Dissertation zur Erlangung des Doktorgrades

der Fakultät für Chemie und Pharmazie

der Ludwig-Maximilians-Universität München

Elucidating virus uptake and fusion

by single virus tracing

Dorothee Carolin Schupp

aus

Ravensburg, Deutschland

2012

für Benno

Summary

Viruses are known to cause many diseases, from the common cold and cold sores to more serious diseases such as the Ebola virus disease and AIDS. Most viruses have evolved with their host over thousands of years and are experts in cell entry. On the one hand, this can complicate the development of efficient drugs against virus infections. On the other hand, one can make use of the virus entry skills to cure diseases using them as shuttles to target a therapeutic agent to particular cells in the body. Prior to their application as therapeutic agents, it is crucial to understand how cells are infected by these viruses. Viruses have evolved different strategies to enter and infect cells. In order to infect a cell, viruses have to overcome the cell membrane barrier to deliver their genome to the site of replication. Enveloped viruses can either fuse directly at the plasma membrane or with an endosomal membrane after endocytic uptake. Upon fusion the viral capsid is released into the cytoplasm.

The aim of this work is to investigate the early steps in virus entry of herpes simplex virus 1 (HSV-1) and foamy virus (FV) by means of fluorescence microscopy. The virus particles contain two different labels, one located at the envelope and the other at the capsid so that fusion can be detected upon separation of the two colors in space.

The first dual-color HSV-1 preparations contained only very few dual-color particles. Therefore, a screen for the best preparation conditions was performed. The amount of capsid particles colocalizing with an additional envelope signal was increased from about 40 % to around 70 %. In addition, the presence of envelope-only particles was significantly reduced although still about 50 % envelope-only particles were present in the optimized virus preparations.

Live-cell imaging experiments in Vero cells revealed a decrease in the colocalization percentage over time, indicating fusion. However, pH-dependent quenching of the fluorescence intensity in acidic cellular compartments could also lead to this observation. Evaluation of the fluorescence intensity of the pH-sensitive GFP-tag, located at the in-

side of the virus envelope, revealed significant quenching at acidic pH values.

In order to account for pH-dependent quenching, colocalization experiments were performed in fixed and permeabilized Vero and HeLa cells. Permeabilization ensures neutral pH throughout all cellular compartments. In the case of Vero cells, no clear decay in the colocalization percentage was observed during 3.5 hours post attachment. In contrast, HeLa cells showed a small decay over time.

The use of fixed cells is intrinsically accompanied by a lack of kinetics on a single-cell level over time. Consequently, colocalization analysis of dual-color viruses was performed in live HeLa cells with an additional marker of endosomal compartments. This 3-color experiment revealed that fusion takes place to a small extend in HeLa cells, consistent with the experiment in fixed HeLa cells. Moreover, the uptake of individual virus particles was investigated in real-time, but no fusion event was detected.

Thus, the use of GFP can result in critical artifacts in live-cell imaging, but tools are presented to circumvent this issue. Furthermore, one can take advantage of the pH-sensitivity to distinguish extra- and intracellular virus particles.

The entry of two types of dual-color foamy virus particles was investigated, namely of prototype foamy virus (PFV) and macaque simian foamy virus (SFVmac). The virus particles contained a GFP-tag at the capsid and an mCherry-tag at the envelope. First, the percentage of dual-color virus particles was characterized for each virus preparation. In all virus preparations, more than 90 % of detected capsid particles colocalized with an mCherry-envelope signal. The amount of envelope particles that contained an additional GFP-capsid signal ranged between 30 to 60 %.

FV glycoproteins possess highest fusion activity at acidic pH values which suggests a pH-dependent endocytic uptake pathway. However, PFV in contrast to the other FV species, already shows significant fusion activity at neutral pH. Hence, it may take an additional pH-independent entry route. In the case of endocytosis, the virions encounter a low pH environment on their journey towards the nucleus in late endosomes. Under these pH conditions, the fluorescence intensity of the dual-color particles was still detectable and a slight reduction was only observed for the GFP-tag. The pH-dependent GFP-tag is located at the capsid and protected by the surrounding lipid bilayer envelope. Live-cell imaging experiments were performed with spinning-disk confocal microscopy in 3D to gain insights into virus uptake and fusion. In order to determine the time-scale when virus fusion occurs, the percentage of virions containing both envelope and capsid signals was evaluated over time in live HeLa cells for PFV and SFVmac particles. In the case of PFV, the obtained colocalization percentage already decreased significantly within the first few minutes post attachment whereas for SFVmac, the decay was less

pronounced. This experiment demonstrates that there are differences between the uptake of PFV and SFVmac in HeLa cells. PFV already fuses within the first minutes. In contrast, fusion of SFVmac occurs at later times and less fusion events were observed during the measurement time of 90 minutes. The highest probability to detect FV fusion is expected during the first 30 minutes post attachment.

Subsequently, single virus tracing experiments were performed with high time resolution to investigate individual fusion events in real-time. Sixteen fusion events, visualized by color separation, were observed. In the case of PFV, four fusion events were observed at the plasma membrane and nine fused with an endosomal membrane after endocytic uptake. For SFVmac, only three intracellular fusion events were observed in total, consistent with the previous colocalization experiment. Moreover, an intermediate stage during the fusion process of foamy viruses was identified that lasted over minutes. This stage was characterized by an increase in the distance between mCherry-envelope and GFP-capsid signals before the final color separation event.

Hence, it was possible for the first time to visualize single fusion events of foamy virus in real-time and characterize the corresponding dynamics. The results provide new insights into the entry pathway and fusion process of this unconventional retrovirus.

Contents

1 Introduction

Since 9/11 2001, there is an increasing fear of terrorist attacks all around the globe. Dirty bombs, anthrax attacks, strikes resulting in small pox pandemic, to mention only a few weapons that threaten the safety of people all around the world. Do you consider this to be a horror scenario of a science fiction novel? Experts are sure that the danger of terrorist attacks – besides the conventional arsenal of weapons – will be more and more extended toward biological weapons. In President Obama's *State of the Union address* in 2010, he announced a new plan to address the potential of bioterror attacks in order "[...] to protect Americans from bioterror or infectious health threats.[1]", as the spokesman of the White House specified [314]. Do you think that this is only supposed to happen in the US? Potential targets are everywhere, including crowded places such as big cities, public transportation systems and festivals. As a result, are you going to avoid visiting the *Oktoberfest*? Even if you do so, your family and friends, without being aware of it, might bring a highly contagious virus directly home to you as a souvenir. In a globalized world, the distribution of virus is no longer locally limited. Traffic hubs such as airports entail a high risk of spreading a virus throughout the whole world, transmitted by people who have not even recognized that they are carriers – the beginning of a pyramid-scheme: neither detectable by body scanners nor personal security check. Such a virus can hit anyone, anywhere, at any time.

Bioterrorism is not the only possible cause for virus pandemics. One of the most deadly diseases was the influenza pandemic in 1918/19, also known as the "Spanish flu" (H1N1). It is estimated that over 50 million people lost their lives due to this pandemic [221, 313], even more lives than have been claimed by World War I. That was probably one of the reasons why many people reacted with panic over the outbreak of avian influenza (H5N1) in humans reported by the media a couple of years ago [35].

Currently, this topic is very explosive since researchers have created a more disastrous

---

[1] `www. hudson. org`, downloaded 2012/05/12 [314]

H5N1 variant that is more efficiently transmitted between mammals [94, 132]. The consequence was an intense public debate – e.g. the German newspaper *F.A.S.* dedicated it's actual title story to this topic [89] – whether the results should be published in *Science* or not. The results help to develop vaccinia against flu. However, the publication could serve as a blueprint for the construction of a horrible bioweapon.

Viruses are part of our daily life, being present in various situations, from a common cold to serious diseases such as Ebola virus disease and AIDS. Even cancer can be a result of a virus infection. Investigation of virus infection and spread are crucial in order to limit new infections, treat outbroken diseases and restrict the opportunity of natural or terroristic-driven pandemics by providing vaccinia. Development of vaccines and drugs for antiviral defense is one important aspect of virus research. Viruses infect people, thus they know how to enter cells. Studying virus entry in cells helps to unravel new cellular pathways, e.g. caveolae-mediated endocytosis was elucidated by investigation of the entry process of simian virus 40 [5, 243, 290]. Moreover, we can exploit viruses as transport system to deliver therapeutic agents to particular cells in the body with high efficiency. This way, viral vectors can be employed for the treatment of cancer or other diseases [51]. Before application as therapeutic agents, it is crucial to understand how cells are infected by each individual type of virus. A detailed understanding of virus entry into cells is also important for the development of antiviral drugs. Viruses can enter cells through multiple pathways. The chosen entry pathway can differ among viruses and even one virus can exploit various entry pathways. One aspect that all viruses have in common is that they need to overcome the cell-membrane barrier to infect a cell. Enveloped viruses cross this barrier by fusion of the viral envelope with the cellular membrane. For some viruses, e.g. herpes simplex virus 1, the entry pathway differs among investigated cell lines. However, the exact factors that determine which pathway is taken by the virus are currently poorly understood. In the case of other viruses, such as foamy virus, it is still unclear which pathways they exploit. Hence, many aspects of the entry process still remain to be elucidated under biologically relevant conditions. A non-invasive technique that enables the study of kinetics and dynamics of virus entry into live cells is required and a suitable method is fluorescence microscopy.

I studied the entry of herpes simplex virus 1 (HSV-1) and foamy virus (FV) in cells by applying fluorescence microscopy. The basics of fluorescence microscopy are outlined in chapter 2 and an introduction to virology is given in chapter 3. In chapter 4.1, the focus is on different cellular entry pathways utilized by viruses as well as on the process of virus fusion in order to deliver the viral genome for replication. The applied methods

to investigate the different steps in virus entry are described in chapter 5. More than 70 % of the world's population are infected with HSV-1 world-wide [341]. Usually, the virus does not lead to severe diseases in immuno-competent persons. Mutant forms of HSV-1 are promising candidates as viral vectors in cancer therapy due to their large genome size in combination with the ability to specifically target HSV-1 to cancer cells [27, 51]. In order to investigate the uptake of HSV-1, fluorescent virus particles were optimized and then applied to study the entry and amount of fusion in two different cell lines (chapter 6). Besides HSV-1, foamy virus is another promising viral vector for application in gene therapy. This virus can infect humans but no associated disease has been documented so far [190]. Fluorescent FV particles were used to elucidate the details of virus fusion. Thereby, a novel intermediate phase during the fusion process was observed (chapter 7). In chapter 8, the obtained results for HSV-1 and FV are compared.

2 Fluorescence microscopy

In the first half of the 20th century, invention of the electron microscope revolutionized the field of microscopy as the achievable resolution could be increased due to the smaller wavelength of electrons in comparison to photons. Electron microscopy (EM) provides excellent resolution for viruses but no dynamic information can be obtained. Nowadays, many high-resolution techniques are available to investigate biological systems. Over the years, it became possible to obtain insights into e.g. the structure of a virus with near-atomic resolution [36] by applying cryo-EM. Cryo-EM is a useful technique for the investigation of biological samples as, unlike other EM techniques, this method preserves biological structures very well. However, it is limited for studying viral interactions with a cell, as only a snapshot at a certain time-point can be observed. By using X-ray diffraction, protein structures and their conformational changes, e.g. upon binding of a viral glycoprotein to its cellular receptor, can be determined, given that crystallization is possible. A powerful method for unraveling dynamics in biological systems is fluorescence microscopy. In the meanwhile, resolution beyond the diffraction limit became possible by techniques such as tip-enhanced near-field optical microscopy [119], stimulated emission depletion (STED) [130], photoactivated localization microscopy (PALM) [21] and stochastic optical reconstruction microscopy (STORM) [264]. However, these super-resolution techniques are still limited for investigation of dynamics. Dynamic processes can be investigated in real-time with high-resolution fluorescence microscopy. As fluorescence microscopy is a non-invasive technique, it is widely utilized to investigate biological systems, e.g. for unraveling dynamic processes in live cells or to investigate the life cycle of a virus. Fluorescence microscopy complements static techniques such as X-ray diffraction and electron microscopy with valuable dynamic information.

The first part of this chapter introduces the principles of fluorescence. Thereafter, advantages and disadvantages of fluorescent microscope techniques for live-cell imaging will be discussed. Fluorescent proteins are useful tools to light up biological systems as they

can be stably introduced in an organism. A description of fluorescent proteins, focusing on those used in this thesis, and exemplary applications are given in the last part of this chapter.

2.1 Principles of fluorescence

Photoluminescence is the overall phenomenon of photon emission after absorption by a molecule. At ambient temperature or temperatures around 37 °C, excitation mainly occurs from the electronic ground state S_0 of lowest vibrational energy, as higher vibrational states are not significantly populated at these temperatures. These transitions occur within approximately 10^{-15} s [111], so that there is no significant movement of the relatively heavy nuclei during this time (Born-Oppenheimer approximation[1] [24]). Therefore, the most likely transition is the vertical transition between states with overlapping nuclear coordinates, which is known as the Franck-Condon principle [54, 55, 95]. An intuitive illustration to explain the different absorption and emission processes was proposed by Jabłoński [140] and can be seen in figure 2.1.

Fluorescent molecules are excited to higher electronic, vibrational and rotational states. Absorption is followed by vibrational relaxation, typically to the ground state of S_1. Vibrational relaxation is often referred to as internal conversion (e.g. [154, 179]), however, in some literature internal conversion is exclusively used for an isoenergetic conversion from a lower vibrational level of a higher electronic state to a higher vibrational level of a lower electronic state (e.g. [111, 187]). Vibrational relaxation to the ground state of S_1 takes around 10^{-12} s [179] and is faster compared to fluorescence lifetimes of around 10^{-8} s [179]. Therefore, dissipation to the S_1 ground state is normally complete before emission, and the emission wavelength is independent of the excitation wavelength. This is known as the Kasha-rule as he stated that *"The emitting electronic level of a given multiplicity is the lowest excited level of that multiplicity[2]"* [154]. The excited molecule can return to the electronic ground state S_0 by fluorescence ($S_1 \rightarrow S_0$) or via non-radiative decay channels. The molecule can also undergo spin conversion to the triplet state T_1, called intersystem crossing. In this case, the electron has the same spin orientation as the electron in the ground state. Therefore, T_1 is usually energetically below S_1 because no spin-pairing energy is required. The emission from T_1 to S_0 is called phosphorescence. This transition is spin-forbidden resulting in a relatively long lifetime of ms to s or even

---

[1]E. U. Condon commented on *"The paper of Born and Oppenheimer [that it] is among those difficult ones that are more often cited than read"*, Condon 1947, p.368, [56]

[2]Kasha 1950, p.15, [154]
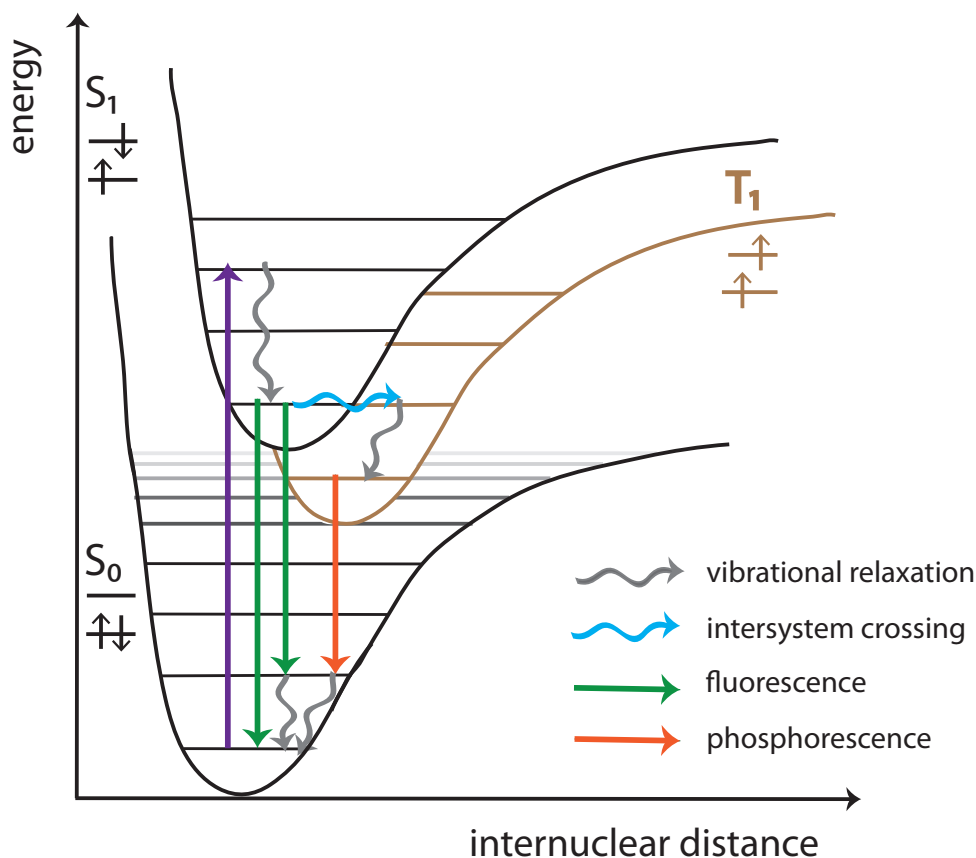
Figure 2.1: *Quasi-Jabłoński diagram. After absorption of a photon, the molecule is excited to a higher electronic state. From there it typically reaches the ground state of S_1 by vibrational relaxation. From S_1, the molecule can go to the ground state of S_0 via non-radiative decay channels or by emission of a photon, called fluorescence. Furthermore, there can be intersystem crossing to a triplet state, which is energetically below the singlet state. The emission from T_1 to S_0 is called phosphorescence.*

longer [179].

Molecules in the triplet state are not available for excitation and are removed from the detection pool until they return to the ground state [187]. Photochemical reactions that lead to photobleaching are mostly assumed to occur from the triplet state as it has a longer lifetime than the singlet state [75].

According to the Franck-Condon principle, the most likely transition occurs between states with overlapping nuclear coordinates, which is usually an electronic state of higher vibrational energy [54, 55, 95]. Fluorescence is typically emitted from the vibrational ground state of S_1 to higher vibrational levels of S_0, resulting in a lowered energy of the
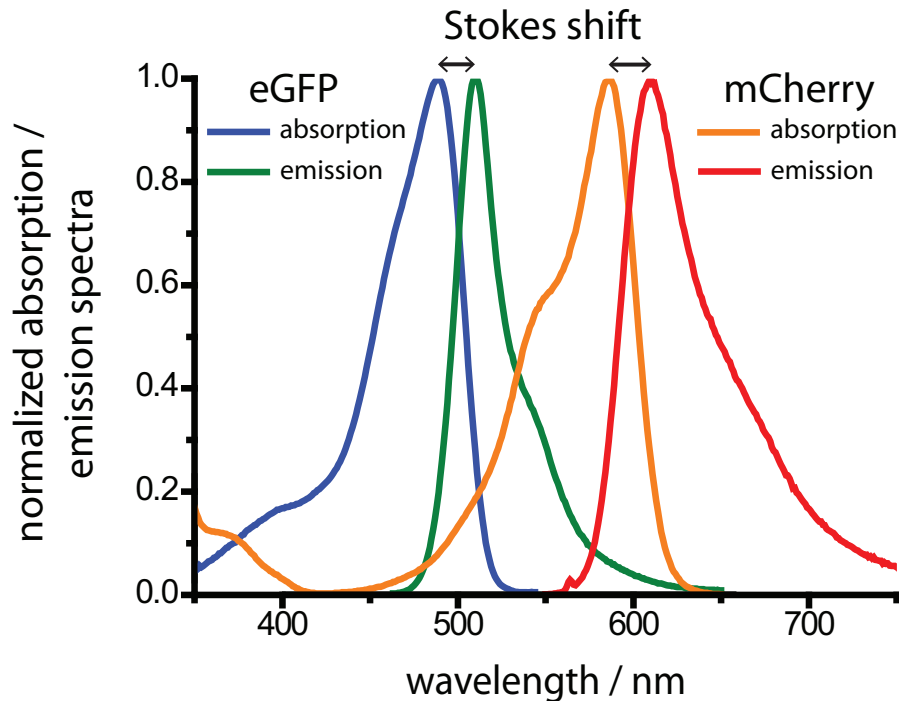
Figure 2.2: *Absorption and emission spectra of the fluorescent proteins eGFP and mCherry, illustrating the Stokes shift. Spectral data downloaded from [316].*

emitted photon relative to the absorbed one. The effect is even more prominent in the case of phosphorescence as the triplet state is energetically below the singlet state. This shift to lower energy from the absorption to emission spectrum is called Stokes shift and illustrated in figure 2.2 [297]. The Stokes shift of fluorescent molecules enables separation of excited and emitted light and makes fluorescent based methods an efficient tool for investigation of various processes.

2.2 Fluorescent microscope techniques

Fluorescent microscope techniques used for live-cell imaging should fulfill several criteria: it should be possible to image a whole cell, requiring a large field of view and an additional z-motor to get the full 3D view of a cell. The introduced fluorophores as well as image acquisition should be minimal invasive to the investigated specimen. Furthermore, the images should have a good contrast, which can be difficult if the background increases due to autofluorescent cellular structures. Obtaining a good contrast can be even more demanding if the cell membrane or the cellular cytoskeleton is stained in addition. Above all, image acquisition should be possible in real-time. Depending on the biological system studied and the questions addressed, one has to choose the appropriate

microscope configuration.

In the following paragraph, basic principles of light microscopy are explained. Description of different fluorescent microscope techniques with regard to live-cell imaging is given in the subsequent section.

The resolution of imaging a point-like object is limited by diffraction of the light on the aperture of the objective lens. The observed diffraction pattern is called the Airy disk [2]. As a rule of thumb, the Rayleigh criterion [252] is used to estimate the achievable resolution. According to this criterion, two nearby point-like objects can be resolved if the center of the Airy disk from one object corresponds to the first minimum of the other object or is further apart [224]. Thus, the resolving power of a microscope is given by

$$d_{lateral} = 0.61 \cdot \frac{\lambda}{\text{NA}} \tag{2.1}$$

where $d_{lateral}$ corresponds to the minimal distance between two objects that can be resolved, λ is the wavelength and NA is the numerical aperture of the objective. The numerical aperture depends on the refractive index n of the medium (for oil immersion objectives n equals 1.512 at 37 °C) and the half angle of the light cone collected by the objective (θ). The NA is given by $\text{NA} = n \cdot sin(\theta)$. For a typical oil immersion objective used in this thesis with a NA of 1.49 and an excitation wavelength of 488 nm, the best possible lateral resolution is 200 nm.

However, the actual resolution depends also on the signal-to-noise ratio of the obtained image. Contributions from out-of-focus light or autofluorescent cellular structures increase the background signal. The lower signal-to-noise ratio limits the achievable resolution.

In the following subsection, an overview of wide-field and confocal microscopy are given. A detailed description of the experimental setups used in this thesis can be found in the section 5.2 of the materials and methods.

2.2.1 Wide-field microscopy

In wide-field microscopy, the laser beams used for sample illumination are expanded and focused on the back focal plane of the objective. The light exiting the objective is collimated and used to excite fluorescent particles in the sample as illustrated in figure 2.3. Not only particles within the focal plane are excited but rather a broad volume of the sample, including particles above and below the focal plane. The emitted light is col-

lected via the same objective (epi-fluorescence) and separated from the excitation light by a dichroic mirror. The detection path is simple and photons are detected with high sensitivity by an EMCCD camera.

The contribution from out-of-focus light increases the background signal and limits the theoretical available resolution. Especially, the axial resolution is deteriorated compared to confocal microscopy. As a broad area of the sample is illuminated at once, one does not need to scan the sample or the excitation beam, and image acquisition is fast, with frame rates up to 30 ms. Cameras with a large field of view of 512×512 pixels or even in the mega-pixel range enable imaging of one or more cells at once with high magnification. Hence, imaging can be done with high temporal and spatial resolution. Moving particles that show a small displacement in z-direction can still be detected. This can be advantageous for imaging particle uptake in live cells, given that the signal-to-noise ratio is sufficient.

An alternative approach to minimize out-of-focus contributions is total internal reflection fluorescence (TIRF) microscopy (figure 2.3). The evanescent field resulting from total internal reflection at the cover-slide/medium interface is used to excite the sample. The depth of the evanescent field is typically around 100 nm and contrast is enhanced in comparison to normal wide-field mode [14, 308]. However, using this approach, only fluorophores in the bottom area of the sample can be excited and hence, only cellular structures that are close enough to the glass surface can be observed. In the case of cells, TIRF microscopy is restricted to the ventral membrane.

2.2.2 Confocal microscopy

Confocal microscopy offers the advantage of an increased image contrast in comparison to wide-field microscopy.

The laser excitation beam is fed parallel into the objective. The objective focuses the light on the specimen as diffraction limited spot. Fluorescence is collected via the same objective and separated from the excitation light via a dichroic mirror, as can be seen in figure 2.3. A pinhole, positioned in a conjugated image plane in front of the detector, ensures that only emitted light originating from the focal volume is detected. This leads to increased contrast compared to the wide-field mode, although with some cost to the total signal. Confocal microscopy is beneficial for thicker samples or if e.g. virus particles need to be detected in the presence of labeled cellular structures, such as tubulin or actin, that led to an increase of the background signal.
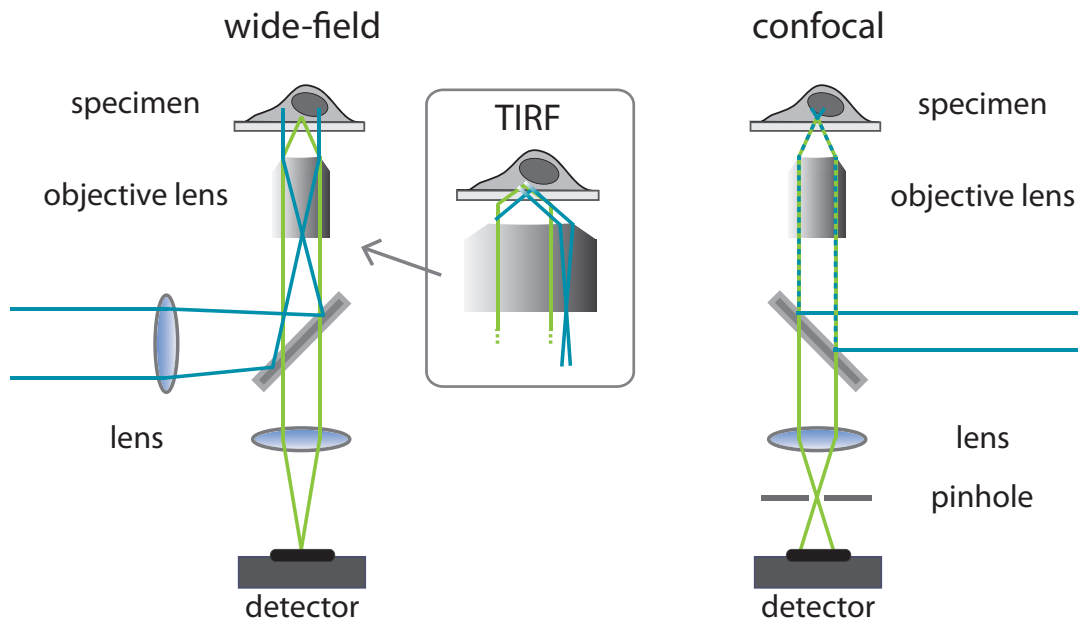
Figure 2.3: *Comparison of a wide-field and a confocal microscope configuration. The excitation light is shown in blue color and the emitted light from the sample in green color. In wide-field mode the sample is uniformly illuminated, whereas in confocal microscopy only a defined volume of the sample is excited. The confocal pinhole ensures that only light originating from the focal volume is detected. Therefore, out-of-focus contributions are minimized and image contrast is enhanced in comparison to wide-field microscopy. However, as only a small spot of the sample is illuminated in confocal microscopy, the sample needs to be scanned to obtain the whole image. An alternative approach to minimize out-of-focus contributions is total internal reflection fluorescence (TIRF) microscopy since only the lower bottom of the sample is excited by the generated evanescent field.*

However, in confocal microscopy one needs to scan the sample, either by moving the stage or the laser beam, to obtain a whole image of a cell. The scanning process for obtaining a comparable field of view as in wide-field microscopy can be time consuming and hence, problematic for imaging in live cells, when a large field of view is required. For experiments with live cells, one wants to combine the improved contrast with fast image acquisition times (near real-time) and a large field of view. By combining these features, spinning-disk confocal microscopy is usually the instrument of choice for studying dynamics inside live cells in real-time.

2.2.2.1 Spinning-disk confocal microscopy

Spinning-disk confocal microscopy uses a different scanning mode than in conventional confocal microscopy. As indicated by the technique's name, a disk comprising multiple pinholes, is spun. This disk is called a Nipkow disk. The pinholes and the spacing between them are arranged in such a way that every point in the specimen gets the same amount of illumination when the disk is rotating [224]. The majority of the excitation light is blocked and only very little light passes through the pinholes. In order to improve the irradiation efficiency, the Nipkow disk is combined with a second disk that contains an array of microlenses, corresponding to the pinholes of the Nipkow disk (figure 2.4) [199]. The combination of these disks, devised by the Yokogawa Electric Corporation and known as Yokogawa CSU, comprises 20,000 microlenses and the same amount of pinholes [199]. It can be rotated between 1800 to 10,000 rotations per minute [228, 343]. A dichroic mirror is positioned between the two disks, so that the emitted light passes through the pinholes and can then be detected by an EMCCD camera as illustrated in figure 2.4. Combination with a piezo system for z-stacking allows the whole 3D information of a cell to be collected.

The advantages of the spinning-disk confocal system compared to laser scanning confocal microscopes are that the whole confocal image can be directly seen and detected by an EMCCD camera and image acquisition can be done with higher time resolution. However, one looses flexibility in adjusting the pinhole size and the optical sections are thicker [224], but the image contrast is still improved in comparison to wide-field microscopy. Therefore, spinning-disk confocal microscopy is ideally suited for analysis of live cells.

2.3 Fluorescent proteins

Fluorescence microscopy is a powerful tool for unraveling dynamic processes in living systems as it is a non-invasive technique. Fluorescent proteins are ideal markers of biological systems, e.g. viruses or as markers of different cellular compartments. Figure 2.5 gives an example how fluorescent proteins can be used to highlight cellular structures. The gene encoding for the fluorescent protein can be introduced into an organism, so that it is stably expressed. In principle, fluorescent proteins can be fused to any protein, but one has to validate that fusion does not affect protein functionality. Fluorescent proteins typically have a molecular mass of around 26 kDa or more [31, 200, 250] and
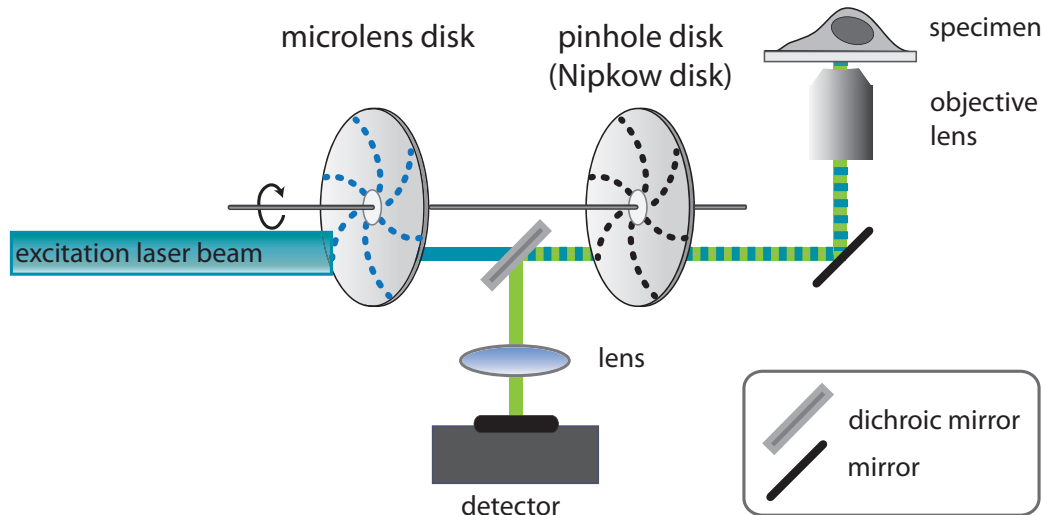
Figure 2.4: *Spinning-disk confocal microscope combining a Nipkow disk, comprised of multiple pinholes, and a microlens disk. The microlens disk increases the illumination efficiency by focusing the excitation laser beam (blue color) on the pinholes. The Nipkow disk is located in a conjugated image plan. Fluorescent light (here in green color) passes through the pinholes and is reflected by a dichroic mirror positioned between the two disks. The emitted light can be detected by an EMCCD camera.*

hence, one can imagine that this might alter kinetics to a variable extent, depending on the investigated system. Despite that fact, fluorescent proteins enable insight into living systems that would not be possible without them.

In comparison to organic dyes, fluorescent proteins offer the advantage that they can be introduced into wider ranges of tissues and organisms and they can be used to specifically label different cellular compartments [349]. By using fluorescent proteins for labeling, the biological functions of the modified system can be reliably characterized, e.g. infectivity of viruses.

Since the discovery of the green fluorescent protein (GFP) in the jellyfish *Aequorea* by Shimomura *et al.* in 1962 [281], fluorescent proteins have revolutionized the field of fluorescence-based applications in living organisms. The first application of GFP as a marker of cellular gene expression was developed by Chalfie *et al.* [34], based on the nucleotide sequence published by Prasher and co-workers [249]. Tsien and co-workers contributed to obtain more fluorescent proteins with improved brightness and with absorption and emission spectra in a different spectral range, most of them derived from the red fluorescent protein DsRed [31, 122, 123, 124, 275]. The contributions of O. Shimomura, M. Chalfie and R. Y. Tsien were awarded with the Nobel prize in chemistry in the year 2008 [235].

Nowadays, fluorescent proteins over the whole visible spectral range are available [276].
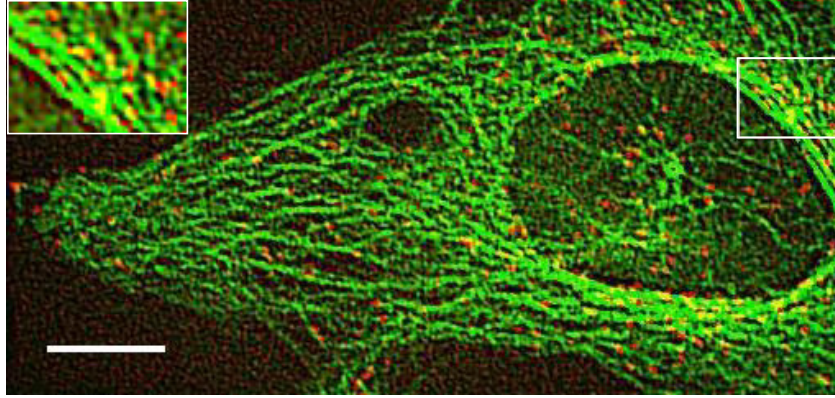
Figure 2.5: *Application of fluorescent proteins to highlight the microtubule network in a live cell. HeLa cells, transiently expressing tubulin-GFP (green color), are shown after infection with foamy virus particles containing the fluorescent protein mCherry (red dots). Virus particles colocalize with microtubules as can be seen in the figure inset. Transport of viruses along microtubules can be studied by live-cell imaging. Scale bar 10 μm.*

In this work, the fluorescent proteins GFP, mRFP and mCherry are used (figure 2.2). The absorption and emission spectra of mRFP and mCherry are in the same spectral range with the emission spectra of mCherry being slightly red-shifted [31, 275]. Furthermore, mCherry shows improved photostability in comparison to mRFP [275, 276]. The pK_A of mRFP is around 4.5 and even lower for mCherry [275, 276]. The most prominent fluorescent protein, GFP, consists of 238 amino acid residues, which fold into eleven β-strands and one α-helix. The tertiary structure can be described as a hollow cylinder with the chromophore in the middle (figure 2.6) [249, 315]. The chromophore is formed in an autocatalytic reaction involving Serin-65, Tyrosin-66 and Glycin-67, leading to an imidazolinone ring structure (*p*-hydroxybenzylidene-imidazolinone) (figure 2.6.B, green highlighted structure) [123, 234, 315]. Protonation of the hydroxyl group of Tyr-66 leads to a non-fluorescent state (figure 2.6.B, red box) [120, 159]. This conversion between a fluorescent state and a dark state is reversible, at least in a certain pH-range [159]. This explains the pH-sensitivity of GFP fluorescence. The wild-type (wt) form of GFP has a pK_A near 4.5 [315]. However, mutated forms of wtGFP with enhanced spectral properties at neutral pH, like the enhanced GFP (eGFP), are more sensitive to high proton concentrations [315]. The pK_A of eGFP is around 6.0 [120, 276].

Beyond the possibility of highlighting cellular structures by genetically encoding fluorescent proteins, the possibility to engineer their photophysical properties offers versatile novel applications. Fluorescent proteins can be used as intracellular sensors, e.g. to investigate the redox potential or proton concentration in cells [22, 117, 294]. Novel
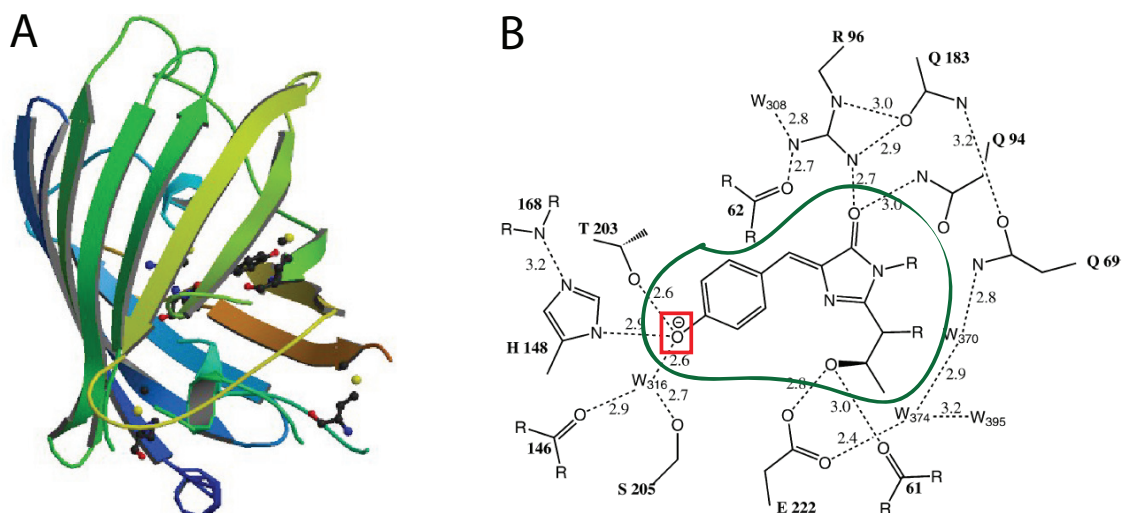
Figure 2.6: *Structure of GFP from Aequorea victoria based on the crystal structure obtained by Ormö et al. [237]. (A) Tertiary structure of GFP made up of eleven β-strands and one α-helix. The chromophore is located inside the protein matrix. Structure downloaded from Protein Data Bank, entry 1EMA. (B) Structure of the chromophore (highlighted in green) together with the first and second coordination spheres. The red box indicates the hydroxyl group of Tyr-66 that is protonated at lower pH, leading to a non-fluorescent state. Probable hydrogen bonds are shown as dashed lines, the corresponding distance between the heteroatoms is given in Ångstroms. Adapted from [315].*

fluorescent proteins that emit in the far-red, like Neptune, make it possible to perform deep tissue imaging in living animals [188].

Several fascinating applications became possible by the development of fluorescent proteins that can be photochemically modulated. Photoactivatable proteins, such as Dronpa or the more recently developed rsTagRFP [299], can be reversibly switched from a fluorescent state to a dark state. Thus, particles tagged with e.g. Dronpa, can be detected in the presence of cellular fluorescent structures in the same spectral range [126]. Moreover, photochromic FRET has now become possible with fluorescent proteins [299]. By using rsTagRFP as acceptor fluorophor together with EYFP as donor, Subach *et al.* have studied intracellular protein-protein interaction in live cells [299]. Another amazing group of photoactivatable fluorescent proteins, such as Kaede [6] or EosFP [334], can be converted from green to red fluorescence, enabling their application in super-resolution techniques like PALM, FPALM and STORM [21, 135, 149, 298].

3 Introduction to viruses

Viruses are complex carriers of genomic information that are dependent on a host cell for their replication. They are classified on basis of the nucleic acid they contain, their capsid morphology, their lipid membrane containment (envelope) and their genome architecture [91]. On basis of their genome, we distinguish between RNA- and DNA-viruses. RNA-viruses can be further divided into Retro- and Riboviruses. In Retroviruses, replication takes place via a DNA-intermediate whereas, in Riboviruses, replication occurs only via an RNA-intermediate. Satellite viruses constitute a class of viruses that does not only depend on a host cell for replication but also requires helper functions of other viruses to be infectious. Examples of satellite viruses are the delta virus and the adeno-associated virus which depend on helper functions of hepatitis B virus and adeno- or herpesvirus, respectively [17].

Despite many differences reflected in the numerous classes of different virus families, they also share some structural features. In general, the viral genome is enclosed in a protective protein shell called the capsid, which is build up of highly regularly protein assemblies that form different capsid symmetries. Known capsid structures are classi-fied as helical (e.g. tobacco mosaic virus) or icosahedral symmetry (e.g. herpesviruses) [60, 91]. The icosahedral structure is the most economic way to build a shell with a minimal surface area but maximal internal volume. There are also viruses that contain a so-called complex capsid (e.g. vaccinia virus) where the structural elements are not well understood up to now [53, 91].
For enveloped viruses, the capsid structure is surrounded by a lipid bilayer envelope acquired from host-cell membranes during egress. The envelope accommodates viral surface proteins that are required for binding to cellular receptors and cell penetration. In contrast, naked viruses contain no envelope. Enveloped viruses have a higher capacity for adaption compared to naked viruses and furthermore, protect the inner capsid from environmental influences. Enveloped viruses can release their capsid into the cytosol by

fusion of the envelope with a cellular membrane, so that there is no need for destruction of the host-cell membrane, e.g. through lysis, to achieve release [197].

Although all viruses, without exception, need a host cell for replication, their strategies differ significantly. Most RNA-viruses replicate in the cytoplasm [17, 76]. However, Retroviruses transcribe their RNA genome into dsDNA, which thereafter is then integrated into the host-cell genome for efficient replication. Thus, transcription of the resulting integrated virus genome (provirus) to the viral RNA takes place in the nucleus [109]. The replication of DNA-viruses typically takes place in the host-cell nucleus except for pox- and iridoviruses, which replicate in the cytoplasm [76, 197]. The genome of most RNA-viruses is single-stranded RNA with the exception of viruses from the reo- and birnavirus family whose members contain double-stranded RNA. [91]. In principal, DNA-viruses have a double-stranded DNA genome, whereas members of the parvo- and circovirus family use single-stranded DNA for replication [91].

Both, RNA- as well as DNA-viruses can undergo spontaneous mutations. The mutation rate is typically much higher for RNA- than DNA-viruses which allows rapid adaption to the host but can lead to accumulation of lethal mutants if the mutation frequency is too high [52, 76]. Well-adapted viruses induce few side effects in their natural host organism whereas transmission to a non-natural host (from one species to another) often provokes severe diseases as seen for HIV or the outbreak of avian influenza virus in humans [8, 35, 91, 116, 277].

3.1 Herpesvirales

One main part of this work focuses on the entry of a herpesvirus into cells. Herpesviruses are very old viruses which are found in vertebrates and in invertebrates. Genetically, there are three different groups that are only slightly related, which should be considered for their classification [67, 68, 318]. The International Committee on Taxonomy of Viruses therefore revised the classification of the former *Herpesviridae*, which had included all known herpesviruses, into the new order of *Herpesvirales*. A sketch illustrating the classification is given in figure 3.1. *Herpesvirales* is consisting of the three families *Alloherpesviridae*, *Herpesviridae* and *Malacoherpesviridae* [138]. The updated family of *Herpesviridae* contains mammal, bird and reptil viruses [69]. There are eight different herpesviruses known so far where humans are the natural host [244]. The focus of this work is on entry of a human herpesvirus (HHV), therefore the main similarities and differences of this group will be described in more detail in the following section.
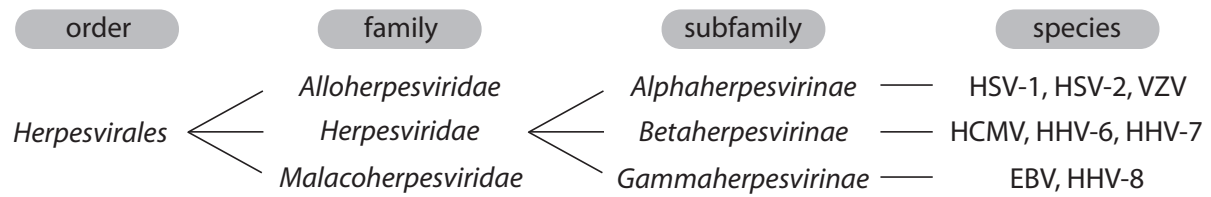
order	family	subfamily	species

Herpesvirales
Alloherpesviridae
Herpesviridae
Malacoherpesviridae

Alphaherpesvirinae — HSV-1, HSV-2, VZV
Betaherpesvirinae — HCMV, HHV-6, HHV-7
Gammaherpesvirinae — EBV, HHV-8

Figure 3.1: *Classification of the order Herpesvirales. All human herpesviruses belong to the family of Herpesviridae. For the sake of simplicity only the subfamilies of Herpesviridae are given together with the human herpesvirus species belonging to this subfamily.*

Herpesviruses are complex viruses with a lipid bilayer membrane envelope [84, 258]. They contain an amorphous proteinaceous layer called the tegument, which surrounds the capsid [260]. Inside the capsid resides the double-stranded DNA genome with a huge size ranging from 125 kbp to 236 kbp for HHV [244]. The viruses are comparably large with a virion diameter ranging from 120 nm to 250 nm [68]. This broad size spectrum is, in part, assigned to variability in the dimensions of the tegument [244].

Herpesviruses are ubiquitous and found worldwide in animals and human beings [244]. The numbers of infected people are in general lower for the sexually transmitted virus HSV-2 and for HHV-8 [76, 285]. In nature, virus infection is usually in close association with a single host species indicating evolution of the viruses with their hosts [68, 318]. By being well adapted to their natural hosts, the virus shows modest pathogenity [68, 244, 318].

Among the biological features that all herpesviruses share are the nuclear synthesis of viral DNA and capsid assembly [244, 258]. All herpesviruses have the capacity to establish lifelong, latent infections in specific host cells [244, 258]. Latency is defined as a state in which the viral genome is continuously present in the host tissue but no infectious progeny virions are produced from this cell [244, 292]. However, the mechanism differs by which the virus remains latent and in which cells [244, 258, 262].

Among the different families in the order of *Herpesvirales* as well as within each family, the viruses show distinct features concerning (i) the cells in which latency is established, (ii) whether the viruses have a broad or a narrow host cell range, (iii) a short or long replicative cycle and (iv) in the clinical manifestations of the resulting diseases [244, 258, 262]. Therefore the family of *Herpesviridae* is further divided into the subfamilies of *Alpha-, Beta- and Gammaherpesvirinae* (figure 3.1), as is indicated by the ending *-virinae* [259]. Initially, this division was based on biological characteristics as the nucleotide sequence was not known. Nowadays, the viruses have been further classified

based on molecular criteria like sequence homology [244, 262].

Similarities shared within the *Alphaherpesvirinae* are a variable host range, a short replication cycle followed by a rapid spread in cell culture and cell lysis; latency is established in neurons, mainly in the trigeminal and dorsal root ganglia [50, 258, 259, 293]. The neurotropic viruses belonging to this group are herpes simplex 1 and 2 (HSV-1, HSV-2) and varicella-zoster (VZV), with HSV-1 being the prototype alphaherpesvirus [50, 244, 258]. Primary infection with HSV is asymptomatic whereas reactivations can be either symptomatic resulting in oral or genital blisters, or asymptomatic. Asymptomatic shedding can arise in more than 65 % of HSV-2 seropositive patients [293]. Primary VZV infection causes the highly contagious varicella that are also known as chickenpox. Reactivation from latency typically results in herpes zoster, also called shingles [49, 50, 293].

Characteristics of the *Betaherpesvirinae* are a restricted host range, a relatively long replication cycle, slow spread of infection from cell to cell in culture with cells frequently becoming enlarged before lysis and that latency is usually established in secretory glands and the lymphoreticular system [50, 258, 259, 262]. Human cytomegalovirus (HCMV), roseolovirus (HHV-6) and the human herpesvirus 7 (HHV-7) belong to this group [244]. Primary infection with the prototypical betaherpesviruses HCMV rarely causes serious illness in healthy adults but can lead to severe, life-threatening diseases in immunocompromised individuals [50, 99].

Gammaherpesviruses also show a narrow host range[1]. The viruses replicate *in vitro* in lymphoblastoid cells and are usually specific for either T- or B-lymphocytes where latency is established. The lytic cycle of the virus leading to destruction of the infected cell as well as the cytopathology of its infection are variable [50, 76, 258, 259]. The prototype gammaherpesvirus Epstein-Barr (EBV) and human herpesvirus 8 (HHV-8) are currently grouped into this subfamily [244]. Some latently with EBV infected B-cells undergo spontaneous lytic replication, so that virus can be found in the saliva of nearly all seropositive persons. This may explain why more than 90 % of humans are infected. EBV and HHV-8 are both associated with tumor formation, especially in immunocompromised persons. Clinical syndromes of EBV infections can be infectious mononucleosis, nasopharyngeal carcinoma, Burkitt's lymphoma, Hodgin's disease and peripheral T-lymphoma (reviewed in [48, 76]).

---

[1]Experimental hosts are usually limited to the family or order of the natural hosts [262]

3.1.1 Herpes simplex virus 1

Herpes simplex virus is a highly prevalent virus that causes lifelong infections, the vast majority of adults are infected. Due to their large genome size, mutant forms of this virus are promising candidates as viral vectors in cancer therapy [27, 51]. In order to develop efficient drugs and vaccines as well as to optimize the virus for use in cancer therapy, it is crucial to gain detailed insights into the life cycle of this virus.

3.1.1.1 Pathology

Infection with herpes simplex virus is normally obtained through direct contact with an infected lesion or infected body fluid, typically saliva but also genital fluids of a seropositive patient [9]. Primary infection involves mucocutaneous surfaces or damaged skin and is usually asymptomatic [9, 50, 293].

Following local replication, the virus enters sensory nerve endings and reaches the cell body of the neurons by retrograde axonal transport where latency is established [9, 261, 293]. Latent virus was mainly found in trigeminal ganglia and to a lower extend in sacral and vagal ganglia [9, 261]. In order to maintain latency, HSV-1 expresses latency-associated transcripts (LATs) to circumvent programmed cell death in neuronal cells [9, 42, 121, 293, 318].

Reactivation of latent virus from the sensory ganglia can be triggered by a number of endogenous or exogenous factors such as emotional stress, fever, menstruation, oral and facial surgery, immunosuppression or exposure to UV light [9, 261].

Symptomatic reactivations, termed recrudescence, lead to cutaneous and mucocutaneous herpetic infections, mainly manifested as herpes labialis in the case of HSV-1. However, about 17 % of genital herpes are caused by HSV-1, probably acquired via oral-genital contact [174]. Additionally, oral HSV-2 shedding has also been reported, meaning that the virus is excreted or spread e.g. into the saliva and other people can be infected upon close contact [9, 164, 293].

Reactivation can also be asymptomatic, resulting in unperceived transmission of HSV and could thus explain the high contagious rate. The numbers for asymptomatic HSV-1 shedding vary among different investigations: 2-9 % of adults were reported in antecedent studies reviewed by Corey and Spear [59], around 18 % of children between 3 to 14 years (reviewed in [261]) and Knaup *et al.* reported even 68 % of asymptomatic HSV-1 shedding [160]. However, the statistics were quite poor.

A study from Wutzler *et al.* in Germany revealed that, on average, 73 % of the population are infected with HSV-1. The numbers increased steadily with age, reaching 90 %
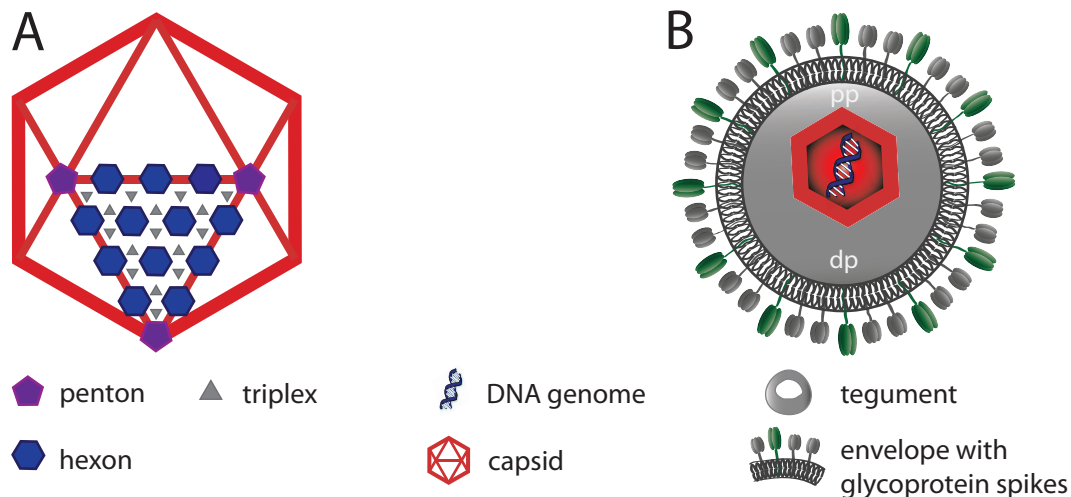
Figure 3.2: *Structure of HSV-1. (A) Illustration of the icosahedral capsid symmetry. The capsid consists of 150 hexons and 12 pentons that are at each vertix. The connecting triplexes are at each trigonal site. Figure after [230]. (B) Complete virus structure consisting of DNA genome, capsid, tegument and lipid bilayer envelope with protruding glycoprotein spikes. The virus is about 225 nm in diameter, pp - proximal pole, dp - distal pole.*

or more in people over 50 years [341]. Comparable high prevalence numbers are reported worldwide in adults, though the time-point in life at which infection was acquired differs [285].

Besides orolabial and genital blisters, HSV diseases can have morbid outcome including blindness through infection of the eye, encephalitis, which is associated with a high mortality, and neonatal infections [293, 318]. In immunocompromised patients, recrudescence can be more extensive and aggressive [9]. Whether other neurological diseases like Alzheimer's disease, multiple sclerosis, acute disseminated encephalomyelitis or Bell's palsy are associated with HSV is still under debate [9, 293].

3.1.1.2 Virus structure

Herpes simplex virus 1 particles contain a double-stranded DNA with a genome size of 152 kbp [80, 203]. The DNA core is enclosed in the capsid. The capsid itself is composed of 12 pentons, 150 hexons and 320 connecting triplexes and has a triangulation number of $T = 16$, resulting in icosahedral symmetry as is illustrated in figure 3.2.A [355]. The outer capsid layer is composed of four viral proteins, namely VP5 (UL19), VP26 (UL35), VP23 (UL18), and VP19C (UL38) and has a molecular mass of 0.2 billion daltons. The capsid protein VP 5 (149 kD) is the main component forming the capsid
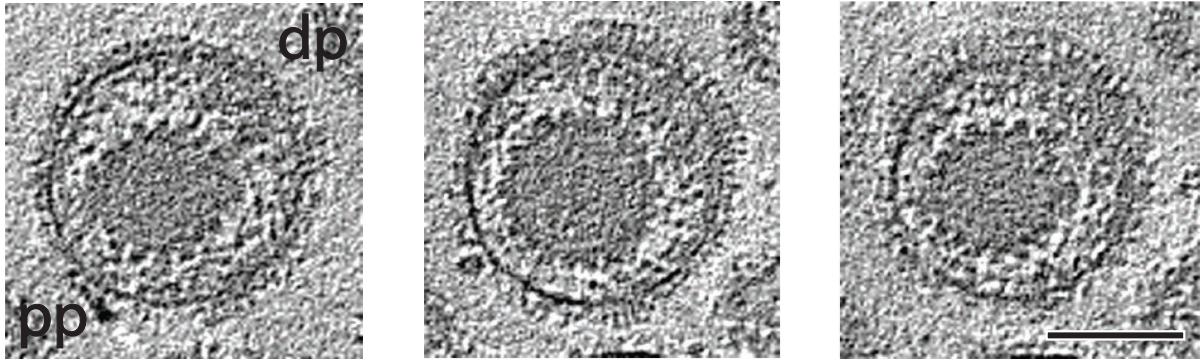
Figure 3.3: *Slices through a HSV-1 particle obtained by tomographic reconstruction. The image illustrates the assymetric cap formation of the tegument. The capsid can be seen in dark gray. The side closely located to the envelope (dark gray line) is called the proximal pole (pp), the side with larger spacing is called the distal pole (dp), scale bar 100 nm. Figure adapted from [114].*

lattice of pentons and hexons. Each VP5 hexameric subunit is capped by a VP26 (12 kD) hexameric ring [261, 354, 355]. The number of VP26 proteins per virion can therefore be roughly estimated to around 900 copies.

The capsid is surrounded by an amorphous proteinaceous layer called the tegument which forms an asymmetric cap (figure 3.3) [260]. Grünewald *et al.* have shown with cryo-electron tomography that the capsid is on one side closely located to the surrounding envelope which they call the proximal pole (pp). On the distal pole (dp), capsid and envelope are separated by around 35 nm of tegument layer (figure 3.3, 3.2.B). They further observed filamentous structures of approximately ∼7 nm in width within the tegument, which they assumed to result from actin [114]. The tegument is wrapped up by a lipid bilayer envelope. Around two-thirds of the volume enclosed by the envelope is occupied by the tegument and the remaining volume by the capsid [114]. The envelope membrane is ∼5 nm thick with an envelope diameter ranging from 170 nm to 200 nm [114]. The lipid composition of the viral envelope is most likely determined by the host cell. The high concentrations of sphingomyelin and phosphathidylserine in the viral envelope are found in the Golgi apparatus as well as in the plasma membrane of cells [322].

The envelope contains around 660 glycoprotein spikes that are protruding out of the membrane. The glycoproteins gB, gC, gD, gE, gG, gH, gI, gL and gM are embedded in the viral envelope and the envelope hosts around eleven different glycoproteins [261]. Cryo-electron tomography showed that these glycoprotein spikes vary in length (10 nm - 25 nm) and distribution with an average spacing of 13 nm. The total envelope diameter including the glycoprotein spikes is on average 225 nm [114].

3.2 Retroviridae

Retroviridae are divided into the subfamily of *Orthoretrovirinae* and *Spumaretrovirinae* as is illustrated in figure 3.4. *Orthoretrovirinae* comprises the virus groups of alpha-, beta-, delta-, epsilon- and gammaretroviruses as well as lentiviruses [91, 138]. These groups of viruses with the exception of lentiviruses was formerly referred to as *Oncovirinae* due to their oncogenetic potential [76, 326].
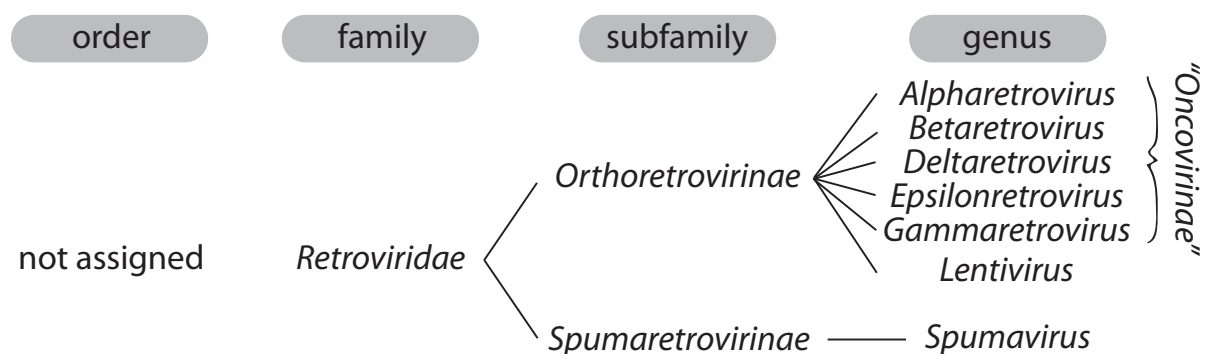

Figure 3.4: *Classification of the family Retroviridae that comprises the subfamilies Orthoretrovirinae and Spumaretrovirinae. Orthoretrovirinae comprises the group of so-called "oncoviruses" and the lentiviruses. Spumaviruses or foamy viruses are the sole members of Spumaretrovirinae.*

Spumaviruses, or foamy viruses, are the sole viruses currently belonging to the group of *Spumaretrovirinae*. They comprise their own subfamily within the *Retroviridae* due to some distinct features. Their infectious genome is rather DNA than RNA and they differ in the replication pathway, e.g. budding of virus particles requires the expression of both proteins that form capsid and envelope [191, 218, 346]. In some aspects e.g. virus budding, foamy viruses share more similarities with the group of *Hepadnaviridae* [16, 192]. Hepadnaviruses, like for example hepatitis B virus, are enveloped DNA viruses that replicate via an RNA intermediate [91, 274].

Retroviruses are enveloped single-stranded RNA viruses with positive polarity[2] and a genome size ranging from 7 kb to 13 kb [52, 91, 326]. They are diploid as they contain two copies of their RNA genome [324, 326, 328]. Capsid structures can be spherical, cylindrical, conical or have an immature appearance [52, 326]. The outer lipid bilayer

---

[2]By convention, the polarity of messengerRNA is defined of positive sense as the information can be immediately translated. Accordingly, viruses with an RNA genome of positive polarity have the same sense as mRNA and can directly serve as mRNA. Although, Retroviruses have a (+) strand RNA genome, they replicate via a DNA-intermediate [91].

envelope contains glycoprotein spikes and measures between 80 nm to 140 nm in diameter [26, 339, 326].

All retroviruses contain the three coding sequences *gag*, *pol* and *env* for the major proteins. The core proteins that form the matrix, capsid and nucleoprotein structures are encoded by *gag*, while viral enzymes are encoded by *pol*, and *env* encodes the envelope glycoproteins [324, 326, 328]. The smaller coding domain *pro* encodes the viral protease that cleaves the Gag polyprotein during virus maturation, leading to infectious particles [25, 326]. Interestingly, the amount of Gag polyproteins found in the capsids of mature virus particles was lower than in immature virions, at least for HIV and rous sarcoma virus [25, 26, 33]. It is estimated that mature virus particles are formed by around 1200 to 2000 Gag molecules, whereas the amount of Env is more variable among the different viruses [33, 109].

Retroviruses are further differentiated into simple and complex viruses, depending on the coding sequences that they contain. Simple viruses like most oncoviruses contain *gag*, *pol*, *env* and *pro*. Lentiviruses, like HIV, spumaviruses (FV) and the deltaviruses, like HTLV, are complex viruses that contain coding sequences for additional regulatory proteins [326, 328].

Retrovirus particles infect a wide range of vertebrates and are diverse in the biological manifestations of the diseases they cause. The RNA genome of retroviruses is reversely transcribed into dsDNA and integrated into the host genome, leading in some cases to uncontrolled cell growth and finally to cancer [326]. Autoimmune diseases, acquired immune deficiency syndrome (AIDS), neurological diseases and diseases of bone and joint such as osteopetrosis and arthritis can be the consequences of infection, while other retroviruses, like foamy viruses, do not produce apparent effects [328].

Some retroviruses, like the Human T-lymphotropic virus (HTLV), produce pathogenic affects in only a small percentage of infected people [190]. Although it is claimed that FV has no pathogenic effect, it should be kept in mind that only few infections of human beings have been reported. The deltavirus HTLV causes malignant T-cell lymphoma in around 1 % to 5 % of infected individuals although viral gene expression and replication is poor [176, 190]. This virus can be transmitted through infected blood and from mother to child through breastfeeding. Although sexual transmission is thought to be less efficient, it still plays an important role in infection [176].

The most famous retrovirus is the causative agent of AIDS: the human immunodeficiency virus (HIV). HIV belongs to the genus of lentiviruses which are found worldwide. A report by the Joint United Nations Programme on HIV/AIDS and the World Health Organization estimated that, in the year 2010, around 2.7 million people were newly

infected and around 34 million people are living with HIV at the moment, worldwide [319, 333]. Sadly, this makes HIV the most prominent deadly infection worldwide.

3.2.1 Foamy virus

Foamy viruses (FV) are the oldest known vertebrate RNA-viruses [191]. They were initially described by Enders and Peebles in 1954 who discovered them in monkey kidney cells. They show a foamy cytopathic effect (figure 3.5.B) and thus were named Foamy Virus [82, 157]. In 1971, the primary laboratory strain of "human" foamy virus was isolated from a nasopharyngeal carcinoma tissue culture from a Kenyan patient [1]. The obtained virus is closely related to a virus strain found in a chimpanzee species living in Kenia suggesting a zoonotic infection of the patient through a bite from this chimpanzee species [191].

Foamy virus isolated from humans is now referred to as prototype foamy virus (PFV) indicating that the virus, though isolated from a human being, is not of human origin. Virus isolated from monkeys is called simian foamy virus (SFV). When making general statements I will use the term foamy viruses (FV) which refers to all the different isolates. Otherwise, the terms PFV or SFV are utilized to indicate the host of the virus isolates.

FVs are found in many vertebrates such as cats, cows, horses and in non-human primate species [191, 202]. Monkeys show a high rate of infection [205]. A SFV prevalence of 40 % or higher was found in wild animals whereas animals in captivity showed higher prevalence rates ranging from 80 % to 100 %, probably resulting from close housing [157].

Modes of transmission are thought to be saliva-based and occur through biting and licking [191, 205]. These modes of transmission are strengthened by the following observations: Murray *et al.* found high levels of FV viral RNA in the oral tissue of immunocompetent rhesus macaques [226]. Another examination of baboons in a primate center revealed that almost all adults were infected with SFV. Interestingly, SFV antibodies were detected in around 40 % of juvenile animals prior to sexual maturity. The newborns were routinely removed from the breeding harems and hence, interactions with adult animals were restricted [23, 191]. This emphasizes the contribtuion of saliva-based modes of transmission, although it does not rule out sexual modes of transmission.

Zoonotic infection of humans with FV are rare, but has been reported for people in close contact with primates. An infection arising from a laboratory accident has also been documented [272, 304]. The few humans that tested positive for FV generally reported severe monkey bites earlier in their life [272]. No human-to-human transmission of FV
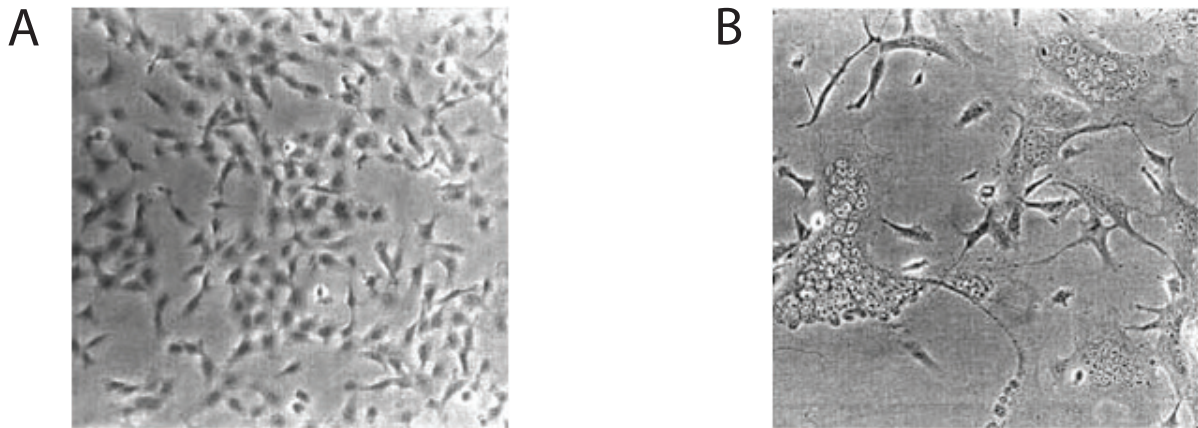
Figure 3.5: *Cell culture images illustrating the foamy cytopathic effect. (A) Cell culture images of non-infected human fibroblasts. (B) Syncytia formation of human fibroblasts upon infection with foamy virus. Images are courtesy of T. Pietschmann.*

has been observed so far, but statistics are poor as only few humans have been infected with FV [131, 191].

3.2.1.1 Pathology

FVs infect a broad range of cells and are highly cytopathic in cell culture. Productively infected cells undergo cell fusion resulting in multinucleated synctia, *id est*, the cells are not separated any more but rather a mass of protoplasm with scattered nuclei. The cytoplasm is highly vacuolating and of foamy-appearance. In some cell lines, no synctium formation or cell death is observed as infection is rather persistent or latent than lytic [191].

Despite their cytopathic effect in cell culture, there is no associated disease known so far. Although association with Grave's disease or multiple sclerosis have been under discussion, it was not confirmed by further studies [205]. Accidentally as well as naturally infected hosts show unapparent, long-term persistence of the infection and low levels of virus replication [191, 202].

A pathogenic potential of FV gene expression could be demonstrated in experiments with transgenic mice when it was targeted to the central nervous system and striated muscle cells (reviewed in [205]).

3.2.1.2 Virus structure

The majority of foamy virus particles contains two copies of the RNA [85] (figure 3.6.A). In contrast to other retroviruses, around 20 % of released foamy virus particles contain double-stranded DNA, which is rather believed to be the infectious form of genome as compared to the RNA genome [72]. The following experiments from Moebes *et al.* and Yu *et al.* led to this conclusion: Moebes *et al.* inhibited reverse transcription. Viral titers were significantly reduced when the inhibitor was added during virus production whereas only a minor effect was oberved when added prior to infection [218]. In addition, Yu *et al.* demonstrated successful virus production in cells after transfection with DNA extracted from PFV particles [346].

The proviral genome has a size of 12 kb to 13 kb and encodes the classical retroviral genes *gag*, *pol* and *env*, and at least two additional genes referred to as *tas* and *bet* [191, 192, 205].
The capsid of PFV is around 65 nm to 70 nm in diameter [222]. Another difference to orthoretroviruses is the immature appearance of the capsid. This immature morphology arises from incompletely cleaved Gag protein. Mature particles do not contain a separate matrix, capsid and nucleocapsid but comprise two Gag cleavage products differing by 3 kDa [192, 205]. The carboxyl terminus of the Gag protein, which contains the positively charged amino acids that are part of the nucleic acid binding domain, is very likely oriented towards the inside of the virus particle [191].
The surrounding envelope is about 100 nm to 140 nm in diameter (figure 3.6) and comprises highly prominent glycoprotein spikes that are between 5 nm to 15 nm in length [72, 202, 267]. Electron microscopy of negatively stained PFV particles revealed a trimeric nature of the surface glycoproteins. Wilk *et al.* could further observe an arrangement of these trimers in hexagonal rings with adjacent hexameric rings sharing two trimers [335].
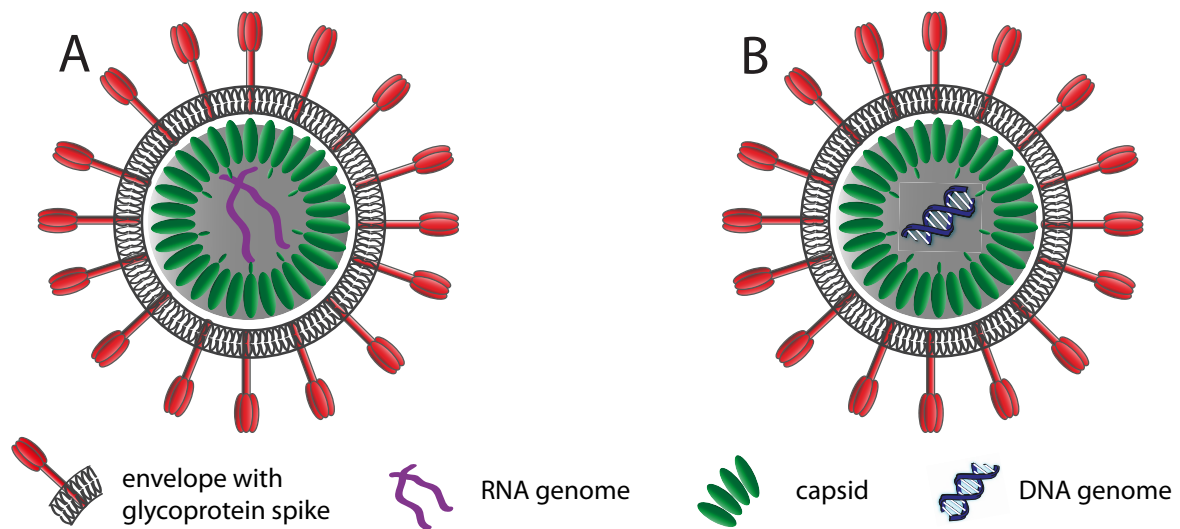
Figure 3.6: *Structure of FV containing the immature capsid out of Gag proteins and a lipid bilayer envelope with prominent glycoprotein spikes. Figure adapted from [189]. (A) Structure of FV containing two ssRNA genomes linked near their 5´ ends [85]. (B) Structure of FV containing a dsDNA genome [267].*

4 Virus entry and replication

The virus replication cycle can be roughly divided into virus entry and virus egress. The focus of this work will be on the entry of enveloped viruses. During early steps of entry, viruses already face their first barrier - the cell membrane. Viruses allow their genetic material to cross this barrier by fusion of the viral envelope with the cellular membrane. During this process, the virus envelope is integrated into the cellular membrane and the capsid - which contains the virus genome - is released into the cytosol. This process may either occur directly at the cell surface or later inside endocytic vesicles. The fusion process is mediated by the interaction of viral glycoproteins with cellular receptors. Besides the obvious criteria that cellular receptors are available, it is believed that other parameters such as virus size, cell type and cell stage are important for definition of the viral entry pathway.

4.1 Endocytic modes of entry

Endocytosis offers several advantages to the virus, such as efficiently transporting it from the cell membrane to the perinuclear area as opposed to inefficient diffusion through the crowded cytoplasm. During "transportation" toward the cell nucleus, the endosomes undergo maturation and the pH inside endosomes decreases. Some viruses make use of this increase in proton concentration within maturing endosomes as a trigger to facilitate virus fusion. However, for entry to be infectious, the virus needs to escape before degradation occurs within the low pH environment.

Viruses exploit the same pathways by which the cell internalizes nutrients and other physiological ligands. Various endocytic mechanisms such as phagocytosis ("cell eating") and pinocytosis ("cell drinking") are known. Pinocytosis is subdivided into macropinocytosis, clathrin- or caveolae-mediated endocytosis and further clathrin- and caveolin-independent mechanisms (figure 4.1). Depending on the endocytosis pathway, differ-

ent cellular factors, such as scission and regulatory factors, are involved that assist the formed vesicles in pinching of the plasma membrane. Almost all known mechanisms involve actin [211].

Large particles can be taken up by *Phagocytosis*. Phagocytosis implicates a major transient reorganization of the plasma membrane and is restricted to a few cell types such as macrophages. This process is strictly particle-driven and depends on dynamin-2 and actin [57, 210, 211].

Macropinocytosis is a transient, usually growth-factor stimulated, actin-mediated process that involves radical, cell-wide plasma membrane ruffling leading to membrane protrusions [211]. These ruffles fuse back upon the plasma membrane thereby forming large, endocytic vesicles, the macropinosomes, reaching up to 10 μm in diameter [156, 211]. Macropinocytosis can take place in almost all cell types [210]. Depending on the cell type, the macropinosomes are either recycled back to the plasma membrane or targeted toward the endosomal system, where they undergo acidification [156, 211]. The whole process does not depend on dynamin [242].

Clathrin-mediated endocytosis (CME) occurs constitutively in all mammalian cells and many distinct viruses utilize it for internalization [57, 211]. Clathrin has a three-legged structure, called triskelion, that consists of three heavy chains. Every heavy chain is associated with a light chain [320, 158]. After formation of clathrin-coated pits and propagation of the clathrin lattice, the coated vesicles are pinched off, transported away from the membrane and the clathrin-coat is removed. This whole cycle happens within one minute. The outside diameter of the clathrin lattice can vary from 60 nm to 200 nm [158].

Caveolae-mediated endocytosis involves lipid rafts and is dynamin-2 dependent [211]. Caveolae are cholesterol-enriched, flask-shaped invaginations in the plasma membrane that contain caveolin-1 and are roughly 50 nm to 70 nm in diameter [241, 242]. Individual caveolae are dynamic and undergo short-range cycles of internalization and fusion, referred to as kiss-and-run, whereas assembly states of several caveolae are static [240]. Simian virus 40 (SV40) is one of the viruses that enter cells via caveolae-mediated endocytosis. Pelkmans *et al.* observed a two-step transport pathway for SV40 from the initial plasma membrane caveolae, via an intermediated organelle - the caveosome, to the endoplasmatic reticulum. The pH-value found in caveosomes is about neutral [243]. More endocytic pathways are known and further exploration of the uptake mechanisms of viruses may lead to the discovery of additional novel pathways.
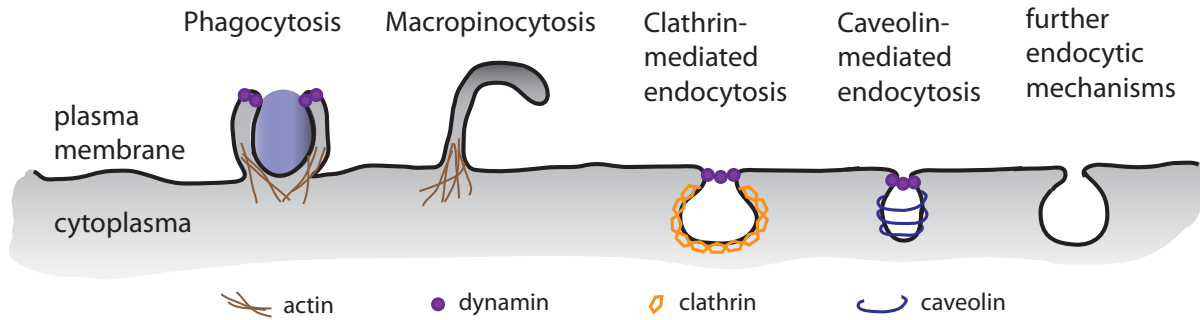
Figure 4.1: *Different endocytic mechanisms. Fluids and small particles are taken up via pinocytic mechanisms such as macropinocytosis, clathrin- or caveolin-mediated endocytosis. Further entry mechanisms are known and may be discovered. Macropinocytosis and phagocytosis involve severe actin rearrangement but other pathways are also actin-dependent. Figure after [57] and [211].*

4.1.1 The endosomal system

After the virus particles have been internalized within primary endocytic vesicles, they are usually fed into the endosomal system, which is responsible for sorting of the cargo for recycling, degradation and trafficking. The main organelles of the endosomal system are the early endosomes (EE), maturing endosomes (ME), late endosomes (LE), lysosomes and recycling endosomes (RE) [211]. Depending on their state of maturation, the endosomes contain different Rab proteins that are often used as a marker to trace the different endosomal classes. EEs contain Rab5, MEs contain Rab5 and Rab7, and LEs Rab7 and Rab9 [211, 255].

Maturation of EEs to LEs is coupled to an increase in proton concentration from around pH 6.5 - 6.0 in EEs, pH 6.0 in MEs, to around pH 6.0 - 5.0 in late endosomes; lysosomes have an acidic pH around 5.0 - 4.5 [136, 208, 211]. Endosomal acidification can most likely be explained by different subunit compositions of the vacuolar ATPase along the endocytic pathway and a net influx of negative charge for electroneutrality by some isoforms of the CLC-family of chloride channels acting as Cl^-/H^+ exchangers [144, 145, 175, 208].

4.2 Virus membrane fusion

In order to replicate, virus have to overcome the cell-membrane barrier to release the capsid in the cytoplasm. Enveloped viruses overcome this barrier by fusion of the viral membrane with the host-cell membrane, either directly at the plasma membrane or after endocytic uptake. Fusion of these two lipid bilayer membranes is thermodynamically favorable but nevertheless, it has a very high kinetic barrier [38, 118]. Viruses contain

one or more proteins on the viral envelope which facilitate the fusion process probably by lowering the activation energy for fusion [37, 98]. A detailed understanding of the fusion process is essential for the development of antiviral strategies [206].

For some viruses, such as influenza virus and HIV-1, the fusion proteins are identified and well characterized [118]. Crystal structures are available of the fusion proteins in their conformation on the viral surface (prior to interaction with the cell, "pre-fusion") and after fusion is completed ("post-fusion"). Based on structural motifs in the post-fusion state, the membrane fusion proteins are divided into three classes [329]. Despite some structural differences, all fusion proteins known so far are trimeric in their fusion-competent state and follow a common mechanism how fusion is mediated between these two lipid bilayer membranes [118, 329]. The generic steps of this so-called "cast-and-fold" mechanism are sketched in figure 4.2. The first step in this model is the interaction of viruses with the host-cell membrane and subsequently, both membranes are brought in close contact (figure 4.2.A-C). In the next step, the hemifusion intermediate is formed by lipid mixing of the contacting leaflets of both lipid bilayers (figure 4.2.D) and hemifusion is classified by lipid mixing without content mixing. The hemifusion stalk proceeds forward to form a small, expanding fusion pore. Fusion is completed when both, proximal and distal leaflets have merged (lipid and content mixing, figure 4.2.E) [38].

In the pre-fusion state (figure 4.2.A), there is no specific interaction between viral fusion proteins and cellular receptors. The two membranes are still separated by about 10 nm to 20 nm due to electrostatic repulsion between the bilayers, hydration force and steric interaction of cellular and viral membrane proteins [37, 171]. The pre-fusion state of most fusion proteins is metastable. Binding of a cellular receptor or viral protein and/or protons in acidic cellular compartments (figure 4.2.B) induces conformational changes in the fusion protein leading to interaction with both membranes and probably destabilization of the membranes [329, 331]. The evidence for such an extended intermediate is only indirect and the life-time may range from seconds to minutes, depending on the type of virus [118].

Subsequently, the two membranes are pulled toward each other (figure 4.2.C), resulting in distortion of the two bilayers [118]. Insertion of the viral protein in the target membrane may lower the distortion energy [118]. The energy necessary for membrane bending and deformation as well as for overcoming the hydration force must be generated during the rearrangement of the viral fusion proteins [118, 329]. If the membranes are pulled close enough together, the contacting bilayer leaflets merge and form a hemifusion stalk (figure 4.2.D) [118]. The energy barrier for hemifusion is approximately $170 \text{ kJ} \cdot \text{mol}^{-1}$ [37, 38, 171]. For some viral fusion proteins, such as HIV gp41, a single fusion protein is in principle sufficient to overcome this energy barrier [118]. Other viruses require several
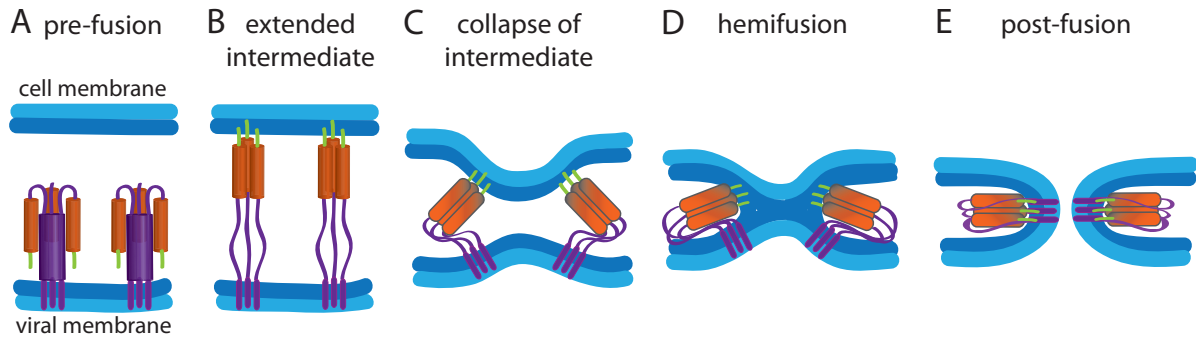
Figure 4.2: *A schematic illustrating the steps in the "cast-and-fold" model of virus fusion with a host-cell membrane. (A) The viral fusion protein, in it's pre-fusion conformation, before ligand binding. (B) Upon ligand binding (cellular or viral proteins and/or protons), the protein opens up and interacts with the cell membrane. There is currently only indirect evidence for this extended intermediate [118]. (C) Collapse of the extended intermediate draws the two membranes toward each other. (D) Hemifusion occurs when the two membranes are pulled in close contact so that the contacting bilayers can merge. (E) Formation of the fusion pore. The small pore may flicker between closed and open states before it expands to complete fusion. Figure after [118].*

fusion proteins, e.g. influenza virus hemagglutinin [118].

In order to complete fusion, the hemifusion stalk opens to form a fusion pore (figure 4.2.E). The small fusion pore can close and reopen (pore flickering) before it expands to form a larger pore [38, 118]. In the case of intracellular fusion events, pore flickering is often referred to as "kiss-and-run" [38]. The transition from a flickering pore to complete fusion is probably the most energy-demanding step [38, 206]. Hence, a greater number of active fusion proteins is required to complete this transition [196, 206]. The transition from the hemifusion stalk to formation of a fusion pore can happen almost instantaneously in some cases, last for a few seconds or even take several minutes, depending on the investigated virus, the cell line and other experimental settings [92, 146, 150, 196, 217]. Generally, the majority of investigated viruses proceeded from hemifusion to complete fusion within one minute [92, 146, 150, 196].

Different approaches have been applied to elucidate the time-scale of the fusion process from simulations to experiments with viruses on supported lipid bilayers as well as in the biological context of live cells. Simulation of lipid membrane fusion yielded a complete fusion process within microseconds [155]. Kyoung et al. investigated fusion of synthetic vesicles with reconstituted synaptic proteins, triggered by the addition of Ca^{2+}. Lipid and content mixing occurred for the majority of vesicles within milliseconds and for a slower minority within a few seconds [173].

Melikyan *et al.* studied the different fusion steps of the retrovirus avian sarcoma and leukosis virus (ASLV). They co-labeled the viral envelope with DiD and palmitylated enhanced YFP (pYFP). Redistribution of DiD in the virus and cell membrane indicated lipid mixing, whereas pYFP was located in the distal leaflet of the viral membrane and could only be transferred after a fusion pore was established [207]. Low pH was used to trigger fusion as fusion of ASLV is pH-dependent [207]. The authors reported that the time from low pH until hemifusion was about 25 s for the majority of particles [207]. For 50 % of the fusion pores formed after hemifusion, they measured a delay of about 10 s to 100 s, indicating that hemifusion is a true and relatively long-lived intermediate of ASLV fusion [207]. The fusion process proceeded through formation of small pores. These pores either enlarged, remained small or even closed [207]. The small pores need to enlarge in order to initiate infection [207]. Similar observations were reported by Jha *et al.*, who investigated ASLV fusion with early endosomes. The average lag time between lipid and content transfer was around one minute [146]. However, they observed differences in the fusion process depending on whether a transmembrane receptor (TVA950) or a lipid-anchored receptor (TVA800) was expressed [146]. Formation of larger and more stable fusion pores was observed in cells expressing the transmembrane receptor TVA950. Fusion was more rapid and efficient in these cells, consistent with a higher infectivity [146]. In contrast, smaller and less stable fusion pores were formed in TVA800 cells. The pores showed transient closing and reopening [146]. Pore flickering was also observed in cells with a lower density of the TVA950 receptor [146].

Markosyan *et al.* investigated fusion of pseudotyped viruses expressing HIV-1 Env. Fusion was triggered upon temperature shift from about 18 °C to 37 °C and lipid mixing occurred about 50 s to 200 s afterwards [196]. The transition from lipid to content mixing ranged between > 0 s to 300 s. Transition was fast in 30 % of the cases and no delay was detectable within their time resolution of 10 s, whereas 70 % of the fusion events were delayed [196]. Furthermore, they reduced the number of fusion-competent Env by addition of a fusion blocking peptide (C34) in various concentrations. Content mixing was more sensitive to C34 than lipid mixing, indicating that more active copies of Env are required for content than for lipid mixing [196]. Differences in the fraction of viruses that exhibited lipid and content mixing were also observed among different cell lines [196]. Interestingly, Miyauchi *et al.* observed that HIV-1 fusion at the plasma membrane did not proceed beyond the lipid mixing stage in the investigated epithelial and lymphoid cells. Lipid mixing at the plasma membrane occurred without an apparent delay when the temperature was increased from 12 °C to 37 °C [217]. In contrast, content mixing took place in endosomes with a lag time of about 14 minutes relative to the increase in temperature [217]. These findings suggest that hemifusion is a long-lived

intermediate in the fusion process of HIV-1.

A relatively long-lived fusion intermediate was also observed in experiments with influenza virus [92]. Floyd *et al.* investigated fusion of influenza virus with supported bilayers. Fusion was triggered by an increase in the pH and lipid mixing happened faster at lower pH values. Below pH 5, the lag time until lipid mixing was about 25 s and increased to around 100 s at pH 5.3 [92]. The decay time of the hemifusion stalk was relatively independent of the pH value [92]. Pore formation occurred within 50 s after hemifusion [92]. Somewhat contradictory results were obtained by Joo *et al.* with lentiviral particles containing the fusion protein of influenza virus. No delay was detected between lipid and content mixing for 85 % of the influenza particles [150]. In the same study, fusion of influenza virus particles was compared to Sindbis virus particles. Hemifusion occurred rapidly for Sindibs virus and took around 30 s for influenza virus after increasing the pH to the optimal fusion value of each virus (pH 5.5 and pH 5.0, respectively) [150]. Pore formation was delayed for Sindbis virus with a lag time of about 3 s to 6 s relative to hemifusion [150]. The authors attributed the discrepancy between their results with influenza virus particles and the relatively long-lived intermediate obtained by Floyd *et al.* to the differences in the applied labeling method [150]. Joo *et al.* incorporated their dye into the inner leaflet of the viral membrane and pore formation was detected upon loss of the fluorescent signal. Floyd *et al.* monitored the pore formation by diffusion of dye into the fluid bilayer support after the fusion pore had opened, which may be kinetically slower [150]. Moreover, the presence and density of receptors and additional cellular factors probably play a role and may contribute to the observed differences as was reported for ASLV and HIV viruses [146, 196, 217].

4.2.1 Virus trafficking

In order to infect the host cell and produce progeny virus particles, release of the viral genome into the cytosol is not sufficient. In order to reach the site of viral replication and assembly, viruses have to cover large distances through the crowded cytoplasm. In the case of enveloped DNA viruses, these distances typically span from the entry site (plasma membrane) to the nucleus for replication. In addition, these distances are covered in the opposite direction during virus egress to allow the exit of viral particles from the cell.

Viruses within cellular vesicles such as endosomes rely on the transport mechanisms of the host cell machinery along the cytoskeleton network. In contrast, virus particles residing in the cytosol can no longer rely on cellular organelles for transport and need to

bind to motor proteins for efficient transport [286]. Indeed, proteins of several viruses have been shown to interact with molecular motors [198, 247, 287, 342].

It becomes clear that there is no single common viral entry pathway. Viruses often rely on several strategies to ensure successful entry into various cell types under different conditions as has been shown for simian virus 40 and influenza virus [64, 265].

In the subsequent two sections, the current state of research regarding the entry mechanism of HSV-1 and FV will be discussed.

4.3 Herpes simplex virus 1

The lifecycle of a virus is a complex multi-step process. It can be roughly divided into (i) attachment and entry of the virus to deliver its DNA genome to the nucleus for replication, followed by (ii) assembly and egress of new progeny virus. For every step of the viral lifecycle, a variety of requirements must be accomplished for successful replication. Different cellular receptors are exploited by the virus for attachment to the cell surface, as well as for mediation of virus entry and fusion with a cellular membrane to overcome the cell membrane barrier.

4.3.1 Attachment and entry

The first step in virus entry involves binding of viruses to the cell surface. An overview about virus attachment and entry is given in figure 4.4. Many viruses make use of heparan sulfate proteoglycans (HSPG) on the plasma membrane for attachment to the cell surface (figure 4.3) [83, 283]. Interactions with these negatively charged polysaccharides are usually electrostatic and not very specific [211]. One should be aware that viruses grown in cultured cells may show a stringent use of proteoglycans [197].
The initial attachment sites for HSV-1 to the cell surface are also heparan sulfate proteoglycans [340]. Several studies in the group of Patricia G. Spear revealed that HSV-1 contains even specific glycoproteins in the viral envelope that mediate binding to HSPGs on the cell surface. The glycoproteins B (gB) and C (gC) can interact independently with heparan sulfate to promote reversible virus binding to the cell surface [133, 134, 280, 340]. In the absence of gC, virus binding and infectivity were reduced [134]. Glycoprotein B can mediate virus binding in gC deficient viruses. Mutant viruses lacking both gC and gB are severely detracted from binding to the cell surface [133]. Glycoprotein C seems to have an higher impact on binding to HSPGs than gB [134, 180]. Cells devoid of heparan sulfate due to mutation or enzymatic digestion showed reduced virus binding and were partially resistant to infection [280, 340]. Pertel *et al.* could show in a cell-cell fusion assay[1] that heparan sulfate was not required for cell-cell fusion [246].
These results imply that although HSPGs play an important role in initial attachment, they are not essential for infection, at least not in cultured cells. Prebinding to heparan sulfate tethers and concentrates the virus on the cell surface, thereby increasing the probability to encounter a less available entry receptor [168, 288]. Virus binding to one

---

[1]In a cell-cell fusion assay, it is investigated whether cells upon expression of viral glycoproteins fuse with nearby cells.

of its entry receptors is crucial for entry to be infectious. The viral glycoproteins and cellular receptors that play a major role in viral entry and fusion will be discussed in the subsequent section.

4.3.1.1 Receptors and viral glycoproteins involved in the fusion process

After initial attachment to the cell surface, viruses can enter cells either directly by fusion with the plasma membrane or via one or several of the endocytosis pathways (figure 4.4 ① and ②-④, respectively). Following endocytosis, the virus also needs to fuse with the cellular membrane to escape from intracellular vesicles and deliver its genome to the nucleus. Each pathway seems to involve the same set of viral glycoproteins for membrane fusion and a gD receptor on the cellular side [232, 233]. An overview on the different entry receptors and the involved viral glycoproteins is given in figure 4.3.

In cell-cell fusion assays, it was shown that the viral glycoproteins gD, gB, gH and gL are required and sufficient to cause cell-cell fusion [246, 317]. The same was observed for HSV-2 [223]. From the cellular side, a gD receptor is required [246].

Known gD receptors for HSV-1 include the herpes virus entry modulator (HVEM), nectin-1 and 3-O-Sulfated heparan sulfate proteoglycan [102, 220, 282]. Each of these receptors is sufficient as receptor for gD and binds gD with affinities in the micromolar range [168, 169, 193, 282, 330]. There is increasing evidence that additional receptors and co-receptors are involved in the fusion process through interaction with gB and perhaps with the heterodimer gH-gL [10, 20, 104, 153, 270].

The first gD receptor to be identified was *HVEM*, also known as HveA (herpesvirus entry modulator A) [220]. HVEM is a member of the tumor necrosis factor (TNF) family and expressed in many different cell types such as T- and B-lymphocytes, other leucocytes, fibroblasts and epithelial cells as well as in human tissues of the lung, liver, kidney and brain [153, 220, 288]. This receptor is a regulator of the immune response that can either lead to co-stimulation of T-cells, which is required for their activation in addition to antigen-specific stimulation, or to inhibition depending upon ligand binding [61, 273]. A second class of receptors comprises the *nectins*, which are members of the immunoglobulin superfamily [102]. Nectin-1 and nectin-2 are broadly expressed in human cell lines like epithelial, endothelial, fibroblastic, neuronal, B- and T-lymphocytic cell lines. They are found in human tissues of the central nervous system, ganglia, skin, thyroid, kidney, lung, prostate and liver [29, 153, 288]. Nectins are cell adhesion molecules found at cadherin-based adherens junctions (that connect neighboring cells), and are anchored to
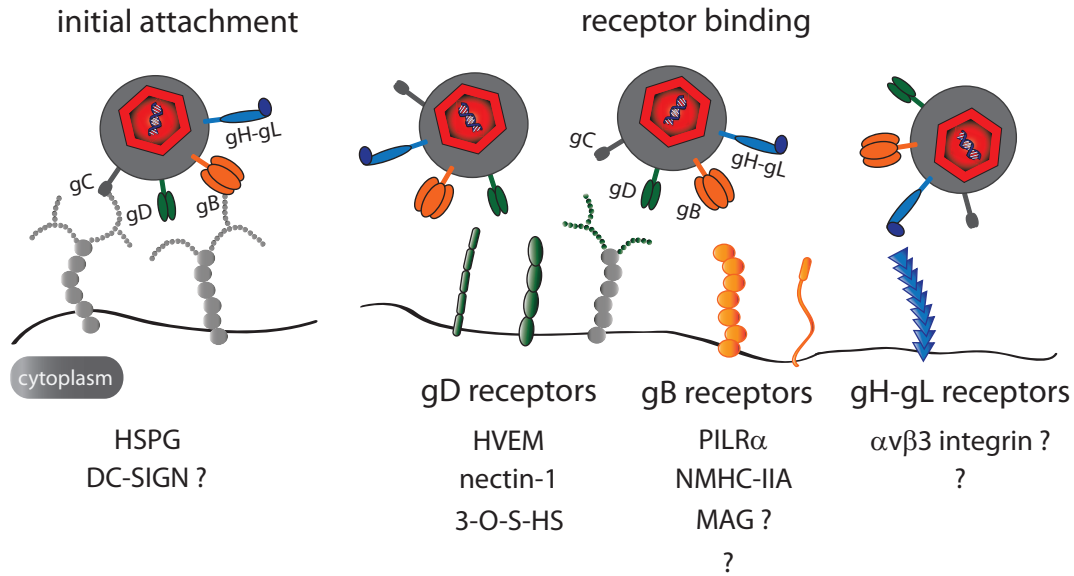
Figure 4.3: *Interaction of HSV-1 glycoproteins with different cellular receptors. Initial attachment to the cell surface occurs through binding of the viral glycoproteins B (gB) and C (gC) to HSPGs. A similar role is suggested for DC-SIGN on certain cell lines. Initial attachment probably increases the chance to encounter a less abundant entry receptor. Known entry receptors for the viral glycoprotein D (gD) are HVEM, nectin-1 and 3-O-HS. Receptors for gB are PILRα and NMHC-IIA. A role of MAG is discussed on some cell lines and there may be further, still unknown receptors involved in virus entry and fusion. The heterodimer gH-gL was found to interact with αvβ3 integrin and may have a potential role as co-receptor.*

the cytoskeleton via the actin-binding protein afadin [306, 307]. Nectin-1 or HveC (earlier also referred to as Prr1) serves as receptor for HSV-1 and HSV-2. Nectin-2 (HveB or Prr2) only serves as receptor for HSV-2 or mutated forms of HSV-1 [102, 254, 309, 327]. Nectin forms homo- or heterodimers which need to be disrupted to allow binding of gD to its receptor [344]. Krummenacher *et al.* could show that soluble forms of gD were able to disrupt already formed cell aggregates and prevented nectin-1 mediated cell aggregation [167]. In a subsequent study, they observed modifications in the localization of nectin-1 at adherens junctions upon infection with HSV-1. Nectin-1 and gD were found to colocalize at the contact areas of infected and non-infected cells, indicating an important role in cell-to-cell spread of the virus [165].

Whether viruses can use a specific receptor for infection depends on the presence as well as accessibility of the receptor. Therefore, it seems likely that nectins are mainly used for infection of neuron cells and in cell-to-cell spread of viruses, whereas HVEM might be present in intact epithelium and could, therefore, be used in primary infection [46, 115, 254, 269, 288].

The third class of gD receptors are *3-O-Sulfated heparan sulfate proteoglycans* (3-O-S HS)

[282]. These are highly sulfated heparan sulfate proteoglycans generated by the enzyme 3-O-Sulfotransferase (3-OST) [153, 282]. 3-OSTs are found in epithelial cells of human, rat and mouse, in neurons and in tissues of the liver, heart, kidney, pancreas and brain [29, 181]. Tiwari *et al.* showed that the presence of soluble 3-O-S HS can induce HSV-1 entry into otherwise resistant Chinese hamster ovary (CHO-K1) cells and, furthermore, induce cell fusion of CHO-K1 cells with cells expressing the viral glycoproteins gB, gD, gH and gL [311]. This receptor probably plays an important role in entry into primary cultures of corneal fibroblasts [310].

Besides the classical gD receptors, co-receptors are thought to be involved during the entry/fusion process, which interact with gB or gH-gL, at least in certain cell lines [10, 20, 104, 153, 270]. A lot of progress has been made in this field over the last few years.

The *paired immunoglobulin-like type 2 receptor* α (PILRα) is one co-receptor that interacts with gB. PILRα is a regulator of the immune system, like HVEM. It has an inhibitory effect and is expressed on monocytes, granulocytes and dendritic cells [270]. Satoh *et al.* could show that the interaction of both glycoproteins, gD and gB with HVEM and PILRα, respectively, are required for infection of human primary cells [270]. Another co-receptor is *non-muscle myosin heavy chain IIA* (NMHC-IIA), a subunit of non-muscle myosin IIA (NM-IIA) which interacts with gB [10]. It is ubiquitously expressed in cells and human tissue [10]. Non-muscle myosin II is an actin-binding protein engaged in processes of cell reshaping and movement like cell adhesion, cell migration and cell division [325]. Arii *et al.* found that the percentage of infected human promyelocytic HL60 cells increased if the cells stably expressed high levels of NMHC-IIA compared to normal HL60 cells. In an additional cell-cell fusion experiment they investigated the role of endogenous NMHC-IIA. Fusion of Vero cells expressing the viral glycoproteins gD, gB, gH and gL with NMHC-IIA knockdown Vero cells was significantly decreased in relation to normal Vero cells. Another interesting observation was the enrichment of NMHC-IIA at the plasma membrane of virus-incubated Vero cells within a few minutes after shifting the temperature from 4 °C to 37 °C, although NMHC-IIA mainly functions in the cytoplasm [10].

The *myelin-associated glycoprotein* (MAG) was shown to associate with gB and the efficiency of infection in MAG-expressing promyelocytes was decreased in the presence of antibodies against MAG [302]. However, MAG is not naturally expressed in epithelial and neuronal cells and its importance as receptor during infection is unclear [153].

The glycoproteins gB and gC were found to interact with *DC-SIGN* on dendritic cells (DC) [70]. Binding was dependent on DC-SIGN and HSPG, suggesting a similar role of

DC-SIGN in initial attachment to the cell surface. Infection of DCs was severely reduced in presence of antibodies against DC-SIGN [70].

It was shown for the heterodimer gH-gL that it binds to $\alpha v\beta 3$ *integrin*, but binding was dispensable for virus entry [58]. As shown by Gianni *et al.*, virus infection and cell-cell fusion could be inhibited by prebinding of soluble forms of gH-gL, and gH-gL binding was independent of $\alpha v\beta 3$ integrin [104].

The protein *B5*, which is ubiquitously expressed on cell lines and in human primary tissue, was also suggested as potential receptor. HSV infection in B5-expressing porcine cells was inhibited by binding of a peptide that contains part of the B5 sequence [245]. However, another study showed a role of B5 in viral protein translation but not during entry [41].

Furthermore, studies with mutated HSV-1, which contained additional binding sequences in gD, were able to use novel virus receptors for entry like the urokinase plasminogen activator, HER2/neu and the interleukin-13 receptor subunit $\alpha 2$ (IL-13Rα2) [151, 209, 352, 353]. This is an important feature for application of the virus as therapeutic gene vector in cancer therapy, as it enables specific targeting of virus particles to cancer cells [27].

4.3.1.2 Mechanism of fusion

For the fusion process to begin, it is thought that binding of gD to one of its receptors leads to conformational changes in gD, which then transmits a signal to gB and the heterodimer gH-gL to initiate the fusion process [32, 153, 170, 253]. Crystal structure of unliganded gD showed that the C-terminus is anchored near the N-terminus and masks the receptor binding sites [170]. Krummenacher *et al.* and Lazear *et al.* found that movement of the C-terminus is required for triggering fusion by implementing intracellular disulfide bonds, thereby lowering the flexibility of the C-terminus in gD [170, 182]. Mutants having insertions or substitutions in their C-terminal region were unable to mediate fusion, even though receptor binding was unaffected [45, 127, 347]. These results strongly suggest that flexibility of the C-terminus of gD plays a crucial role in activating the fusion process, although it is not required for receptor binding. This assumption was further confirmed in experiments with soluble forms of gD or its receptor. Cocchi *et al.* could rescue infectivity of a gD-null HSV mutant by adding soluble forms of gD [45]. Kwon *et al.* and Tiwari *et al.* could trigger infectious HSV-1 entry into resistant CHO-K1 cells by adding soluble forms of the nectin-1 binding domain or 3-O-S HS, respectively [172, 311]. This leads to the conclusion that gD's role in triggering the fusion process upon conformational changes is more important than binding to the cell membrane,

given that other receptors, such as HSPGs, are available [172, 311].

The core fusion machinery consists of the glycoproteins gB and gH-gL which act in concert to mediate virus fusion [58, 253]. How this fusion machinery works in detail is not completely understood up to now. The crystal structure of gB shares similarities with the post-fusion state of vesicular stomatitis virus glycoprotein G (VSV-G), suggesting a role as fusion protein [128, 257]. However, gB alone is not sufficient to promote fusion [13, 58]. Subramanian and Geraghty reported a hemifusion state without involvement of gB by lipid mixing of gD and gH-gL [301]. However, recent cell-cell and virus-cell based hemifusion assays by Jackson and Longnecker revealed that gD and gH-gL alone are not sufficient to induce hemifusion [142]. In addition, the crystal structure of gH-gL shows no similarities with known fusion proteins [43]. Different experiments with insertional mutations in gH or gL indicate that gH-gL plays a role as regulator of the fusion process [86, 141]. Atanasiu *et al.* performed a cell-cell fusion assay using gD receptor positive cells expressing gH and gL together with gD receptor negative cells that express gB. Preincubation of the gH-, gL-expressing cells with soluble gD led to fusion with gB-expressing cells. In contrast, gB-expressing cells were not able to fuse with the gH-, gL-expressing cells after preincubation with gD [12]. These findings suggest a model where binding of gD to its receptor activates the heterodimer gH-gL, which than regulates the fusion activity of gB [12, 30].

4.3.1.3 Factors determining the site of fusion

As described earlier, enveloped viruses either penetrate the cell-membrane by direct fusion with the plasma membrane or via fusion with an endosomal membrane after endocytic uptake (figure 4.4 ① and ⑥-⑦, respectively). Depending on the virus and/or the investigated cell line, intracellular fusion can either occur in a pH-independent way ⑥ or require endosomal acidification to initiate fusion ⑦.
In order to address the issue of endosomal acidification, a lot of studies have been carried out using lysosomotropic agents to inhibit endosomal acidification. The lysosomotropic weak bases ammonium chloride ($NH_4Cl_{aq.}$) and chloroquine serve as proton acceptors and thereby neutralize acidic cellular compartments [96, 232]. Drugs such as bafilomycin A1 (BFLA) block endosomal acidification by inhibition of the vacuolar ATPase [215]. Treatment with energy depletion medium is often used to investigate involvement of endocytic uptake as endocytosis is an energy-dependent process, which is sensitive to inhibitors of ATP synthesis [215]. The endocytic entry of many viruses such as adenovirus, influenza virus or HHV-8, requires cellular kinase activities [233]. Wortmannin is used to inves-

tigate the role of cellular kinase activities during endocytosis as it inhibits PI 3-kinases with high selectivity [323]. It has been reported as an inhibitor of fluid-phase mediated endocytosis and phagocytosis but not receptor-mediated endocytosis [225]. Some studies also use a proteinase protection assay to distinguish between extra- and intracellular virus particles. In these assays, virus incubated cells are treated at different time points with proteinase K, which digests surface-bound glycoproteins. Intracellular viruses are protected from digestion. The ratio of degraded to non-degraded viruses gives evidence how many virus particles have entered the cell via endocytosis [215]. Recombinant β-galactosidase expressing reporter viruses are often used to probe infection of cells by the resulting β-galactosidase activity [4, 44].

For HSV-1, it was believed that fusion at the plasma membrane is the main route of infectious uptake [162, 194]. However, endocytic uptake has also been reported in earlier studies [137] and is required for infection in certain cell lines [28, 44, 215, 251]. In some cell lines, fusion was observed to be pH-dependent [231, 232]. This is an astonishing fact as for fusion exposure to low pH was not required in cell-cell fusion assays [66, 246]. What factors determine whether fusion takes place at the plasma membrane or with an endosomal membrane? The following section gives an overview about observed entry pathways in various cell lines. Experiments with normally non-permissive cell lines are an excellent tool to address the question of pathway determining factors, since the entry pathway of the virus can be directly compared upon expression of e.g. different gD receptors. An overview of herpesvirus entry pathways into cells is given in figure 4.4.

In African green monkey (Vero) cells, fusion at the plasma membrane is the major entry pathway of HSV-1. Koyama *et al.* observed that entry into Vero cells was not dependent on endosomal acidification in experiments with ammonium chloride [162]. Detailed studies by Nicola *et al.* using inhibitors of endosomal acidification showed no significant reduction of infectivity in Vero cells as was measured by β-galactosidase activity [232]. Treatment with wortmannin had no effect on Vero cells [232, 233]. Wittels *et al.* obtained similar results upon inhibition of endosomal acidification or ATP synthesis [337]. A proteinase assay revealed that the HSV-1 glycoproteins were digested, thus they were still present at the cell surface [215]. These results strongly suggest entry via direct fusion at the plasma membrane in Vero cells, which was further confirmed by EM and cryo-EM data [201, 232, 233, 287]. Vero cells express the gD receptor HVEM and nectin-1 [93, 166].
Using cryo electron tomography, Maurer *et al.* observed cytosolic capsids after two min p.i. in Vero cells, rat kangaroo kidney cells (PtK$_2$) and human foreskin fibroblasts (HFF).

Identification of the corresponding fusion sites by dense clusters of glycoproteins spikes and the outer tegument at the plasma membrane suggests entry via direct fusion in these cell lines [201]. Entry via fusion at the plasma membrane has also been reported in human epidermoid cells (HEp2) using EM as well as by inhibition of endosomal acidification and endocytosis [97, 103, 337].

In several cell lines, infectious uptake involves an endocytic pathway. Milne *et al.* investigated the uptake of HSV-1 upon expression of nectin-1 or HVEM in normally non-permissive murine melanoma (B78H1) cells. A proteinase assay showed that protection of the viral glycoproteins from digestion occurred rapidly in B78C10 cells expressing nectin-1, indicating endocytic uptake [215]. In a similar assay using nectin-1 expressing B78C10 cells and HVEM expressing B78A10 cells, protection of gB was measured and protection was independent of the expressed gD receptor [215]. Further experiments revealed that virus entry was energy-dependent but endosomal acidification was not required [215]. Theses results suggest a pH-independent endocytic pathway into gD receptor expressing B78 cells.

Entry into usually non-permissive J-cells expressing nectin-1 or HVEM was not sensitive to inhibition of endosomal acidification [103]. Similar results were obtained in COS and BHK cells as well as in neurons and different neuroblastoma cell lines [103, 231]. The obtained data imply that entry into these cell lines occurs in a pH-independent manner. In contrary, requirement of endosomal acidification for infectious entry was reported for various cell lines including HCjE, HaCaT, primary human keratinocytes, HeLa and RPE cells [4, 231, 233, 251, 312].

Nicola and co-workers investigated the entry mode in HeLa cells by energy depletion and different lysosomotropic agents. Infectivity was measured by β-galactosidase expression. Vero cells were included as control since fusion can occur at the plasma membrane. All agents significantly reduced successful entry in HeLa cells relative to the baseline of Vero cells [232]. Treatment with wortmannin also inhibited infectious uptake in HeLa cells [233]. HeLa cells express the three known gD receptors HVEM, nectin-1 (and nectin-2) as well as 3-O-HS [4, 47, 166].

Comparison of entry kinetics into gD receptor deficient CHO-K1 cells and CHO cells expressing nectin-1 occurred rapidly in both cell lines, half of the internalized viruses were already taken up within ten minutes [233]. Thus, uptake in CHO-K1 cells is not dependent on nectin-1 and presumably leads to degradation of viruses in lysosomes as entry is non-infectious. Infectious entry in CHO nectin-1 cells is achieved by pH-dependent endocytosis [233].
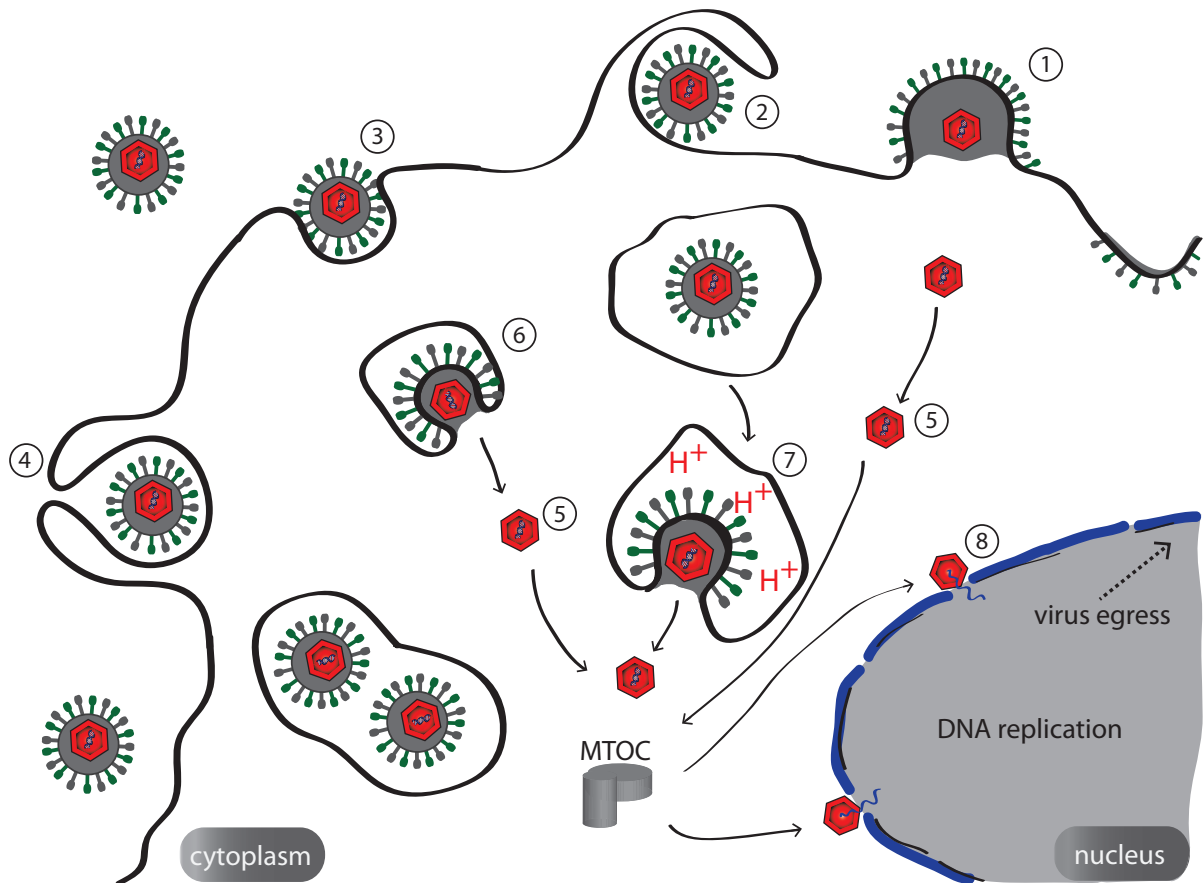
Figure 4.4: *Different pathways of herpesvirus entry. HSV-1 can enter cells either by direct fusion with the plasma membrane ① or via endocytosis pathways ②-④. Endocytic uptake can occur through e.g. macropinocytosis ②, a non further classified endocytic pathway ③, or phagocytosis ④. Following endocytic uptake, virus particles need to fuse with the vesicular membrane in order to release their capsid into the cytoplasm ⑤. Fusion with an endosomal membrane can already occur around neutral pH in some cell lines ⑥, whereas, in other cells, endosomal acidification is required for fusion ⑦. Currently, the pathway determining factors are not well understood. Internalized virus particles and released capsids ⑤-⑦ are transported to the MTOC, from there they move further to the nucleus to release the DNA genome in the nucleoplasm for replication ⑧.*

Further experiments were performed to investigate the role of gD receptor expression in determining the entry pathway. Gianni *et al.* created different nectin-1 expression sites in usually non-permissive J cells using J-nectin-GPI and J-nectin-EGFR1. These new nectin expression sites were located at the plasma membrane and functional uptake of HSV-1 was proven [103]. Treatment with inhibitors of endosomal acidification revealed a pH-dependent entry pathway in these J-nectin-GPI and J-nectin-EGFR1 cells, whereas entry into J-nectin1 or J-HVEM cells was pH-independent [103]. Hence, modification of the expression site of nectin-1 altered the entry pathway.

Using a cell-cell fusion assay, Stiles *et al.* have shown that interaction with gD leads to downregulation of nectin-1 in cell lines where endocytic entry has been reported, such as B78C10 or HeLa cells, but not in Vero cells [295].

Delboy *et al.* found that entry of a synctial HSV strain (ANG path) into CHO-nectin1 cells is pH-dependent, whereas entry into CHO-nectin2 cells occurred preferentially via direct fusion at the plasma membrane [71].

Taken together, the observed cell-type dependency in viral entry indicates that the entry pathway is determined from the cellular side. Acidification seems not to be a pre-condition for the viral glycoproteins to initiate fusion since fusion always involves the same set of glycoproteins from the viral side [232, 233]. The reported experiments from Gianni, Stiles and Delboy support a role of gD receptor expression [71, 103, 295]. However, gD receptor expression alone is not sufficient to explain why there are different entry mechanisms in several nectin-1 expressing cell lines like Vero, HEp2, B78C10, CHO-nectin1 and HeLa [215, 232, 337]. Involvement of further cellular receptors in triggering the entry pathway seems therefore likely.

Indeed, studies of Arii *et al.* using the non-permissive CHO cell line have shown that expression of the gB receptor, PILRα, led to HSV-1 entry via fusion at the plasma membrane and not via pH-dependent endocytosis as observed in CHO-nectin1 cells [11].

Involvement of co-receptor expression in mediating an alternative entry pathway was also reported by Gianni and co-workers. Entry into CHO-nectin1 cells became dependent on cholesterol-rich rafts and dynamin-2, if αvβ3 integrin was expressed in addition. Infection was inhibited by blocking the αvβ3 integrin pathway [105]. Expression of αvβ3 integrin in J-nectin1 cells and 293T cells modified the entry from a neutral pathway to a pH-dependent route, that became also dependent on cholesterol-rich rafts and dynamin-2 [105].

Besides an entry pathway dependent on cholesterol and dynamin-2 [105, 251], involve-

ment of macropinocytosis (figure 4.4 ②) has also been suggested for some cell lines (e.g. HeLa and CHO-nectin1) [231]. Clement *et al.* reported a role of phagocytosis-like uptake ④ in primary human corneal fibroblasts and CHO-nectin1 cells [44]. HSV-1 particles were found to associate with cell membrane protrusions, uptake was actin-dependent and involved RhoA activation [44].

Cheshenko *et al.* suggested an involvement of Ca^{2+} signaling pathways to trigger HSV entry [39, 40]. Cells were incubated with viruses in the cold and then shifted to 37 °C, whereat they observed an increase of calcium in the plasma membrane and a global release of intracellular calcium in CaSki cells. In contrary, the calcium responses were impeded after knock-down of either the initial HSPG-receptors (syndecan-2) or the nectin-1 receptor, indicating that both receptors play a role in triggering Ca^{2+} signaling pathways [40]. So far, HSPGs have been mainly reported as dispensable attachment receptors for the virus to the cell surface [168, 246, 288].

4.3.1.4 Virus transport

In order to reach their site of viral replication, herpesviruses are efficiently transported along microtubules to the microtubule-organizing center (MTOC), usually located in close proximity to the nucleus [163, 195, 287]. Viruses can be transported within endocytic vesicles, or following membrane penetration, by direct interaction with motor proteins. The interaction of several tegument and capsid proteins with the motor proteins dynein, kinesin and the dynein and kinesin-2 cofactor dynactin has been reported [77, 78, 79, 195, 287, 338]. From the MTOC, capsids have to move further to the nucleus and dock to the nuclear pore (figure 4.4 ⑧) [78, 236, 287]. The viral genome is released and translocated in the nucleoplasm for replication [78, 100].

4.3.2 Assembly and egress

The events involved in virus assembly and egress are shown in figure 4.5. After transcription and replication of the viral genome in the nucleus, the DNA is packaged into pre-assembled capsids (procapsids) in the nucleus (figure 4.5 ①, ②) [212, 214]. According to the envelopment – de-envelopment mechanism first observed in EM-studies of a frog herpesvirus by Stackpole [289], HSV maturation can now be best described by an extended envelopment – de-envelopment – re-envelopment model [112, 212, 216, 227, 284, 332]. This model is supported by the observation that primary enveloped viral particles con-

tain a different particle composition than mature virus particles [112, 214, 216].

According to this model, intranuclear capsids ③ bud through the inner leaflet of the nuclear membrane into the perinuclear region ④, thereby acquiring their primary envelope [88, 112]. Fusion of this primary envelope with the outer nuclear membrane results in non-enveloped cytosolic capsids ⑤ [112].

Subsequently, the viral tegument is completed and the viral envelope is acquired by budding into vesicles of the trans-Golgi network (TGN) [212]. Tegumentation occurs around the cytosolic capsid ⑥ and at the future envelopment site ⑦, both subassemblies combine during secondary envelopment ⑧ [213, 214]. Secondary envelopment can also occur in the absence of capsids ⓘ, thereby producing so-called L-particles that consist of the tegument proteins and a functional viral envelope, but lack the nucleocapsid ⓘⓘ [204, 212, 256, 305].

Mature viruses and L-particles enclosed in cellular vesicles (⑨ and ⓘ, respectively) are transported to the plasma membrane and released through exocytosis, a process in which the vesicular membrane fuses with the plasma membrane (⑩ and ⓘⓘ, respectively) [15, 214].

In addition to the glycoproteins gD, gB and gH-gL involved in initial entry of extracellular virus particles, cell-to-cell spread of progeny viruses requires the heterodimer of gE and gI [3, 87, 148].
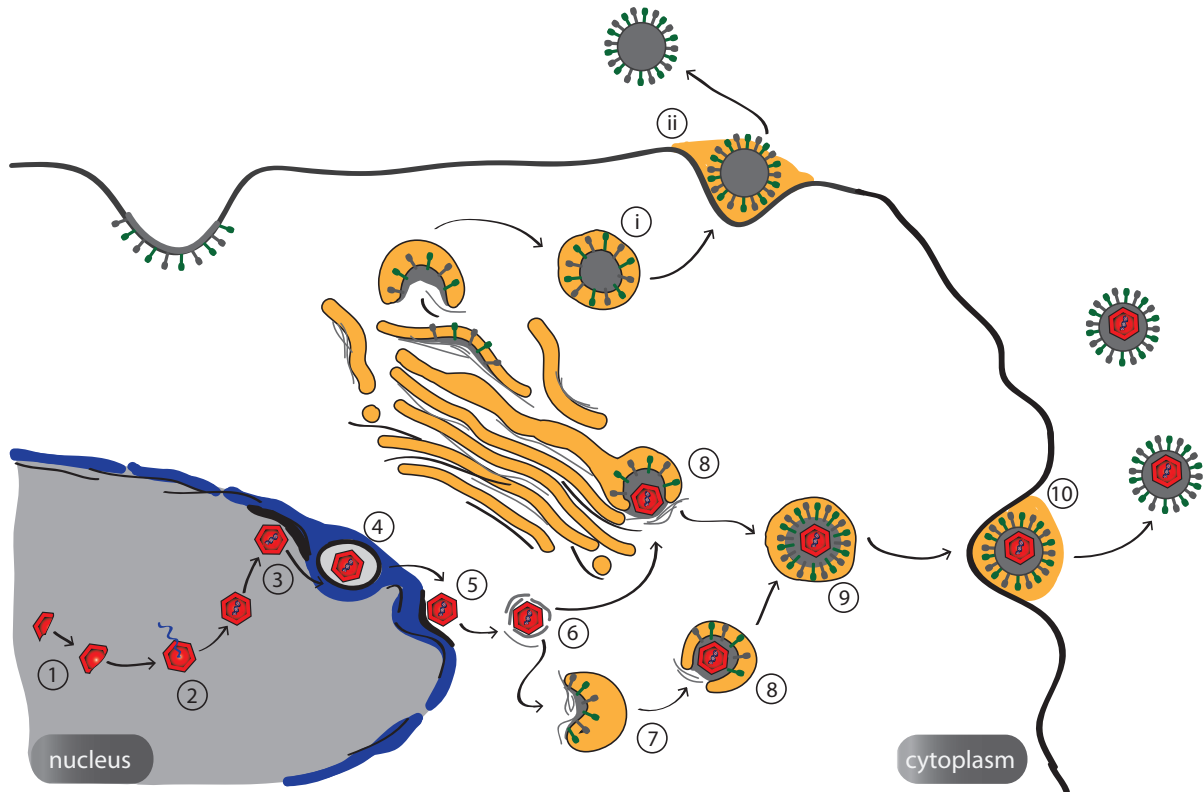
Figure 4.5: *Herpesvirus assembly and egress. Capsids assemble in the nucleus ① and the viral DNA is packaged into these pre-assembled capsids ②. DNA-containing capsids bud through the inner nuclear membrane ③ and acquire their primary envelope ④. Capsids escape from the perinuclear region into the cytoplasm by fusion of their primary envelope with the outer nuclear membrane ⑤. Tegumentation occurs around the cytosolic capsid ⑥ and at the future envelope site ⑦. Both subassemblies combine during secondary envelopment ⑧. Virion containing vesicles are transported to the plasma membrane ⑨, and viral particles are released through fusion of the vesicular membrane with the plasma membrane ⑩. Secondary envelopment can also occur in the absence of capsids (i), and L-particles are released that lack the nucleocapsid (ii). Figure after [214].*

4.4 Foamy virus

Successful virus replication requires several steps. First, viruses need to enter the cell and cross the cell membrane by fusion with the virus envelope. In order to produce new progeny, the viral genome is transcribed, new virus particles are assembled and released from the cell. The replication cycle of foamy viruses is in some features more closely related to hepadnaviruses than to the classical retroviruses, e.g. concerning particle budding during virus egress.

4.4.1 Attachment and entry

A crucial step in the entry process of viruses is binding to cellular receptors, that mediate virus fusion with the cellular membrane. An overview about virus attachment and entry is shown in figure 4.6. The first step in the entry process is usually binding to an initial receptor for attachment, that helps to concentrate the virus on the cell surface and increases the probability to encounter an entry receptor. Initial attachment sites are often ubiquitously expressed cellular receptors, such as proteoglycans. Recently, a role of HSPG in FV entry was reported [229]. Cells lacking HSPGs showed reduced FV transduction but were still permissive [229], suggesting that HSPGs play a role in initial attachment of the virus to the cell surface.

The receptor(s) that is responsible for mediation of foamy virus entry has not yet been identified. The viral receptor(s) seems to be ubiquitous as foamy viruses show a broad cell tropism [72, 191, 205]. Identification of the viral receptor(s) was difficult as no non-susceptible cells were found [191]. Stirnnagel *et al.* succeeded in identifying two cell lines, the zebrafish cell line Pac2 and the human erythroid precursor cell line G1E-ER4, that were resistant to PFV Env-mediated vector transduction. Although they still observed FV Env specific attachment of the virus particle suggesting that both cell lines contain a receptor responsible for virus attachment, no infectious uptake was observed [296].

Only very little is known about the entry mechanism of foamy viruses. It is still unclear whether they are capable of fusion at the plasma membrane and which endocytic mechanisms they usurp for infectious uptake.

Dermott and Samuels investigated the entry of SFV particles into Hep2 cells by electron microscopy. Virus particles where mainly found inside intracellular vesicles suggesting an endocytic entry mechanism [74]. A study of Picard-Maureau *et al.* with FV Env pseudotyped murine leukemia virus (MLV) vectors, where they tested the effect of var-
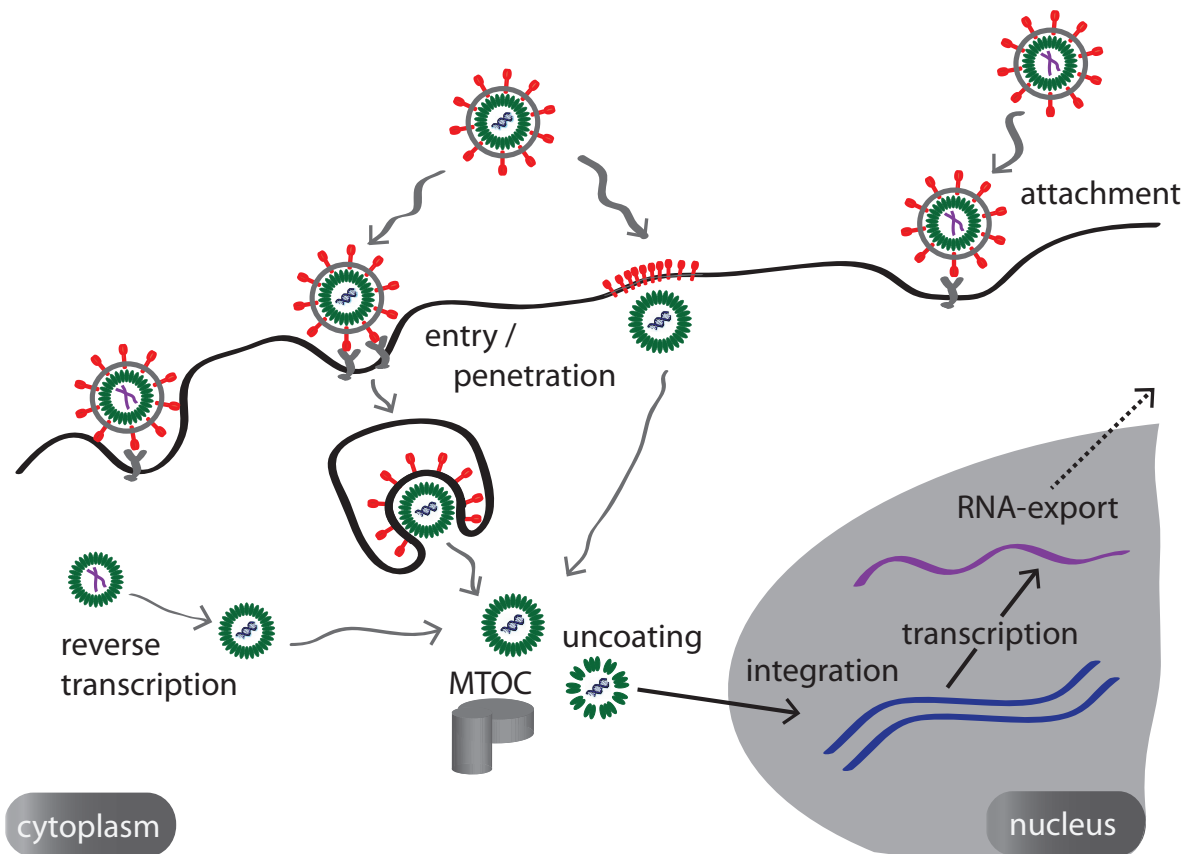
Figure 4.6: *Cell entry of foamy virus. After attachment to a yet unknown receptor(s), the virus may be taken up by fusion at the plasma membrane or via endocytosis. Virus particles containing an RNA genome may be reversely transcribed into DNA [73, 348]. They are transported along microtubules to the MTOC where capsid and genome were found to concentrate [247, 268]. Following virus uncoating, the viral DNA is integrated into the host-cell genome [191]. After transcription of the provirus, the resulting RNA genome is exported and virus particles assemble to form new progeny viruses.*

ious lysosomotropic agents, strongly suggests a pH-dependent entry route of FV. They performed additional control experiments using MLV-A Env and vesicular stomatitis virus G protein (VSV-G) pseudotypes that show a pH-independent and a pH-dependent entry process, respectively. The reduction in infectivity upon exposure to lysosomotropic agents was comparable for the PFV Env MLV pseudotype and the VSV-G pseudotype. The reduction in infectivity was even more prominent when pseudotyping the envelope with glycoproteins from other FV species. However, one inconsistency was observed after treatment with the lysosomotropic agent chloroquine, which resulted in a loss of VSV-G infectivity, but only a slight reduction in the relative infectivity of the FV Env pseudotypes. Additional cell-cell fusion assays with FV Env glycoprotein expressing cells yielded the highest fusion activities around pH 5.5. This was also the case for PFV Env

expressing cells whereas these cells alone already showed a significant fusion activity at neutral pH [248].

As the highest fusion activities were observed at acidic pH, productive FV entry via caveolae-mediated endocytosis (section 4.1) seems not likely. Virus particles within caveosomes do not undergo acidification and the size of foamy virus, with 100 nm to 140 nm in diameter, is larger than the typical size of caveolae, which are about 50 nm - 70 nm in diameter [72, 202, 242, 267]. Virus size and the ability to infect a broad range of cells would favor a clathrin-mediated entry mechanism during infection. PFV share similarities with VSV for which entry through clathrin-coated vesicles was reported [62]. However, the differing effect of chloroquine, which resulted in significant loss of VSV-G but not PFV infectivity, suggests that the entry pathway of PFV deviates to some extend in the investigated cell lines. Furthermore, the fact that PFV already showed significant fusion activity at neutral pH suggests that they are capable of fusing at the plasma membrane as well as already within early endosomes.

After penetration, the virus is transported along microtubules to the microtubule-organizing center (MTOC). Capsid and genome were found to concentrate at the centrosome [247, 268]. The Gag protein itself can target the MTOC through interactions with the cytoplasmic light chain 8 (LC8) of dynein to ensure successful targeting of capsid and genome [247]. This is crucial for virus particles that have already fused at the plasma membrane or for those that have escaped from endosomes. LC8 also interacts with the actin based motor myosin V, therefore likely facilitating transfer from the plasma membrane (rich in actin) to the microtubule network [19, 110].

At the MTOC, viral uncoating takes place in order to release the viral genome (figure 4.6). Lehmann-Che *et al.* observed a cell cycle dependence of virus uncoating in primary fibroblasts and peripheral T-cells [186]. Cleavage of the Gag proteins by the viral protease is required for infection [185]. In contrast to orthoretroviruses, the cleavage happens early during infection rather then later during assembly [191]. Subsequently (after virus uncoating) the viral DNA is integrated into the host genome [191].

4.4.2 Assembly and egress

The FV Gag protein contains a cytoplasmic targeting and retention signal (CTRS). This CTRS is essential for assembly as FV Gag does not have a myristylation signal that would allow an alternative targeting for assembly e.g. to the plasma membrane [191]. The assembly process of FV takes place in the cytoplasm similar to the assembly

pathway of betaretroviruses (B/D type retroviruses). Yu *et al.* have shown that PFV Gag proteins assemble near a pericentriolar site in the cytoplasm [345].

Similar to hepadnaviruses, reverse transcription is a late event that takes place before the virus is released from infected cells [218]. Therefore a considerable extent of the released virus particles contains infectious viral DNA [218, 346]. This viral DNA can also be re-integrated in the infected host-cell, a process called retrotransposition. Heinkelein *et al.* showed that the intracellular retrotransposition of FV DNA was increased if particle release was hampered by co-expression of mutated Env [125]. More recent experiments from Delelis *et al.* and Zamborlini *et al.* suggest that FVs are also able to undergo an early reverse transcription process in agreement with their retroviral counterparts [73, 348]. Consequently, the viral RNA genome as well as the DNA genome might both be infectious [348].

An important feature during assembly and egress is that particle budding and release requires expression of Gag and Env. In the absence of Env glycoproteins, PFV particles are assembled but only rarely detected in the cell culture supernatant [16, 90]. This clearly distinguishes FVs from orthoretroviruses that only require Gag for production of virus-like particles [72]. In contrast, Shaw *et al.* could demonstrate that the FV Env alone is sufficient for particle budding [278]. Concerning these features, FVs share more similarities with hepadnaviruses than with orthoretroviruses [16, 192].

FV Env contains an endoplasmatic reticulum (ER) retrieval signal suggesting a preference for intracytoplasmical budding cites [107, 108]. However, budding was found to occur from intracellular membranes as well as through the plasma membrane [107]. Experiments with mutant viruses missing the ER retrieval signal led to relative increase of viral budding from the plasma membrane, but had neither an effect on the amount of extracellular particles nor alter infectious viral titers [107]. Whether the ER retrieval signal plays an important role in virus assembly is therefore questionable. Yu *et al.* could not detect FV Gag at the ER whereas Gag and Env were found to colocalize at the trans-Golgi network (TGN) suggesting the TGN as site for interaction of Gag and Env [345].

5 Materials and methods

5.1 Sample preparation

All virus particles used throughout this thesis were tagged with fluorescent proteins to allow fluorescent imaging. Virus preparations were done by our collaborators and safety was provided by them. In the case of HSV-1, the viruses were provided by the group of Prof. Dr. Beate Sodeik, Hannover Medical School, Institute of Virology. Foamy virus particles were provided by the group of Prof. Dr. Dirk Lindemann, Technische Universität Dresden, Institute of Virology.

5.1.1 Herpes simplex virus 1 particles (HSV-1)

For experiments on HSV-1, virus particles were tagged with two different fluorescent proteins, namely GFP and RFP/mCherry. An overview on the different virus preparations is given in table 5.1. In general, the viruses have GFP fused to the C-terminus of the envelope glycoprotein D (gDGFP) and RFP N-terminally fused to the capsid protein VP26 (RFPVP26) [227]. A second type of dc virus particles was constructed, where the GFP was attached to the outer tegument protein VP11/12 (VP11/12GFP), sometimes also referred to as pUL46 [350]. In this case, GFP is either C-terminally fused to VP11/12 or inserted into a H*in*dIII restriction site near the C-terminus, as described in [336]. The RFP-tag at the capsid protein VP26 was replaced by mCherry.

Table 5.1: *Overview of received dual-color virus preparations from our cooperation partners in Hannover. The first row indicates an acronym, which was used in this work to assign the different virus preparations. The two virus strains HSV1(17*)bblueLox and HSV(17*)Lox are given in addition. The two virus strains HSV1(17*)blueLox and HSV(17*)Lox were generated with a bacterial artificial chromosome [227]. In HSV1(17*)blueLox, but not HSV1(17*)Lox, the gene encoding for the viral thymidine kinase is lost. Wild-type HSV-1 refers to the recombinant virus without insertion of a gene encoding for a fluorescent protein. Virus preparations were done by KD – Katinka Döhner, CN – Claus-Henning Nagel, JJ – Jessica Janus, TK – Thalea Koithan, KG – Katharina Goris, MC – Michela Cappucci.*

label of virus prep.	denotation of received virus preparations	ratio of dcHSV : wtHSV	date, person of virus prep	viral titer [pfu/mL]
Pdc 1	HSV(17*)blueLox RFPVP26-gDGFP	1 : 0	25.04.2006, KD	$3.4 \cdot 10^7$
Pdc 2	HSV(17*)blueLox RFPVP26-gDGFP	1 : 0	06.11.2006, CN	$3.3 \cdot 10^7$
Pdc 3	HSV(17*)blueLox RFPVP26-gDGFP	1 : 0	17.12.2007, CN	$1.8 \cdot 10^6$
Psp.dc 1	HSV(17*)blueLox RFPVP26-gDGFP; HSV(17*)blueLox	8 : 2	03.04.2009, JJ/KD	$1.7 \cdot 10^7$
Psp.dc 2	HSV(17*)blueLox RFPVP26-gDGFP; HSV(17*)blueLox	8 : 2	18.09.2009, JJ	$5.4 \cdot 10^6$
Psp.dc 3	dc RFPVP26-gDGFP; HSV(17+)Lox	8 : 2	02.07.2010, TK	$5.4 \cdot 10^7$
Pteg.dc 1	HSV(17+)Lox mCherryVP26-UL46GFP	1 : 0	21.01.2011, KG	$3.2 \cdot 10^8$
Pteg.sp.dc 2	HSV(17+)Lox mCherryVP26-VP11/12mGFP; HSV(17+)Lox	8 : 2	30.04.2010, MC	$5.1 \cdot 10^8$

Incorporation of fluorescent proteins in viruses generally diminishes the infectivity of obtained virus particles. Therefore, some virus preparation were spiked with 20 % of recombinant wild-type virus to rescue viral titers. The obtained titer in plaque forming units per mL is given in the last row of table 5.1. Highest viral titers were observed for virus preparations with GFP fused to the outer tegument protein VP11/12.

5.1.2 Foamy virus particles (FV)

Foamy virus particles used in this work were fluorescently tagged at the capsid and the viral envelope. These double-tagged virus particles were generated by our cooperation partners using a replication-deficient 4-component vector system (Gag, Env, Pol, and genomic RNA). Gag proteins were C-terminally tagged with eGFP (Gag-eGFP) and viral envelope proteins were N-terminally tagged with mCherry (Env Ch).
The viral envelope proteins were generated with different fusion competent wild-type proteins of PFV Env (PE) or SFVmac Env (SE) and fusion incompetent variants (PE iCS, SE iCS). These iCS variants possess no significant fusion activity through inactivation of the furin cleavage site between SU and TM domains. Viral particles with different envelope proteins and Gag composition were generated by co-transfection of PFV or SFVmac Env expression vectors with packaging vectors encoding untagged PFV Gag, Gag-eGFP or Gag : Gag-eGFP at a ratio of 3:1.

Adding a fluorescent tag to the viral Gag protein reduced infectivity, but infectivity of the virus particles could be restored to almost wild-type levels by co-transfection of untagged PFV wild-type Gag with PFV Gag-eGFP at a ratio of 3 : 1, as can be seen in figure 5.1 (bars 1, 5, 9) [296]. Particles containing an mCherry-tag at the viral envelope (PE Ch and SE Ch) showed only marginal reduction in relative infectivity (figure 5.1 bars 1, 3 and 14, 16 for particles with untagged Gag)(Stirnnagel *et al.*, manuscript in preparation). Therefore, it was not necessary to spike with untagged Env proteins. In agreement with single-tagged particles, the infectivity of double-tagged PE Ch particles composed of Gag-eGFP and Ch-Env could be increased to almost wild-type levels by spiking with Gag : Gag-eGFP at a ratio of 3 : 1. Viral titers of double-tagged SFVmac Env could be increased to 40 % of wild-type infectivity. Transfection of cells with plasmids from the fusion deficient PE Ch iCS and SE Ch iCS variants showed a 1,000 to 5,000-fold reduction in infectivity (figure 5.1, bars 4 and 17). A more detailed characterization of the generated viral particles can be found in [296], Stirnnagel *et al.* (manuscript in preparation).

An overview on the virus preparations obtained from our collaboration partner is given
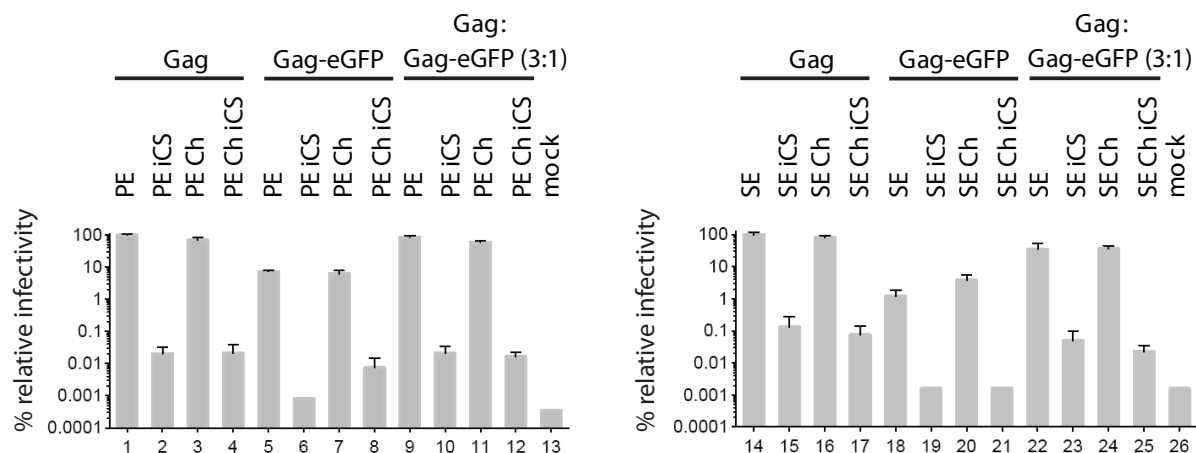
Figure 5.1: *Infectivity of virus particles relative to the corresponding wild-type virus. The infectivity values of the wild-type virus (bars 1, 14) were set to 100 %. HT1080 cells were infected with PFV env (bars 1-13) or SFVmac (bars 14-26) and the relative infectivity of the harvested cell culture suspernatant was determined by FACS analysis. Different Gag compositions of the capsid were analyzed: bars 1-4 and 14-17 show virus particls with untagged Gag, bars 5-8 and 18-21 show virus particles with tagged Gag-eGFP, and bars 9-12 and 22-25 are spiked virus particles with a ratio of Gag to Gag-eGFP of 3:1. The different envelope proteins are indicated as the following: PE or SE are envelope proteins driven from PFV or SFVmac, iCS indicates the fusion incompetent variants and the abbreviation Ch indicates the mCherry-tag. Cells transfected with an empty vector serve as negative control (bars 13, 26). Mean values and standard deviation were calculated from titration of the cell culture supernatant. Figure adapted from Stirnnagel et al. (manuscript in preparation)*

in table 5.2. All virus preparations contained 100 % Ch-Env and PFV Gag : Gag-eGFP at a ratio of 3 : 1, besides the first virus preparation (PFV P1), which contained 100 % Gag-eGFP. The first two virus preparations (P1, P6) were purified via ultracentrifugation, whereas the other preparations were purified via Pierce protein concentrators.

5.1.3 Cell culture

HeLa and Vero cells were grown in an incubator at 37 °C in a 5 % CO_2–atmosphere. Cell culture media (DMEM, DMEM/F12) were supplemented with 10 % fetal bovine serum (FBS). Media and supplement were purchased from Invitrogen GmbH/Life Technologies (Carlsbad, California, USA). Vero cells were provided by the group of Dr. Kay Grünewald, University of Oxford, Nuffield department of Clinical Medicine. Cells were seeded in chamber slides at a density of $2.0 \cdot 10^4$ cells/well or at a density

Table 5.2: *Different foamy virus preparations provided by our cooperation partners from Dresden.*

label of virus preparation	viral envelope protein	amount of PFV Gag : Gag eGFP	purification method
PFV P 1	PE Ch	0 : 1	ultracentrifugation
PFV P 6	PE Ch	3 : 1	ultracentrifugation
PFV P10	PE Ch	3 : 1	Pierce
PFV P11	PE Ch iCS	3 : 1	Pierce
SFV P12	SE Ch	3 : 1	Pierce

of $1.0 \cdot 10^4$ cells/well 24 hours or 48 hours before the experiment, respectively. For the experiments on HSV-1, sterile μ–slides from ibidi were taken that are already tissue culture treated (μ–slide 8 well with ibiTreat, ibidi, Martinsried, Germany). The surface of these μ–slides is physically modified for improved cell adhesion (ibiTreat). Sterile Lab-Tek cell chambers (8 chambers, VWR, Ismaning, Germany) were taken for all other experiments. The Lab-Tek chambers were incubated with collagen A-solution (Biochrom AG, Berlin, Deutschland) according to the manufacturer's protocol, prior to seeding of the cells. Prior to the measurement, media in the camber-slides was replaced with CO_2–independent media (Invitrogen GmbH/Life Technologies, Carlsbad, California, USA) supplemented with 0.2 % w/v BSA (bovine serum albumin, PAA Laboratories GmbH, Cölbe, Germany) or Leibovitz's L15 medium (Invitrogen GmbH/Life Technologies, Carlsbad, California, USA) containing 10 % FBS.

5.1.4 Live-cell imaging conditions

In order to do fluorescence imaging experiments of viral particles in live cells, the cells were incubated previously with virus particles at lower temperatures around 4 °C to 10 °C to ensure virus binding to the cell surface. This way, the uptake of virus particles can be synchronized by an increase in the temperature to 37 °C, a temperature allowing virus uptake. Additionally, some experiments were performed using different markers of cellular compartments. An overview of the protocols for the different conditions are given in the following subsections.

5.1.4.1 Virus incubation in the cold

Since the virus uptake is slowed down considerably at lower temperatures, virus binding was carried out at reduced temperatures. This is a useful tool to synchronize the entry of virus particles into cells, as it allows virus binding to cells without being taken up. The protocol was adapted from [129] and [287]. However, low temperatures are not physiological and can lead to depolymerization of actin microfilaments and microtubules. The rearrangement of the cytoskeleton is visible as cells become smaller after only few minutes of incubation at low temperatures. After increase of the temperature to 37 °C, the cells spread again. Preincubation at low temperatures may lead to differences in the entry pathway of viruses relative to the direct addition of virus particles at 37 °C, the biologically more relevant condition. However, fusion is a rare event, which was seldom observed in real-time. The probability to detect fusion can be increased by a preincubation step in the cold as it increases the amount of surface-bound particles and helps to synchronize the uptake. However, the incubation time in the cold should be short.
Cells were pre-cooled at temperatures around 4 °C to 10 °C for eight minutes, then the virus particles were added and allowed to bind to the cells for another 10 - 15 minutes in the cold. Virus incubation was followed by three washing steps on ice to remove unbound virus particles. Incubation time in the cold was kept as short as possible (< 30 minutes).

5.1.4.2 Markers of endosomal compartments

To look for HSV-1 fusion in live cells, the endosomal compartments were labeled with fluid phase marker. For this purpose, HeLa cells were incubated with 32 μg per well fluid phase marker dextran Alexa Flour 647 for four hours at 37 °C (dextran, Alexa Fluor 647, 10 000 MW, Invitrogen GmbH/Life Technologies, Carlsbad, California, USA). Depending on the experiment, either LysoTracker Red or dual-color virus particles were added during the last or last two hours of incubation and subsequently cells were washed four times (LysoTracker Red DND-99, Invitrogen GmbH/Life Technologies, Carlsbad, California, USA).

5.1.5 Fixation and permeabilization

To analyze the pH-sensitivity of the fluorescence intensity of dual-color viruses, the virus particles were fixed and permeabilized. Experiments, evaluating the amount of HSV-1

fusion in cells were also performed in fixed and permeabilized cells after different time-periods of virus incubation.

Cells incubated with virus or samples containing only virus particles were fixed in 3 % paraformaldehyde (PFA) solution in D-PBS for 20 minutes at room temperature (PFA, 16 % w/v aqueous solution, EM grade, Electron Microscopy Sciences, Hatfield, PA, USA; D-PBS, Invitrogen GmbH/Life Technologies, Carlsbad, California, USA). Afterwards samples were washed three times with PBS.

In some cases, fixation was followed by permeabilization. Permeabilization was used to avoid low pH environment in cellular compartments or to make fluorescent proteins inside the viral envelope accessible for protons prior to pH-quenching experiments. Therefore samples were incubated for exact five minutes with 0.1 % Triton X-100 solution in PBS (Triton X-100, Sigma-Aldrich Chemie GmbH, Taufkirchen, Germany), followed by several washing steps with PBS. The freshly prepared samples were then measured in PBS.

5.1.5.1 Screening for optimization of the dual-color virus preparation

Fixed samples of dual-colored HSV-1 particles were obtained from the group of Prof. Dr. Beate Sodeik, Hannover. In order to find the best preparation conditions, the supernatant of infected cells was analyzed with respect to particle number and colocalization percentage. Samples were prepared by Dr. Jessica Janus. A short summary of Jessica's protocol is given hereafter. A more detailed description of the sample preparation can be found in Jessica's thesis [143].

Four different cell lines: Vero, BHK, HEp-2 and HeLa CNX cells were infected with different amounts of the dual-color strain HSV-1(17*)blueLox-RFPVP26-gDGFP and the wild-type strain HSV-1(17*)blueLox. In order to rescue viral titers, dual-color viruses were spiked with wild-type virus. Five different infection conditions containing 100 %, 80 %, 50 %, 20 % and 0 % dual-color and respectively 0 %, 20 %, 50 %, 80 % and 100 % wild-type virus were tested.

Cells were seeded in 6 well plates and infected with virus 12 hours later. Supernatants were taken every four hours from 12 hours to 44 hours post binding. Supernatant at zero hour post binding was taken as control. Obtained supernatants were spotted on diagnostic object plates with a volume of 20 μL per spot. After further incubation steps, samples were fixed with 3 % PFA for 20 minutes, embedded in Mowiol supplemented with 100 mg/mL DABCO and sealed with a coverslip on top of each diagnostic object plate.

5.1.5.2 Samples of fixed Vero and HeLa cells for colocalization analysis

To determine the amount of HSV-1 fusion in Vero and HeLa cells, samples of virus-incubated cells were fixed and permeabilized after different time-periods. The samples for this experiment were obtained from the group of Prof. Dr. Beate Sodeik, Hannover, and prepared by Dr. Katinka Döhner using the dc viruses from the preparation Psp.dc 3 (table 5.1). A short summary of Katinka's protocol is given below.

HeLa and Vero cells were pre-cooled for 10 - 15 minutes on ice; virus binding was carried out for two hours on ice before washing three times with cold medium. Virus incubated cells were shifted to 37 °C for different time-periods ranging from zero minutes to 3.5 hours. Afterwards, cells were washed with cold medium and samples were fixed at room temperature with 3 % PFA in PBS for 20 minutes, followed by permeabilization with 0.1 % Triton X-100 for five minutes. Samples were washed three times with PBS and embedded in Mowiol supplemented with 100 mg/mL DABCO on a cover slide. The coverslips were sealed with clear finger nailpolish on the next day.

5.1.6 Quenching of virus particles at low pH

Quenching experiments were performed to investigate the pH-sensitivity of fluorescent proteins in the viral context. Virus particles were spotted on a chamber-slide and analyzed with and without a previous permeabilization step. Citrate buffer (50 mM, 260 μL) at different pH values was added to a chamber-slide, containing 150 μL D-PBS with a pH around 7.0.

5.2 Experimental setup in details

For the analysis of virus entry into cells, two different experimental setups were used. A wide-field microscope, enabling experiments with a higher time resolution and a spinning-disk confocal microscope, having the advantage of a higher spatial resolution.

The majority of experiments was based on the detection of the fluorescent proteins GFP and RFP or mCherry. Experiments with virus particles containing for instance a GFP-tag at the capsid and an mCherry-tag at the envelope allow to detect virus fusion with a host-cell membrane by the separation of the capsid and envelope signals. For the experiments, one has to consider that there can be cross-talk from GFP into the red spectral channel after 488 nm excitation. Additionally, there can be direct excitation of
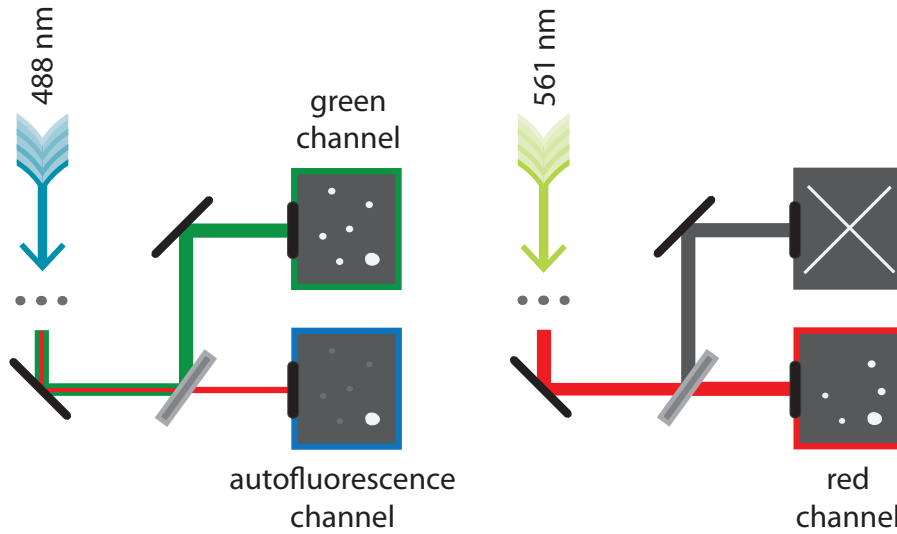
Figure 5.2: *Resulting channels after alternating-laser excitation (ALEX). Namely the green channel after 488 nm excitation (GFP), the red channel after 561 nm excitation (RFP/mCherry) and the autofluorescence channel, which is the red channel after 488 nm excitation. Autofluorescent cellular structures are characterized by a broad excitation and emission spectra and can be detected after 488 nm excitation in the green and red spectral channels, as well as in the red spectral channel after 561 nm excitation (the agglomerate showing up in all three channels). ALEX allows to identify the autofluorescence signal in the additional autofluorescence channel. This is especially important for colocalization analysis of green and red signals as otherwise the large autofluorscent agglomerate detected in all three channels would yield a false-positive colocalization result.*

RFP or mCherry at this wavelength. Furthermore, for imaging with cells, one has to keep in mind that the cell itself possesses autofluorescent structures, which are usually more prominent at shorter excitation wavelengths. Autofluorescence is characterized by a broad excitation and emission spectra and can be detected after 488 nm excitation in the green spectral (GFP) and red spectral (autofluorescence) channels, as well as in the red spectral channel (RFP/mCherry) after 561 nm excitation.

In order to account for spectral cross-talk and direct excitation as well as to identify autofluorescent structures properly, alternating-laser excitation (ALEX) was used [152, 266]. A scheme of the recorded channels after ALEX is shown in figure 5.2. For analysis, the green spectral channel, the red spectral channel and the so-called autofluorescence channel, which is the red spectral channel after 488 nm excitation, are considered. However, ALEX comes at cost of time resolution. Depending on the purpose of the experiment, time resolution may be essential and one would use simultaneous excitation. In this case, one needs to ensure that, at the chosen acquisition conditions such as filter settings and laser power, neither autofluorescent cellular structures, spectral cross-talk or direct

excitation are disturbing issues.

5.2.1 Wide-field microscopy

The wide-field microscope used in this work was a home-built setup, previously designed and built by Dr. Sergey Ivanchenko to allow a combination of wide-field (WF) and total internal reflection fluorescence (TIRF) microscopy. A detailed description can be found in the supporting material of Ivanchenko *et al.* [139]. For the capabilities necessary we had to upgrade the system to a Nikon Ti corpus with perfect focus system. Furthermore, an additional camera was implemented in the detection part to allow correction for chromatic aberration as now the two different channels can be detected on two separate cameras, having the additional advantage of a larger field of view. A schematic diagram of the actual setup is shown in figure 5.3.

Four different lasers for excitation were available: a 405 nm diode laser for photoconversion (PhoxX 405-120, Omicron-Laserage, Rodgau, Germany), a 488 nm frequency doubled diode laser for GFP excitation (Picarro Cyan Laser, Picarro, Sunnyvale, California, USA), a 561 nm diode pumped solid state laser for the excitation of RFP/mCherry (Crystal Laser, Reno, Nevada, USA) and a 642 nm diode laser for excitation of Alexa647 (PhoxX 642, Omicron-Laserage, Rodgau, Germany). Selection of excitation wavelength and laser power was achieved using an acousto-optic tunable filter (AOTF, AA Opto-Electronic Company sa, Orsay Cedex, France) coupled into a multi-mode fiber (AMS Technologies, Martinsried, Germany). The fiber was shaken during the experiments to eliminate speckles and ensure homogeneous sample illumination.

The fibre output was split into two different excitation pathways for WF and TIRF illumination mode by a polarizing beamsplitter (Newport Corporation, Irvine, California, USA), allowing alternating excitation between these two modes due to switching of two electronic synchronized shutters (Uniblitz VS14S2ZM0 (WF) and VS14S2S0 (TIRF), Vincent Associates, Rochester, New York, USA). In wide-field mode, the laser beam was focused on the back focal plane of the objective, resulting in parallel light for sample illumination. In the TIRF path, the excitation beam was focused onto the edge of the back focal plane of the objective so that the angle of incidence for illuminating the sample is larger than the critical angle for the coverslip/medium interface. This two paths were reunited by a second polarizing beamsplitter (Newport Corporation, Irvine, California, USA) before being fed into the microscope. The excitation beam was reflected into the objective by either a Z488/568rdc (Chroma Technology Corporation, Vermont, USA) or
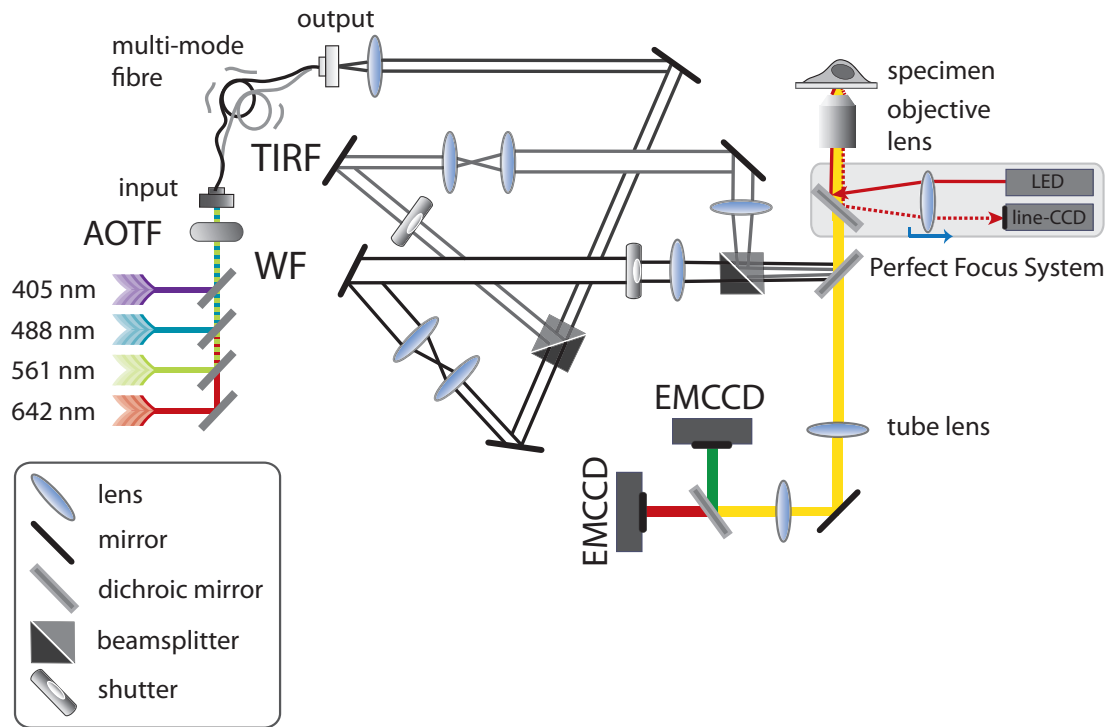
Figure 5.3: *Schematic of the wide-field microscope based on a Nikon Ti corpus. The excitation mode can be alternated between WF and TIRF by using two shutters. The fluorescence is divided into two beams and each channel is detected on a separate EMCCD camera, allowing to correct for chromatic aberration.*

a FF416/500/582/657-Di01 dichroic mirror (Semrock, Rochester, New York, USA). Depending on the desired magnification, different oil immersion objectives were used: either a 100X or 60X Apo TIRF with a NA of 1.49 or a 40X Plan Fluor with a NA of 1.30 (all from Nikon Corporation, Tokyo, Japan).

The Nikon eclipse T*i* base (Nikon Corporation, Tokyo, Japan) with integrated perfect focus system is equipped with a motorized xy-stage (LUDL Electronic, Hawthorne, New York, USA) and a heating table (PeCon GmbH, Erbach, Germany). To ensure ambient temperature around 37 °C for live-cell imaging experiments and in order to avoid drift caused by a large temperature gradient, the heating table was covered with a lid (non heated) and the objective itself was heated with a heating ring (PeCon GmbH, Erbach, Germany).

Fluorescence was collected via the same objective that was used to excite the specimen and transmitted through the same dichroic mirror to separate the emitted light from the laser light. The detection pathway consisted of a Q565LP dichroic mirror (Chroma Tech-

nology Corporation, Vermont, USA) to split the emitted light into a lower and higher wavelength spectral channel. The channel suited for detection of red dyes was equipped with a motorized filter wheel with six filter positions (LUDL Electronic Products Ltd., Hawthorne, New York, USA), allowing multicolor detection with switching times of down to 50 ms. For two-color experiments with GFP and either RFP or mCherry, a combination of 525/50 and 617/73 filters was used (both Semrock, Rochester, New York, USA). The emitted light was focused onto two separate EMCCD cameras (both DU 897E-CSO-#BV Ixon$^+$, Andor Technology plc., Belfast, Northern Ireland), resulting in an area of 512×512 pixel for each channel. The corresponding image size in micrometer per pixel was determined with an USAF Pattern (USAF test target, CVI Melles Griot, Albuquerque, New Mexico, USA) and are given in table 5.3 for the different magnifications. Please note that the tube lens can be changed, which results in additional magnification.

Table 5.3: *Resulting pixel size in micrometer at WF*

objective	tube lens	resulting pixel size in μm
60 X	1.5	0.138
60 X	1.0	0.210
40 X	1.0	0.305

The setup was controlled via Andor IQ software. For faster acquisition mode, the second camera as well as the different lasers were externally triggered using the output/fire pulse of the first camera to ensure synchronized image acquisition. In this case, the individual laser powers were controlled externally. A box to modulate laser power was built from Axel Gersdorf in the electronic workshop. Trigger pulses were distributed via a FPGA device (NI cRIO-9073, National Instruments Corporation, Austin, Texas, USA), the corresponding software to address the device was written by Dr. Volodymyr Kudryavtsev.

5.2.2 Spinning-disk confocal microscopy

The spinning-disk confocal microscope (SDCM) used within this work was a commercially available Revolution System from Andor (Andor Technology plc., Belfast, Northern Ireland) and purchased via BFI Optilas. It is controlled via Andor IQ software. A scheme of the setup is shown in figure 5.4.

The system is based on a Nikon eclipse TE2000-E corpus (Nikon Corporation, Tokyo, Japan) and equipped with a CSU-10 confocal spinning-disk unit from Yokogawa Electric
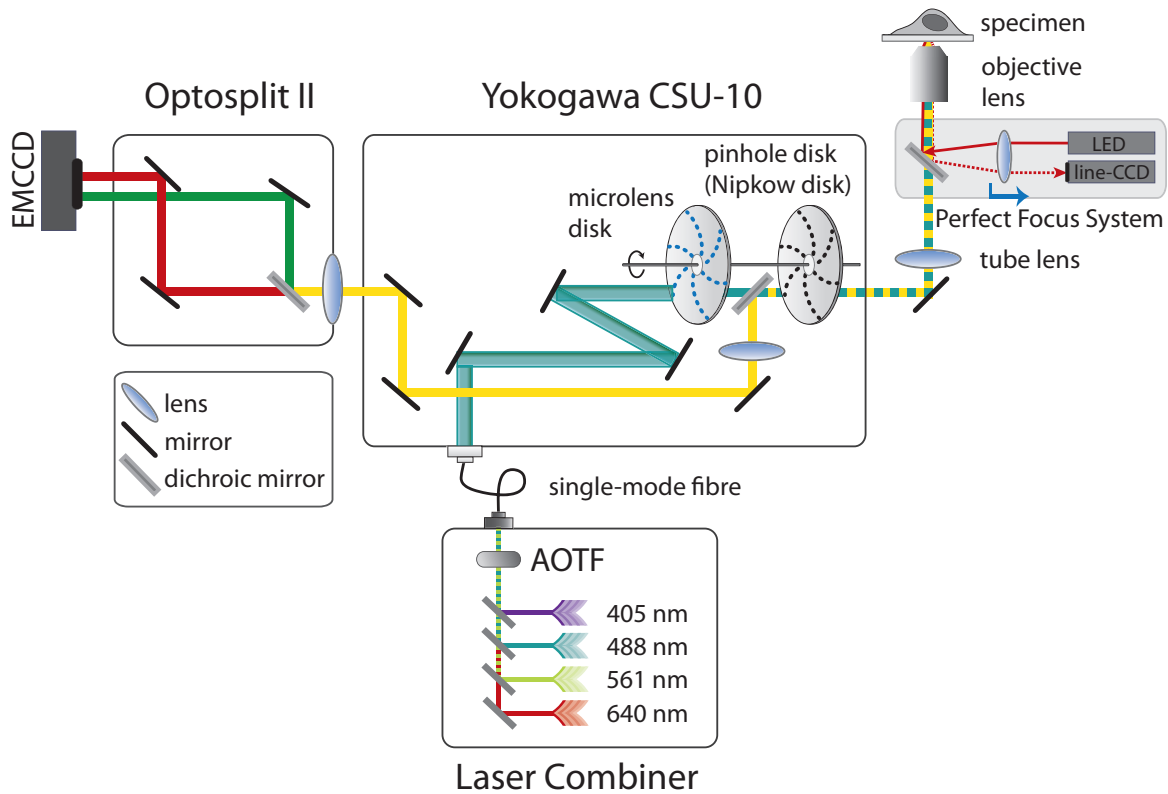
Figure 5.4: *Schematic of the spinning-disk confocal microscope. The system is based on a Nikon corpus and equipped with a CSU-10 confocal spinning-disk unit and an Optosplit system for separation of the different fluorescence wavelength. A perfect focus system is implemented to avoid focus drift. An additional magnification can be applied by switching the tube lens.*

Corporation (Tokyo, Japan), a perfect focus system (Nikon Corporation, Tokyo, Japan), a motorized xy stage ProScan II in conjunction with a piezo stage system NanoScanZ (both from Prior Scientific, Inc., Rockland, Massachusetts, USA) and a laser combiner. The laser combiner includes four solid state lasers allowing excitation with 405 nm, 488 nm, 561 nm and 640 nm, respectively. Selection of excitation wavelength and laser power is possible via an AOTF, after which the excitation beam is coupled into a single-mode fiber.

A 100X or 60X Apo TIRF oil immersion objective with a numeric aperture of 1.49 was used to focus the beam into the sample (Nikon Corporation, Tokyo, Japan).

Fluorescence emission was collected via the same objective and separated from the excitation wavelength with a dichroic beamsplitter Di01-T405/488/568/647 (Semrock, Rochester, New York, USA). The detection path consisted of the spinning-disk unit, where the pinhole disk (Nipkow-disk) is located in an intermediate image plane, and an Optosplit II (Cairn Research Limited, Faversham, United Kingdom) equipped with different filter sets, depending on the experimental demands.

In the case of two color experiments with GFP and RFP or mCherry, a BS 562 dichroic mirror (Semrock, Rochester, New York, USA) in combination with a HC 525/50 filter (Semrock, Rochester, New York, USA) and an ET 605/70 filter (Chroma Technology Corporation, Vermont, USA) were used. For three color experiments a dichroic mirror FF662-FDi01 (Semrock, Rochester, New York, USA) in combination with a HC GFP/DsRed dualband filter (Semrock, Rochester, New York, USA) and a HQ 730/140 bandpass filter (Chroma Technology Corporation, Vermont, USA) were used.

In the two and three color experiments, the different spectral channels were projected onto two separate areas of an EMCCD camera (DV887DCS-BV Ixon, Andor Technology plc., Belfast, Northern Ireland) resulting in two areas of 256×512 pixel per channel. The corresponding image size in micrometer per pixel was determined with an USAF Pattern (USAF test target, CVI Melles Griot, Albuquerque, New Mexico, USA) and are given in table 5.4 for the different magnifications.

Table 5.4: *Resulting pixel size in micrometer at SDCM*

objective	tube lens	resulting pixel size in μm
100X	1.0	0.140
60X	1.5	0.147
60X	1.0	0.217

For live-cell experiments, an objective heating ring (PeCon GmbH, Erbach, Germany) as well as a heating table and heating lid (ibidi GmbH, Martinsried, Germany) were used in order to provide physiological temperatures around 37 °C.

5.3 Data analysis

For a first analysis of the obtained movies, the freely available ImageJ software was used. For a more detailed analysis, different softwares have been written in the group of Prof. Don Lamb, PhD.

Throughout the work, dual-color virus particles have been used to study virus uptake and fusion via color separation. Therefore, average changes in the fraction of colocalizing capsid and envelope particles were analyzed as a function of time to get a general impression of the fusogenity possessed by the different viruses. Interval times of up to several minutes were used for this analysis analysis in order to cover a broad time range.

Therefore, single particles cannot be followed with time but kinetics are available on a single cell level. Furthermore, individual virus trajectories were analyzed to obtain insights into the dynamics of the fusion process. Movies for single particle analysis were acquired with high time resolution to enable tracking of single particles over time.

5.3.1 Image calibration

Fluorescence was separated spectrally and detected on different areas of an EMCCD camera. Depending on the excitation and emission wavelengths, the measured channels were assigned to green, red and autofluorescence, as shown in figure 5.2. For colocalization analysis, it is crucial to have a excellent mapping of the different channels. Therefore, image calibration needs to be done prior to analysis.

Before each day of experiments, an image of TetraSpeck microspheres spotted on a cover slide was recorded (TetraSpeck microspheres, 0.1 μm, fluorescent blue–green–orange–dark red, Invitrogen GmbH/Life Technologies, Carlsbad, California, USA). These microspheres are fluorescent over a large spectral range and could be detected in all spectral channels in this work. For experiments on the spinning-disk confocal microscope, the white light through the stationary pinhole array of the confocal disk could be alternatively used for mapping of the two channels. A Matlab program which enables the calibration of one channel with respect to the other was written by Dr. Aurélie Dupont. Corresponding particles in both channels were selected manually and fitted by a 2D Gaussian to determine the accurate xy-coordinate of the particle's position in each channel. A polynomial fit of 2$^{\text{nd}}$ order was applied to obtain the transformation matrix.

5.3.2 Colocalization analysis of virus-only samples in 2D

In order to determine the colocalization percentage of different dual-color virus preparations, a software that performed intensity-based colocalization analysis in two dimensions was written by Dr. Volodymyr Kudryavtsev.

Particles in each channel were selected by the following criteria: an intensity threshold that is adjusted dynamically, particle size and the minimum distance between two neighboring particles to exclude aggregates. The dynamic intensity threshold was calculated for each image, based on the intensity distribution of all pixels within this image and determined by a 1D Gaussian fit of this distribution (figure 5.5). In our case, the total number of pixels covered with particles was low compared to the sum of background pixels. We assumed a normal distribution of intensities. The most common background

intensity is given by I_{center} of the Gaussian fit of the pixel intensity distribution and the width of the distribution is given by the standard deviation σ (figure 5.5). I_{center} is only weakly affected by the presence of the fluorescent particles. An additional parameter, n, is used to adjust of how many σ's above the background level are required for detection. This parameter remained constant throughout the analysis. The resulting threshold was given by: $threshold = I_{center} + n \cdot \sigma$.

The detected particles were then fitted with a 2D Gaussian using the Levenberg-Marquart algorithm. To speed up the analysis, the initial values were calculated using a center of mass approach. Detection of colocalizing capsid and envelope particles was based on the background corrected intensity ratio of the green to red channels. In the case of colocalizing particles, this ratio should be close to one. In addition, intensities in the autofluorescence channel (section 5.2) were taken into account allowing impurities to be identified. Thus, the analysis could be performed for example with virus inocculum. Particles with intensities above a certain threshold in the autofluorescence channel were excluded from the colocalization analysis. The upper threshold limit ensures that only the described autofluorescent particles were excluded and not fluorescent virus particles, as their corresponding GFP-signal may also be detected with low intensities in the autofluorescence channel. This is due to cross-talk of GFP being observable in the autofluorescence channel. The cross-talk of GFP was evaluated to around 9 % of its intensity in the GFP-channel. Direct excitation of RFP with 488 nm is negligible.

5.3.3 Colocalization analysis of virus-incubated cells in 3D

Evaluating the colocalization percentage of dual-color viruses in living cells over time requires particle detection and colocalization analysis in three dimensions. A software for 3D colocalization analysis was written by Dr. Volodymyr Kudryavtsev. The analysis was based on the whole 3D information of the recorded image stack rather than using a z-projection of the images, and colocalization was determined based on the distance between particles in the green and red channels.

Images were pre-processed by a Spot Enhancing Filter before particle detection with an empirically determined Kernel size of 7 pixel and width σ_w of 1.3 pixel. Particles were detected independently in the green and red channels for each plane in every z-stack using the detection approach that was described previously. The calculation of the dynamic intensity threshold was based on all images within one z-stack. In addition, intensities in the autofluorescence channel (section 5.2) were taken into account allowing impurities to be identified. To avoid that occasionally detected agglomerates are counted as
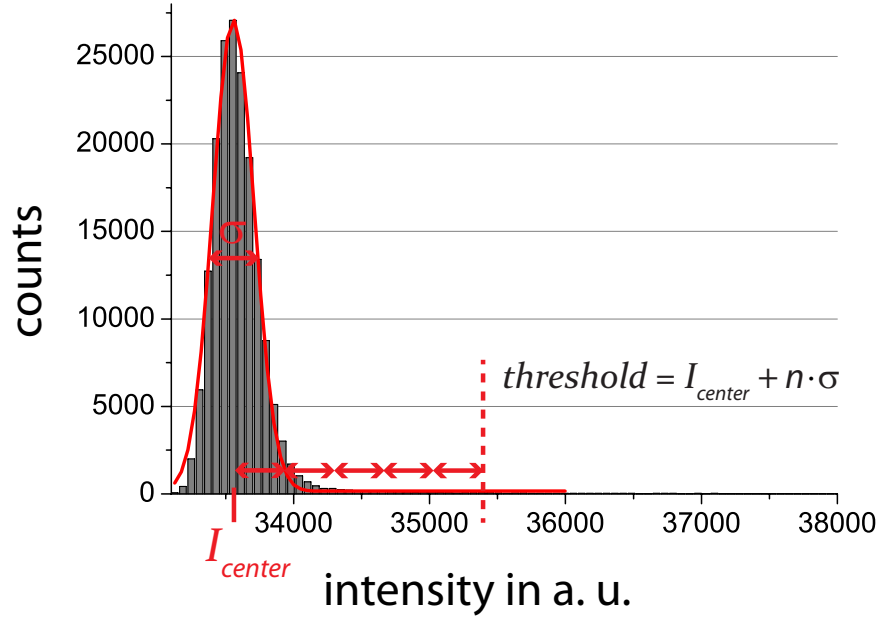
Figure 5.5: *Intensity threshold for particle detection. The intensity threshold is based on the intensity distribution of all pixels within each image and determined by a 1D Gaussian fit of this distribution. The most common background intensity is given by I_{center} of the Gaussian fit and the width of the distribution is given by σ. The additional parameter, n, is used to adjust of how many σ's above the background level are required for detection. This parameter remained constant throughout the analysis.*

multiple particles, additional parameters were implemented in the software: the range of the allowed particle size as well as a minimal distance between two neighboring particles required to consider them in the analysis. Particle size and minimal distance parameters were optimally adjusted for the colocalization analysis. The position of each particle was estimated by calculating the center of mass of the fluorescence intensity for each spot. To ensure that each particle was only counted once per z-stack, the image plane within the z-stack containing the highest intensity coming from the particle was taken as the axial position. The lateral position of the particle was determined by fitting the intensity to a 2D Gaussian function.

If movies were recorded with alternating-laser excitation in live cells, the green and red channels were collected sequentially rather than simultaneously and colocalized particles can be slightly displaced between frames as consequence of their motion. Hence, criteria for detecting colocalization in live cells were set by the maximal allowed distance in x, y and z between particles in the green and red channels; the higher the time resolution, the lower the limits can be for displacement in x, y and z. Particles actively transported along microtubules exhibit velocities of up to 2 μm·s^{-1} or even higher peak velocities.

The two channels were recorded alternatively with $\sim$ 150 ms delay, allowing a displacement of 0.3 μm during that time. Not only the x-y position of moving dual-color particles differs, the z-position may also be distinct due to movement as well as chromatic aberrations. The lag time from one channel to the second channel in the next image plane is approximately 500 ms, allowing a displacement of 1 μm during that time or even of 2 μm during 1 s, the lag time between both channels for two image planes. Relatively high parameters for the allowed displacement in live cells were chosen to ensure that all moving dual-color particles undergoing transport are identified as colocalizing particles and do not yield false positive fusion results. In this way, a detectable decrease in colocalization percentage would clearly imply that fusion is occurring since the amount of fusion is not overestimated.

The following parameters were used for colocalization analysis of foamy or herpesvirus particles in live cells: in the x-y plane, the maximal allowed distance was set to 2.2 μm and 600 nm were allowed in z. An exemplary illustration of these criteria are given in figure 5.6. For experiments in fixed cells, no offset due to movement of particles was required. However, a slight offset in the z-position (one z-plane, 300 nm) was allowed to account for chromatic aberrations.

5.3.4 Single particle tracking

Single particle tracking was either done manually using the plugin 'Manual Tracking' for ImageJ from Fabrice Cordelières (PhD) or automatically, using the 'vtracker' in ImageJ, which was developed from William J. Godinez *et al.* [106].

Manual Tracking was done using the local barycenter correction. Only the obtained x and y position per frame were recorded for further analysis.

For automatic particle tracking, a probabilistic approach was applied. This approach consists of particle detection with either a spot-enhancing filter or 2D Gaussian fitting and connection of particles from one frame to the following frame, based on a global nearest neighbor scheme in combination with a spatial-temporal filter [106]. For spatial-temporal filtering, a Kalman filter was used to predict the current particle position for each track. In addition to the particle position in x and y over time, the particle intensity as well as a local background corrected intensity for each particle were determined with this automated tracking routine.

In the case of 3D movies recorded at the SDCM, the particles were first tracked in two dimensions using a maximum intensity projection of each z-stack. Afterwards, the
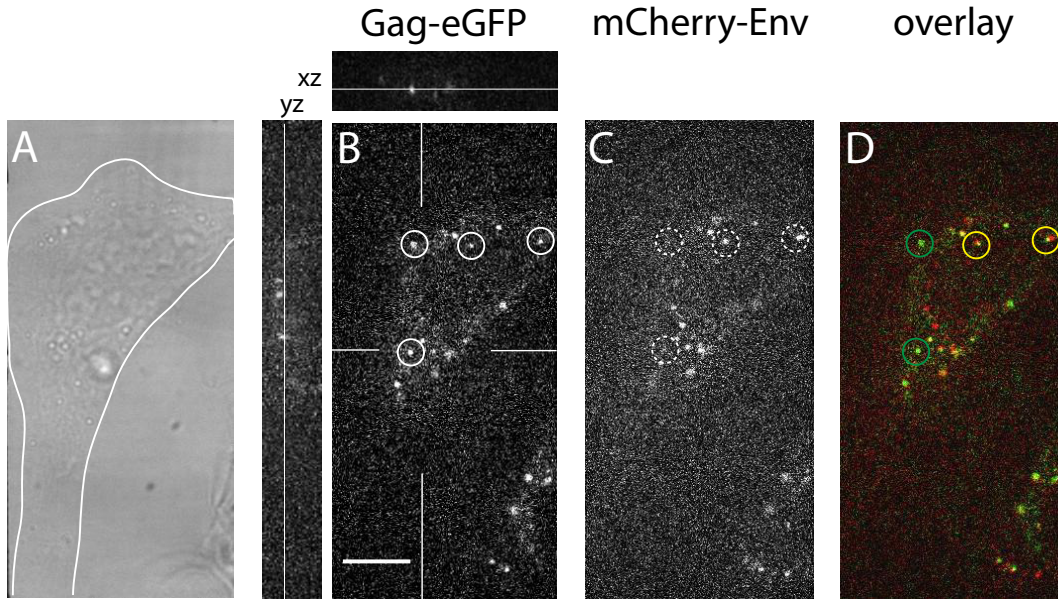
Gag-eGFP   mCherry-Env   overlay

Figure 5.6: *Exemplary images of a PE Ch incubated HeLa cell after 22 min at 37 °C, illustrating the colocalization criteria for displacement in x and y. (A) Bright-field image of the corresponding HeLa cell. Membrane boarders are indicated by a white line. (B)-(D) Images show one z-slice through the 3D cell volume. The circle indicates the allowed displacement parameter in x and y of 2.2 µm around the center of each Gag-eGFP particle (the RFP-capsid in the case of HSV-1). If a red particle (green particle in the case of HSV-1) is detected within this area (dashed circle), particles are defined as colocalizing (yellow circle), given that they are separated by less than 600 nm in z. If no particle is detected in the corresponding channel within this area, the particle is defined as non-colocalizing (green circle). Scale bar 10 µm.*

z-coordinates were retrieved by determining the z-plane with the particle's maximum intensity in the original movie, using the 'TrIC' software described in the subsequent paragraph.

5.3.5 Dynamic colocalization analysis of single virus trajectories

A software aimed to combine single particle tracking with image correlation was developed by Dr. Aurélie Dupont and is called Tracking Image Correlation (TrIC) (Dupont *et al.*, manuscript in preparation).

This method enables quantitative 3D colocalization analysis along the trajectory of moving dual-color particles. Typically, colocalization is determined visually and/or by an intensity-based comparison of the corresponding channels. This approach can be problematic due to bleaching of the fluorophores. The recently developed image cross-correlation method has the great advantage that it is more sensitive than intensity-based

methods and colocalization can be determined based on an automatic threshold criteria. In addition, information about the particle position in both channels relative to each other can be obtained. Furthermore, by performing cross-correlation along the whole particle trajectory, one can take into account the colocalization information obtained at different time-points and rule out colocalization events obtained through crossing of two individual particles.

The detection channels were first calibrated using TetraSpeck microspheres as explained in subsection 5.3.1 and a transformation matrix to map the two channels was thereby obtained. In order to analyze colocalization of dual-color particles, the virus particles were first tracked in the corresponding z-projection (2D track) of one channel as described previously in the subsection 5.3.4 and further analyzed in 3D with the TrIC software.

The obtained 2D track of the particle together with the z-projection of the movie is loaded into the TrIC software and the particle is re-tracked in 3D (3D track) based on the initial 2D track. Therefore, the software requires the original movie acquired in both channels (including all z-planes) and the obtained transformation matrix. Colocalization is measured through local 3D image cross-correlation of the two channels. This cross-correlation is performed in an area of 21×21 pixels^2 around the tracked particle position in x and y and the whole z-stack. In the case of colocalizing particles, the output stack shows a well-defined peak with high intensity as is illustrated in figure 5.7.A, and the resulting cross-correlation amplitude yields theoretically a value of 1 for the peak of the autocorrelation function. Experimentally obtained values are lowered due to background noise. When particles do not colocalize, the second channel contains only background noise, and the resulting output stack contains no defined intensity peak (fig. 5.7.D). As negative control, the pixels of the second channel are randomized and the resulting cross-correlation values serve as internal threshold criteria (fig. 5.7.E). In some cases, random particles show up in the analyzed area of 21×21 pixels^2 that are brighter than the particle of interest. Unlike typical cross-correlation methods, the presence of a random particle is not compensated by statistics and, therefore, the cross-correlation at that time-point gives the position relative to the brighter particle. Such random particles are present typically for only a few frames and easily identified by the resulting spikes in the cross-correlation amplitude and in the relative distance.

By applying this analysis, one gets the 3D trajectory, the particle's velocity, the corresponding background-corrected fluorescence intensity values of the particles in both channels and the 3D colocalization information. This cross-correlation output also provides information about the relative position of the particles in both channels with an accuracy of 30 nm. A more detailed description of the developed software is given in
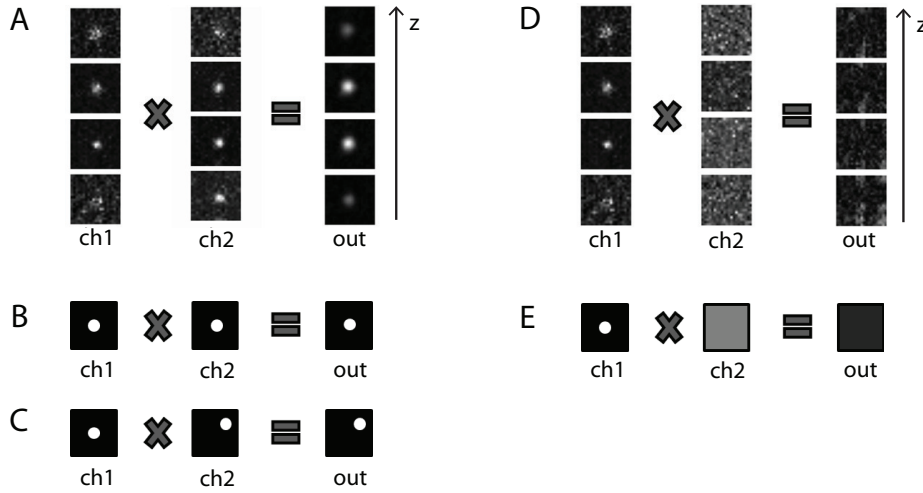
Figure 5.7: *Illustration of the image cross-correlation method. The output stack (out) shows the 3D cross-correlation of the two channels (ch1, ch2) around an area of 21 × 21 pixels² in x and y and the whole z-stack along the particle trajectory. (A) The resulting output stack of colocalizing particles shows a well-defined peak with high intensity. (B, C) The position of this peak reflects exactly the relative position between the peaks in the first and the second channels. In this way, information can be obtained on the relative movement of the capsid signal with respect to the envelope signal of a virus particle. (D) When the second channel contains only background noise, the result is a 3D stack of images with low intensities and no clear peak. (E) To define a threshold criteria for colocalization taken into account the intensity statistics of the input stacks, a cross-correlation of the first stack with the randomized second channel was performed. Figure adapted from Dupont et al. with permission (manuscript in preparation).*

Dupont *et al.* (manuscript in preparation).

6 Study of herpes simplex virus entry

To investigate the entry and fusion of enveloped viruses by means of fluorescence microscopy, the viruses have been labeled with two different fluorescent tags: one located at the envelope and another at the capsid. Thus, the fusion event itself should be observable via the separation of envelope and capsid signals. However, fusion has been rarely observed in real time. Experiments evaluating the average percentage of dual-color viruses as well as experiments analyzing the uptake of individual viruses, both, profit from a high percentage of dual-color (dc) viruses. First, decreases in the colocalization percentage over time can be a sign of fusion. Secondly, a high percentage of dc viruses increases the probability of observing a fusion event during a measurement.

The main goal was to investigate the entry kinetics by evaluating the percentage of dual-color virions over time. To do this, following experiments have been performed: A screen for the best virus preparation conditions was carried out to optimize the percentage of dual-color particles present in the virus preparation. Having optimized the virus preparation, colocalization experiments were performed in cells to get a general idea whether fusion takes place and on what time scale. Therefore, the initial colocalization percentage of each dc virus preparation was determined on coverslips. Then, the colocalization percentage was evaluated over time in cells incubated with dc virus. When fusion takes place, the percentage of dc viruses in cells should be below the initial value of the virus preparation and show a decrease over time.

Successful infection of a cell comprises several steps including virus uptake, separation of envelope and capsid by fusion with a cellular membrane, and transport of the capsid toward the nucleus for replication of the DNA genome. Viruses can enter cells either by fusion at the plasma membrane or via endocytic uptake, followed by fusion with an endosomal membrane. Endocytosis offers several advantages to the virus, such as efficiently transporting it from the cell membrane to the perinuclear area. During transport within maturing endosomes, virus particles face an increasing proton concentration,

which can serve as trigger for fusion. For entry to be infectious, the virus needs to escape before degradation takes place within the low pH environment. However, the emission of some fluorescent proteins is known to be pH-dependent. Thus, the effect of the proton concentration on fluorescent proteins in the viral context was evaluated by performing quenching experiments with virus particles on coverslips. The issue of potential quenching of the fluorescence intensity in acidic cellular compartments was further addressed by experiments with permeabilized cellular membranes in fixed cells to ensure neutral pH, or by performing triple color experiments with an additional marker of acidic compartments.

All these approaches reveal the average behavior of virus particles within one cell. The experiments are suitable to evaluate to which extend fusion takes place and on what time scale most fusion events are expected but no dynamic information is available. Hence, further experiments were performed to investigate the entry of individual virus particles in live cells with high time resolution.

6.1 Optimization of virus preparation

To obtain a high percentage of particles that contain both labels, the conditions for dual-color (dc) virus preparations were optimized. The herpes simplex 1 virus particles used throughout this work were labeled with two different fluorescent proteins, namely GFP and RFP (or mCherry instead of RFP). Most of the investigations were performed with viruses that have GFP fused to the C-terminus of the envelope glycoprotein D (gDGFP) and RFP N-terminally fused to the capsid protein VP26 (RFPVP26) [227] as is illustrated in figure 6.1.A. In addition, a second type of dc virus was constructed, which has GFP attached to the outer tegument protein VP11/12 (VP11/12GFP), sometimes also referred to as pUL46 (figure 6.1.B) [350]. The RFP-tag at the capsid protein VP26 was replaced by mCherry. Also in the case of these dc virus particles, the fusion event should be visible by separation of the GFP and mCherry signals, as this outer tegument protein detaches from the virus upon fusion [7, 78, 81, 113, 336]. A detailed description of the different virus strains is given in subsection 5.1.1 on page 57.

Analysis of the first double-tagged virus preparations revealed a very low percentage of colocalizing capsid and envelope particles. In these preparations, the percentage of RFP-tagged capsid particles containing also a GFP-envelope ranged between 33 % to 43 %, with 38 % on average. In addition, a large number of GFP-tagged envelope-only
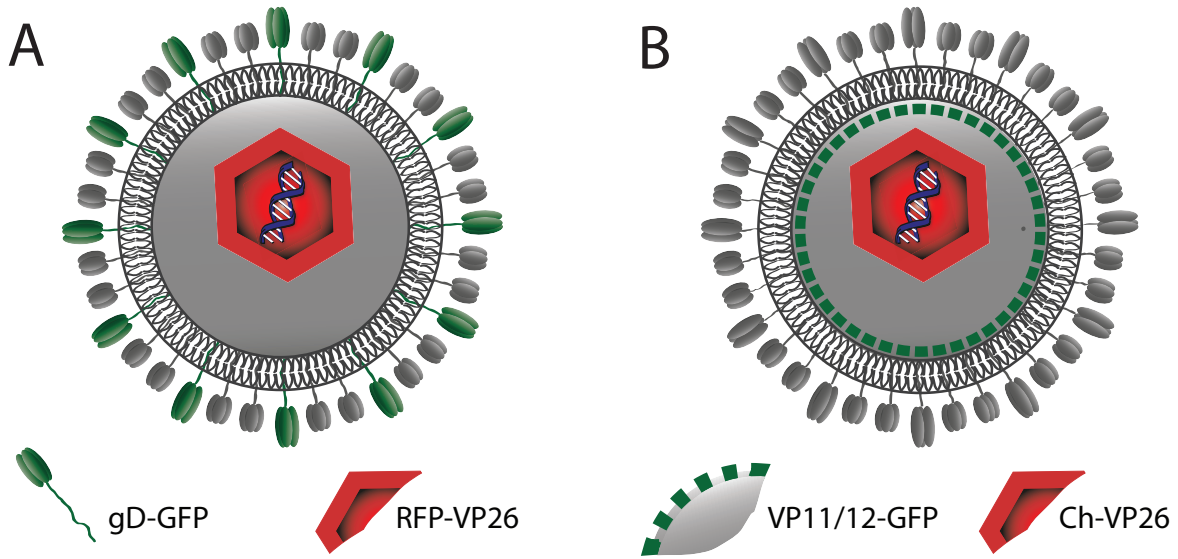
Figure 6.1: *HSV-1 structure with fluorescent proteins. The dsDNA is enclosed in the icosahedral capsid and the capsid is further surrounded by the tegument. The tegument is wrapped up by a lipid bilayer envelope with protruding glycoprotein spikes. (A) GFP is C-terminally fused to the envelope glycoprotein D (gDGFP) and RFP fused to the N-terminus of the capsid protein VP26 (RFPVP26). (B) GFP is fused to the outer tegument protein VP11/12 (VP11/12GFP) and mCherry to the capsid protein VP26 (ChVP26).*

particles was present as can be seen in the first row of images in figure 6.2 (A-D). The percentage of colocalizing GFP-tagged envelope-only particles varied between 3 % to 16 % and hence, was even below the percentage of colocalizing capsid particles. The presence of many envelpe-only particles can be attributed to the replication mechanism of HSV-1. In addition to functional viruses that contain envelope and nucleocapsid, there are also particles produced that lack the nucleocapsid (L-particles) [204, 212, 256, 305]. In order to increase the percentage of dual-color particles, a screening for the best preparation conditions was performed. A direct comparison of purified virus particles from preparations before optimizing the conditions and with optimized protocol are shown in figure 6.2, first and third row, respectively. The middle row of figure 6.2 shows virus particles from the non-purified supernatant obtained under the optimized conditions. The content of colocalizing RFP-capsids could be increased to about 70 %, and the fraction of envelope-only particles was significantly reduced (figure 6.2.I-L in comparison to A-D). This increase in the colocalization percentage was achieved by adjustment of many different parameters, such as the cell line of virus preparation and the time-scale of virus harvest. As fluorescent protein tags diminish the infectivity of double-tagged viruses, the effect on infectivity by reducing the amount of label was evaluated. Since comparison of all these parameters is very time-consuming, the screening was performed

in two iterations to keep it fast forward. The aim of the first screening round was to obtain a general trend of the best conditions, which allows to narrow the conditions for the subsequent screening round. The screening was constructed such that no purification of the virus was necessary. This was achieved by taking into account the signal arising from autofluorescent cellular structures (figure 6.2.F).

Autofluorescence is characterized by a broad excitation and emission spectra and can be detected after 488 nm excitation in the green spectral (GFP) and red spectral (autofluorescence) channels, as well as in the red spectral channel (RFP) after 561 nm excitation. An illustration of the resulting channels is given in figure 5.2 on page 65. The autofluorescence signal consisted mostly of aggregates that can be easily separated from viruses due to the larger size. However, smaller autofluorescent spots resembling the virus particles could also be detected (figure 6.2.F). These spots would cause false positive colocalization numbers when only the GFP and RFP channels are considered. However, alternating-laser excitation allows identification of the autofluorescence signal in an additional channel [152, 266]. This so-called autofluorescent channel is defined as the red detection channel after 488 nm excitation. Images of double-tagged virus particles in the green, autofluorescence and red channels (green, blue and red color, respectively) and their corresponding overlay (last row) are shown in figure 6.2. Autofluorescent spots appear in white in the corresponding overlay as can be seen in the right part of image H. Truly colocalizing dc viruses show up in yellow color (e.g. image L or lower bottom of image H) and thus, are distinguishable from autofluorescent cellular structures. A software was developed that allows determination of the number of colocalizing capsid and envelope particles in the presence of autofluorescent cellular structures. A detailed description of the software is given in section 5.3.2.

6.1.1 First screening round of virus optimization

The parameters, that were compared in the screen were different cell lines, time point of harvesting and different spiking ratios with wild-type virus. The virus samples for this experiment were prepared by our cooperation partners. A description of the sample preparation can be found in the subsection 5.1.5.1.
The supernatant from four cell lines: Vero, BHK, Hep2 and HeLa MZ cells, was analyzed every four hours from 12 h to 36 h post binding. As the infectivity of viruses decreases after the fluorescent tags are introduced, the amount of label was reduced by spiking the dual-color viruses with various amounts of wild-type virus. Four different
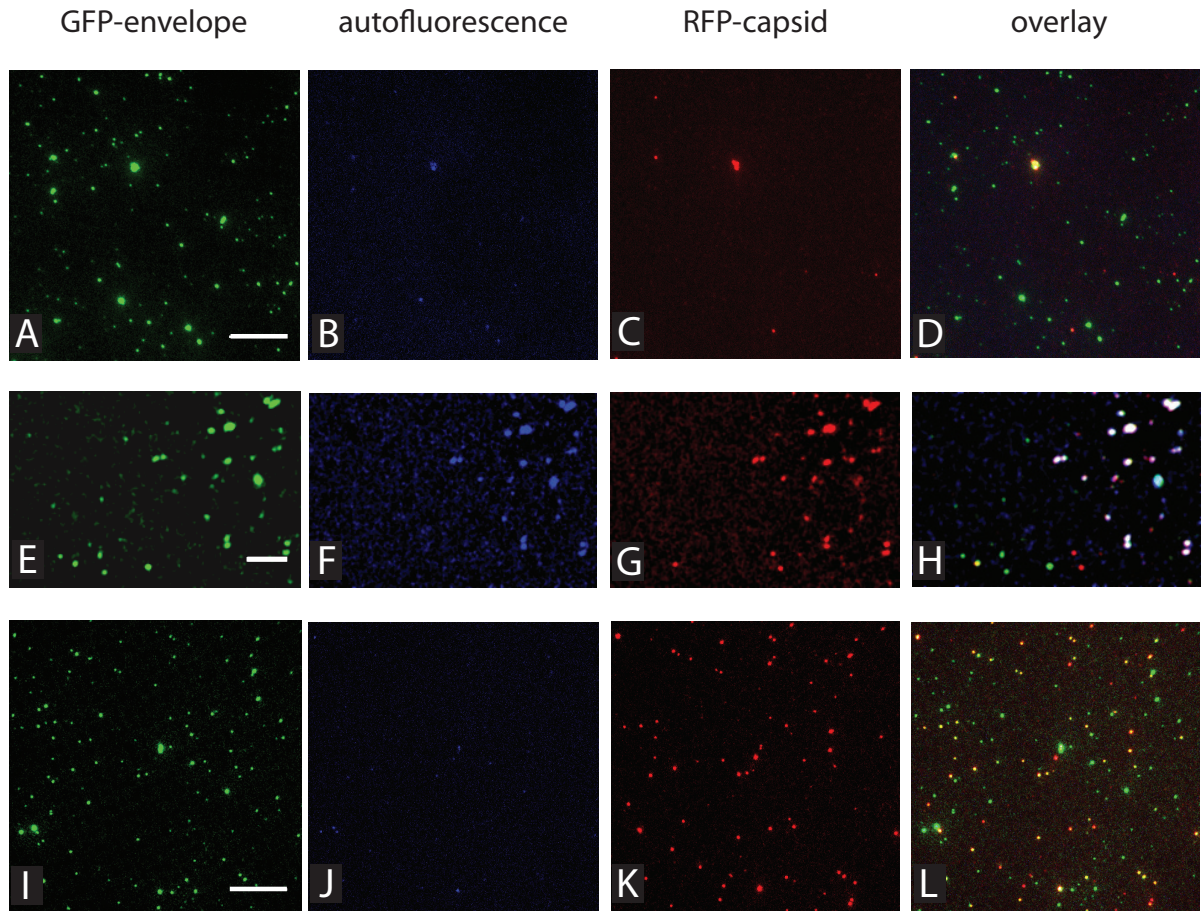
GFP-envelope   autofluorescence   RFP-capsid   overlay

Figure 6.2: *Comparison of double-tagged virus preparations obtained under different conditions. (A-D) Purified virus preparation before optimization of the conditions. (E-H) Non-purified supernatant obtained under optimized conditions. (I-L) Purified virus preparation obtained after optimization. Wide-field images of the green channel containing the GFP-envelope signal are shown in green color (first row). Fluorescence signal arising from potential autofluorescent cellular structures or impurities can be observed in all spectral channels and can lead to false positive colocalization results. Therefore, autofluorescence was identified using the red detection channel after 488 nm excitation (second row, blue color) and accounted for in the analysis. The RFP-capsid signal is detected in the red channel (third row). The last row shows the corresponding overlay of the three channels. Colocalizing spots of true double-tagged virus particles appear in yellow color, whereas colocalizing structures resulting from cell debris are white. The purified virus preparations in the upper and lower panel contain almost no autofluorescent structures (B, J), whereas many autofluorescent spots are observed in the unpurified supernatant (F). Scale bar 10 µm.*

spiking conditions containing 0 %, 20 %, 50 % and 80 % wild-type virus were tested. The number of dual-color particles and red particles evaluated under each condition for the four different cell lines are shown in figure 6.3 and figure 6.4, respectively.

For experiments in cells, a high percentage of dual-color virus particles is required. In addition, it is important to know when the highest numbers of dual-color particles are produced. In the screen, the main focus was on the total number of dc particles, rather than on the colocalization percentage as screening was performed in the virus inoccolum and free capsid and envelope particles will be removed to a certain extent upon purification due to their lighter weight. The first large scale screening was aimed at giving an overall trend. A few samples contained almost no virus particles, which most likely arose from difficulties in sample preparation. Therefore, samples containing less than 12 dc particles were not included in the analysis. These time-points are labeled in gray in the corresponding figures 6.3 and 6.4.

From all four cell lines included in the screen, Vero cells showed the highest density of dual-color particles, followed by BHK cells (figure 6.3.A and B, respectively). A lower number of produced double-tagged particles was observed in HEp2 and HeLa MZ cells (figure 6.3.C and D, respectively). The highest yields of dual-color virions were generally observed for virus particles spiked with 0 % or 20 % wild-type virus (e.g. figure 6.3.A). Double-tagged particle numbers were lower when the amount of wild-type virus was increased to 50 % or 80 %. However, the obtained dc particle numbers in Vero cells spiked with 50 % or 80 % wild-type virus were still higher than the average numbers observed from preparations in HEp2 or HeLa cells. In HeLa MZ cells, the number of dual-color particles was the highest when no wild-type virus was added (figure 6.3.D). In contrast, the effect of spiking on the obtained double-tagged particle numbers was not so clear in the data of BHK and HEp2 cells. In these two cell lines, low dual-color particle numbers were obtained, which were mainly below 200 particles per 1 mm^2, and no significant variation among the different spiking ratios was observed (figure 6.3.B, C). The time for harvesting the virus was best between 28 to 36 hours post binding. The time-point of virus harvest gives only a trend as it depends on various factors of the cells used for the virus preparation, such as passage number, cell-density and cell-cycle at the time of infection. At time points of 28 hours or later, the chance to obtain a large number of dual-color particles was higher. On the other hand, virus harvest should not be too late, as the risk of cell rupture due to virus infection is higher at later time-points. Cell rupture leads to release of capsid-only particles.

During the time of our screen from 12 h to 44 h post binding, no general increase in the number of capsid-only particles was observed (figure 6.4 in comparison to figure 6.3).

Occasionally, a higher number of particles in the red channel was obtained at later time points, such as in HEp2 cells with 20 % spiking or in HeLa cells with 0 % or 80 % spiking (figure 6.4.C and D, respectivly). In general, an increase in the number of produced red particles was accompanied by an increase in the number of dual-color particles. In Vero cells, not only the total number of capsid and double-tagged particles was the highest, but also the percentage of RFP-capsid particles that colocalized with GFP-envelope signal was the highest among the four cell lines investigated.

Altogether, the first screening round revealed that the most promising conditions for a virus preparation with a high content of double-tagged virions are Vero cells with 0 % or 20 % spiking with wild-type virus. A subsequent screening round was performed to fine-tune the obtained preparation conditions.
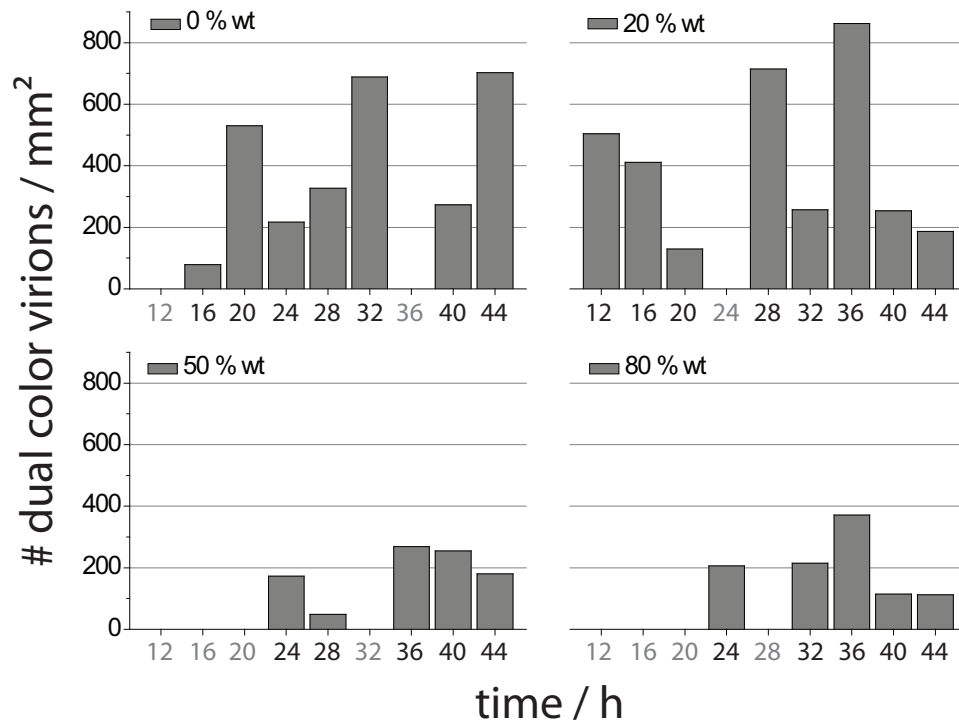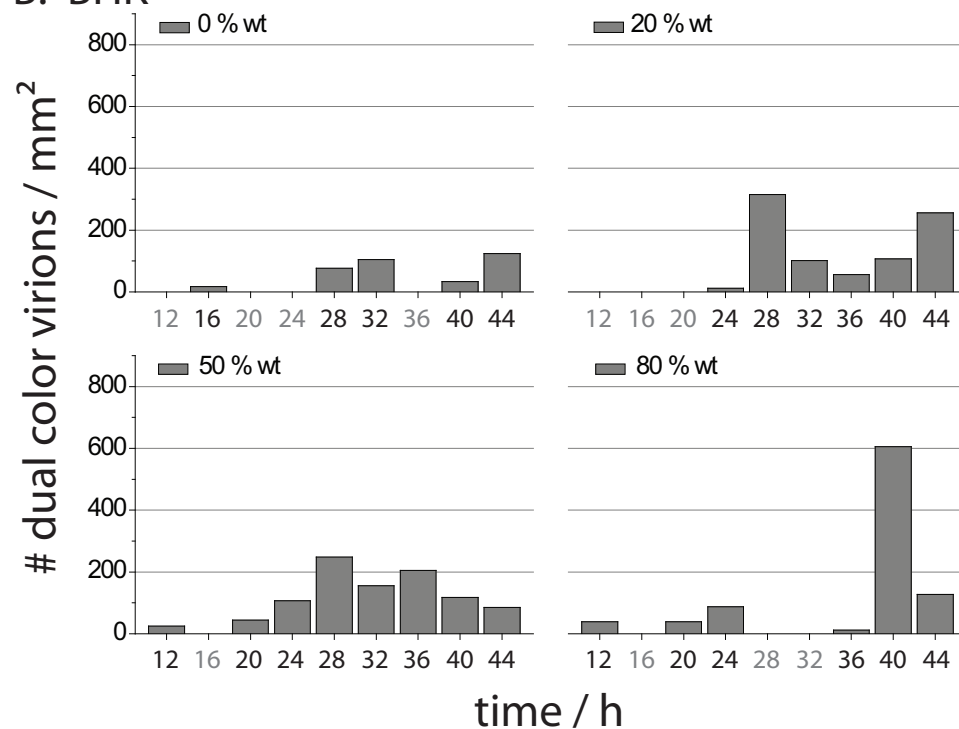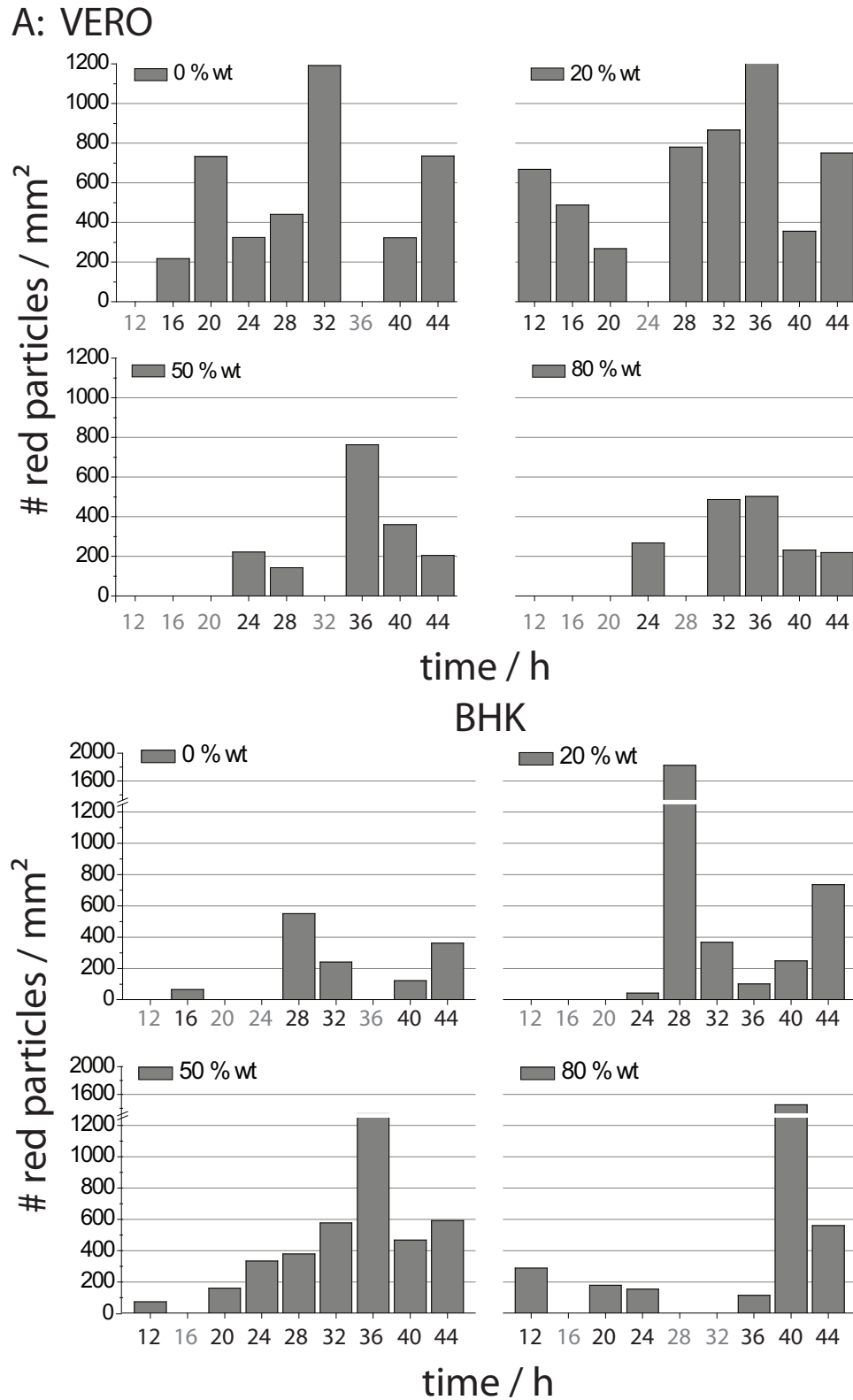
Figure 6.3: *Screen 1. Number of dual-color virus particles per 1 mm². (A) Vero, (B) BHK, (C) HEp2 and (D) HeLa MZ cells were infected with four different spiking ratios of dual-color and wild-type virus. The plots are shown in the order of increasing wild-type concentration: 0 %, 20 %, 50 % and 80 % wt virus. The cell culture supernatant of the four different cell lines was harvested every four hours during 12 to 36 hours post binding. The unpurified supernatant was pipetted on coverslips (20 μL) and the number of dual-color virions was counted.*

C: HEp2
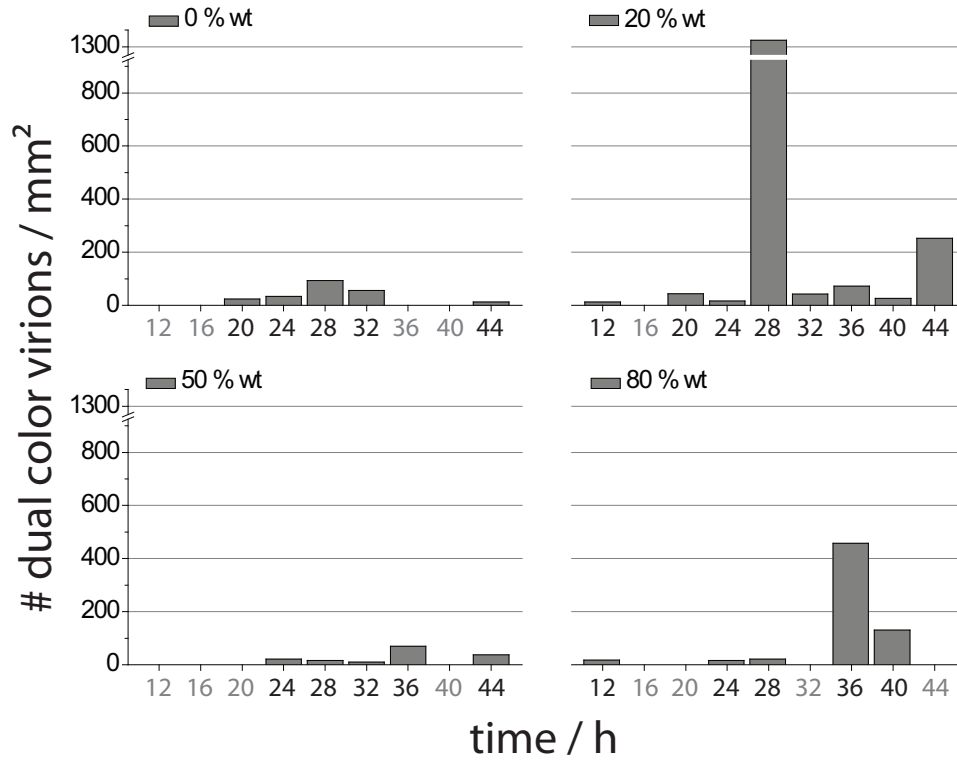
D: HeLa MZ
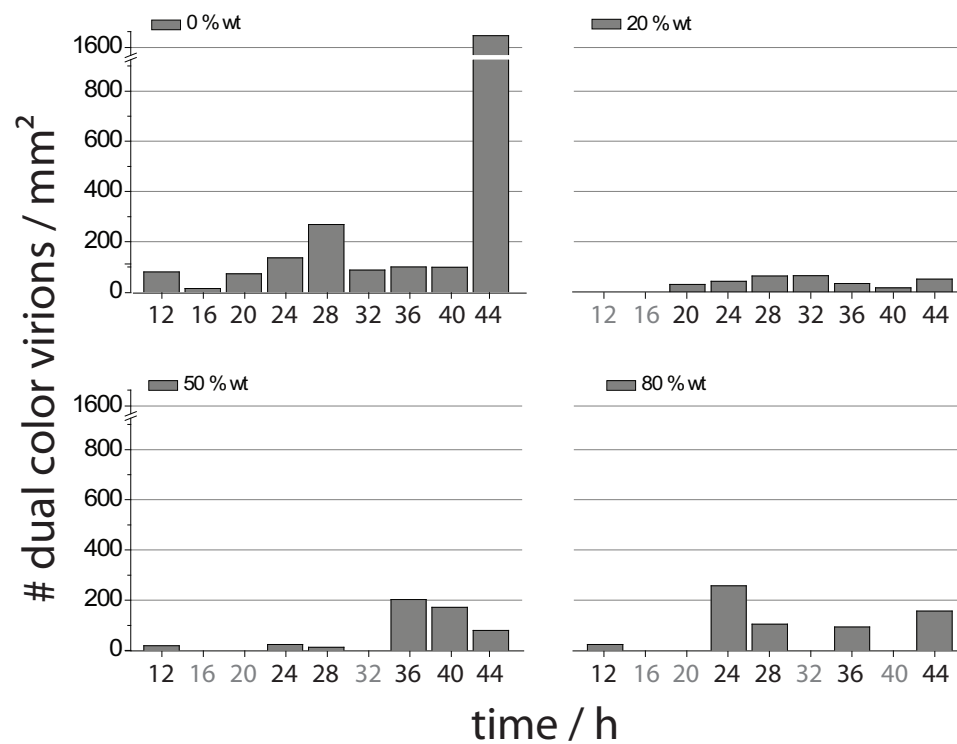
Figure 6.3: *Continued. This first large scale screening was aimed to give an overall trend. Occasionally, almost no virus particles were detected. Therefore, samples containing less than 12 particles were excluded from the analysis. These time-points are labeled in gray. Note the different scaling of the y-axis in the case of HEp2 and HeLa MZ cells.*

Figure 6.4: *Screen 1. Number of RFP-capsid particles per 1 mm². (A) Vero, (B) BHK, (C) HEp2 and (D) HeLa MZ cells were infected with four different spiking ratios of dual-color and wild-type virus, ranging from 0 %, 20 %, 50 % and up tp 80 % of wt virus. The cell culture supernatant of the four cell lines was harvested at the indicated time-points. The unpurified supernatant was pipetted on coverslips (20 μL) and the number of capsid particles was counted.*
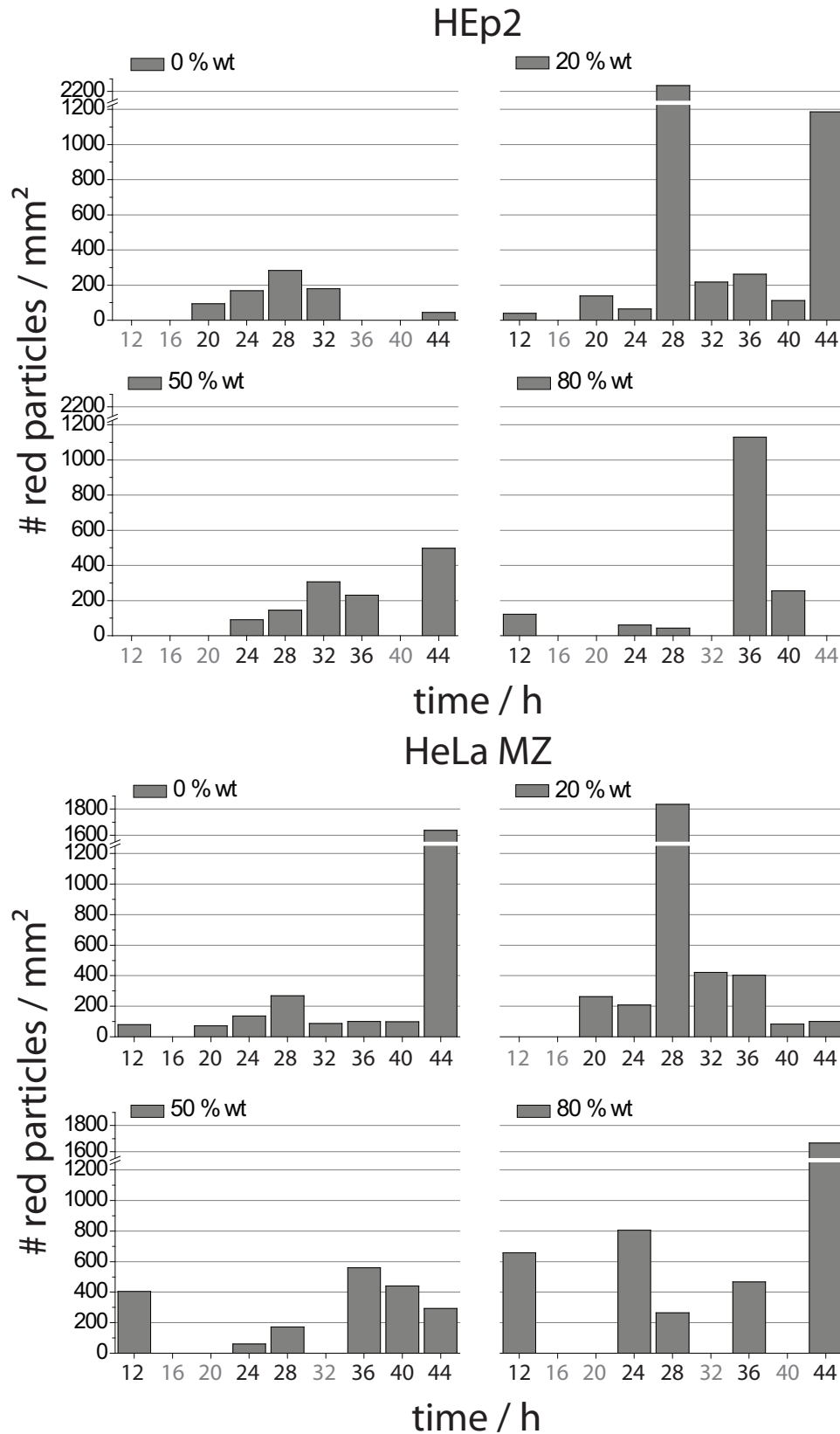
Figure 6.4: *Continued. This first large scale screening was aimed to give an overall trend. Occasionally, almost no virus particles were detected. Therefore, samples containing less than 12 particles were excluded from the analysis. These time-points are labeled in gray. Note the different scaling of the y-axis in the case of HEp2 and HeLa MZ cells.*

6.1.2 Second screening round of virus optimization

The aim of the second screen was to refine the overall trend obtained in the first screen by analyzing more samples near the optimal conditions. The number of dual-color particles was evaluated in Vero and BHK cells after 28 hours and 32 hours post binding. The four different spiking ratios with wild-type virus were compared and the effect of spiking on the infectivity of the obtained virus particles was measured. Although BHK cells showed lower particle numbers than Vero cells, they were included in this screen as virus preparations are more easily done in this cell line.

A higher production of dual-color particles was observed at 32 hours post binding than after 28 hours (figure 6.5.A and figure 6.6.A). This was the case for virus preparation in Vero cells (figure 6.5.A) as well as for preparation in BHK cells (figure 6.6.A). In Vero cells, the number of the obtained double-tagged and red particles was significantly higher than that of virus preparations in BHK cells (figure 6.5.A, B and 6.6.A, B, respectively), which is consistent with the results from the first screening round. Furthermore, the percentage of colocalizing capsid particles was about twice as high in Vero cells than in BHK cells. Most dual-color virions were detected in Vero cells at a spiking ratio with 20 % of wild-type virus after 32 hours post binding (figure 6.5.A). Overall, an increase in spiking with wild-type virus led to a decrease in the number of detected virus particles. Again, the effect of spiking was not so prominent in BHK cells, but the highest number of dual-color virions was detected with 20 % spiking of wild-type virus, which is comparable to the results from preparations in Vero cells.

In Vero and BHK cells, spiking of the attenuated double-tagged virus particles with wild-type virus increased the infectivity as can be seen in figure 6.5.C and 6.6.C, respectively. Viral titers are given in plaque forming units (pfu) per mL for each condition. Briefly, the cell culture supernatant was harvested for the specified conditions and diluted to ensure that a single cell within the cell monolayer can only be infected with one virus particle. Replication of the virus led to infection of the neighboring cells and cell death. After a certain time period, this accumulation of dead cells can be visualized as plaque. Hence, by counting the plaques, the concentration of infectious virus particles was determined. The titer of the wild-type virus (100 % wt), harvested under the same conditions, is shown for comparison.

The higher the spiking ratio with wild-type virus, the higher the viral titers that were obtained (figure 6.5.C and 6.6.C). Already at a spiking ratio with 20 % of wild-type virus, the titer significantly increased in comparison to non-spiked dual-color virions. For virus
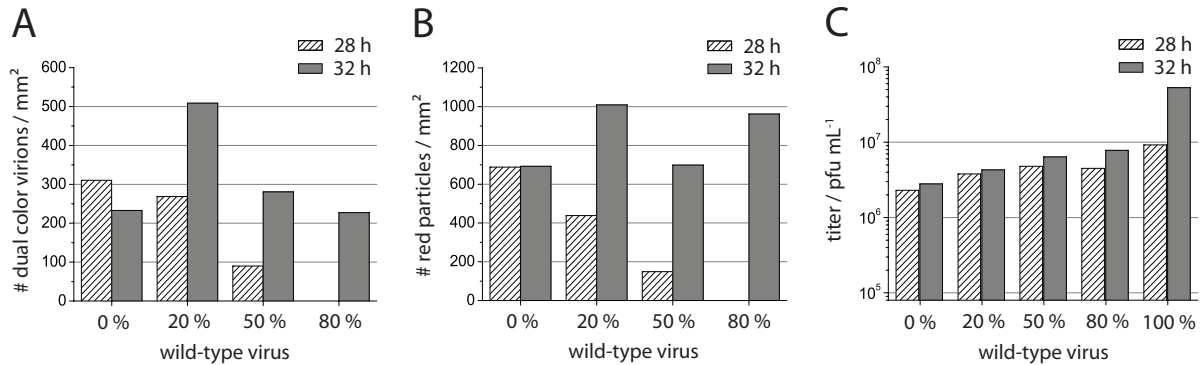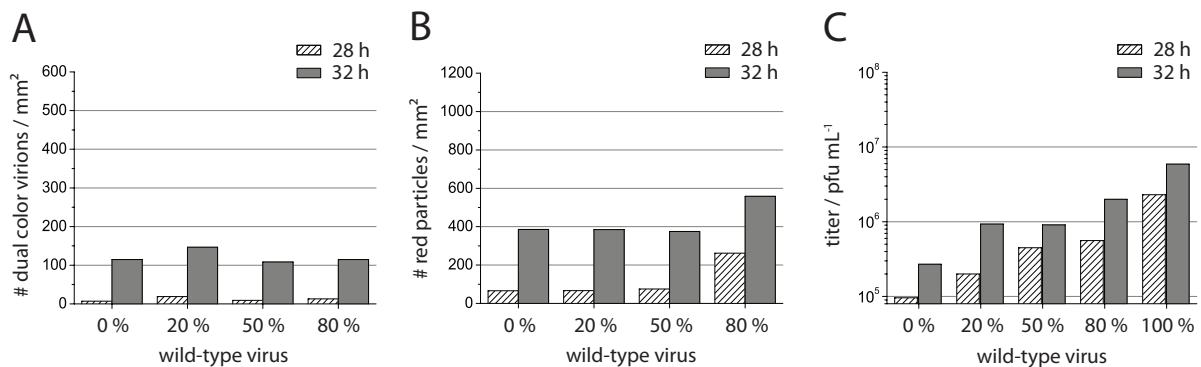
Figure 6.5: *Screen 2. Vero cells were harvested at 28 hours (hatched bars) and 32 hours (gray bars) post binding. The effect of spiking double-tagged virions with an increasing amount of wild-type virus was evaluated. (A) The number of dual-color particles was determined for the different spiking ratios. Detected particle numbers in samples with 80 % wt at 28 h post binding were much lower than for the other conditions and are therefore not visible within this scaling. (B) The number of detected red particles for the different spiking ratios. (C) Viral titers were determined in terms of plaque forming units per mL cell culture supernatant for the different spiking ratios with wild-type virus. For comparison, the titer of 100 % wild-type virus is given in addition. Note the logarithmic scaling of the y-axis.*

Figure 6.6: *Screen 2. BHK cells were harvested at 28 hours (hatched bars) and 32 hours (gray bars) post binding. The effect of spiking double-tagged virions with an increasing amount of wild-type virus was evaluated. (A) The number of dual-color particles was determined for the different spiking ratios. (B) The number of detected red particles for the different spiking ratios. (C) Viral titers were determined from the supernatant obtained under each conditions. For comparison, the titer of 100 % wild-type virus is given in addition. Note the logarithmic scaling of the y-axis.*

preparations in Vero cells, the viral titer was almost doubled upon spiking with 20 % wild-type virus (figure 6.5.C). Further increase in the amount of wild-type virus to 50 % or even 80 %, was accompanied by an increase in viral titers of about 25 % for each step. Thus, the increase in relative infectivity was lower compared to the first step from 0 % wild-type virus to 20 % wild-type virus. This effect is even more prominent in BHK cells (figure 6.6.C). Lower viral titers were obtained for preparations in BHK cells than in Vero cells and hence, less infectious viral particles were present in the supernatant of BHK cells.

From a biological point of view, the virus with the highest infectivity is the most desirable, which would favor a spiking ratio with 80 % wild-type virus. However, for imaging, a high fluorescence signal is desirable. To investigate details in virus uptake, movies need to be recorded with high time resolution over a time period of 20 minutes or more. The higher the amount of labels per virus, the lower the laser power that is required for imaging, resulting in less phototoxicity. Hence, measurements with high time resolution are possible over longer time periods. The best compromise from the conditions tested is a spiking ratio with 20 % wild-type virus as it combines reasonable infectivity with a high dual-color virus yield suited for live-cell imaging.

Taken together, the two screening rounds revealed that a preparation with high dual-color virus yield can be achieved using Vero cells after about 32 hours post binding with 80 % double-tagged virus and 20 % wild-type virus. Under these conditions, about 50 % of the RFP-tagged capsids contained also a GFP-tagged envelope in the unpurified cell culture supernatant. In contrast, only about 30 % of the GFP-tagged envelope particles contained an RFP-tagged capsid as can be seen in figure 6.7 (middle red and green bar, respectively). Exemplary purified virus preparations that were obtained before optimization (figure 6.7, left-hand bars), as well as under optimized conditions (figure 6.7, right-hand bars) are given for comparison. Upon purification, the percentage of dual-color virus particles was further increased. In purified virus preparations, performed under the optimized conditions, about 70 % of the RFP-tagged capsids colocalized with a GFP-tagged envelope. Furthermore, the amount of colocalizing GFP-tagged envelope was about 50 % on average. These results confirm the successful and reproducible optimization of dual-color virus preparations and highlight the importance of careful purification. However, there is still a significant amount of envelope-only particles present in the optimized virus preparations, although the amount could be reduced compared to the preparations before the optimization as can be seen by comparing image L and D of figure 6.2 on page 83.
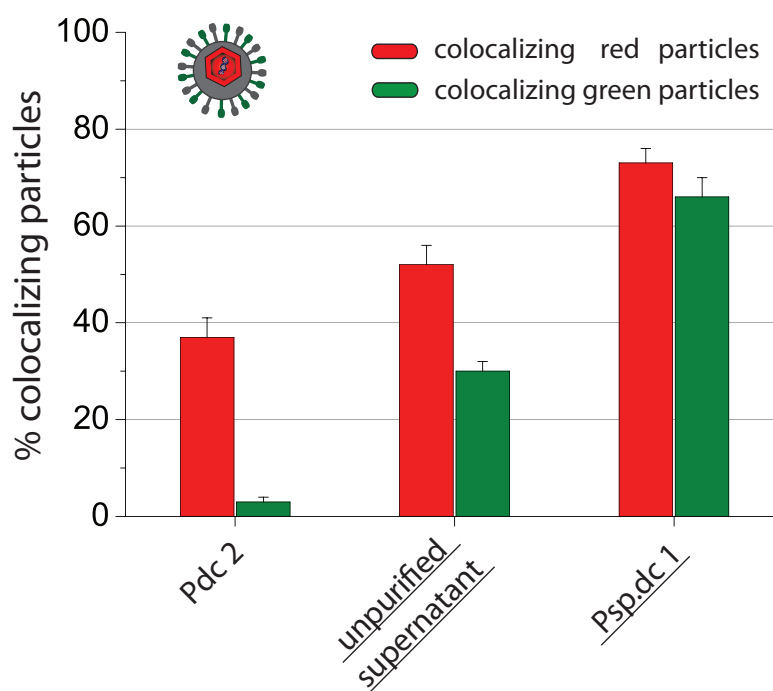
Figure 6.7: *Comparison of the colocalization percentage of double-tagged virus preparations before and after optimization. The colocalization percentage is given with respect to the total number of detected red particles (red bars), as well as relative to the total number of green particles (green bars). The virus preparation Pdc2 was obtained before the optimization, whereas the two underlined preparations were obtained under optimized conditions. The colocalization percentage of the unpurified supernatant could be increased upon purification (Psp.dc 1). An overview on the percentage of dual-color viruses in all the obtained virus preparations is given in the subsequent section.*

The presence of such a high number of envelope-only particles can be explained by the replication cycle of herpes simplex viruses (figure 4.5 on page 51). During egress of herpes simplex virus, progeny capsids are assembled in the nucleus and released into the cytoplasm by budding through the nuclear membrane (figure 4.5) [88, 112]. In a subsequent step, tegumentation is completed and the viral envelope is acquired by budding into vesicles of the trans-Golgi network (TGN) [212]. This final envelopment step can also occur if no capsid is present. Subsequently, particles are released that contain a functional viral envelope and tegument proteins, but lack the nucleocapsid and viral genome [204, 212, 256, 305]. Hence, the release of these so-called L-particles is the reason why so much fluorescent envelope-only signal is detected in the dual-color virus preparations. Although theoretically L-particles and complete dc virus particles should be separable due to the different weight, they are practically not completely separated as the bands are close enough together.

Despite the fact that the presence of many envelope-only particles complicates imaging-based investigation of virus entry, it is interesting to know that these L-particles probably play an important role in virus infection. These virus-like particles may aid defective virions by complementing the defective functions [300]. Indeed, addition of L-particles to cells transfected with viral DNA resulted in a fivefold enhancement of DNA infectivity according to plaque forming assays [65]. However, the role of L-particles in the natural infection pathway is not completely clear. The fact that these virus-like particles are produced in most tissue culture cell lines of different species in comparable quantities and that they are produced by all α-herpesviruses, implies an important biological function [65].

Furthermore, L-particles are promising vaccine candidates. They are not infectious as they lack the viral genome but nevertheless, they are functional in entry and can stimulate the development of immunity [300]. Synthesis of another type of virus-like particles can be induced by blocking the viral DNA synthesis. This leads to the production of so-called PREP-particles, which also lack the viral genome and are morphologically similar to L-particles [300]. In comparison to L-particles, the production of PREP-particles occurs without the new synthesis of infectious virus progeny, which makes them attractive as potential vaccines [300].

6.1.3 Colocalization analysis of purified dual-color virus preparations

Now having optimized the conditions for dual-color virus preparations, different dc virus preparations were done. Some of the obtained virus preparations were still prepared under non-optimized conditions or have been already prepared by our cooperation partners before the optimization of the protocol. With regard to fluorescence experiments focusing on virus entry into cells and fusion, it is crucial to characterize the initial colocalization percentage of each purified virus preparation, as fusion is visualized by the separation of capsid and envelope signals and hence, an overall decrease in the colocalization percentage. Therefore, the colocalization percentage of each virus preparation was determined prior to experiments in cells.

An illustrative comparison of the obtained colocalization percentages from all dc virus preparations is given in figure 6.8. The figure comprises virus preparations under optimized and non-optimized conditions. Virus preparations performed under optimized conditions are underlined in the figure. The calculated colocalization percentage is given with respect to the RFP-capsid signal (red bars), as well as relative to the number of
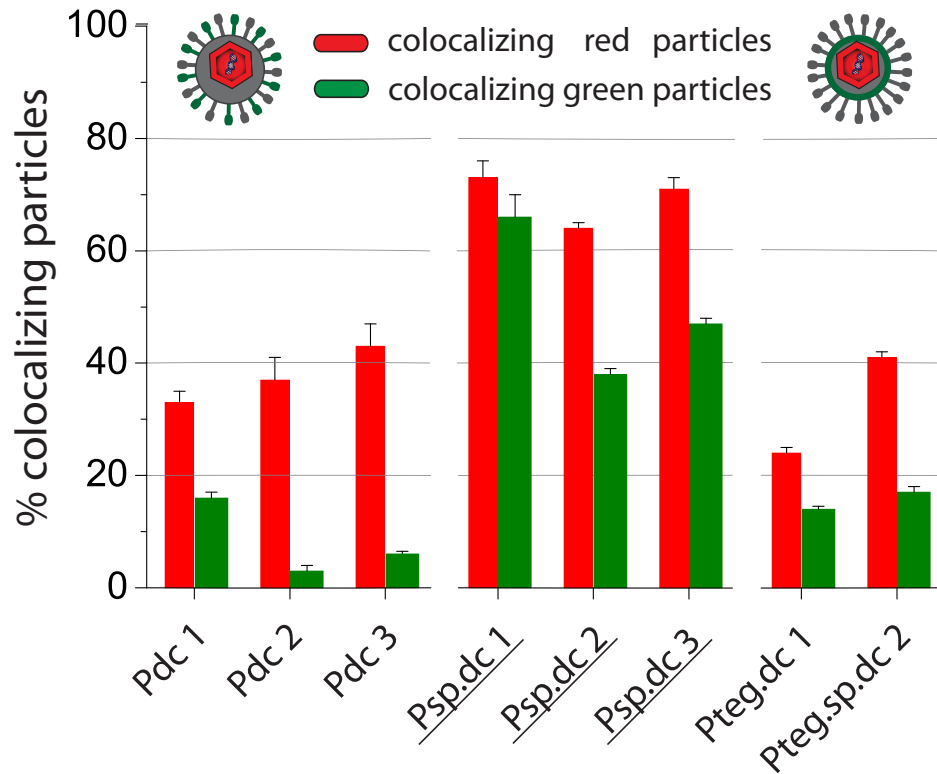
Figure 6.8: *Percentage of dual-color particles in different virus preparations with respect to the total number of RFP-capsid signal (red bars), and relative to the total number of GFP-envelope or -tegument signal (green bars). Error bars represent the standard error of the mean. The three underlined virus preparations were obtained under optimized conditions. The numbers as well as the total sum of analyzed particles are given in the corresponding table 6.1. Pdc - non-spiked dc virus preparation, Psp.dc - spiked dc virus preparation (20 % wt virus), Pteg.xy - non-spiked (dc) or spiked (sp.dc) virus preparations with GFP fused to the tegument instead of the envelope glycoprotein D. The numbers as well as the total sum of analyzed particles are given in the corresponding table 6.1.*

GFP-envelope or GFP-tegument signal (green bars).

Details on the preparation conditions for each virus preparation, as well as the corresponding colocalization percentage, are summarized in table 6.1. Virus preparations contain different abbreviations to indicate the most important conditions of their preparation. Non-spiked dual-color virus preparations contain the abbreviation dc: Pdc, and virus preparations that were spiked with 20 % wild-type virus are indicated by the addition of sp: Psp.dc. All virus preparations with the abbreviation Pdc contain the GFP-tag at the envelope, whereas virus preparation that have GFP fused to the tegument protein VP11/12 are indicated by the addition of teg: Pteg.dc, Pteg.sp.dc. The three virus preparations Psp.dc 1, 2 and 3 were prepped under the optimized conditions

in Vero cells, whereas all other preparations were harvested from BHK cells. For each virus preparation, the colocalization percentage was calculated with respect to the capsid signal, as well as relative to the envelope or tegument signal. The results are given together with the standard error of the mean (SEM) and the total numbers of particles that were counted in the green and red channels (table 6.1).

Table 6.1: *Preparation conditions and corresponding fraction of dual-color particles in obtained HSV-1 preparations. The preparation conditions, such as cell line and whether dc viruses were spiked with wt-virus, are given in the second column. The abbreviation for the different virus preparations are assigned in the following: Pdc - non-spiked dc virus prep, Psp.dc - spiked dc virus prep (20 % wt virus), Pteg.xy - non-spiked (dc) or spiked (sp.dc) virus preparations with GFP fused to the tegument instead of the envelope glycoprotein D. The determined colocalization percentage is given relative to the number of RFP-capsid particles (coloc. red) and relative to the number of GFP-envelope or GFP-tegument (coloc. green), together with the standard error of the mean (SEM). The total number of detected red (capsid) and green (envelope/tegument) particles are listed in addition.*

label of virus prep.	cell line; % wt virus	sum red particles	% coloc. red $\pm$ SEM	sum green particles	% coloc. green $\pm$ SEM
Pdc 1	BHK; 0 % wt	871	33 $\pm$ 2	1,861	16 $\pm$ 1
Pdc 2	BHK; 0 % wt	193	37 $\pm$ 4	2,130	3 $\pm$ 1
Pdc 3	BHK; 0 % wt	253	43 $\pm$ 4	1,892	6 $\pm$ 0.5
Psp.dc 1	Vero; 20 % wt	686	73 $\pm$ 3	753	66 $\pm$ 4
Psp.dc 2	Vero; 20 % wt	1,483	64 $\pm$ 1	2,537	38 $\pm$ 1
Psp.dc 3	Vero; 20 % wt	7,823	71 $\pm$ 2	11,737	47 $\pm$ 1
Pteg.dc 1	BHK; 0 % wt	8,302	24 $\pm$ 1	13,611	14 $\pm$ 0.5
Pteg.sp.dc 2	BHK; 20 % wt	2,578	41 $\pm$ 1	6,078	17 $\pm$ 1

Most dc virus preparations have GFP C-terminally fused to the glycoprotein D. This glycoprotein plays an important role in the fusion process, as gD binding to a cellular gD receptor is required to initiate fusion [12, 232, 233]. More precisely, movement of the C-terminus of gD upon binding to its cellular receptor plays an essential role in triggering the fusion process [170, 182]. Hence, the C-terminal insertion of GFP to gD might reduce the flexibility of the C-terminus and lower the infectivity of these virus particles. The viral titers are given in table 5.1 on page 58. Therefore, our cooperation partners cloned a new virus strain with GFP fused to the outer tegument protein VP11/12. VP11/12 is not essential for infection in cultured cells [351]. However, it is also incorporated into L-particles [65], which still leads to the presence of GFP-only particles in dc virus preparations. The most recent virus preparation that have GFP fused to the tegument protein

VP11/12, showed increased viral titers in comparison to the dc preparations that have GFP fused to gD (table 5.1).

Comparison of the colocalization percentage obtained for the different virus preparations once again confirmed the successful optimization of the preparation conditions. Highest colocalization percentages were obtained for the optimized virus preparations Psp.dc 1, 2 and 3. The fraction of colocalizing red particles was above 60 % colocalization for the optimized preparations, whereas it ranged between 20 % to 50 % for the non-optimized preparations. Although the fraction of colocalizing GFP-tagged envelopes was significantly increased in the optimized virus preparations, there were still a lot of envelope-only particles present in these preparations. These results imply that the colocalization percentage should rather be calculated with respect to the total capsid number, than to the total number of envelope particles.

The latest dc virus preparations have GFP attached to the tegument and are very promising candidates to study virus fusion as they are less attenuated than the corresponding gDGFP-tagged viruses. However, the received virus preparations show a very low colocalization percentage. Only around 25 % or 40 % of the detected red particles were found to colocalize with GFP-tegument signal, and the fraction of colocalizing GFP-particles was even below 20 %. These low colocalization numbers make it difficult to determine changes in the overall colocalization percentage over time due to fusion, as well as lower the chance to detect an individual fusion event. Thus, it would be desirable to prepare these dc tegument preparations also under the optimized conditions in Vero cells. Consequently, this should help us to obtain infectious virus preparations with a high percentage of dual-color viruses.

6.2 Colocalization analysis in live cells

The optimized dc virus preparations in hand were now used to investigate virus entry and fusion in live cells. First, we wanted to get a general overview of the fusogenity possessed by the virus particles and the time-scale at which fusion occurs. Therefore, the colocalization percentage of virus particles was evaluated over time in live cells. Vero cells were chosen for this experiment since fusion at the plasma membrane is reported as the main entry pathway in this cell line [201, 215, 232, 233, 287, 337].

Vero cells were incubated with dc virus particles (preparation Psp.dc 1, table 5.1) at around 4 °C to ensure synchronous binding to the cell surface. Unbound virus particles were removed by several washing steps. Time lapse of virus incubated Vero cells were

recorded with alternating-laser excitation on a spinning disk confocal microscope. The setup is described in detail in subsection 5.2.2 on page 68. The movies were started shortly after warming the cells to 37 °C. An additional movie was recorded, starting about 30 minutes later, to check whether photobleaching plays a role. Every five minutes, a z-stack through the whole cell was taken. The number of dual-color particles throughout the whole cell was determined using the software for colocalization analysis in 3D, which is described in subsection 5.3.3.

Altogether, 13 cells were analyzed. The initial colocalization percentage of the virus preparation was 73 ± 3 % with respect to the total capsid signal. As can be seen in figure 6.9.A, the number of colocalizing capsid particles decreased within 60 minutes from around 60 % to around 30 % - 20 %, corresponding to a reduction of around 50 % of detected dual-color virus particles. After 60 minutes, the colocalization percentage remained more or less constant. The evaluated colocalization percentage of both movies started shortly after the increase in temperature to 37 °C (figure 6.9.A, hatched bars) coincides for the starting values as well as for the observed decay in the colocalization percentage, confirming the reproducibility of the experiment. Moreover, the obtained values for the colocalization percentage around 30 to 40 minutes post binding are in agreement with the movie where illumination was started around 30 minutes later (figure 6.9.A, black bars), implying that the overall decrease in the colocalization percentage was not provoked by photobleaching. A minor effect of photobleaching was observed after one hour post binding as the obtained values are slightly lower for the movie started earlier (figure 6.9.A, black hatched bars) compared to the movie started around 30 minutes later (figure 6.9.A, black bars). However, the colocalization percentage is still in the same range. As presented in figure 6.9.B, the total number of detected particles in the green and red channel decreased over time, which is attributed to degradation of virus particles. The observed decay in particle numbers does not imply decay in the calculated colocalization percentage, as the percentage is independent of the absolute particle number.

The observed decay in the colocalization percentage can be due to separation of capsid and envelope, which would suggest that about 50 % of the dual-color virus particles undergo fusion within the first hour. The decay of detected GFP-envelope particles happens faster than that of the RFP-capsid particles. This may be explained by dilution of the GFP signal in the cellular membrane after fusion and thus, the signal may not be detectable in the presence of the cellular background. A similar observation was reported
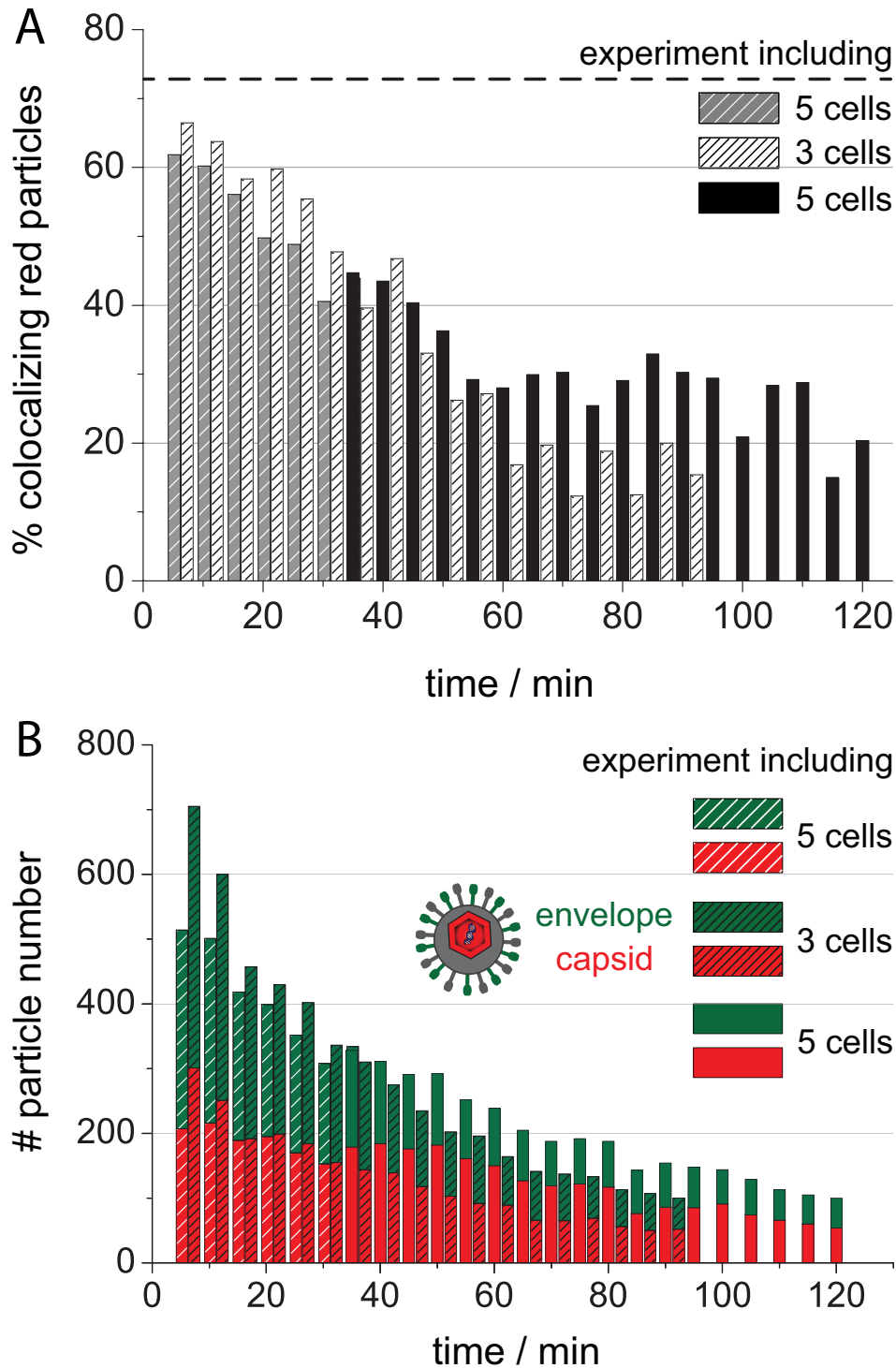
Figure 6.9: *(A) Decrease in the percentage of detected dual-color virus particles over time in live Vero cells. The number of colocalizing RFP-capsid particles was evaluated as a function of time. The dashed line indicates the initial colocalization percentage of the virus preparation. (B) Total number of HSV-1 particles in live Vero cells over time. Signal from detected RFP-capsid particles is drawn as red bars, and the number of detected GFP-envelope particles is shown as green bars. Virus binding was carried out at about 4 °C to obtain a defined starting time-point. The shift to 37 °C was defined as the zero time-point. Confocal microscopy time series with z-stacks throughout the whole cell were started at three different time points with an interval time of five minutes.*

by Koch *et al.* using pseudotyped HIV-1 particles. They reported a loss of the YFP-Env signal of individual virus particles after fusion, which further led to staining of the cell membrane in the case of multiple fusion events [161].

Another explanation could be pH-dependent quenching of GFP in acidic compartments as GFP is pH-sensitive [239, 276, 315]. Quenching of the GFP-envelope signal would lead to an increase of detected "red-only" particles and could therefore provoke the observed decay in the colocalization analysis over time. However, if the decrease in the colocalization percentage is caused by an acidic endosomal pH, this would be an indication that about 50 % of the virus particles are taken up and have reached acidic compartments (e.g. late endosomes) after around one hour.

To clarify whether the observed decay is the result of an efficient fusion process or caused by GFP-quenching, we characterized the pH-dependency of GFP in the viral context.

6.3 pH-dependency of fluorescent proteins in the viral context

In order to investigate the possibility of pH-dependent GFP-quenching in the viral context, quenching experiments with virus-only particles were performed. GFP is attached to the C-terminus of the glycoprotein gD [227] and located inside the viral envelope [170]. Quenching experiments were first performed with disrupted viral membranes to ensure that the GFP inside the viral envelope is directly accessible to protons. To this end, dc virus particles were immobilized and permeabilized with 0.1 % Triton-X to destroy the virus envelope (subsection 5.1.5). Citrate buffer was added at different pH-values as described in 5.1.6. In addition, the pH-dependency of the RFP-tag at the capsid was evaluated.

Background-corrected intensities of ten individual particles were determined over time at several pH-values, ranging from pH 7.0 down to pH 3.3. The corresponding averaged intensity traces are shown in figure 6.10. The intensity traces at neutral pH were measured in PBS buffer and serve as control for bleaching of GFP and RFP (gray lines). The addition of citrate buffer, resulting in a lower pH-environment, was defined as time-point zero in the corresponding plots. A significant decrease in the GFP intensity was already observable at pH 6.0 (figure 6.10.A, blue color). At pH 5.5 (dark cyan color), the GFP intensity dropped immediately down to around 30 % of its initial value at pH 7.0. At lower pH values, all particles were completely quenched. In addition, quenching of GFP was reversible (data not shown). These results show a strong pH-dependency of GFP.
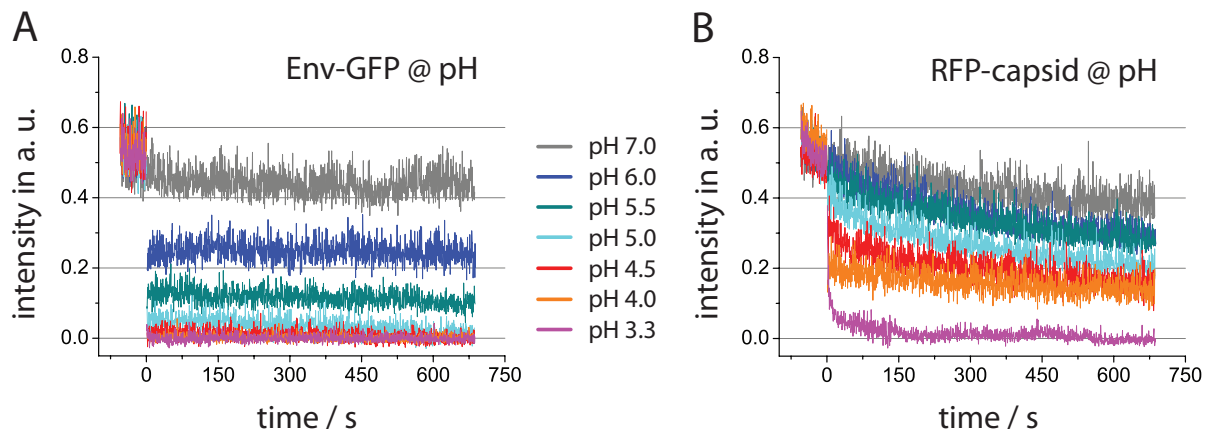
Figure 6.10: *Intensity traces of fixed and permeabilized dc HSV-1 particles at different pH values. Dual-color virus particles were fixed with paraformaldehyde and permeabilized with Triton X-100 to ensure accessibility of the fluorescent proteins to protons. Images were recorded at different pH values, ranging from pH 7.0 down to pH 3.3. The intensity values at neutral pH where measured in PBS and serve as control for bleaching (gray line). The acidic pH-values were obtained by addition of citrate buffer (zero time-point). Background-corrected intensities of ten particles were determined over time and the averaged intensity values are shown. (A) Intensity traces of the GFP-envelope signal of permeabilized dc particles showing a strong pH-dependency. The intensity of the GFP signal was significantly quenched at pH 5.5. At lower pH values, the GFP signal was completely quenched. (B) Intensity traces of the RFP-capsid signal of permeabilized dc particles. Only a minor reduction in the RFP intensity was observed at pH values of 5.5 and above.*

In contrast, the RFP-tag is less pH-dependent (figure 6.10.B). At pH 5.5, only a slight reduction in the RFP intensity was observed in comparison to pH 7.0, whereas the RFP signal was significantly quenched at values below pH 4.5.

In order to study the pH-dependency of virions tagged with fluorescent proteins under the biologically relevant conditions, further experiments were performed with intact virus particles. Therefore, virus particles were adhered on a tissue culture treated coverslip (ibiTreat) without any additional fixation and permeabilization step. Citrate buffer was added at different pH-values and images were recorded under the same illumination conditions as in the case of the fixed virus particles. The obtained intensity traces of GFP-tagged and RFP-tagged virus particles are presented in figure 6.11. GFP-dependent quenching was already observable at pH 6.0 (figure 6.11.A, blue color). At a pH-value of 5.5, the GFP intensity was already significantly quenched, and after ten minutes only around 45 % of the intensity was detectable relative to the value at pH 7.0. At lower pH values, the effect was even faster and more strongly observed. In the case of RFP,

only minor reductions in the intensity were observed for pH values between 6.0 to 4.0 (figure 6.11.B). However, the intensity of the RFP signal was strongly reduced at pH 3.3. Proton concentrations that the virions encounter in late endosomes are typically around $10^{-5.5}$ mol·L^{-1} [136, 211]. Depending on the autofluorescent background of a cell, the reduced intensity of the GFP signal at pH 5.5 may be too low for its detection within late endosomes, whereas the RFP signal should be still detectable.

In light of the GFP-quenching properties, experimental designs are required that deal with the pH-dependency of the GFP-envelope.

6.4 Colocalization analysis in fixed cells

An experimental approach that avoids quenching of the GFP signal in acidic compartments is to use fixed and permeabilized cells. After permeabilization, there are no acidic compartments left and homogenous pH around 7 is ensured throughout the whole cell. Analysis of the 3D colocalization percentage in fixed and permeabilized cell samples, therefore, allows determinination of the fraction of particles that have undergone fusion at certain time points. The analysis is similar to the experiment performed with live Vero cells (subsection 6.2), but any remaining decay in the colocalization percentage over time cannot result from GFP-quenching and must be real.

Vero and HeLa cells were incubated with dual-color virus (virus preparation Psp.dc 3, table 5.1) on ice to allow virus binding. Subsequently, cells were washed to remove unbound virus particles and shifted to 37 °C for different time periods, ranging from 0 hours to 3.5 hours. At the indicated time points after reaching 37 °C, samples were fixed and permeabilized (subsection 5.1.5.2). These samples were provided by our cooperation partners. Z-stacks throughout the whole cell were recorded with alternating-laser excitation on a SDCM (subsection 5.2.2). The colocalization percentage was determined using the 3D colocalization software (subsection 5.3.3) and is given relative to the total capsid number. For each condition, a minimum number of 22 cells and more than 2000 capsid particles were analyzed. In order to estimate the uncertainty of the experiment, 5-6 cells were grouped into one subset. The average colocalization percentage and the standard error of the mean were calculated out of 4-6 cellular data subsets.

The obtained colocalization percentage in Vero and HeLa cells is shown in figure 6.12.A and B, respectively. The initial colocalization percentage of the dc virus preparation used in this experiment was around 71 ± 2 % (relative to the total capsid signal). To verify that no artifact arises for the starting value of the colocalization percentage as
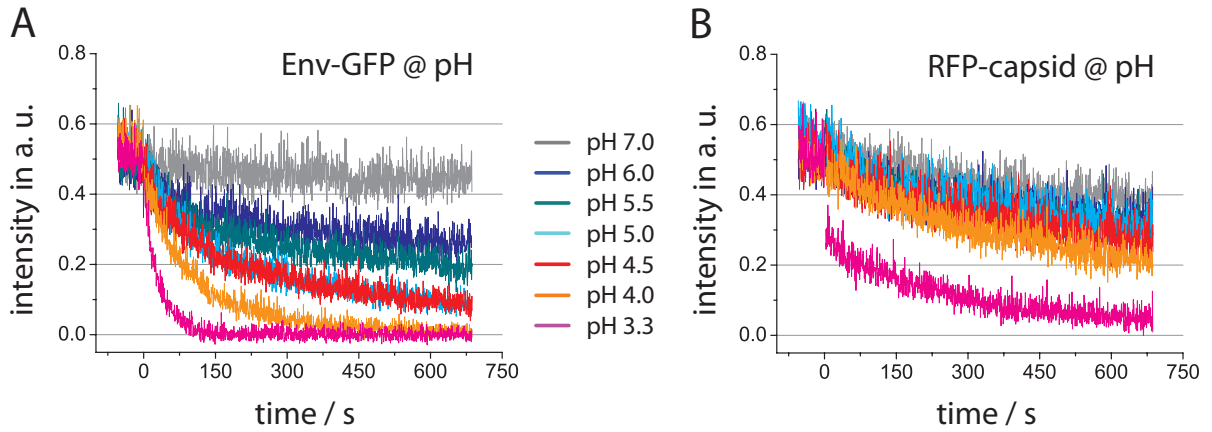
Figure 6.11: *Intensity traces of dc HSV-1 particles at different pH values. Dual-color virus particles were spotted on a tissue culture treated coverslip without fixation and permeabilization. The zero time-point indicates the addition of citrate buffer, resulting in the indicated pH values from pH 6.0 down to pH 3.3. The averaged background-corrected intensities of ten particles are shown. (A) Intensity traces of the GFP-envelope signal of dc particles. The GFP signal from intact virus particles still shows a strong pH-dependency. (B) Intensity traces of the RFP-capsid signal of dc particles. Significant reduction of the RFP intensity was only observed at pH 3.3.*

some virus particles (e.g. capsid-only) may not bind and are removed by washing, we included the zero time-point of virus-incubated cells that were fixed directly in the cold. At this time-point, the obtained value of 69 ± 1 % in HeLa cells is in good agreement with the value determined for the initial virus preparation. In Vero cells, the initial starting value was 65 ± 1 %, which is slightly below the value obtained in HeLa cells. However, no differences among the cell lines are expected for the zero time-point as viruses were incubated on ice, which should prevent endocytosis as well as fusion at the plasma membrane. Therefore, the variation in the determined values gives an estimate of the uncertainety of the experiment. However, if the percentage of colocalizing envelope particles is considered, no differences within the error bars were observed among Vero and HeLa cells at the zero time-point. The fraction of colocalizing envelope particles at the zero time-point was 47 ± 1 % in Vero and 45 ± 1 % in HeLa cells, which is in good agreement with the initial virus preparation (47 ± 1 %, relative to the envelope signal).

In Vero cells, no significant decay was observed with time within the first 3.5 hours post binding. The fraction of colocalizing capsid particles always remained above 60 % (figure 6.12.A). Hence, there is no evidence for fusion in Vero cells from the analyzed data. In contrast, HeLa cells showed a decay from around 69 ± 1 % to 55 ± 3 % colocalization within two hours post binding (figure 6.12.B). After 3.5 hours post binding, a further decrease in the colocalization percentage to 45 ± 2 % was observed.
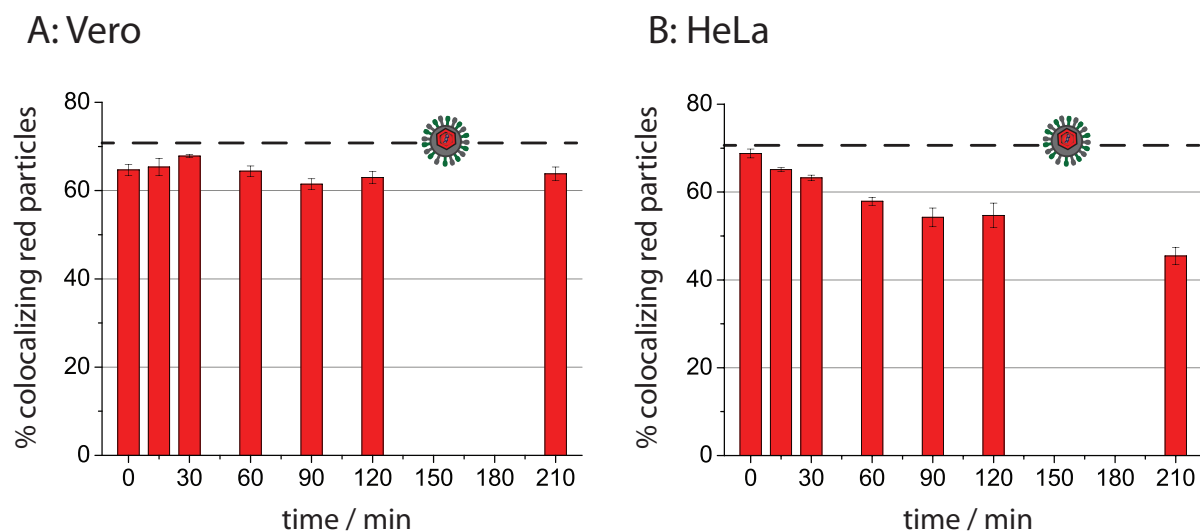
A: Vero

B: HeLa

Figure 6.12: *Fraction of dual-color virus particles at different time-points after virus binding in fixed and permeabilized (A) Vero and (B) HeLa cells. Cells were incubated with virions for different time-periods, ranging from 0 minutes to 3.5 hours post binding. Subsequently, cells were fixed and permeabilized to ensure neutral pH throughout all intracellular compartments. Confocal z-stacks were recorded on a SDCM and the colocalization percentage was analyzed relative to the total number of detected capsid particles. Several cells from multiple samples were recorded for each data point. The dotted black line indicates the colocalization percentage of the initial dc virus preparation.*

The colocalization percentage determined in fixed and permeabilized Vero cells (figure 6.12.A) and the data obtained in living Vero cells over time (figure 6.9.A) show an apparent discrepancy. No differences in the percentage of dc viruses that undergo fusion are expected among the two experiments as both were performed in the same cell line. A reasonable explanation for the significant decay in the fraction of colocalizing RFP-capsid particles in live Vero cells over time (figure 6.9.A) is that the decay resulted from quenching of the GFP-envelope signal in acidic compartments. Quenching experiments with untreated virus particles on a cover-slide (figure 6.11.A) showed that the fluorescence intensity of the GFP-envelope signal is significantly quenched at pH 5.5 or lower values, values which are typically found in late endosomes and lysosomes [136, 208, 211]. Quenching of the GFP-envelope signal of dual-color viruses leads to an increase in the number of detected capsid-only particles and to a lower percentage of detected dual-color particles. Hence, the later the time-points post binding in live cells, the more virus particles have reached acidic compartments and the more capsid-only particles resulting from quenched GFP-envelope signal are detected (figure 6.9.A). Quenching of the GFP-envelope signal is avoided in experiments with fixed and permeabilized Vero cells
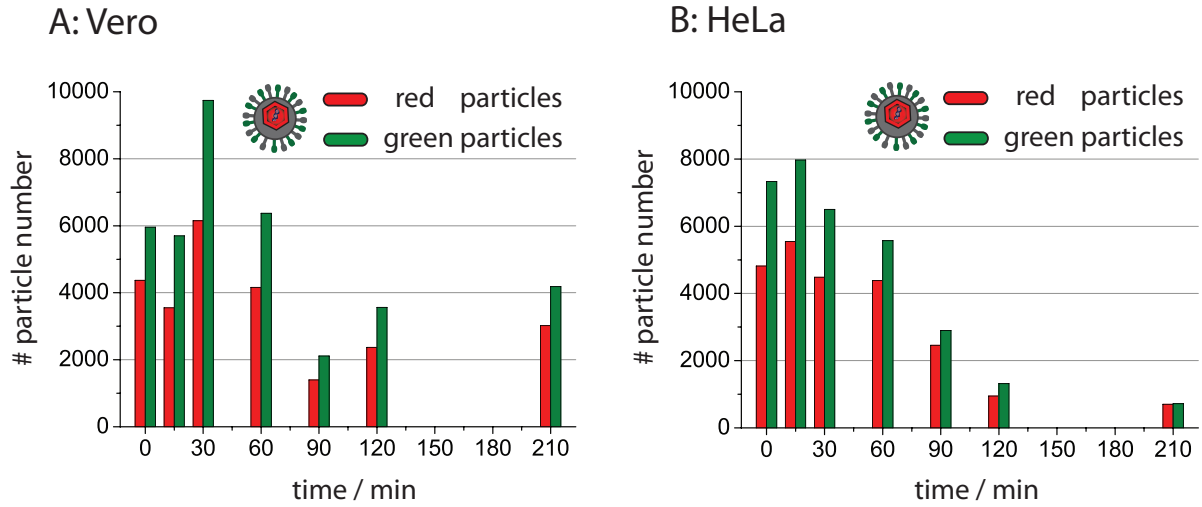
Figure 6.13: *Detected particle numbers of RFP-capsid (red) and GFP-envelope (green) at different time-points after virus binding, ranging from 0 minutes to 3.5 hours, in fixed and permeabilized (A) Vero and (B) HeLa cells. Several cells were analyzed per data point and the sum of particles from one experimental series containing approximately the same number of analyzed cells is plotted for each time-point in order to visualize changes in the detected particle numbers over time.*

since neutral pH is ensured for all cellular compartments and no significant decay in the colocalization percentage over time was observed (figure 6.12.A).

In order to get a general idea of the number of detected particles in fixed Vero and HeLa cells at the different time-points, we analyzed about the same number of cells for each condition. The overall number of detected particles was significantly lower after 1.5 hours or later than during the first hour post binding as shown in figure 6.13. The effect was more prominent in HeLa cells. The observed decay in particle numbers was reproducible, hence, inhomogeneities in sample preparation can be excluded. The reduction in particle numbers is not due to bleaching as illumination was started with the first frame. Therefore, the decrease is assigned to degradation of the virus particles.

The experiment reveals that fusion takes place in HeLa cells, hence, the viruses are able to undergo the fusion process. In contrast, no fusion was observed in Vero cells. This experimental approach allows qualitative analysis of the amount of fusion in different cell lines, but it does not tell where the fusion events took place. In literature, it is reported that fusion in HeLa cells requires endosomal acidification [232], whereas the main entry pathway for HSV-1 in Vero cells is via fusion at the plasma membrane [201, 215, 232, 287, 337]. Whether the higher numbers for possible fusion events in HeLa cells compared to Vero cells are related to the site of fusion or the involvement of different co-receptors remains speculative. In Vero cells, involvement of the gB receptor

non-muscle myosin heavy chain IIA (NMHC-IIA) has been reported [10]. NMHC-IIA mainly functions in the cytoplasm. However, Ari *et al.* reported an enrichment of NMHC-IIA at the plasma membrane of virus incubated Vero cells a few minutes after shifting the temperature from 4 °C to 37 °C [10]. From this observation, one would expect an increase in the number of detected fusion events after preincubation in the cold. Therefore, it is astonishing that no significant amount of fusion was observed in Vero cells. Experimental evidence for the different fusion sites among the cell lines comes from Cryo-EM data and inhibitor studies, that were mainly performed after preincubation of cells with virus particles on ice [201, 215, 232, 287]. Hence, it is not likely that fusion numbers in Vero cells were altered relative to these other experiments due to virus incubation in the cold. Nonetheless, the entry pathway after preincubation on ice might well be somewhat changed relative to the direct addition of virus particles at 37 °C, the biologically more relevant condition. However, as fusion is a rare event, it is beneficial to include a preincubation step at low temperatures to increase the number of surface-bound particles and remove unbound viruses prior to imaging.

The pH dependency of GFP located at the viral envelope can be used to distinguish extra- from intracellular virus particles on cells as is shown in figure 6.14. In this experiment, live Vero cells were incubated with virus particles at 4 °C and washed to remove unbound virus particles. Few minutes after the increase in temperature to 37 °C, a movie was recorded at the wide-field microscope. Figure 6.14 shows an image of a Vero cell with virus particles before and after addition of citrate buffer at pH 4.5 (B and C, respectively). The green encircled particle showed movement with velocities around 0.5 μm·s^{-1}, indicating that the particle was already taken up. The GFP signal of this particle was still detectable after addition of citrate buffer, whereas the GFP signal of most other particles was quenched (e.g. the particle highlighted in magenta), indicating that these were extracellular virus particles. As expected, the RFP signal of these particles was still detectable after addition of citrate buffer.

6.5 Studying influence of pH dependency in live cells

The use of fixed and permeabilized cells is one way to circumvent the issue of GFP-quenching, but it is intrinsically accompanied by a lack of kinetic information on a single-cell level over time. Another possibility to account for GFP-quenching is by using a marker of acidic cellular compartments. In this approach, acidic endosomes are monitored separately with a third color and therefore, experiments can be performed in live
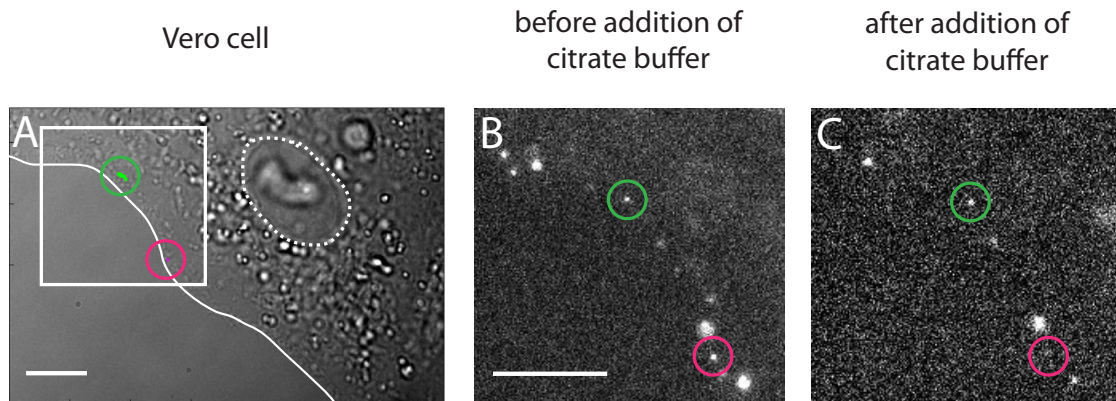
Figure 6.14: *Quenching of the GFP signal of extracellular virus particles on a live Vero cell. (A) Corresponding bright field image of the recorded Vero cell. Nucleus and plasma membrane are highlighted in white. The white box indicates the enlarged area shown in panel B and C. The corresponding trajectory of a non-quenched particle is shown in green and in magenta for a non-moving, quenched particle over a duration of 30 s. (B, C) Images show the GFP-envelope signal of virus particles (B) before and (C) after addition of citrate buffer at pH 4.5. The GFP signal of most particles is quenched after addition of citrate buffer, indicating that these were extracellular virus particles. An exemplary quenched virus particle is highlighted in magenta. The green encircled particle showed rapid movement, indicating that it was already taken up. This presumably intracellular virus particle was still detectable after addition of citrate buffer. Scale bar 10 µm.*

cells.

In order to evaluate whether the GFP signal is still detectable within acidic compartments in live cells, colocalization studies of virus particles were performed together with a marker of endosomal compartments. HeLa cells were used for this purpose, as fusion is dependent on a low pH environment [232]. Hence, virus particles cannot escape from early endosomes and should therefore colocalize with the marker in acidic organelles after a certain incubation period. For this purpose, a specific marker of acidic organelles is best suited such as the commercially available LysoTracker probes, in which the fluorophor is linked to a weak base [219]. At neutral pH, cellular membranes can be permeated, whereas in a low pH environment, the base gets protonated and the LysoTracker is trapped in the membrane of acidic compartments. For experiments with a third color, a fluorophor is required that shows no spectral overlap with the GFP- and RFP-emission of the dc virus particles. Unfortunately, the emission spectra of the commercially available LysoTracker probes does overlap and is therefore not suitable. A fluorophor with a more red-shifted emission spectrum is desirable such as Alexa647. There is no spectral overlap of Alexa647 and GFP and samples can be excited simultaneously with 488 nm and

640 nm to speed up the acquisition time. For the three color experiment, the excitation wavelenghts 488 nm and 640 nm were alternated with 561 nm laser excitation. GFP- and RFP-emission were detected in the same spectral channel, emission of Alexa647 in a second channel. Alexa647 is available as dextran-based fluid phase marker (fpm), which serves as marker of cellular membranes. However, it is not a specific marker of acidic organelles, but is expected to accumulate in late endosomes and lysosomes after a certain incubation period. The incubation period should not last too long, as otherwise the fluid phase marker gets degraded in lysosomes.

In order to evaluate whether fpm dextran Alexa647 can be used as a marker of acidic compartments after four hours of incubation, colocalization experiments were performed together with LysoTracker Red. HeLa cells were incubated with fpm dextran Alexa647 for four hours at 37 °C, and LysoTracker Red was added during the last hour of incubation (subsection 5.1.4.2). The cells were washed several times and z-stacks were recorded with alternating-laser excitation on a SDCM (subsection 5.2.2). Extensive colocalization of fpm dextran Alexa647 with LysoTracker Red was observed as can be seen in figure 6.15. Around 96 % of all detected compartments labeled with fpm Alexa647 were found to colocalize with LysoTracker Red. Occasionally, compartments were detected that contained only fpm dextran Alexa647 but no LysoTracker Red. The pH values found in these compartments are probably above pH 5.5. The other way around, approximately 90 % of all detected compartments labeled with LysoTracker Red contained an additional fpm dextran Alexa647 signal. A few acidic compartments were not labeled with fluid phase marker. Hence, fluid phase marker dextran Alexa647 can be used as marker of acidic compartments in HeLa cells after four hours of incubation, with the limitation that few acidic compartments remain unlabeled.

Having established fpm dextran Alexa647 as marker of acidic organelles, colocalization experiments were performed together with dc virus particles in HeLa cells (virus preparation Psp.dc 2, table 5.1). HeLa cells were pretreated with dextran Alexa647 at 37 °C as above and dc virus particles were incubated during the last one to two hours. A relatively long incubation period with virus particles was chosen to ensure that viruses had enough time to reach acidic compartments. Afterwards, cells were washed to remove unbound virus particles and extracellular fpm dextran Alexa647, which otherwise would increase the background signal dramatically. Confocal z-stacks of the virus incubated cells were recorded with a SDCM. The intracellular distribution of the GFP, RFP and Alexa647 signals was investigated to elucidate whether the GFP signal is still detectable in acidic compartments. Exemplary images are given in figure 6.16. The GFP and RFP signals of
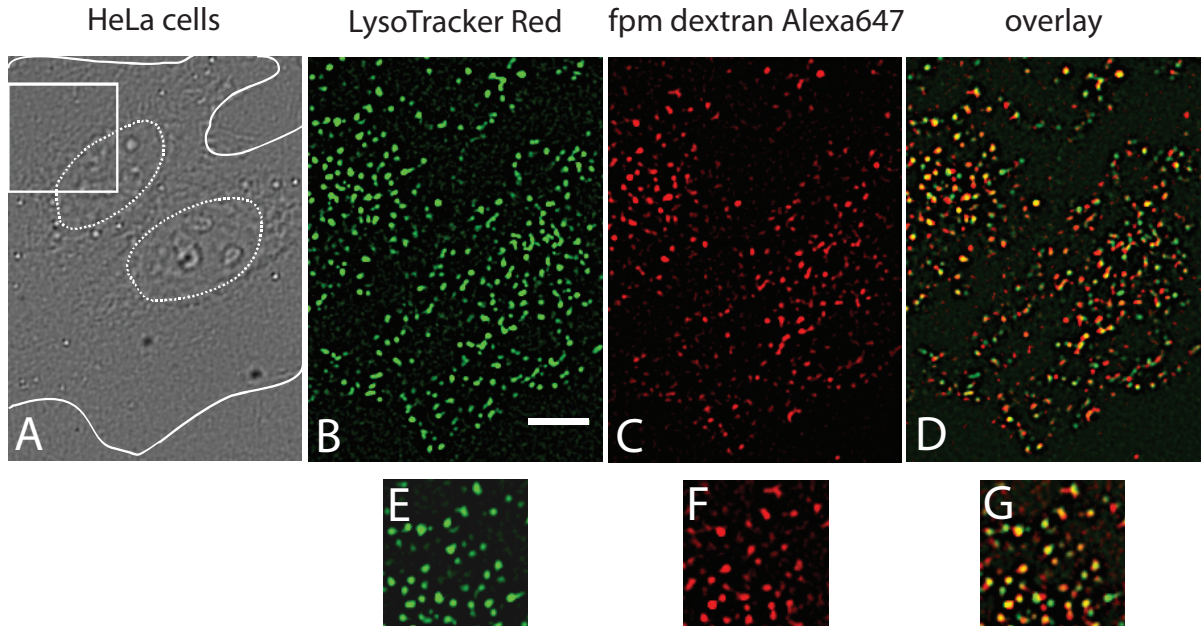
Figure 6.15: *Conditions for the use of fluid phase marker as a marker of acidic cellular compartments. HeLa cells were incubated with fpm dextran Alexa647 (red color) for four hours, and co-incubated with a specific marker of acidic organelles, Lyso-Tracker Red (green color). (A) Bright field image of the recorded HeLa cells. Nuclei and plasma membrane are highlighted in white. Fluorescence signal of (B) LysoTracker Red and (C) fpm dextran Alexa647 were recorded with alternating-laser excitation on a SDCM. (D) Overlay of images B and C. Colocalizing spots of fluid phase marker with LysoTracker Red appear in yellow color. The high percentage of yellow spots attests that fpm dextran Alexa647 is mainly a marker of acidic compartments after four hours of incubation in HeLa cells. Figures (E), (F) and (G) correspond to panels B - D, respectively, showing an enlarged image of the area that is indicated by the white box in D. Scale bar 10 μm.*

the dc virus particles are visualized in green and red color, respectively. Signal from fpm dextran Alexa647 is shown in blue color. Double-tagged virus particles, capsid-only and envelope-only particles were detected together with fpm dextran Alexa647, as well as in some cases without the additional Alexa647 signal (figure 6.16.D). For each of these different color combinations, the number of colocalizing particles was evaluated. The absolute particle numbers, which were withdrawn from two movies recorded after 75 and 110 minutes post binding, are plotted in figure 6.17.
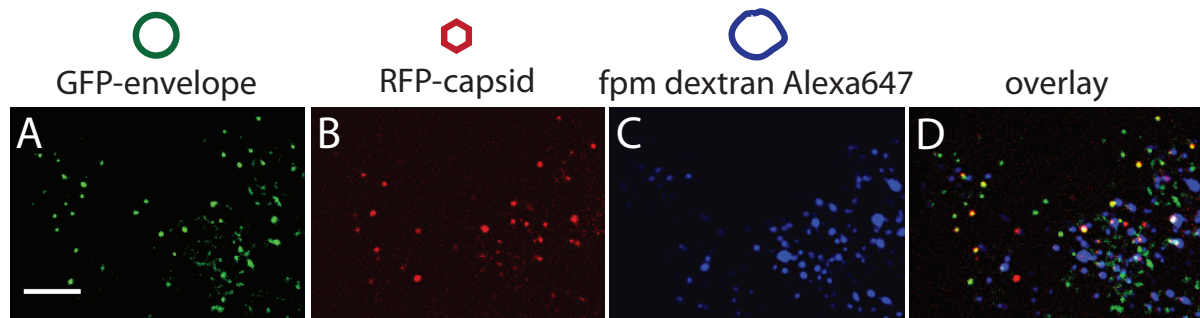
Figure 6.16: *Triple colocalization experiment of dc HSV-1 with fpm in live HeLa cells. HeLa cells were incubated with fpm dextran Alexa647 for four hours, and dc viruses were added during the last two hours of incubation. Confocal z-stacks were recorded on a SDCM. For clarity, a corresponding z-projection of three slices taken from the middle of the cell is shown. Fluorescence signal of (A) GFP-envelope (green color) and (B) RFP-capsid (red color) were recorded in the same channel with alternating-laser excitation. Fluorescence signal of (C) fpm dextran Alexa647 (blue color) was detected in a separate channel. (D) Overlay of panels A - C. Double-tagged virus particle appear in yellow color, and in white if they are additionally colocalizing with fpm. Capsid-only or envelope-only particles remain in red or green color, respectively. Scale bar 10 µm.*

In the initial virus preparation, 64 ± 1 % of the RFP-capsid particles were found to colocalize with GFP-envelope signal. The value of the initial colocalization percentage is indicated in the plot by a dotted black line (figure 6.17). From the movies, a total of 160 particles contained an RFP-capsid signal (100 %). Thereof, 39 particles contained an additional GFP-envelope signal, corresponding to 24 % of double-tagged virus particles (total dc virus). Only a minor fraction of 15 double-tagged particles (9 % of all capsid particles) were observed together with fluid phase marker (dc virus + fpm). The vast majority of capsid particles neither colocalized with GFP-envelope signal nor with fpm dextran Alexa647, yielding 54 % of capsid-only particles. However, 22 % of capsid-only particles were found to colocalize with fpm dextran Alexa647 (capsid + fpm). This number could result from (i) capsid-only particles still present in the initial virus preparation ($\sim$ 36 %) and taken up by the cell, (ii) from dc viruses with quenched GFP-envelope signal, assuming that the capsid-only particles detected together with fluid phase marker were in acidic compartments or capsid-only particles colocalizing with fluid phase marker resulting from fusion. The last explanation is unlikely as the capsid-only particles were still observed inside an endosome. Taking into account the most likely quenching of GFP signal in acidic compartments (explanation (ii)) the correct number of dc particles will be somewhat higher than the observed 24 %. To estimate this number, the maximal number of possible dc viruses was calculated out of all detected dual-color virus particles (dc virus - fpm, dc virus + fpm) and the capsid-only particles colocalizing with
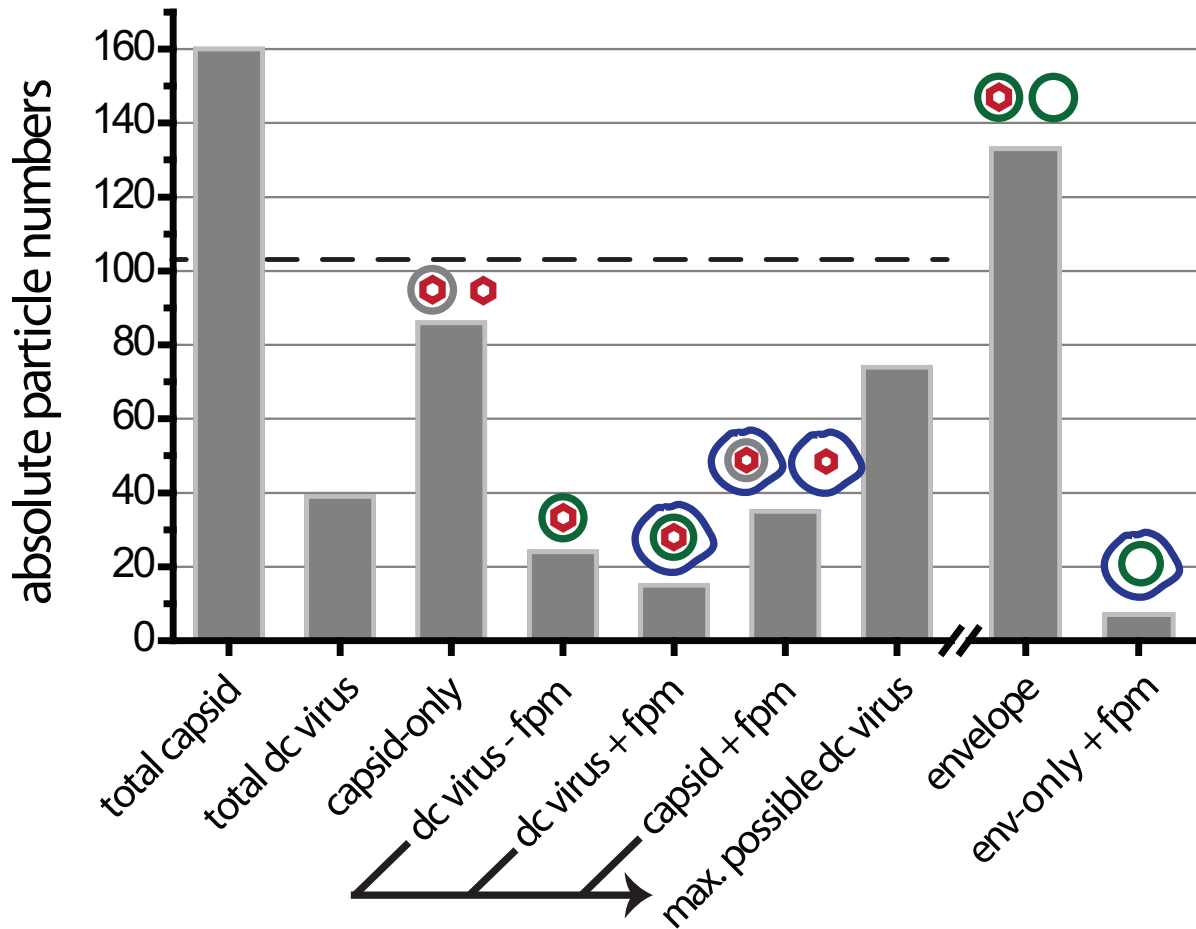
Figure 6.17: *Evaluated particle numbers of the triple colocalization experiment with dc HSV-1 and fluid phase marker in live HeLa cells. Confocal z-stacks of HeLa cells were analyzed for colocalization of capsid (red), envelope (green) and fpm (blue). Absolute particle numbers are given, which were obtained from two movies after 75 and 110 minutes post binding. The number of all detected capsid particles, as well as of all detected dc viruses, are given in the first two bars (total capsid, total dc virus). Capsid-only particles have a capsid signal that neither colocalized with GFP-envelope nor fpm. Detected dc virus particles were further differentiated depending on whether or not they colocalized with fpm (dc virus - fpm) or whether triple colocalization was observed (dc virus + fpm). Capsid particles colocalizing with fpm but not with GFP-envelope are plotted in the sixth bar (capsid + fpm). The sketches above the bars indicate different combinations, which would lead to the same observation. On some occasions, the virus envelope is drawn in gray color to illustrate putative GFP-quenching in acidic organelles, and hence, these actual dc virus particles would only show an RFP-capsid signal. Therefore, the number of maximal possible dc virus was estimated out of (i) dc viruses without fpm, (ii) dc viruses with fpm, and (iii) the number of capsid particles colocalizing with fpm. These capsid + fpm particles may, in part, result from dc viruses with quenched GFP-envelope signal. The dotted black line indicates the fraction of colocalizing capsid particles expected from the initial dc virus preparation. Please note that the estimated number of max. possible dc virus is still below the colocalization percentage of the initial virus preparation.*

fpm (capsid-only + fpm). That is all capsid-only particles colocalizing with fluid phase marker were assumed to be dc particles. The correct dc particle number will be a bit below the estimated maximum, since some of the capsid-only + fpm particles are true capsid-only particles from the virus preparation. The percentage of possible dc viruses was estimated around 46 %, which is below the initial colocalization percentage of about 64 % of the virus preparation.

Regarding the GFP signal, 133 envelope particles were detected in total. Only about 17 % of the detected envelope particles were found to colocalize with fpm dextran Alexa647 (env + fpm, dc virus + fpm). The estimated number of dc virus particles one to two hours post binding is below the initial value of the virus preparation. Hence, this data imply that fusion takes place in HeLa cells. The number of fused virus particles may even be underestimated, as it is only possible to calculate a maximum number of possible dc virus particles. Furthermore, there are about 54 % of capsid-only particles present that do not colocalize with fluid phase marker. These capsid-only particles are probably not in acidic compartments and therefore GFP-quenching should not play a role, *id est*, the particles are assumed to be true capsid-only particles without any quenched GFP-envelope. However, a few acidic compartments are not labeled with fpm dextran Alexa647 (figure 6.15) so that the percentage of true capsid-only particles may be slightly below the observed 54 %. Thus, we assume that the residual capsid-only particles either have undergone fusion or result directly from capsid-only particles present in the virus preparation. The inital virus preparation contained only about 36 % capsid-only particles. This clearly indicates that fusion has occurred, in particular since some of the initial capsid-only particles will be observed in the fraction of capsid-only particles colocalizing with fluid phase marker.

To compare all the results where kinetics of virus fusion have been measured by colocalization analysis of RFP-capsid and GFP-envelope signals, let us go back to the previous experiments.

First, we compare the experiments where quenching of the GFP-envelope signal was taken into account. In experiments with fixed and permeabilized cells (figure 6.12), quenching of the GFP-envelope signal was avoided by ensuring neutral pH through permeabilization of cellular membranes. In the three color experiment (figure 6.17), quenching was taken into account by using an additional marker to highlight acidic compartments. The initial colocalization percentage of the virus preparations used in the two experiments were different as was evaluated with virus particles on coverslips (table 6.1, Psp.dc 3 and Psp.dc 2). In order to compare the number of dc particles that have fused, the percentage of fused dc viruses is given relative to the total number of dc particles

present in the virus preparation. The experiment with fixed and permeabilized HeLa cells (figure 6.12.B) yielded about 55 % of dual-color particles after two hours, whereas only 71 % of dc particles were present in the inital virus preparation. This suggests that 23 % of all detected dual-color particles have fused after two hours post binding in HeLa cells. In the three color experiment, the percentage of dual-color particles was estimated to around 46 % by taking into account red-only particles with putatively quenched GFP-envelope signal (figure 6.17, total dc virus, capsid + fpm). Approximately 64 % of dc particles were present in the initial virus preparation, indicating that 28 % of all dc viruses have undergone fusion. Consequently, both experiments reveal that fusion takes place in a small fraction of HeLa cells. The results are consistent among the different experiments if quenching of the GFP signal is considered. For real-time experiments, one has to keep in mind that the probability to detect a fusion event does not only depend on the fraction of dc particles that fuse but also on the percentage of dc particles present in the virus preparation.

If we do not account for pH-dependent quenching of the GFP-envelope signal, let us go back and compare the experiment in live Vero cells (figure 6.9.A) with the results of the three color experiment in HeLa cells, assuming that the rate of endocytic uptake is similar in both cell lines. The three color experiment offers the advantage that we (i) obtain the number of detected dc particles in live cells that is lowered by quenching of the GFP-envelope signal and (ii) we can estimate the total number of dc particles by considering quenching in acidic compartments labeled with fpm. In the experiment with live Vero cells (figure 6.9.A), about 20 % of dc particles were detected after two hours post binding. The initial colocalization percentage of the virus preparation was approximately 73 % (table 6.1, Psp.dc 1). Hence, around 73 % of all dc particles had no detectable GFP-envelope signal after two hours post binding. In the three color experiment, around 24 % of dc particles (figure 6.17, total dc virus) were observed after two hours post binding compared to 64 % of dc particles present in the initial virus preparation and thus, around 63 % of all dc particles contained no detectable GFP-envelope signal any more. The loss of the detectable GFP-envelope signal may be due to fusion and quenching of the GFP signal in acidic compartments.

Around 65 % of all dc particles contained no detectable GFP-envelope signal after two hours post binding in experiments not accounting for quenching of GFP, whereas in experiments circumventing GFP-quenching, only around 25 % of all dc viruses have fused. The difference between these two type of experimental analysis is striking and implies together with the quenching experiments with virus particles on coverslips (figure 6.11.A), that the loss of the GFP-envelope signal is mainly due to quenching of the fluorescence intensity in acidic compartments. The issue of GFP-quenching is fur-

ther emphasized by the fact that less GFP-envelope particles than RFP-capsid particles were detected in the three color experiment, although more GFP-envelope particles were present in the initial virus preparation (table 6.1, Psp.dc 2). Only a few GFP-envelope particles were found to colocalize with fluid phase marker, whereas the vast majority of detected GFP-envelope particles did not colocalize with fpm. The data reveal that the vast majority of GFP-envelope signal encountered in acidic endosomes cannot be detected within the cellular background. Altogether, these results strongly indicate that GFP-quenching is a crucial issue in imaging, though tools were presented how this issue can be addressed.

6.6 Analysis of individual HSV-1 trajectories

To gain more insights into the entry pathway of HSV-1 on a single particle level, experiments were performed during the first hour post binding of virus particles to live Vero cells. Movies were recorded with high time resolution using the spinning-disk confocal microscope (subsection 5.2.2). Virus particles having GFP attached to the tegument and mCherry to the capsid (ChVP26-VP11/12GFP, preparation Pteg.dc 1, table 5.1) were chosen, as these particles showed a five to 100-fold higher viral titer, although only a small fraction of 25 % of dual-color particles were present in these preparations. First, live Vero cells were incubated with virus particles at around 10 °C to allow attachment to the cell surface without being taken up. Before the experiment, cells were washed to remove unbound virus particles and then warmed to 37 °C (zero time-point). This defined shift to 37 °C, a temperature allowing virus uptake and fusion, helps to synchronize the virus uptake. Movies were either started few minutes after reaching 37 °C or about 40 minutes later and recorded over a duration of 20 minutes. In order to acquire movies with high time resolution and to avoid an offset between particle positions in the green and red channels, which otherwise would complicate the analysis of individual fusion events, samples were simultaneously excited with 488 nm and 561 nm. Thus, we do no longer have an autofluorescence channel. Only cells were selected with a low level of autofluorescence as was validated with 488 nm excitation before recording a movie and as we are tracking, autofluorescent cellular structures are less of a problem. To obtain the whole 3D volume of the cell, around 20 to 25 planes were recorded with a z-distance of 300 nm and an exposure time of 130 ms per frame, resulting in typical interval times between 4 to 5 s. The recorded image series were analyzed to determine three-dimensional virus trajectories. A colocalization analysis of the tracked particles was performed in 3D using the TrIC software described in subsection 5.3.5 on page 75.

Low virus concentrations, ranging between 20 to 70 capsid particles per cell, were utilized to avoid saturation of the cell surface and model biologically relevant conditions. Low virus concentrations simplify the tracking procedure and minimize tracking errors due to crossing particles. Altogether, a total of 570 capsid and 790 tegument particles were detected. Thereof, only about 120 particles contained both labels, which is consistent with the low colocalization percentage of the initial virus preparation (24 ± 1 % of colocalizing capsid particles). All dc particles exhibiting movement were tracked, yielding a total of 64 trajectories. The analysis of an exemplary trajectory of a dual-color particle is shown in figure 6.18. A bright field image of a Vero cell is overlaid with the corresponding z-projection of the virus trajectory (figure 6.18.A). The particle is located in vicinity to the nucleus (panel A, white dashed circle). The virus exhibited movement over small distances and the trajectory, shown in yellow color, almost looks like a dot (panel A). Instantaneous velocities were mainly below 0.1 μm (panel Bii), suggesting that the particle was still bound to the plasma membrane [18, 271]. As expected for a dual-color particle, the cross-correlation amplitude (panel Biii, blue) is always above the threshold criteria (gray) determined by randomization of the GFP channel (black). The values for the cross-correlation amplitude are smaller at the end of the track as the GFP-tegument and mCherry-capsid signals photobleach over time (panel Bi). The relative distance between capsid and envelope is within the localization accuracy of the measurement (80 nm) and no significant increase in the relative distance was observed (figure 6.18.Biv), confirming the colocalization of the envelope and capsid signals throughout the whole trajectory. The colocalization of the two signals can also be seen in the corresponding images in panel C.

Out of the 64 virus trajectories, no fusion event was detected. Fusion would be detectable by the separation of the capsid and envelope signals which would result in a drop in the cross-correlation amplitude (below the threshold criteria, gray line in figure 6.18.Biii) as well as in an increase in the relative distance between the two signals. The increase in the relative distance is depending on whether capsid and envelope remain closer together or e.g. the capsid is transported away from the site of fusion, which would result in a large increase in the relative distance.
The probability to detect a fusion event within the 20 minutes of the movie duration can be estimated below a couple of per cent from the analysis on a single-particle level with the given virus preparation. This result matches with the previous analysis of a somewhat different virus construct (RFPVP26-gDGFP) in fixed cells (section 6.4), which revealed that only a small fraction of viruses undergoes fusion. In the experiment with fixed cells, virus particles had GFP fused to the glycoprotein gD which plays an

important role during virus fusion [12, 232, 233]. Binding of gD to its cellular receptor leads to conformational changes in gD that require the flexibility of the C-terminus and are essential for activating the fusion process [170, 182]. Further studies with mutant viruses having insertions or substitutions in their C-terminal region of gD revealed that these viruses were unable to mediate fusion, although receptor binding was unaffected [45, 127, 347]. In the case of the RFPVP26-gDGFP virus, GFP is fused to the C-terminus of gD, which probably reduces the flexibility of the C-terminus and accounts for the lower infectivity of these virus particles. Therefore, our cooperation partners prepared new viruses having GFP fused to the outer tegument protein VP11/12. VP11/12 is not essential for infection in cultured cells [351] and these preparations showed higher viral titers (table 5.1 on page 58). These virus particles were chosen for the analysis of individual fusion events as a higher fraction of dual-color viruses is expected to undergo fusion. However, the initially low fraction of dual-color particles reduces the chance to observe individual fusion events. To obtain a higher probability for the detection of virus fusion, the colocalization percentage of these preparations needs to be increased. Our collaborators did not prepare the dual-color virus with GFP fused to the tegument under the optimized conditions. It would be desirable to do these virus preparations under the optimized conditions (section 6.1) in order to obtain infectious virus particles with a high colocalization percentage.

The majority of the virus particles were either green- or red-only particles. Due to the high number of single-colored viruses, occasionally green- and red-only particles were located close to each other in the experiment as can be seen in figure 6.19. When two distinct particles are located next to each other and separate with time, this may appear similar to virus fusion. Therefore, an adequate analysis method is required that allows to distinguish between (i) true fusion events and (ii) particles located accidentally close to each other and then moving further apart. The analysis of such as critical event is shown in figure 6.19. A bright field image of a Vero cell is overlaid with the corresponding z-projection of the virus trajectories of the green- and red-only particles located next to each other (figure 6.19.A). The two particles clearly did not colocalize at the beginning of the movie (panel B, 0 min, highlighted by a white circle). A displacement in the particle's position between the two channels due to movement can be excluded as movies were recorded with simultaneous excitation. The channels were mapped onto each other so that there was no offset between the two channels as can be seen from the example of the fully colocalizing particle in panel B, highlighted by a yellow box. In figure 6.19, panels Ci and Di, the background-corrected intensity values are plotted for the GFP-tegument
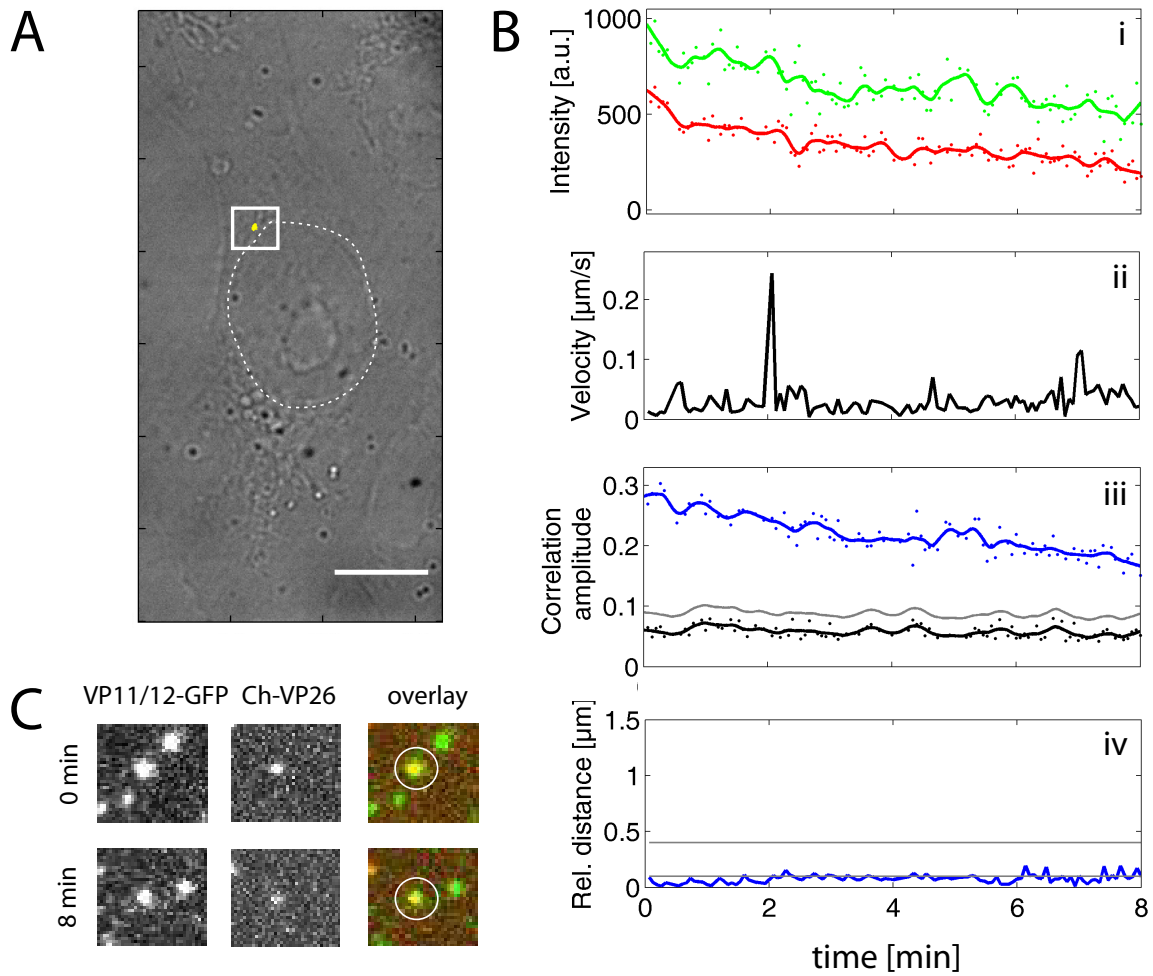
Figure 6.18: *Dual-color HSV-1 trajectory close to the cell surface. Vero cells were incubated with HSV-1 particles at low temperatures. After warming the cell to 37 °C, images of z-stacks (20 planes) were recorded on a SDCM with an interval time of 4.0 s. The results of the single virus tracking and 3D colocalization analysis are given in panels (A)-(C). (A) Bright field image of a Vero cell with overlaying virus trajectory showing movement at the cell surface. The white box indicates the area shown in C. (B) Results of the TrIC analysis along the virus trajectory: (i) the intensity of the GFP-tegument (green) and mCherry-capsid (red) signals, (ii) the instantaneous velocity of the capsid, (iii) the cross-correlation amplitude (blue) together with the determined threshold (gray) out of the negative control (black), and (iv) the relative distance between the GFP-tegument (green) and mCherry-capsid (red) signals. (C) Images of selected time points at the beginning and at the end of the track. Z-projections are given for the GFP-tegument (VP11/12-GFP) and the mCherry-capsid (Ch-VP26) channels together with the corresponding overlay. The tracked dc particle is highlighted in white in the image overlay. The selected images have a width of 5 μm. Scale bar 10 μm.*

and mCherry-capsid signals of the tracked green- and red-only particles together with the corresponding background-corrected intensity values in the second channel in an area of 9×9 pixel^2 around the tracked particle. In each case, only the analyzed particle shows intensity values above the background level, whereas in the corresponding second channel, the intensities are at the level of the background. In the case of a dual-color virus, the intensity values of both channels are above the background level (figure 6.18.Bi). Hence, the analysis of the corresponding intensity values in the second channel confirms that we tracked two distinct green- and red-only particles. Another clear signal that the green- and red-only particles move independently of each other are the different values of the instantaneous velocities (figure 6.19.Cii and Dii, respectively). The red-only particle exhibited movement with higher velocities compared to the green-only particle. The obtained values of the cross-correlation amplitude (panels Ciii and Diii) are the same for both particles as in principle, it makes no difference whether the first channel is correlated with the second channel or *vice versa*. In the beginning of the trajectory, the cross-correlation amplitude (blue) is above the threshold criteria (gray), which would indicate colocalization of the two particles. After about nine minutes, the values of the cross-correlation amplitude drop below the threshold criteria, which would indicate fu-

---

Figure 6.19 *(facing page)*: *Analysis of the trajectories of two red- and green-only particles that are located close to each other. Images of z-stacks (24 planes) of virus-incubated Vero cells were recorded on a SDCM with an interval time of 4.8 s. The results of the single virus tracking and 3D colocalization analysis are given in panels (A)-(D). (A) Bright field image of a Vero cell with overlaying virus trajectories of the GFP-tegument (green) and mCherry-capsid (red) particles. Nucleus and membrane boarders are highlighted in white. The white box indicates the region shown in B. (B) Images of z-projections are given for the GFP-tegument (VP11/12-GFP) and the mCherry-capsid (Ch-VP26) channels together with the corresponding overlay for selected time-points along the trajectories. The tracked particles are highlighted in white in the image overlay and were located close to each other at the start of the movie (0 min). The yellow box highlights a fully colocalizing particle, confirming that there is no offset between the two channels. (C, D) Results of the TrIC analysis along the virus trajectory of the (C) green and (D) red particles: (i) the intensity of the GFP-tegument (green) and mCherry-capsid (red) signals, (ii) the instantaneous velocity of each particle, (iii) the cross-correlation amplitude (blue) together with the determined threshold (gray) out of the negative control (black), and (iv) the relative distance between the GFP-tegument (green) and mCherry-capsid (red) signals. Scale bar 5 μm.*
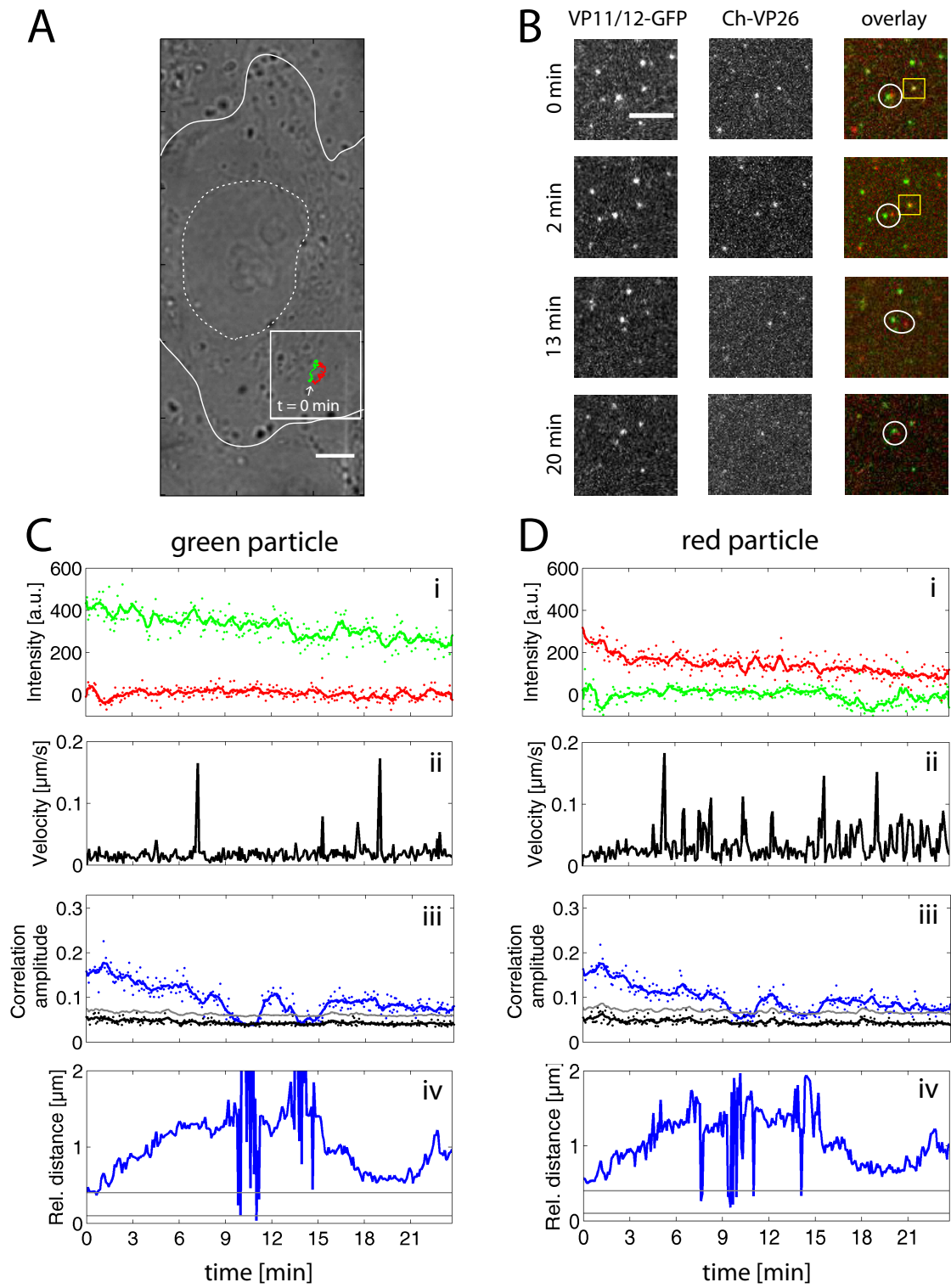
sion. From 15 minutes onwards, the cross-correlation is above the threshold criteria. The obtained values from 15 minutes on are lower than in the beginning of the trajectory as the GFP-tegument and mCherry-capsid signals photobleach over time. The image cross-correlation is performed around an area of 21×21 pixel^2 in x and y and the whole z-stack along the tracked particle. As long as there is a particle within this area in the second channel, the cross-correlation amplitude will be above the threshold. When the particles move further apart, the value drops below the threshold criteria. Considering only one criteria can be critical to correctly distinguish between (i) true fusion events and (ii) particles located accidentally close to each other. As an additional criteria, the position of the peak of the image cross-correlation is taken into account. The position of this peak reflects exactly the relative position between the peaks in the first and the second channels and is plotted as relative distance in panels Civ and Div. In the case of a fully colocalizing particle, the relative distance between capsid and envelope signals is within the localization accuracy of the measurement (80 nm)(figure 6.18.Biv). The relative distance between the analyzed green- and red-only particles is above 400 nm, confirming that the particles did not colocalize at the start of the movie. After about six minutes, the distance between the particles increased to around 1.5 μm (figure 6.19.Civ and Div). After 18 to 21 minutes, the two particles were again located closer together. The variation in the distance between the green- and red-only particles can also be seen in the images in panel B. The spikes in the relative distance (panels Civ and Div), e.g. between nine to twelve minutes, are a result of random particles that show up in the analyzed area and are brighter than the particle of interest. Overall, the two particles moved about each other over a duration of 20 minutes, indicating that they were confined in the same area. Moreover, the particles showed movement with an underlying flow, resulting from movement of the cell.

In order to detect individual fusion events, one needs to ensure that the particles exhibited clear colocalizing movement over several seconds prior to the final color separation. A high colocalization percentage of the virus preparation increases the chance to observe fusion and narrows the possibility that green- and red-only particles are accidentally located in the same cellular compartment, which complicates the analysis. However, the TrIC software is able to correctly identify such a critical event of two particles close by, taking into account all the information obtained by the image cross-correlation analysis.

7 Study of foamy virus entry

Foamy virus are promising vectors for application in gene therapy. They can infect animals and human beings but no disease associated with infection has been reported. Prior to their development and application as therapeutic agents, it is crucial to understand how cells are infected by this virus. Many aspects of the entry process remain to be elucidated. It is not yet clear whether foamy virus can directly fuse at the plasma membrane or only with an endosomal membrane after endocytic uptake.

By means of fluorescence microscopy, the entry and fusion process of double-tagged foamy virus particles can be studied in detail. To investigate if fusion takes place and at which time point most fusion events are expected, an analysis of many virus particles at a time were performed on a single-cell level. Subsequently, experiments were performed with high time resolution to investigate individual fusion events in real-time. We addressed questions such as (i) how soon after virus addition can the first fusion events be observed?, (ii) are there differences observed in the fusion process depending on the site where fusion takes place (plasma membrane vs. an endosomal membrane)?, (iii) how long does the fusion process take? and (iv) what characteristics are associated with the fusion process? Thereby, a novel intermediate phase in the fusion process of foamy viruses was identified. This intermediate phase can be described by dancing of the capsid and envelope signals around each other, prior to their final separation.

The investigation of foamy virus entry was conducted in cooperation with Dr. Kristin Stirnnagel and Prof. Dr. Dirk Lindemann, a virological group in Dresden. Preparation of the virus particles and characterization were done in their laboratory. The live-cell imaging experiments focusing on single fusion events were performed here in Munich together with Dr. Kristin Stirnnagel as well as Dr. Aurélie Dupont and Florian Perrotton from the group of Prof. Don Lamb, PhD.

7.1 Characterization of viral particles

The goal of this project is to investigate virus entry and fusion by fluorescence microscopy, similar to our experiments on HSV-1 (chapter 6). Virus particles are required that contain two different fluorophores, one located on the envelope and one at the capsid. In this case, virus fusion can be detected by separation of the envelope and capsid signals. Investigation of virus entry and fusion requires infectious particles which are functional in virus entry, fusion and intracellular transport to the site of replication. Moreover, it is crucial to really obtain double-tagged virus particles, connoting a high percentage of viruses with colocalized capsid and envelope signals.

Taken into account the fact that fusion is a rare event, which has been rarely observed for viruses in real time, this becomes even more important. A high percentage of dual-color virus particles increases the chance to observe individual fusion events.

The clearest signal for fusion is the direct observation of the separation of the capsid and envelope signals in real time. Fusion can also be detected by a decrease in the average colocalization percentage over time. As we saw earlier (chapter 6), one has to ensure that this decrease is not provoked by quenching of the fluorescence intensity in acidic cellular compartments. For all different virus preparations, the percentage of colocalized capsid and envelope signals was determined. Furthermore, I investigated whether the fluorescence intensity

Figure 7.1: *Foamy virus structure with mCherry (Ch) at the envelope glycoprotein (Env) and the capsid composed of Gag-eGFP.*

of the virus particles tagged with fluorescent proteins changes upon decrease in the pH value encountered in live cells.

All dual-color FV particles used throughout this work were C-terminally tagged with eGFP at the Gag shell (Gag-eGFP) and had an mCherry-tag at the N-terminus of Env (Ch-Env), their location is illustrated in figure 7.1. Adding a fluorescent tag to virus particles decreased infectivity, but viral titers could be rescued to almost wild-type (wt) levels by spiking of wtGag with Gag-eGFP at a ratio of 3 : 1. Adding the mCherry-tag to Env only marginally influenced viral titers, therefore no spiking with wtEnv was neces-

| Gag-eGFP | Ch-Env | overlay |

Figure 7.2: *Wide-field image of dual-color foamy virus particles, preparation PFV P1, spotted on a coverslip. (A) The Gag-eGFP channel is shown in green color and (B) the Ch-Env channel in red color. (C)Corresponding overlay of the two channels, dual-color particles appear in yellow color. Scale bar 10 μm.*

sary. Fusion competent and fusion incompetent viruses were generated by using different viral envelope proteins. Fusion competent viruses contained either wild-type proteins of PFV Env (PE) or SFVmac Env (SE). Fusion incompetent variants of PFV Env and SFVmac Env were generated and are assigned as PE iCS and SE iCS, respectively. These iCS variants are fusion deficient due to the inactivation of the furin cleavage site between the Env surface subunit (SU) and the transmembrane subunit (TU). The infectivity of dual-color viruses with a spiked Gag shell and Ch-Env reached almost wild-type levels in the case of PFV and could be increased to 40 % of wild-type infectivity in the case of SFVmac, whereas the iCS variants showed a 1,000 to 5,000-fold reduction in infectivity even if no fluorescent proteins were added. More detailed information concerning the virus preparation is given in the section 5.1.2 of the Materials and Methods.

7.1.1 Colocalization analysis of initial dual-color virus preparations

Prior to live-cell imaging experiments addressing viral entry and fusion, we first quantified the fraction of dual-color FV particles in the initial virus preparations. Virus fusion results in a separation of the two colors and hence, a decrease in the colocalization percentage over time can be a reporter of fusion. Therefore, the percentage of colocalizing Gag-eGFP and mCherry-Env signals was evaluated for all virus preparations.

Viruses were spotted on a coverslip and measured with an alternating-laser excitation at the wide-field setup described in subsection 5.2. An exemplary image of the dual-color virus particles is given in figure 7.2. The fraction of colocalizing capsid and envelope

particles within the different virus preparations was determined by using the software for colocalization analysis described in subsection 5.3.2.
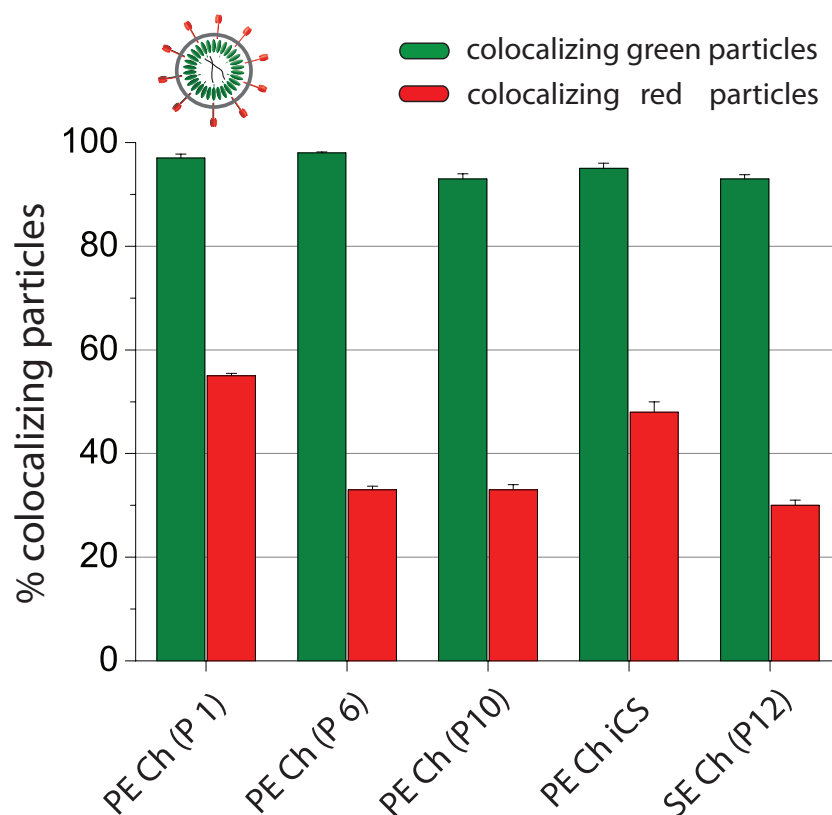
Figure 7.3: *Percentage of dual-color particles in different foamy virus preparations with respect to the total number of the detected Gag-eGFP signal (green bars), and relative to the total number of the detected Ch-Env signal (red bars). Error bars represent the standard error of the mean. The numbers as well as the total sum of analyzed particles are given in the corresponding table 7.1.*

The percentage of dual-color particles was determined with respect to the total number of detected Gag-eGFP particles, as well as relative to the number of Ch-Env particles. The obtained colocalization percentage for the different virus preparations are given in table 7.1.

In all virus preparations, the fraction of labeled capsid colocalizing with envelope signal was very high and ranged between 93 % to 98 %, as can be seen in figure 7.3. In contrast, the fraction of Ch-Env particles that colocalized with Gag-eGFP was between 30 % to 55 % and hence, many particles containing only the mCherry signal were present in the virus preparations, as can be seen in figure 7.2.C.

The high colocalization percentage of Gag-eGFP particles can be explained by a particularity in the foamy virus replication cycle. Virus budding and release requires co-

Table 7.1: *Percentage of dual-color particles in obtained foamy virus preparations. The colocalization percentage is given relative to the detected Gag-eGFP particles (coloc. green) and relative to the detected Ch-Env signal (coloc. red) together with the standard error of the mean (SEM). The sum of analyzed green and red particles is given in addition.*

label of virus prep.	viral env. protein	sum green particles	% coloc. green ± SEM	sum red particles	% coloc. red ± SEM
PFV P 1	PE Ch	6,666	97 ± 0.8	12,649	55 ± 0.5
PFV P 6	PE Ch	2,365	98 ± 0.2	7,683	33 ± 0.7
PFV P10	PE Ch	1,476	93 ± 1	4,022	33 ± 1
PFV P11	PE Ch iCS	542	95 ± 1	1,159	48 ± 2
SFV P12	SE Ch	944	93 ± 0.8	3,290	30 ± 1

expression of Gag and Env (subsection 4.4.2). In the absence of Env glycoproteins, only a few particles if any are released into the cell culture supernatant [16, 90]. However, the expression of Env glycoproteins alone is sufficient for particle budding [278] and subviral particles without capsid are released into the supernatant. This explains the presence of red-only particles. Furthermore, Stanke *et al.* observed an increase in subviral particle release after mutations at the leader peptide of the virus envelope [291]. Therefore, it seems likely that introducing an mCherry-tag to the virus envelope, which is located between the N-terminus and the leader peptide, may lead to an increased subviral particle release.

Another interesting observation was that only virus particles of the first preparations (P1, P6), which were purified via sucrose ultracentrifugation, attached rapidly to the coverslip. In contrast, virus particles purified via centrifugation with Pierce protein concentrators (P10 - P12) did not adhere well to the coverslip and were therefore fixed with paraformaldehyde for the colocalization experiments. These virus preparations showed, in general, higher infectivity (personal communication of K. Stirnnagel).
The obtained dual-tagged virus particles showed high viral titers, especially PFV, which had an infectivity close to that of wild-type viruses. In addition, the percentage of dual-color particles was very high, with mainly all Gag-eGFP particles colocalizing with an mCherry envelope. The presence of red-only particles is not a significant problem since colocalization is always determined relative to the Gag-eGFP signal of the capsid.

7.1.2 pH-dependency of fluorescently tagged virus particles

The fluorescent proteins eGFP and YFP are known to be pH-sensitive [239, 276, 315]. Viruses entering cells by endocytosis have to face a decreasing pH value from early ($\sim$ pH 6.5) to late endosomes ($\sim$ pH 5.5) and lysosomes ($\sim$ pH 4.5) in live cells [136, 208, 211]. Therefore, we investigated the effect of a lower pH environment on the fluorescence intensity of the virus particles tagged with eGFP and mCherry.
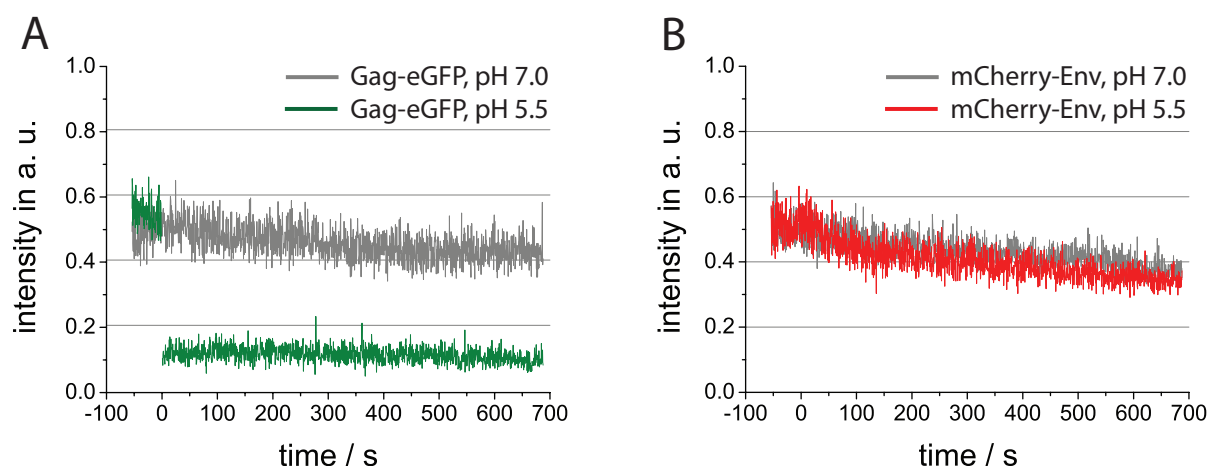

Figure 7.4: *Intensity traces of fixed and permeabilized double-tagged PFV particles at different pH values. Virus particles were fixed with paraformaldehyde and permeabilized with Triton X-100 to ensure accessibility of protons to the fluorescent proteins. Images were recorded at pH 7 as control and at pH 5.5 after addition of citrate buffer (green and red line). The addition of citrate buffer is set as time-point zero. The corresponding intensities recorded at neutral pH serve as control for photobleaching (gray line). Background-corrected intensities of ten particles were determined over time and the averaged intensity values are shown. (A) Averaged intensity traces of the Gag-eGFP signal from permeabilized dc particles at pH 7 (gray line) and pH 5.5 (green line). (B) The corresponding intensity traces of the mCherry-Env signal at pH 7 (gray line) and pH 5.5 (red line).*

In a first step, we focused on the pH-dependency of the fluorescent proteins and performed experiments with disrupted viral membranes. Virus particles were fixed with paraformaldehyde and permeabilized with Triton X-100 to ensure that the fluorescent proteins are accessible to protons. The obtained results are shown in figure 7.4. The intensities of eGFP and mCherry were recorded at pH 7 (gray line), and at pH 7 followed by a decrease to pH 5.5 after addition of citrate buffer (green and red line). The addition of citrate buffer is indicated by the zero time-point. Background-corrected intensities of ten individual dual-color particles were determined over time and the averaged intensity trace is shown. The average intensity trace obtained at neutral pH serves as a control
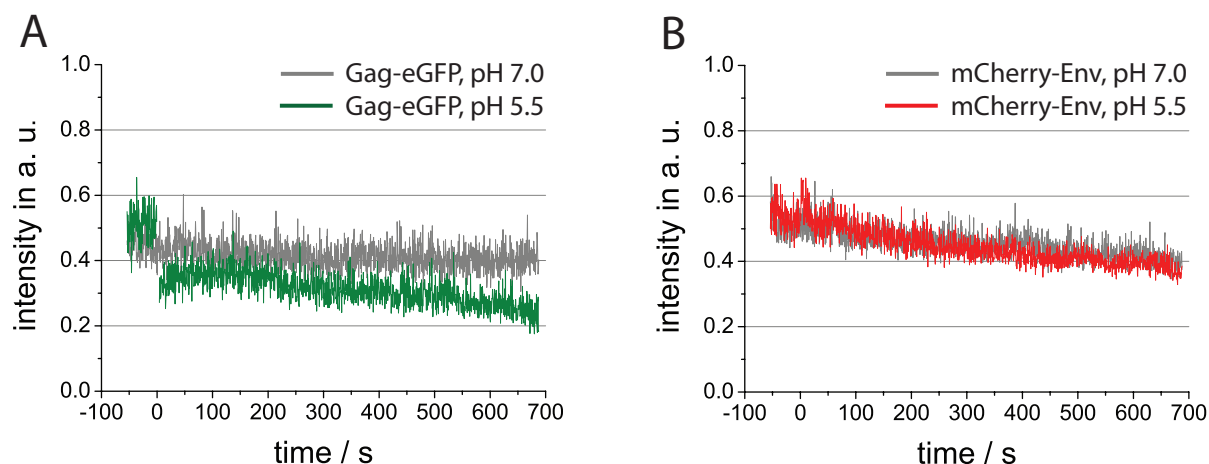
Figure 7.5: *Intensity traces of double-tagged PFV particles at different pH values. Virus particles were adhered on a tissue culture treated coverslip without fixation and permeabilization. The zero time-point indicates the addition of citrate buffer, resulting in pH 5.5. Background-corrected intensities of ten particles were determined over time and the averaged intensity values are shown. (A) Intensity traces of the Gag-eGFP signal of dc particles at pH 7 (gray line) and pH 5.5 (green line). (B) The intensity traces of the corresponding mCherry-Env signal at pH 7 (gray line) and pH 5.5 (red line).*

for photobleaching of the fluorescent proteins.

The Gag-eGFP signal is significantly quenched upon addition of citrate buffer. At pH 5.5, the Gag-eGFP intensity is only around 20 % of the initial value at pH 7 (figure 7.4.A). Hence, eGFP shows a strong pH-dependency, which is expected for a pK_A value around 6.0 [276]. In contrast, no significant decrease in the mCherry-Env signal was observed at pH 5.5, compared to the values obtained at neutral pH (figure 7.4.B). The pK_A value of mCherry is reported to be below 4.5 [275, 276].

After having addressed the general pH-sensitivity of eGFP and mCherry in the viral context, we addressed the pH sensitivity of the fluorescent proteins under biologically more relevant conditions. Virus particles were adhered on a tissue culture treated coverslip (ibiTreat) without further treatment. Particle intensities were recorded under the same illumination conditions as the fixed and permeabilized virus particles. An overview of the obtained intensity traces at pH 7 and pH 5.5 is given in figure 7.5. The fluorescence intensity at neutral pH was recorded (gray line) to account for bleaching of the fluorescent proteins.

After addition of citrate buffer to non-permeabilized virus particles, the intensity of the Gag-eGFP signal decreased slightly to around 60 % (figure 7.5.A), and around 50 % of the initial intensity was still detectable after eleven minutes at pH 5.5. The mCherry-Env signal did not show a decay in the recorded intensity at pH 5.5 compared to pH 7.0 (figure 7.5.B), as was observed for permeabilised virus particles (figure 7.4.B).

The obtained data give evidence that the Gag-eGFP signal should be detectable at pH values found in late endosomes, although eGFP shows a strong pH dependency. It is reasonable that the eGFP signal of the dc particles is still detectable at pH 5.5, considering that eGFP is located at the capsid and protected by the surrounding lipid bilayer envelope and probably also by untagged Gag. A further advantage of labeling the capsid with the pH sensitive fluorescent protein is that particles with potentially quenched capsid signal are not included in the analysis as the colocalization percentage is always calculated relative to the total number of detected capsid particles. The viral envelope contains the less pH sensitive mCherry-tag. This is the beneficial tag on the envelope as it encounters the harshest pH conditions. Thus, quenching of the double-tagged FV particles in live-cell experiments should not be a critical issue.

7.2 Time-lapsed analysis of colocalization in live cells

After having characterized the virus particles and determining the initial colocalization percentage, we investigated the time scale on which viral entry and fusion occur. The percentage of colocalized capsid and envelope signals was analyzed in live cells over time. Live HeLa cells were incubated with double-tagged virus particles at around 10 °C to allow particle binding and synchronize the uptake. Unbound virus particles were removed by several washing steps. Thereafter, cells were shifted to 37 °C, a temperature that allows virus uptake. Cells were imaged in 3D with alternating-laser excitation on a spinning-disk confocal microscope (SDCM) described in subsection 5.2.2. Multiple cells were measured sequentially with z-stacks of 30 planes. The interval time was varied between five and ten minutes. The number of dual-color particles was evaluated using the software for colocalization analysis in 3D described in subsection 5.3.3 on page 72. High virus concentrations were avoided to minimize the possibility of random colocalization of capsid and envelope signals and to ensure more virological relevant conditions. Only cells containing less than 180 Gag-eGFP labeled particles were included in the analysis although the typical number of virions varied between 50 and 100 particles per cell. Even with 180 Gag-eGFP labeled particles, the number of particles detected within one z-plane was low enough to perform a reliable colocalization analysis. The colocalization percentage was determined over time for PFV Gag-eGFP labeled virions, containing one of three different envelope proteins: PE Ch, PE Ch iCS and SE Ch (figure 7.6). The PE Ch iCS particles served as control, as they possess no significant fusion activity. All virus particles utilized in this experiment were spiked with wt-Gag and Gag-eGFP at a ratio of 3 : 1 and purified via Pierce protein concentrators. In order to estimate the uncertainty

of the measurement, the obtained data of individual cells were divided into five to seven subsets, gathered from two to four cells, and binned in ten minute intervals starting from the shift to 37 °C. In the case of PE Ch and PE Ch iCS particles, five subsets out of 13 and 16 cells, respectively, were analyzed. For SE Ch particles, seven subsets out of 23 cells were evaluated. Potential artifacts in the colocalization percentage resulting from quenching of the fluorescent proteins in acidic compartments can be minimized if the percentage is given relative to the number of detected Gag-eGFP particles.

In the event of the non-fusogenic PE Ch iCS viruses, the percentage of colocalizing Gag-eGFP particles remained constant around 96 % over the measurement time of 90 minutes (figure 7.6, black data points). This is in agreement with the colocalization percentage evaluated for the initial virus preparation spotted on a coverslip, which was 95 ± 1 %. The obtained colocalization values of PE Ch iCS serve as control and test of the sensitivity of the method: calculated colocalization values must be below the values obtained for PE Ch iCS to assign that virus particles have undergone fusion.

The initial colocalization percentage obtained for SE Ch particles spotted on a coverslip was 93 ± 1 %. In live HeLa cells, the fraction of double-tagged SE Ch particles showed a slow decay from 92 ± 2 % in the first 20 minutes to around 85 ± 2 % after 90 minutes at 37 °C (magenta data points). The obtained values are below the initial colocalization percentage and below the control with fusion incompetent PE Ch iCS particles, indicating that some of the SE Ch particles have undergone fusion.

PE Ch virus particles spotted on a coverslip showed an initial colocalization percentage of 93 ± 1 %. In live cells, a decay of colocalizing Gag-eGFP particles below 80 % was already observed within the first 30 minutes (blue data points). The percentage of double-tagged particles decreased during the experiment and was significantly below the colocalization percentage determined for both SFVmac and PE Ch iCS. The evaluated percentage of dual-color PE Ch particles in cells was significantly below the value of the virus preparation, suggesting that fusion happened very soon after shifting the cells to 37 °C and to a large amount. A slight increase in the fraction of dual-color PE Ch particles was observable between 30 to 50 minutes post binding. Although the increase is near the limit of statistical relevance, formation of large aggregates of both Gag and Env signals in the perinuclear region made it impossible to analyze individual particles in this region. Both, the limited sensitivity in the perinuclear region as well as capsid disassembly, would lead to a decrease in the detection of green-only particles. A lower number of detected green-only particles results in an increase of the calculated colocalization percentage. The second decay, starting after about 50 minutes post binding, may result from a different entry pathway that is more prominent at this time point, e.g.

fusion with (late) endosomes in contrast to fusion at the plasma membrane or with early endosomes, which would occur at earlier time points, although this remains speculative. In comparison to the other FV species investigated, PE Ch particles showed a significantly lower colocalization percentage throughout the measurement time of 90 minutes than that determined for the non-fusogenic control PE Ch iCS, as well as for the SE Ch particles. The observed decay for the SE Ch particles was slower and less fusion events were observed, which is consistent with their lower infectivity (figure 5.1 on page 60). The slower kinetics observed for SE Ch particles can be attributed to the requirement of low pH for fusion [248]. SE Ch particles probably do not fuse until they are in late endosomes. In contrast, PE Ch particles already possess a significant fusion activity at neutral pH [248], which is consistent with the observation of early fusion events. Accordingly, syncytia formation of cells was only observed after infection with PE Ch particles, but not for SE Ch particles (data not shown).

Based on these findings, most fusion events are expected to occur during the first 30 minutes post binding. Consequently, we focused on this time window for investigating single fusion events with high time resolution. The probability of visualizing these events is the highest for PE Ch particles. In the case of SE Ch particles, the chance to see fusion events is expected to be lower compared to PE Ch.

7.3 Analysis of individual fusion events

To gain more insight into the entry pathway of the two types of FV species, PFV and SFVmac, as well as the fusion process itself, experiments were performed during the first 30 minutes post binding of double-tagged virus particles to live HeLa cells, and movies were acquired in 3D with high time resolution using the spinning-disk confocal microscope (subsection 5.2.2).

First, live HeLa cells were incubated with virus particles at around 10 °C to allow attachment to the cell surface without being taken up. Virus uptake was synchronized by an increase in the temperature to 37 °C (zero time-point), a temperature allowing virus uptake and fusion. Movies were started a few minutes after reaching 37 °C and recorded over a duration of about 20 minutes. Samples were simultaneously excited with 488 nm and 561 nm. Thus, cells were chosen that did not exhibit autofluorescence signal with high intensities which otherwise would interfere with the recorded mCherry signal in the red channel. To obtain the whole 3D volume of the cell, around 20 to 25 planes were recorded with a z-distance of 300 nm and an exposure time of 130 ms, resulting in typical interval times between 3.5 to 4.5 s.
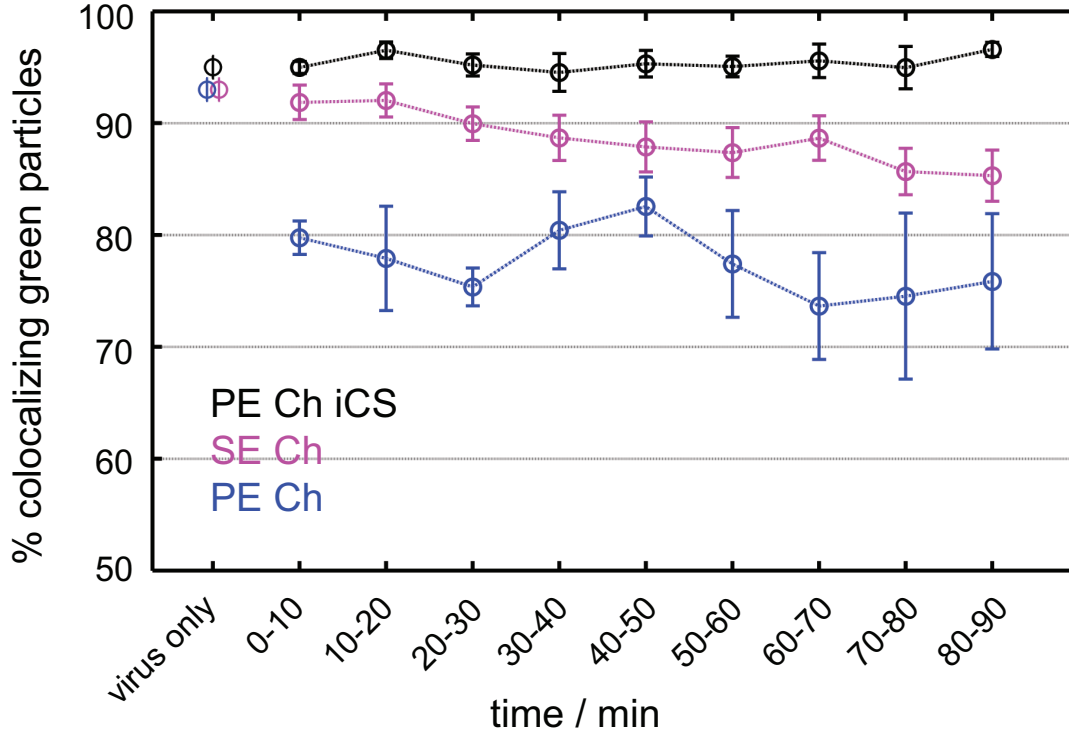
Figure 7.6: *Time-lapsed analysis of the colocalizing capsid signal relative to the envelope signal in live cells over time. The virus particles were composed of a spiked Gag-eGFP capsid and one of three different Env proteins: PE Ch ics (black), SE Ch (magenta) and PE Ch (blue). HeLa cells were incubated with virus particles at 10 °C to allow virus binding and then shifted to 37 °C to synchronize the uptake. Z-stacks of individual cells were recorded on a SDCM with ALEX and an interval time of five to ten minutes. The colocalization percentage obtained from several HeLa cells for the three different FV species is shown as a function of time. The colocalization percentage was determined by grouping individual cells into subsets of 2-4 cells. Cells were averaged together into time bins of ten minutes and the average (circle) and standard error of the mean (error bars) was calculated. For comparison, the initial colocalization percentage of the virus preparations determined on a coverslip are given as zero time-point. Lines are drawn between data points as a guide to the eye.*

From the obtained movies, the particles were first tracked in 2D using a z-projection of the whole cell and then further analyzed with the TrIC software developed by Dr. Aurélie Dupont (subsection 5.3.5 on page 75). This TrIC software is based on image cross-correlation of the Gag-eGFP and mCh-Env channels. Fusion of the double-tagged virions leads to the separation of the two colors. As fusion is rare, long trajectories are required to increase the chance of detecting fusion. Movies were recorded with low laser power to minimize photobleaching. The low signal-to-noise ratio together with photo-bleaching of the fluorophores makes colocalization analysis critical when it is solely based on the fluorescence intensity. Hence, it is important to have additional means for the detection of fusion. Image cross-correlation along the trajectory of a moving dual-color particle is an advantageous method which offers a high sensitivity as noise does not correlate. Applying this analysis, one can extract 3D trajectories of each virus particle from the movies together with its instantaneous velocity, the corresponding background-corrected fluorescence intensity values of the particles in both channels as well as the 3D colocalization information. In addition, the cross-correlation output provides information about the relative position of the particles in both channels with an accuracy of 30 nm.

For the experiments, low doses of virus particles were applied to cells, generally ranging between 20 to 40 virions, in order to have more biological relevant conditions of infection and to avoid saturation of the cell surface. Furthermore, low concentrations allow single particle tracking without crossing of too many other particles. Altogether, about 520 double-tagged PE Ch particles and about 600 double-tagged SE Ch particles were detected. Thereof, viral particles showing active transport or intracellular diffusion were tracked, yielding a total of 88 PE Ch trajectories and 97 SE Ch trajectories. Out of these trajectories, 13 fusion events were detected for the PE Ch viruses and three in the case of SE Ch viruses. The higher number of detected PE Ch fusion events is in agreement with the obtained results of the time-lapsed colocalization experiments described previously (figure 7.6). Out of the 3D colocalization analysis in cells, the probability to detect a fusion event was estimated to be around 6.4 times higher for PE Ch particles compared to SE Ch particles during the first 25 minutes post binding.

After having detected individual fusion events of double-tagged viruses, these fusion events were further classified based on the type of fusion: (i) fusion at the plasma membrane or (ii) fusion after endocytosis. Two criteria were applied to differentiate between extra- and intracellular virus particles: the particle's velocity and the location of the virus particle relative to the plasma membrane. Based on the particle's velocity, it is straightforward to identify particles with active transport along microtubules. Velocities

of actively transported particles ranged between 0.1 to 2 μm·s^{-1}. Prior to virus uptake, particles exhibited velocities below 0.05 μm·s^{-1}, consistent with reported velocities of surface-bound particles [18, 271]. However, this last criteria is ambiguous and velocity-based classification was not possible if no active motion of the virus was observed prior to the fusion event. For that reason, a method was applied to estimate the plasma membrane of the cell based on the 3D position of all virus particles (Dupont *et al.*, manuscript in preparation). This was possible since cells were incubated with viruses around 10 °C and warmed to 37 °C directly at the microscope. Hence, at the beginning of the movie, most virus particles were still located at the plasma membrane. The position of the particle relative to the estimated cell surface was helpful to identify fusion events at the plasma membrane. However, the accuracy of the method is not sufficient to distinguish between fusion at the plasma membrane or a fusion event resulting from a particle that is trapped in the dense actin cortex underneath the plasma membrane.

7.3.1 PFV Env fusion at the plasma membrane and with endosomes

In the experiments with PE Ch viruses, 13 fusion events were detected. Four of them were found to happen at the plasma membrane and nine after cell entry, probably fusing with an endosomal membrane. An exemplary trajectory of a PE Ch fusion event at the plasma membrane, together with the corresponding analysis, is given in figure 7.7. A trajectory of a non-fusing dual-color HSV-1 particle is shown in the previous chapter, figure 6.18. A differential interference contrast (DIC) image of a HeLa cell is overlaid with the corresponding projection of the PE Ch virus trajectory (panel A). The beginning of the trajectory is shown in yellow color, changing to green color after the fusion event was completed. In the beginning, the virus is located at the plasma membrane on the edge of the cell and was mostly immobile. Initial movement of the particle occurred with velocities below 0.05 μm·s^{-1}. This was observed for all analyzed membrane bound virus particles and is consistent with artificial viruses or papillomaviruses bound to the plasma membrane [18, 271]. The instantaneous velocity of the particle was low during the first ten minutes of the movie (panel Bii), suggesting that the particle had not yet been taken up. After ten minutes, the correlation amplitude shows a sudden drop (panel Biii, blue color), pointing out the loss of colocalization and hence, fusion was completed. The separation of the two colors was clearly visible in the movie as can be seen in the still images (panel C, last row). After the color separation, a clear Ch-Env signal could still be measured over minutes after the color separation (panel C, last row). In most fusion events, the Ch-Env signal was lost within five to 15 seconds after the fusion event was

completed. The Gag-eGFP capsid was released into the cytosol and showed active transport towards the cell center with an instantaneous velocity above 1 μm·s^{-1} (panel Bii), whereas the envelope remained at the previous location (panel B, last row in comparison to first rows). Subsequent to the directed active transport towards the cell center, the capsid exhibited short periods of active transport in random directions with velocities of 0.5 μm·s^{-1} (panel Bii). The observed velocities are consistent with dynein-mediated transport of endosomes or viruses along microtubules [101, 177, 178, 265, 303]. PFV Gag is known to interact with the light chain 8 (LC8) of the microtubule motor protein dynein [247]. In turn, LC8 interacts with the actin based motor myosin V, which probably helps to transfer the capsid from the plasma membrane, rich in actin, to the microtubule network [19, 110]. Thus, we assume that the active transport from the fusion site at the plasma membrane towards the cell center is mediated by direct interaction of the capsid with cellular motor proteins and the capsid is transported along microtubules to reach the MTOC.

Figure 7.7 (facing page): *PFV fusion event at the plasma membrane. HeLa cells were incubated with PE Ch particles at low temperatures. After warming the cell to 37 °C, z-stacks (25 planes) were recorded on a SDCM with an interval time of 4.4 s. The results of the tracking and 3D colocalization analysis are given in panels (A)-(D). (A) DIC image of a HeLa cell with the virus trajectory overlaid. The trajectory of the dc virus is shown in yellow, whereas after the fusion event, the movement of the released capsid is plotted in green. (B) Results of the TrIC analysis along the virus trajectory: (i) the intensity of Gag-eGFP (green) and Ch-Env (red) signals, (ii) the instantaneous velocity of the capsid, (iii) the cross-correlation amplitude (blue) together with the determined threshold (gray) out of the negative control (black), and (iv) the relative separation of the Gag-eGFP and Ch-Env signals. An increase in the relative distance was generally observed for the fusion events and divided into three stages: stage 1 (blue) for distances $\leq$ 100 nm, stage 2 (cyan) for separations up to 400 nm and stage 3 (green) when fusion was complete. The time at which fusion was completed is indicated by a black-dotted line through the panels (i)-(iv). (C) Z-projections of the Gag-eGFP and the mCherry-Env channels together with the merged image for selected time points before and after the fusion event. The virus particle undergoing fusion is highlighted by a white circle. Scale bar 5 μm. (D) 3D relative motion of the envelope with respect to the capsid during the fusion process. The color-code is given as in panel (B)iv. Taken from Dupont et al. (manuscript in preparation).*

The further three detected fusion events at the plasma membrane, as well as the nine observed fusion events with an endosomal membrane, appeared similar to the discussed fusion event (figure 7.7). In the case of the intracellular fusion events, steps of active transport were observed prior to fusion. The persistence of a clear Ch-Env signal (figure 7.7.C, last row) was an exception as Ch-Env signals typically disappeared within five to 15 seconds after the fusion event was completed. This is in agreement with observations of other virus fusion events [161, 184]. The loss of the fluorescence signal is attributed to the dilution of the viral glycoproteins in the cellular membrane after the fusion event. The dilution of the Ch-Env signal in the cellular membrane is a further indication that fusion has been completed. The redistribution of the fluorescence signal in the cellular membrane can be utilized to study different steps in the fusion process. When virus particles are incorporated with a lipophilic dye such as DiD, redistribution of the lipophilic dye in the cellular membrane can occur as soon as the contacting leaflets merge. It is frequently used to indicate the hemifusion state during virus fusion which is characterized by lipid mixing of the contacting leaflets without content mixing (section 4.2) [207, 217].

7.3.2 SFV Env fusion in endosomes

In the case of SE Ch viruses, only three fusion events were observed out of about 600 double-tagged particles. This is significantly less than detected for the PE Ch viruses, although more SE Ch particles were analyzed in total. This observation is consistent with the results from the 3D colocalization experiment described previously (figure 7.6), in which SE Ch particles showed a slower decrease in the colocalization percentage than PE Ch particles. From the 3D colocalization analysis, the probability to detect a fusion event is expected to be about 6.4 times higher for PE Ch particles than for SE Ch particles during the first 25 minutes post binding. Furthermore, all detected SE Ch fusion events happened after entry, presumably from an endosome. An exemplary fusion event is shown in figure 7.8. The virus particle was already taken up in the beginning of the movie and after three minutes, active transport towards the nucleus was observed with instantaneous velocities up to 0.6 μm·s^{-1}. The final fusion event occurred 21 minutes after the start of data acquisition (figure 7.8.B, black dotted line).

After this fusion event, the Gag-eGFP and the Ch-Env signals were still detectable. In the other two SE Ch fusion events, the Ch-Env signal was lost after fusion as observed for most of the PE Ch fusion events. The disappearance of the Ch-Env signal cannot be attributed to the site of fusion – plasma membrane *vs.* endosomal membrane – as, for both cases, the Ch-Env signal was typically lost after the fusion event. The exceptional persistence of a clear Ch-Env signal was observed for one fusion event at the plasma membrane (figure 7.7.C, last row) and one with an endosomal membrane (figure 7.8.C, last row).

7.3.3 Kinetics of the entry process

In total, 16 individual fusion events were detected. The numbers of detected fusion events in the case of PE Ch and SE Ch virus particles are summarized in figure 7.9.B. The complete uptake process from virus entry until fusion was detected for nine of the fusion events, all from PE Ch viruses: all events at the plasma membrane and five intracellular fusion events. In the case of the remaining seven intracellular fusion events, the virus had already entered the cell before the movie was recorded and the exact time point of entry is not known. Therefore, the intracellular fusion events were divided into (i) complete uptake and (ii) incomplete uptake events (figure 7.9). For complete uptake, the exact time duration from entry until fusion was determined. In the case of incomplete uptake, only a minimum time can be calculated, from the start of the trajectory

until the occurrence of fusion. For fusion events at the plasma membrane, the total time from virus binding until fusion is given (total time at 37 °C). Figure 7.9.C lists the average duration times from entry until fusion. Additionally, the minimum and maximum detected duration values are given.

The four PE Ch fusion events at the plasma membrane happened on average 19 ± 3 minutes after warming the cells to 37 °C and the values ranged between 11 to 25 minutes (figure 7.9.C). For the five intracellular PE Ch fusion events with complete uptake, the time course from virus entry until fusion ranged between 52 s to 420 s with an average of 160 ± 68 s ($\approx$ 3 min) (figure 7.9.C). This reflects that intracellular fusion of PFV can occur shortly after uptake. Four intracellular PE Ch fusion events were observed with incomplete uptake. The minimum time delay from the start of the track until fusion ranged from 342 s to 584 s with an average value of 471 ± 52 s ($\approx$ 8 min). All detected SE Ch fusion events happened intracellularly and only incomplete uptake was observed. The minimum time lag until fusion ranged from 269 s to 1316 s with an average value of 816 ± 303 s ($\approx$ 14 min) (figure 7.9.C).

Figure 7.8 (facing page): *SFV fusion event after endocytic uptake. HeLa cells were incubated with SE Ch particles at low temperatures. After warming the cell to 37 °C, z-stacks (17 planes) were recorded on a SDCM with an interval time of 3.0 s. The results of the tracking and 3D colocalization analysis are given in panels (A)-(D). (A) DIC image of a HeLa cell with the virus trajectory overlaid. The trajectory of the dc virus is shown in yellow, whereas after the fusion event, the movement of the capsid is plotted in green. (B) Results of the TrIC analysis along the virus trajectory: (i) the intensity of Gag-eGFP (green) and Ch-Env (red) signals, (ii) the instantaneous velocity of the capsid, (iii) the cross-correlation amplitude (blue) together with the determined threshold (gray) out of the negative control (black), and (iv) the relative separation of the Gag-eGFP and Ch-Env signals. An increase in the relative distance was generally observed for the fusion events and divided into three stages: stage 1 (blue) for distances $\leq$ 100 nm, stage 2 (cyan) for separations up to 400 nm and stage 3 (green) when fusion was complete. The time at which fusion was completed is indicated by a black-dotted line through the panels (i)-(iv). (C) Z-projections of the Gag-eGFP and the mCherry-Env channels together with the merged image for selected time points before and after the fusion event. The virus particle undergoing fusion is highlighted by a white circle. Scale bar 5 µm. (D) 3D relative motion of the envelope with respect to the capsid during the fusion process. The color-code is given as in panel (B)iv. Taken from Dupont et al. (manuscript in preparation).*

Comparison of the time course of the different virus particles shows that intracellular fusion of PE Ch viruses in HeLa cells occurred faster than for SE Ch. For other viruses, it has been reported from literature that fusion from early endosomes occurs already within one to five minutes after virus uptake (e.g. Vesicular Stomatitis virus (VSV), Semliki Forest virus) [211]. In contrast, fusion with late endosomes is induced 10 to 20 minutes after uptake (e.g. influenza A virus, dengue virus) [211, 321]. These findings suggest that PFV may already fuse with early endosomes as fusion was detected as soon as 52 s after entry. Indeed, fusion of PFV at neutral pH has been reported, although the highest fusion activities were observed at acidic pH values [248]. This is consistent with our findings that PFV is able to directly fuse at the plasma membrane. Fusion of PFV at the plasma membrane was detected ten to 20 minutes after the increase in temperature to 37 °C, whereas in the case of complete uptake events, fusion occurred on average three minutes after the uptake (figure 7.9.C). The short lag time from entry until fusion in the case of endocytosed particles relative to fusion at the plasma membrane is in agreement with the reported pH-dependency of PFV fusion since early endosomes already have a slightly acidic pH value around 6.5 to 6.0 [136, 208, 211]. Infectious uptake of e.g. HIV-1 or HSV-1 can be by direct fusion at the plasma membrane or by endocytosis and is consistent with our observations that PFV is able to induce fusion at different locations [63, 215, 232, 233]. PFV entry shows similarities with VSV (subsection 4.4.1 on page 52), which is known to induce fusion in early endosomes [147]. PFV fusion events with a larger time delay between seven to ten minutes after entry may occur from maturing or late endosomes. Fusion with early and late endosomes in different quantities within the same cell line has been reported for instance for dengue virus [321]. In contrast to PFV, SFVmac requires low pH to fuse [248] and the detected lag time from entry until fusion was larger in the case of SFVmac (figure 7.9.C). The time course of SFVmac fusion, although only a minimum time duration with an average of 14 minutes could be calculated, suggests that fusion is induced in late endosomes as reported for influenza A virus [263].

7.3.4 Dynamics of fusion

The applied image cross-correlation method provides additional information regarding the relative distance between the fluorescence center-of-mass of the Ch-Env and the Gag-eGFP signals during the fusion process (figure 7.7.Biv and 7.8.Biv). In all but one fusion event, three clear stages were observed during the fusion process: (1) The first stage results from fully intact dc particles with tight colocalization of envelope and

A

B

number of	PFV	SFVmac
detected dc particles	520	600
trajectories	88	97
total fusion events	13	3
fusion at plasma membrane	4	0
fusion intracellular	9	3

C

	PFV			SFVmac
	fusion at pm	complete uptake	incomplete uptake	incomplete uptake
number of virions	4	5	4	3
average time [min]	19 *	3	8	14
minimum value [min]	11 *	1	6	5
maximum value [min]	25 *	7	10	22

* time @ 37 °C until fusion
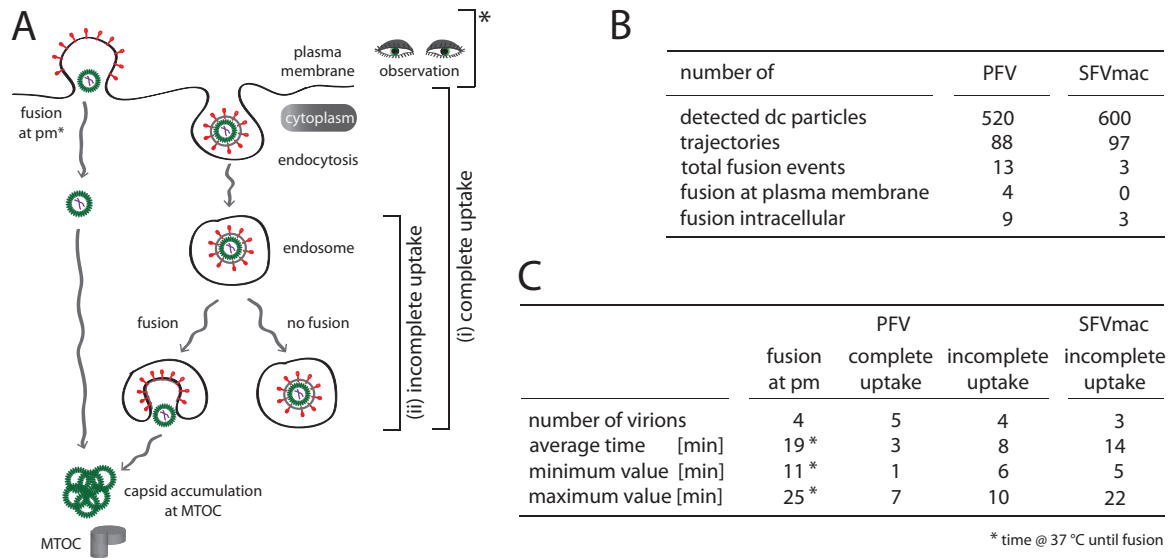
Figure 7.9: *Schematic of different FV entry pathways with corresponding time course. (A) Schematic of different FV entry pathways: Foamy virus can enter cells by direct fusion at the plasma membrane or by endocytic uptake followed by fusion with an endosomal membrane. Subsequent to fusion, capsids are released into the cytoplasm and accumulate at the MTOC. (B) Overview on the number of analyzed trajectories and detected fusion events for HeLa cells infected with PFV or SFVmac. (C) Time course of detected FV fusion events. For fusion events at the plasma membrane, the total time at 37 °C until fusion is given (asterisk). Intracellular fusion events were divided into (i) complete uptake and (ii) incomplete uptake. In the case of complete uptake, the time from virus entry until fusion was calculated. Events where we did not see the uptake were referred to as incomplete uptake. Therefore, only a minimum time is given, referring to the start of the trajectory. In addition to the average duration time until fusion, the minimum and maximum detected values are given for the different fusion events.*

capsid signals (< 80 nm). (2) The second stage is characterized by an increase in distance between the capsid and envelope signals (100 nm $\leq$ r $\leq$ 400 nm). (3) Finally, in the third stage, capsid and envelope signals are completely separated. The relative distance between capsid and envelope in the first stage is within the localization accuracy of the measurement (80 nm). In stage two, the relative distance increased up to 400 nm. In the shown PFV and SFVmac trajectories (fig. 7.7.Biv and 7.8.Biv), the increase in the distance started at four and five minutes, respectively. As can be seen in figures 7.7.D and 7.8.D, the relative movement between capsid and envelope was typically isotropic with the envelope dancing around the capsid. The duration times of stage two are given in table 7.2. On average, stage two lasted for about 392 ± 41 s (≈ 6.5 min) in the case of PFV fusion events and about 649 ± 236 s (≈ 11 min) for SFV fusion events.

In rare cases, relative movement of intracellular dc particles was observed although no fusion event was detected. This stage was observed for three PE Ch particles and two SE Ch particles (table 7.2). The most likely explanation is that these dc viruses had entered stage two but the movie was stopped before fusion had occurred. The minimum duration was on average 290 ± 103 s (≈ 5 min) for PFV. In the case of the two SFVmac events, stage two movement without fusion was observed over 170 s and 1624 s (2.8 min and 27.1 min, respectively). For all observed fusion events, the process of fusion was relatively slow and occurred over minutes. The duration of stage two was 7.5 minutes on average for all detected fusion events. To the best of our knowledge, observation of such an intermediate phase during virus fusion has not been reported before. One explanation for the relative movement could be that (i) fusion already occurred between stage one and stage two, but that capsid and envelope were both confined in a small compartment (e.g. in the dense actin cortex or in an endosome) that only allowed movement over short distances (figure 7.10.A). On the other hand, (ii) capsid and envelope could still be tethered together during this intermediate phase until final separation occurred between stage two and stage three (figure 7.10.B). This tether could be, for instance, the viral genome or filamentous structures of the cell. In the first scenario (i), capsid and envelope would move independently, whereas in scenario (ii), the movement of both would be correlated. In order to distinguish between these two hypotheses, a mean-square-displacement (MSD) analysis was performed on the relative trajectory of the envelope with respect to the capsid and compared with the MSD of the absolute trajectory of the capsid. For case (i), capsid and envelope diffuse independently of each other, the diffusion coefficient of the relative trajectory should be higher than that of either single trajectory: $D_{rel} > D_{abs}$ (figure 7.10.A). In contrast, for case (ii), capsid and envelope are still tethered together, the relative diffusion coefficient is expected to be lower than the

Table 7.2: *Stage two movement was observed for all but one fusion event at the plasma membrane (pm). On average, stage two lasted for 6.5 ± 0.7 min in the case of PFV and 10.8 ± 3.9 min for SFVmac. Occasionally, stage two was observed but no fusion. Probably, the movie ended before the fusion event had happened.*

	PFV		SFVmac	PFV	SFVmac
	pm	intracellular	intracellular	no fusion	
number of virions	3	9	3	3	2
AVG time stage 2 [min]	7.7	6.1	10.8	> 4.8	—
minimum value [min]	6.0	2.3	3.8	> 2.0	> 2.8
maximum value [min]	10.6	9.6	17.4	> 7.9	> 27.1

absolute one: $D_{rel} < D_{abs}$ (figure 7.10.B). The MSD of an SE Ch fusion event is given in figure 7.10.C. Analysis of all 15 fusion events showing relative movement revealed a much lower diffusion coefficient for the relative motion than for the absolute motion of the capsid, suggesting that the occurrence of stage two is not a result of co-confinement. This is further emphasized by the fact that the Ch-Env signal disappeared typically within five to 15 seconds after the final color separation. The loss of the Ch-Env signal is attributed to the dilution of the viral glycoproteins in the cellular membrane after the fusion event and is a further indication that the actual fusion event occurred between stage two and stage three. If fusion would already occur between stage one and stage two, the dilution of the Ch-Env signal in the cellular membrane is expected to occur earlier and hence, no transition from stage two to stage three would be observable any more. Stage two was observed for the fusion events at the plasma membrane as well as for the intracellular fusion events. If stage two would be attributed to co-confinement of capsid and envelope after the actual fusion event, why is it observed independently of the site of fusion? Thus, we conclude that stage two is a real step in the fusion process, although we cannot yet provide a clear explanation of what is happening during that stage.

Stage two may coincide with conformational changes in the envelope protein during the fusion process that are necessary to form and/or enlarge a fusion pore. The current idea of virus fusion with a host-cell membrane involves several steps that are mediated by viral fusion proteins through a common "cast-and-fold" mechanism (figure 4.2 on page 35). The two lipid bilayers are brought in close contact so that the contacting leaflets can merge (hemifusion, figure 4.2). Hemifusion is followed by pore formation, content mixing and pore growth, so that the capsid can be released into the cytoplasm. In order to investigate the different steps of virus membrane fusion, experiments with

fluorescently labeled virus particles have been performed at the single virus level with high temporal resolution [146, 150, 238]. The duration time until hemifusion can be investigated by incorporation of a lipophilic dye (e.g. DiD) in the viral membrane. The dye is diluted in the cell membrane upon lipid mixing of the membranes, which is either detected by an increase or decrease in the fluorescence intensity depending on whether DiD was incorporated in self-quenching concentrations [177] in the viral envelope or with lower concentrations [196, 207]. The time delay until lipid mixing occurred ranged from no apparent delay to a few minutes relative to the onset of the fusion trigger (increase in temperature or acidic pH) [92, 150, 196, 207, 217]. Pore formation can be detected by incorporation of a dye into the inner leaflet of the viral membrane [150, 207]. Incorporation of a fluorescently-labeled mature capsid protein, e.g. MLV Gag NC-FP, is used to dissect content mixing since NC-FP is a relatively small and mobile aqueous marker [146, 196, 207, 217, 238]. Content mixing can happen almost instantaneously with lipid mixing [150], or after a delay, ranging from a few seconds [92, 207, 146, 150] up to several minutes [196, 217]. The small fusion pore can close and reopen before it grows large enough to release the capsid into the cytoplasm [38, 118, 150]. Capsid release can be followed by genetic fusion of fluorescent protein tags to the capsid protein matrix (MA) subunit [161, 279].

Double-labeled viruses having viral glycoproteins and the capsid tagged with fluorescent proteins were only rarely used to study retroviral fusion [161, 279]. It is demanding to obtain infectious double-labeled viruses as incorporation of fluorescent proteins generally diminishes the infectivity. Sherer *et al.* generated infectious double-labeled murine leukemia virus (MLV) particles carrying Env-YFP and Gag-CFP and could show that these particles were able to mediate fusion [279]. During virus entry, Env remained associated with the host-cell membrane while Gag was released into the cytoplasm [279]. Koch *et al.* utilized this functional MLV Env-YFP variant in combination with HIV-1 MA mCherry to investigate virus fusion on a single particle level [161]. From more than 20,000 2D trajectories, they were able to detect 28 fusion events of rapid color separation. In addition, 45 events were detected with simultaneous disappearance of MA and Env signals. Simultaneous loss of MA and Env signals was also observed with fusion deficient virus particles, although to a lower extent [161]. The simultaneous loss of MA and Env signals may result from endocytosed virus particles that are no longer in the focal plane as well as to a certain extend from virus fusion since the simultaneous loss of both signals was observed more often in the case of the fusion competent virus [161]. In contrast to the rapid capsid and envelope separation reported by Koch *et al.*, we observed a much slower fusion process with an intermediate stage where the capsid and

144
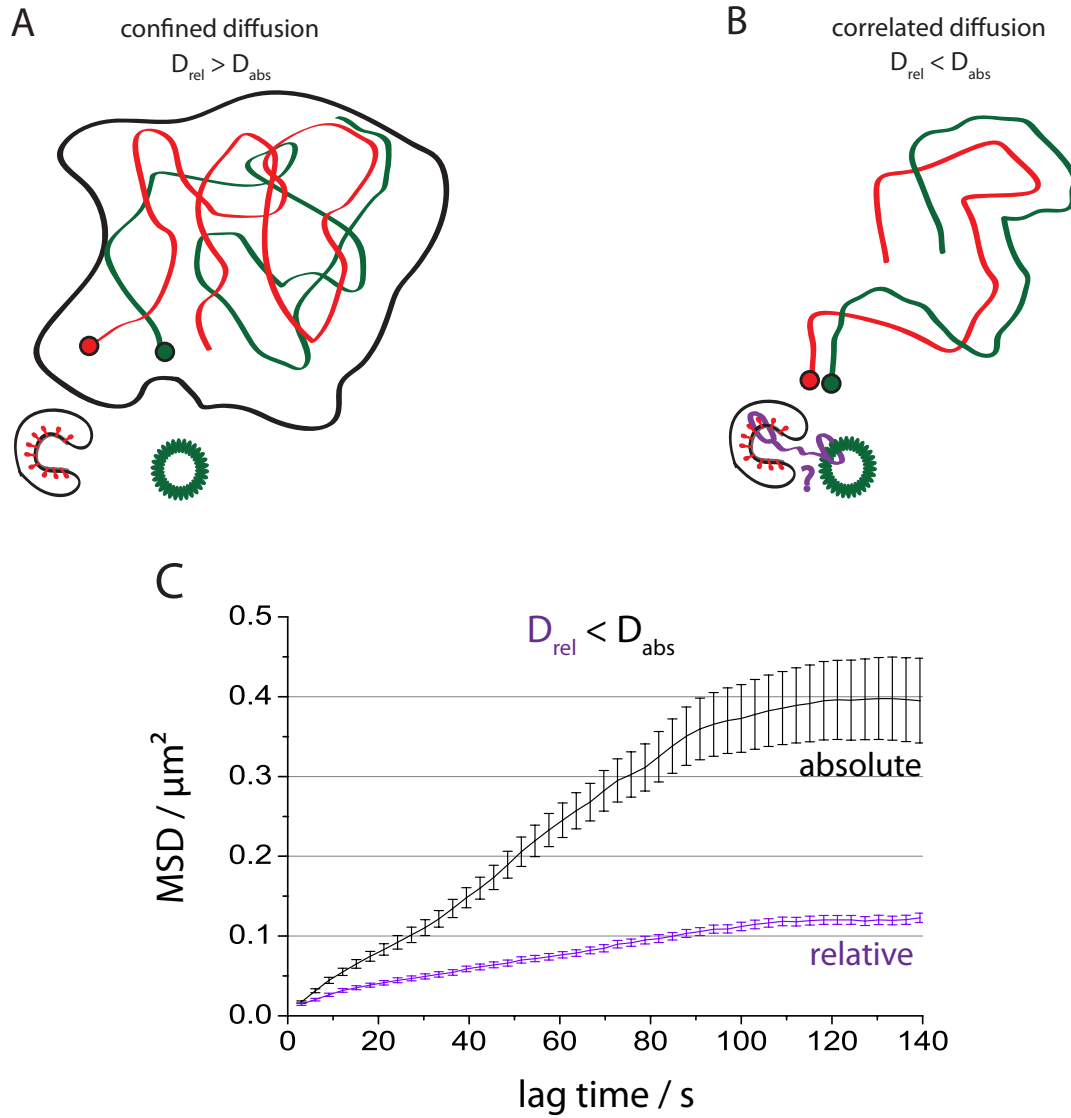
Figure 7.10: *Analysis of the movement of capsid and envelope during stage two. (A) For independent, co-confined diffusion in a restricted area, the relative diffusion coefficient is higher than the absolute diffusion coefficient: $D_{rel} > D_{abs}$. (B) For correlated diffusion of capsid and envelope, the relative diffusion coefficient is lower than the absolute diffusion coefficient: $D_{rel} < D_{abs}$. (C) An MSD analysis of the relative and absolute trajectory during stage two of the SE Ch fusion event shown in figure 7.8. From the MSD analysis of the single trajectory, the diameter of the confinement is estimated to around 0.6 μm. The diffusion coefficient for the relative motion of capsid and envelope (purple) is lower than the diffusion coefficient of the absolute trajectory of the capsid (black). This suggests that capsid and envelope are still linked together.*

envelope are separated by 100 nm to 400 nm. A long duration of the fusion process over more than ten minutes was also reported for HIV entry in epithelial and lymphoid cells [217]. For VSV, it was shown that fusion occurred sequentially. The different steps during fusion were not only temporally separated but also occurred at different locations [183]. Virus particles fused with an endosomal membrane prior to being transported to late endosomes, whereas transport to late endosomes was required in order to release the nucleocapsid in the cytoplasm [183].

At the moment, it is unclear whether the loosened FV capsid – Env interaction overlaps with intermediate fusion steps of the "cast-and-fold" mechanism that have been previously characterized or is a novel intermediate step in the fusion process. Melikyan *et al.* reported that small transient pores can last relatively long so that the capsid is still trapped [207]. Using ASLV particles, Padilla *et al.* observed that the rate of pore enlargement was receptor-dependent [238]. Twice as much capsid particles (or large oligomeric Gag-GFP complexes) were released from endosomes during a time window of two minutes after triggering pore opening in cells expressing a transmembrane receptor (TVA950) than in cells expressing a lipid-anchored receptor (TVA800) [238]. Furthermore, they observed incomplete separation of capsid and Env signals on some occasions [238], resembling to the intermediate stage during the FV fusion process.

This is the first time that the final capsid – Env separation was investigated with such a high temporal and spatial resolution in 3D. We cannot yet determine whether this intermediate stage is generalizable for other retroviruses or a particularity of the foamy virus. The duration of the fusion process can also depend on many variables, for example the cell line. Possibly, FV has developed a somewhat different fusion strategy than other retroviruses. The life cycle of FV differs in some aspects, e.g. particle budding and release requires expression of Gag and Env [72]. However, the recent publication of Padilla *et al.* on ASLV fusion indicates that this retrovirus may also exhibit such an intermediate phase prior to the final separation of capsid and Env [238]. Further investigations are needed to clarify the different steps in the FV fusion process as well as of other (retro)viruses and to clarify whether such an intermediate phase is also observed during membrane fusion of other viruses.

8 Comparison of HSV-1 and FV entry

The focus of this work was on the investigation of virus entry of two enveloped viruses: herpes simplex virus 1 (HSV-1) and foamy virus (FV). The diameter of HSV-1 (225 nm) is about twice the diameter of FV ($\sim$ 120 nm). This difference in size already suggests that HSV-1 and FV exploit somewhat different entry pathways. However, both viruses need to fuse with the cellular membrane to deliver their genome for replication. In the case of HSV-1, the site of virus fusion varies among the investigated cell lines. Depending on the cell line, fusion can directly occur with the plasma membrane or after endocytic uptake by fusion with the membrane of an early or late endosome. Very little is known about the entry mechanism of foamy viruses. Prior to these studies, it was still unclear whether they are capable of fusion at the plasma membrane and which endocytic mechanisms are used for infectious uptake.

In order to investigate the uptake and fusion process, both virus particles were fluorescently tagged by our collaboration partners at the envelope and at the capsid. This way, fusion can be detected by the separation of capsid and envelope signals. HSV-1 particles contained a GFP-tag at the envelope (or outer tegument) and an RFP-tag at the capsid. FV particles had an mCherry-tag at the envelope and a GFP-tag at the capsid.

8.1 Colocalization percentage of dual-color virus preparations

The colocalization percentage of initial dual-color virus preparations was very low in the case of HSV-1. Only about 40 % of the capsid particles contained an additional envelope signal. By performing a large screening procedure for the best optimization conditions, the percentage of colocalizing capsid particles was increased to 70 % (table 6.1). In contrast, already the first double-tagged FV preparations contained about 95 % of colocalizing capsid particles (table 7.1). Approximately 50 % of envelope-only particles were

present in preparations of both viruses.

The observed difference in the colocalization percentage can be attributed to distinct replication mechanism of these viruses. HSV-1 capsids are assembled in the nucleus and released in the cytoplasm by budding through the nuclear membrane [112]. Subsequently, tegumentation is completed, the viral envelope is acquired by budding into vesicles of the trans-Golgi network and virus particles are released through exocytosis [212]. A particularity of foamy virus is that particle budding and release requires co-expression of Gag and Env. In the absence of Env glycoproteins, no or only few particles are released into the cell culture supernatant [16, 90]. This explains why almost all FV capsid particles contain an additional envelope signal.

Envelope-only particles were observed for both types of virus preparations. Final envelopment of HSV-1 can also occur in the absence of capsids, thereby producing envelope-only (or so-called L-particles), consisting only of the tegument proteins and a functional viral envelope [204, 212, 256, 305]. Production of L-particles probably plays an important role in virus infection since infectivity of functional virus particles could be significantly enhanced by addition of these L-particles [65]. Envelope-only particles were also present in FV preparations and it has been reported that the expression of Env glycoproteins alone is sufficient for particle budding [278]. An increased release of subviral particles was reported after mutations at the leader peptide of the virus envelope [291]. Therefore, introduction of the mCherry-tag, located at the leader peptide of the viral envelope, may result in increased subviral particle release.

8.2 Colocalization analysis in cells

In order to obtain insights into the fusion activity of the different viruses and the time scale on which viral entry and fusion occur, we analyzed the fraction of colocalized capsid and envelope signals in cells over time. Fusion of the virus with a cellular membrane leads to the separation of capsid and envelope signals which results in a decrease of dual-color particles. In the case of HSV-1, the pH-sensitive GFP-tag is located at the viral envelope. Quenching experiments revealed that the GFP intensity is significantly reduced at the pH values found in late endosomes (figure 6.11.A on page 103). Therefore, quenching of the GFP-envelope signal in endosomes was avoided by performing experiments on fixed and permeabilized cells to ensure neutral pH throughout all cellular compartments. This allowed the analysis of cells over a broad time range, from 0 hours to 3.5 hours, as photobleaching was no issue (section 6.4). FV contains the pH-sensitive GFP-tag at the capsid and quenching experiments gave evidence that the Gag-eGFP signal should

be detectable at pH values found in late endosomes (figure 7.5.A on page 127). Hence, colocalization of FV particles could be determined in live cells having the advantage that one variable is reduced as the same set of cells is evaluated over time (section 7.2).

For HSV-1 and FV (PE Ch and SE Ch particles), the elucidated percentage of capsid particles colocalizing with an additional envelope signal over time is given in figure 8.1. Initial dc HSV-1 preparations contained a far lower percentage of dual-color particles than FV preparations (71 % compared to 93 %). For comparison of the fraction of dual-color particles undergoing fusion, the plots are normalized to the total number of initially detected dual-color particles (figure 8.1). As samples were fixed in the case of HSV-1, the colocalization percentage of HSV-1 was evaluated over a longer time-window of 3.5 hours. The fraction of colocalizing capsid particles slightly decreased with time (figure 8.1.A). In the case of FV, the colocalization percentage was evaluated in live cells over 90 minutes. Already, within the first 30 minutes, a significant decay in the colocalization percentage of PE Ch particles was observed (figure 8.1.B) and after 30 minutes post binding, more dual-color viruses have fused than in the case of HSV-1 (figure 8.1.A). For SE Ch particles, a slow decrease in the fraction of dual-color viruses was observed during 90 minutes post binding (figure 8.1.C). In the case of PE Ch particles, the percentage of dual-color particles increased after 30 minutes post binding, which is attributed to the formation of large aggregates of both capsid and envelope signals in the perinuclear region that made it impossible to analyze individual particles in this region. Both, the limited sensitivity in the perinuclear region as well as capsid disassembly, would lead to a decrease in the detection of capsid-only particles.

For the investigation of individual fusion events with high temporal resolution, it is important to know when most fusion events are expected. A typical movie with high temporal resolution is started after about five minutes and recorded over a duration of about 20 minutes. After the measurement time of 20 minutes, the signal-to-noise ratio is too low due to photobleaching of the fluorophores. In order to compare how many fusion events are expected for HSV-1 and FV during this duration, the obtained colocalization values over time were fitted with an exponential decay with weighted errors. As an increase in the fraction of dual-color particles was observed for PE Ch after 25 minutes, the time-points after 25 minutes were not included in the fit. Including the later time-points for FV would lower the decay rate during the first 25 minutes and therefore, the calculated number of fusion events during this duration would be underestimated. As the number of viruses undergoing fusion during the first 25 minutes is important, it is appropriate to only include the first data-points of the FV plot.

Out of the fit, the percentage of all dual-color particles that undergo fusion during the

first 25 minutes post binding is expected to be around 7 % in the case of HSV-1, around 19 % for PE Ch and around 3 % for SE Ch. The probability to detect individual fusion events in real-time does not only depend on the number of dc particles that undergo fusion during a certain time window but also on the fraction of dual-color particles present in the virus preparations. To account for the different fractions of dual-color particles in the virus preparations, the number of expected fusion events is given in the following relative to 100 capsid particles. In the case of PE Ch, ten fusion events should occur within the first three minutes, whereas for HSV-1, it would take one hour to detect the same number of fusion events. For SE Ch, only about eight fusion events are expected to occur during the first 90 minutes post binding. After 25 minutes, five HSV-1 particles, 17 PE Ch particles and three SE Ch particles out of 100 capsid particles should have fused. Particle numbers per cell are typically below 100 particles to avoid saturation of the cell-surface and to have biologically more relevant conditions. Hence, detection of an individual fusion event in real-time is challenging.

8.3 Analysis of individual virus trajectories

To gain insight into the entry pathway of HSV-1 and FV on a single particle level, movies were recorded with high time resolution during the first 30 minutes post binding of dual-color particles to live cells. Analysis of individual virus trajectories of PE Ch particles revealed 13 fusion events out of approximately 560 capsid particles ($\sim$ 520 dc particles) (previous chapter 7.3). In the case of SE Ch particles, three fusion events were detected out of about 650 capsid particles ($\sim$ 600 dc particles) (previous chapter 7.3). Estimated from the number of detected fusion events, the probability to detect a fusion event is about five times higher for PE Ch particles compared to SE Ch particles. From the 3D colocalization analysis in cells, the probability for fusion was estimated to be around 6.4 times higher for PE Ch particles during the first 25 minutes post binding (figure 8.1.B and C, respectively).

For HSV-1, no fusion event was detected out of 570 HSV-1 capsid particles ($\sim$ 120 dc particles) (section 6.6). These results are consistent with the 3D colocalization experiment in cells over time, which revealed that the probability to detect fusion within the first 25 minutes post binding is 3.6 times higher for PFV than for HSV-1. Estimated from the results of the individual PFV fusion events, one would need to analyze more than 2000 capsid particles ($>$ 1400 dc particles) to detect 13 events of HSV-1 fusion in the case of the virus preparation used in the 3D colocalization experiment (RFPVP26-gDGFP). However, in the experiment focusing on individual virus trajectories, a somewhat dif-
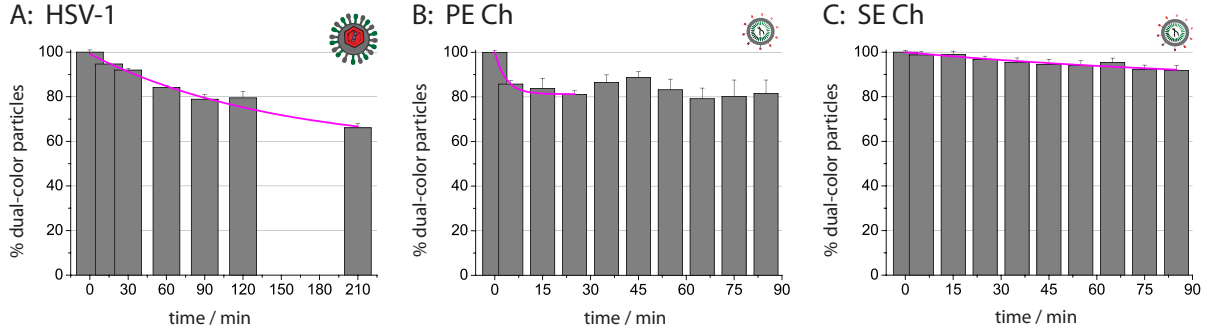
Figure 8.1: *The fraction of dual-color particles in cells over time is compared for HSV-1 (RFPVP26-gDGFP particles) and FV (PE Ch and SE Ch particles). The number of capsid particles colocalizing with an additional envelope signal was evaluated over time. For comparison of the different viruses, the percentage of dc particles was normalized to the total number of initially detected dc particles. The percentage of dc particles is plotted (gray bars) together with the standard error of the mean (error bars). Data points were fitted with an exponential decay with weighted errors, $y = A_1 \cdot e^{-\frac{x}{t_1}} + y_0$. (A) HSV-1: the fraction of colocalizing capsid particles was evaluated in fixed and permeabilized cells due to the pH-sensitivity of the GFP-tag at the viral envelope. Colocalization was evaluated over a duration of 3.5 hours as photobleaching and phototoxic effects were not an issue. $A_1 = 42.4 \pm 6.0$, $t_1 = 144.3 \pm 34.3$ min, $y_0 = 56.8 \pm 6.3$, $R^2 = 0.987$. (B) PE Ch: the fraction of colocalizing capsid particles was determined in live cells over a duration of 90 minutes. Only the first 25 minutes post binding are included in the fit as the colocalization percentage increased afterwards. The number of expected fusion events during the first 25 minutes is important as this is the duration of a typical movie with real-time acquisition. $A_1 = 18.7 \pm 1.9$, $t_1 = 3.5 \pm 1.1$ min, $y_0 = 81.3 \pm 1.6$, $R^2 = 0.998$. (C) SE Ch: the fraction of colocalizing capsid particles was determined in live cells over a duration of 90 minutes. $A_1 = 14.7 \pm 21.3$, $t_1 = 112.2 \pm 223.1$ min, $y_0 = 85.2 \pm 21.6$, $R^2 = 0.946$. The calculated numbers of expected fusion events out of the fit are in the range of the detected numbers from the experiment during 90 minutes post binding.*

ferent HSV-1 construct (ChVP26-VP11/12GFP) was used that should possess a higher fusion activity. The virus preparation, ChVP26-VP11/12GFP, showed a higher viral titer but only very few colocalizing particles (about 25 % of colocalizing caspids). Due to the higher viral titer, more dc particles are expected to fuse. However, the probability to detect a fusion event is reduced by the low colocalization percentage of the HSV-1 particles.

In the case of the detected FV fusion events, an intermediate stage was observed during virus fusion that lasted over minutes. This stage was characterized by an increase in the distance between envelope and capsid signals over 100 nm to 400 nm prior to the final color separation. However, it is not clear to what this intermediate stage can be attributed. One explanation could be that (i) fusion already occurred between stage one and stage two, but that capsid and envelope were both confined in a small compartment (figure 7.10.A on page 145). Another explanation would be that (ii) capsid and envelope were still linked together during this intermediate phase until the final separation occurred between stage two and stage three (figure 7.10.B). For independent, co-confined diffusion in a restricted area, the diffusion coefficient of the relative trajectory should be higher than that of either single trajectory: $D_{rel} > D_{abs}$. In the case of correlated diffusion of capsid and envelope, the relative diffusion coefficient is expected to be lower than the absolute one: $D_{rel} < D_{abs}$. To distinguish between these two hypotheses, we performed a mean-square-displacement (MSD) analysis on the relative trajectory of the envelope with respect to the capsid and compared it with the MSD of the absolute trajectory of the capsid.

For comparison, an MSD analysis was performed on the absolute and relative trajectories of two distinct HSV-1 particles that were located accidentally close to each other. The particles did not colocalize and moved about each other over a duration of 20 minutes as was confirmed by an image cross-correlation analysis with the TrIC software (figure 6.19 on page 119). Both particles exhibited diffusion with an underlying flow, resulting from movement of the cell. As we analyzed two distinct particles, the relative diffusion coefficient is higher than the absolute diffusion coefficient as can be seen in figure 8.2.A. At longer lag times, the MSD of the single trajectory is larger compared to the MSD of the relative trajectory as movement with the underlying flow becomes the dominating term. An exemplary MSD analysis during FV fusion is given in figure 8.2.B. In contrast to the result obtained for the two distinct HSV-1 particles, the relative diffusion coefficient was below the absolute one in all analyzed FV events (figure 8.2). These findings suggest that capsid and envelope are still linked together rather than just being confined in the same compartment during the intermediate stage in FV fusion. It is not clear, whether other viruses also exhibit such an intermediate stage during virus fusion or if this is a
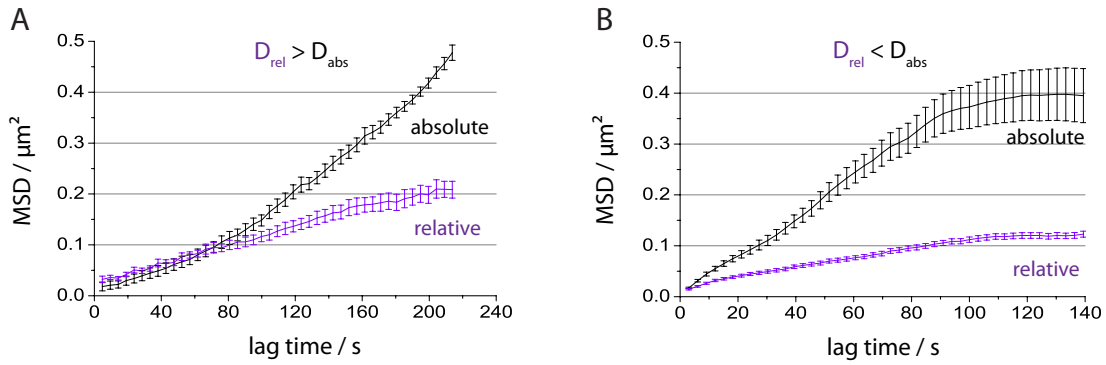
Figure 8.2: *Exemplary MSD analysis of absolute (black) and relative (purple) trajectories. (A) HSV-1: Capsid- and envelope-only particles did not colocalize and moved independently of each other on short time-scales. Both particles showed movement with an underlying flow, resulting from movement of the cell. The relative diffusion coefficient is higher than the absolute diffusion coefficient. At longer lag times, the MSD of the single trajectory is larger compared to the MSD of the relative trajectory as movement with the underlying flow becomes the dominating term. (B) FV: Analysis of the relative movement of capsid and envelope of the SE Ch fusion event shown in figure 7.8. From the MSD analysis of the single trajectory, the diameter of the confinement is estimated to around 0.6 µm. The relative diffusion coefficient is lower than the absolute diffusion coefficient, suggesting that capsid and envelope are still somehow linked together.*

particularity of the foamy virus. On page 144 - 146 of section 7.3.4, the occurrence of this intermediate stage is discussed in relation with different steps assumed to occur during virus fusion and with what has been reported so far for fusion of other viruses.

Bibliography

[1] ACHONG, B. G., MANSELL, P. W., EPSTEIN, M. A., AND CLIFFORD, P. An unusual virus in cultures from a human nasopharyngeal carcinoma. *Journal of the National Cancer Institute 46*, 2 (1971), 299–307.

[2] AIRY, G. B. On the diffraction of an object-glass with circular aperture. *Transactions of the Cambridge Philosophical Society 5* (1835), 283–91.

[3] AKHTAR, J., AND SHUKLA, D. Viral entry mechanisms: cellular and viral mediators of herpes simplex virus entry. *FEBS Journal 276*, 24 (2009), 7228–36.

[4] AKHTAR, J., TIWARI, V., OH, M. J., KOVACS, M., JANI, A., KOVACS, S. K., VALYI-NAGY, T., AND SHUKLA, D. HVEM and nectin-1 are the major mediators of herpes simplex virus 1 (HSV-1) entry into human conjunctival epithelium. *Investigative Ophthalmology and Visual Science 49*, 9 (2008), 4026–35.

[5] ANDERSON, H. A., CHEN, Y., AND NORKIN, L. C. Bound simian virus 40 translocates to caveolin-enriched membrane domains, and its entry is inhibited by drugs that selectively disrupt caveolae. *Molecular Biology of the Cell 7*, 11 (1996), 1825–34.

[6] ANDO, R., HAMA, H., YAMAMOTO-HINO, M., MIZUNO, H., AND MIYAWAKI, A. An optical marker based on the UV-induced green-to-red photoconversion of a fluorescent protein. *Proceedings of the National Academy of Sciences of the United States of America 99*, 20 (2002), 12651–6.

[7] ANTINONE, S. E., AND SMITH, G. A. Retrograde axon transport of herpes simplex virus and pseudorabies virus: a live-cell comparative analysis. *Journal of Virology 84*, 3 (2010), 1504–12.

[8] APETREI, C., ROBERTSON, D. L., AND MARX, P. A. The history of SIVS and AIDS: epidemiology, phylogeny and biology of isolates from naturally SIV infected non-human primates (NHP) in Africa. *Frontiers in Bioscience 9* (2004), 225–54.

[9] ARDUINO, P. G., AND PORTER, S. R. Herpes simplex virus type 1 infection: overview on relevant clinico-pathological features. *Journal of Oral Pathology and Medicine 37*, 2 (2008), 107–21.

[10] ARII, J., GOTO, H., SUENAGA, T., OYAMA, M., KOZUKA-HATA, H., IMAI, T., MINOWA, A., AKASHI, H., ARASE, H., KAWAOKA, Y., AND KAWAGUCHI, Y. Non-muscle myosin IIA is a functional entry receptor for herpes simplex virus-1. *Nature 467*, 7317 (2010), 859–62.

[11] ARII, J., UEMA, M., MORIMOTO, T., SAGARA, H., AKASHI, H., ONO, E., ARASE, H., AND KAWAGUCHI, Y. Entry of herpes simplex virus 1 and other alphaherpesviruses via the paired immunoglobulin-like type 2 receptor alpha. *Journal of Virology 83*, 9 (2009), 4520–7.

[12] ATANASIU, D., SAW, W. T., COHEN, G. H., AND EISENBERG, R. J. Cascade of events governing cell-cell fusion induced by herpes simplex virus glycoproteins gD, gH/gL, and gB. *Journal of Virology 84*, 23 (2010), 12292–9.

[13] ATANASIU, D., WHITBECK, J. C., DE LEON, M. P., LOU, H., HANNAH, B. P., COHEN, G. H., AND EISENBERG, R. J. Bimolecular complementation defines functional regions of herpes simplex virus gB that are involved with gH/gL as a necessary step leading to cell fusion. *Journal of Virology 84*, 8 (2010), 3825–34.

[14] AXELROD, D. Total internal reflection fluorescence microscopy in cell biology. *Methods in Enzymology 361* (2003), 1–33.

[15] BAINES, J. D., AND ROBERTS, K. L. Nuclear egress and envelopment of HSV. In *Alphaherpesviruses*, S. K. Weller, Ed. Caister Academic Press, Norfolk, UK, 2011.

[16] BALDWIN, D. N., AND LINIAL, M. L. The roles of pol and env in the assembly pathway of human foamy virus. *Journal of Virology 72*, 5 (1998), 3658–65.

[17] BALL, L. A. Virus replication strategies. In *Fields Virology*, D. M. Knipe, P. M. Howley, and D. E. Griffin, Eds., 5 ed. Lippincott Williams & Wilkins, 2007.

[18] BAUSINGER, R., VON GERSDORFF, K., BRAECKMANS, K., OGRIS, M., WAGNER, E., BRAUCHLE, C., AND ZUMBUSCH, A. The transport of nanosized gene

carriers unraveled by live-cell imaging. *Angewandte Chemie. International Ed. In English 45*, 10 (2006), 1568–72.

[19] BENASHSKI, S. E., HARRISON, A., PATEL-KING, R. S., AND KING, S. M. Dimerization of the highly conserved light chain shared by dynein and myosin V. *Journal of Biological Chemistry 272*, 33 (1997), 20929–35.

[20] BENDER, F. C., WHITBECK, J. C., LOU, H., COHEN, G. H., AND EISENBERG, R. J. Herpes simplex virus glycoprotein B binds to cell surfaces independently of heparan sulfate and blocks virus entry. *Journal of Virology 79*, 18 (2005), 11588–97.

[21] BETZIG, E., PATTERSON, G. H., SOUGRAT, R., LINDWASSER, O. W., OLENYCH, S., BONIFACINO, J. S., DAVIDSON, M. W., LIPPINCOTT-SCHWARTZ, J., AND HESS, H. F. Imaging intracellular fluorescent proteins at nanometer resolution. *Science 313*, 5793 (2006), 1642–5.

[22] BIZZARRI, R., SERRESI, M., LUIN, S., AND BELTRAM, F. Green fluorescent protein based pH indicators for in vivo use: a review. *Analytical and Bioanalytical Chemistry 393*, 4 (2009), 1107–22.

[23] BLEWETT, E. L., BLACK, D. H., LERCHE, N. W., WHITE, G., AND EBERLE, R. Simian foamy virus infections in a baboon breeding colony. *Virology 278*, 1 (2000), 183–93.

[24] BORN, M., AND OPPENHEIMER, R. Zur Quantentheorie der Molekeln. *Annalen der Physik 389*, 20 (1927), 457–84.

[25] BRIGGS, J. A., SIMON, M. N., GROSS, I., KRAUSSLICH, H. G., FULLER, S. D., VOGT, V. M., AND JOHNSON, M. C. The stoichiometry of Gag protein in HIV-1. *Nature Structural & Molecular Biology 11*, 7 (2004), 672–5.

[26] BRIGGS, J. A. G., JOHNSON, M. C., SIMON, M. N., FULLER, S. D., AND VOGT, V. M. Cryo-electron microscopy reveals conserved and divergent features of Gag packing in immature particles of rous sarcoma virus and human immunodeficiency virus. *Journal of Molecular Biology 355*, 1 (2006), 157–68.

[27] CAMPADELLI-FIUME, G., AMASIO, M., AVITABILE, E., CERRETANI, A., FORGHIERI, C., GIANNI, T., AND MENOTTI, L. The multipartite system that mediates entry of herpes simplex virus into the cell. *Reviews in Medical Virology 17*, 5 (2007), 313–26.

[28] CAMPADELLI-FIUME, G., ARSENAKIS, M., FARABEGOLI, F., AND ROIZMAN, B. Entry of herpes simplex virus 1 in BJ cells that constitutively express viral glycoprotein D is by endocytosis and results in degradation of the virus. *Journal of Virology 62*, 1 (1988), 159–67.

[29] CAMPADELLI-FIUME, G., COCCHI, F., MENOTTI, L., AND LOPEZ, M. The novel receptors that mediate the entry of herpes simplex viruses and animal alphaherpesviruses into cells. *Reviews in Medical Virology 10*, 5 (2000), 305–19.

[30] CAMPADELLI-FIUME, G., MENOTTI, L., AVITABILE, E., AND GIANNI, T. Viral and cellular contributions to herpes simplex virus entry into the cell. *Current Topics in Virology 2*, 1 (2012), 28–36.

[31] CAMPBELL, R. E., TOUR, O., PALMER, A. E., STEINBACH, P. A., BAIRD, G. S., ZACHARIAS, D. A., AND TSIEN, R. Y. A monomeric red fluorescent protein. *Proceedings of the National Academy of Sciences of the United States of America 99*, 12 (2002), 7877–82.

[32] CARFI, A., WILLIS, S. H., WHITBECK, J. C., KRUMMENACHER, C., COHEN, G. H., EISENBERG, R. J., AND WILEY, D. C. Herpes simplex virus glycoprotein D bound to the human receptor HveA. *Molecular Cell 8*, 1 (2001), 169–79.

[33] CARLSON, L. A., BRIGGS, J. A., GLASS, B., RICHES, J. D., SIMON, M. N., JOHNSON, M. C., MULLER, B., GRUNEWALD, K., AND KRAUSSLICH, H. G. Three-dimensional analysis of budding sites and released virus suggests a revised model for HIV-1 morphogenesis. *Cell Host Microbe 4*, 6 (2008), 592–9.

[34] CHALFIE, M., TU, Y., EUSKIRCHEN, G., WARD, W. W., AND PRASHER, D. C. Green fluorescent protein as a marker for gene expression. *Science 263*, 5148 (1994), 802–5.

[35] CHAN, P. K. Outbreak of avian influenza A(H5N1) virus infection in Hong Kong in 1997. *Clinical Infectious Diseases 34 Suppl 2* (2002), S58–64.

[36] CHENG, Y., AND WALZ, T. The advent of near-atomic resolution in single-particle electron microscopy. *Annual Review of Biochemistry 78* (2009), 723–42.

[37] CHERNOMORDIK, L. V., AND KOZLOV, M. M. Protein-lipid interplay in fusion and fission of biological membranes. *Annual Review of Biochemistry 72* (2003), 175–207.

[38] CHERNOMORDIK, L. V., ZIMMERBERG, J., AND KOZLOV, M. M. Membranes of the world unite! *Journal of Cell Biology 175*, 2 (2006), 201–7.

[39] CHESHENKO, N., DEL ROSARIO, B., WODA, C., MARCELLINO, D., SATLIN, L. M., AND HEROLD, B. C. Herpes simplex virus triggers activation of calcium-signaling pathways. *Journal of Cell Biology 163*, 2 (2003), 283–93.

[40] CHESHENKO, N., LIU, W., SATLIN, L. M., AND HEROLD, B. C. Multiple receptor interactions trigger release of membrane and intracellular calcium stores critical for herpes simplex virus entry. *Molecular Biology of the Cell 18*, 8 (2007), 3119–30.

[41] CHESHENKO, N., TREPANIER, J. B., SEGARRA, T. J., FULLER, A. O., AND HEROLD, B. C. HSV usurps eukaryotic initiation factor 3 subunit M for viral protein translation: novel prevention target. *PLoS One 5*, 7 (2010), e11829.

[42] CHOU, J., AND ROIZMAN, B. The gamma 1(34.5) gene of herpes simplex virus 1 precludes neuroblastoma cells from triggering total shutoff of protein synthesis characteristic of programed cell death in neuronal cells. *Proceedings of the National Academy of Sciences of the United States of America 89*, 8 (1992), 3266–70.

[43] CHOWDARY, T. K., CAIRNS, T. M., ATANASIU, D., COHEN, G. H., EISENBERG, R. J., AND HELDWEIN, E. E. Crystal structure of the conserved herpesvirus fusion regulator complex gH-gL. *Natural Structural Biology 17*, 7 (2010), 882–8.

[44] CLEMENT, C., TIWARI, V., SCANLAN, P. M., VALYI-NAGY, T., YUE, B. Y., AND SHUKLA, D. A novel role for phagocytosis-like uptake in herpes simplex virus entry. *Journal of Cell Biology 174*, 7 (2006), 1009–21.

[45] COCCHI, F., FUSCO, D., MENOTTI, L., GIANNI, T., EISENBERG, R. J., COHEN, G. H., AND CAMPADELLI-FIUME, G. The soluble ectodomain of herpes simplex virus gD contains a membrane-proximal pro-fusion domain and suffices to mediate virus entry. *Proceedings of the National Academy of Sciences of the United States of America 101*, 19 (2004), 7445–50.

[46] COCCHI, F., MENOTTI, L., DUBREUIL, P., LOPEZ, M., AND CAMPADELLI-FIUME, G. Cell-to-cell spread of wild-type herpes simplex virus type 1, but not of syncytial strains, is mediated by the immunoglobulin-like receptors that mediate virion entry, nectin1 (PRR1/HveC/HIgR) and nectin2 (PRR2/HveB). *Journal of Virology 74*, 8 (2000), 3909–17.

[47] COCCHI, F., MENOTTI, L., MIRANDOLA, P., LOPEZ, M., AND CAMPADELLI-FIUME, G. The ectodomain of a novel member of the immunoglobulin subfamily related to the poliovirus receptor has the attributes of a bona fide receptor for herpes simplex virus types 1 and 2 in human cells. *Journal of Virology 72*, 12 (1998), 9992–10002.

[48] COHEN, J. I. Epstein-Barr virus infection. *New England Journal of Medicine 343*, 7 (2000), 481–92.

[49] COHEN, J. I., STRAUS, S. E., AND ARVIN, A. M. Varicella-zoster virus replication, pathogenesis, and management. In *Fields Virology*, D. M. Knipe, P. M. Howley, and D. E. Griffin, Eds., 5 ed. Lippincott Williams & Wilkins, 2007.

[50] COHRS, R. J., AND GILDEN, D. H. Human herpesvirus latency. *Brain Pathology 11*, 4 (2001), 465–74.

[51] COLLINS, S. A., GUINN, B. A., HARRISON, P. T., SCALLAN, M. F., O'SULLIVAN, G. C., AND TANGNEY, M. Viral vectors in cancer immunotherapy: which vector for which strategy? *Current Gene Therapy 8*, 2 (2008), 66–78.

[52] CONDIT, R. C. Principles of virology. In *Fields Virology*, D. M. Knipe, P. M. Howley, and D. E. Griffin, Eds., 5 ed. Lippincott Williams & Wilkins, 2007.

[53] CONDIT, R. C., MOUSSATCHE, N., AND TRAKTMAN, P. In a nutshell: structure and assembly of the vaccinia virion. *Advances in Virus Research 66* (2006), 31–124.

[54] CONDON, E. A theory of intensity distribution in band systems. *Physical Review 28*, 6 (1926), 1182–201.

[55] CONDON, E. U. Nuclear motions associated with electron transitions in diatomic molecules. *Physical Review 32*, 6 (1928), 858–72.

[56] CONDON, E. U. The Franck-Condon principle and related topics. *American Journal of Physics 15*, 5 (1947), 365–74.

[57] CONNER, S. D., AND SCHMID, S. L. Regulated portals of entry into the cell. *Nature 422*, 6927 (2003), 37–44.

[58] CONNOLLY, S. A., JACKSON, J. O., JARDETZKY, T. S., AND LONGNECKER, R. Fusing structure and function: a structural view of the herpesvirus entry machinery. *Nature Reviews: Microbiology 9*, 5 (2011), 369–81.

[59] Corey, L., and Spear, P. G. Infections with herpes simplex viruses (1). *New England Journal of Medicine 314*, 11 (1986), 686–91.

[60] Crick, F. H., and Watson, J. D. Structure of small viruses. *Nature 177*, 4506 (1956), 473–5.

[61] Croft, M. Co-stimulatory members of the TNFR family: keys to effective T-cell immunity? *Nature Reviews: Immunology 3*, 8 (2003), 609–20.

[62] Cureton, D. K., Massol, R. H., Saffarian, S., Kirchhausen, T. L., and Whelan, S. P. J. Vesicular stomatitis virus enters cells through vesicles incompletely coated with clathrin that depend upon actin for internalization. *PLoS Pathogens 5*, 4 (2009), e1000394.

[63] Daecke, J., Fackler, O. T., Dittmar, M. T., and Krausslich, H. G. Involvement of clathrin-mediated endocytosis in human immunodeficiency virus type 1 entry. *Journal of Virology 79*, 3 (2005), 1581–94.

[64] Damm, E. M., Pelkmans, L., Kartenbeck, J., Mezzacasa, A., Kurzchalia, T., and Helenius, A. Clathrin- and caveolin-1-independent endocytosis: entry of simian virus 40 into cells devoid of caveolae. *Journal of Cell Biology 168*, 3 (2005), 477–88.

[65] Dargan, D. J., and Subak-Sharpe, J. H. The effect of herpes simplex virus type 1 L-particles on virus entry, replication, and the infectivity of naked herpesvirus DNA. *Virology 239*, 2 (1997), 378–88.

[66] Davis-Poynter, N., Bell, S., Minson, T., and Browne, H. Analysis of the contributions of herpes simplex virus type 1 membrane proteins to the induction of cell-cell fusion. *Journal of Virology 68*, 11 (1994), 7586–90.

[67] Davison, A. J. Channel catfish virus: a new type of herpesvirus. *Virology 186*, 1 (1992), 9–14.

[68] Davison, A. J. Evolution of the herpesviruses. *Veterinary Microbiology 86*, 1-2 (2002), 69–88.

[69] Davison, A. J., Eberle, R., Ehlers, B., Hayward, G. S., McGeoch, D. J., Minson, A. C., Pellett, P. E., Roizman, B., Studdert, M. J., and Thiry, E. The order Herpesvirales. *Archives of Virology 154*, 1 (2009), 171–7.

[70] DE JONG, M. A., DE WITTE, L., BOLMSTEDT, A., VAN KOOYK, Y., AND GEIJTENBEEK, T. B. Dendritic cells mediate herpes simplex virus infection and transmission through the C-type lectin DC-SIGN. *Journal of General Virology 89*, Pt 10 (2008), 2398–409.

[71] DELBOY, M. G., PATTERSON, J. L., HOLLANDER, A. M., AND NICOLA, A. V. Nectin-2-mediated entry of a syncytial strain of herpes simplex virus via pH-independent fusion with the plasma membrane of Chinese hamster ovary cells. *Virology Journal 3* (2006), 105.

[72] DELELIS, O., LEHMANN-CHE, J., AND SAIB, A. Foamy viruses – a world apart. *Current Opinion in Microbiology 7*, 4 (2004), 400–6.

[73] DELELIS, O., SAIB, A., AND SONIGO, P. Biphasic DNA synthesis in spumaviruses. *Journal of Virology 77*, 14 (2003), 8141–6.

[74] DERMOTT, E., AND SAMUELS, J. Electron microscopic observations on the mechanisms of entry of simian foamy virus in HEp-2 cells. *Journal of General Virology 19*, 1 (1973), 135–9.

[75] DITTRICH, P. S., AND SCHWILLE, P. Photobleaching and stabilization of fluorophores used for single-molecule analysis with one- and two-photon excitation. *Applied Physics B: Lasers and Optics 73*, 8 (2001), 829–37.

[76] DOERR, H., AND ADRIAN, T. *Medizinische Virologie.* Thieme, 2002.

[77] DOHNER, K., NAGEL, C. H., AND SODEIK, B. Viral stop-and-go along microtubules: taking a ride with dynein and kinesins. *Trends in Microbiology 13*, 7 (2005), 320–7.

[78] DOHNER, K., RADTKE, K., SCHMIDT, S., AND SODEIK, B. Eclipse phase of herpes simplex virus type 1 infection: Efficient dynein-mediated capsid transport without the small capsid protein VP26. *Journal of Virology 80*, 16 (2006), 8211–24.

[79] DOHNER, K., WOLFSTEIN, A., PRANK, U., ECHEVERRI, C., DUJARDIN, D., VALLEE, R., AND SODEIK, B. Function of dynein and dynactin in herpes simplex virus capsid transport. *Molecular Biology of the Cell 13*, 8 (2002), 2795–809.

[80] DOLAN, A., JAMIESON, F. E., CUNNINGHAM, C., BARNETT, B. C., AND MCGEOCH, D. J. The genome sequence of herpes simplex virus type 2. *Journal of Virology 72*, 3 (1998), 2010–21.

[81] Douglas, M. W., Diefenbach, R. J., Homa, F. L., Miranda-Saksena, M., Rixon, F. J., Vittone, V., Byth, K., and Cunningham, A. L. Herpes simplex virus type 1 capsid protein VP26 interacts with dynein light chains RP3 and Tctex1 and plays a role in retrograde cellular transport. *Journal of Biological Chemistry 279*, 27 (2004), 28522–30.

[82] Enders, J. F., and Peebles, T. C. Propagation in tissue cultures of cytopathogenic agents from patients with measles. *Proceedings of the Society for Experimental Biology and Medicine 86*, 2 (1954), 277–86.

[83] Endress, T., Lampe, M., Briggs, J. A., Krausslich, H. G., Brauchle, C., Muller, B., and Lamb, D. C. HIV-1-cellular interactions analyzed by single virus tracing. *European Biophysics Journal* (2008).

[84] Epstein, M. A. Observations on the fine structure of mature herpes simplex virus and on the composition of its nucleoid. *Journal of Experimental Medicine 115* (1962), 1–12.

[85] Erlwein, O., Cain, D., Fischer, N., Rethwilm, A., and McClure, M. O. Identification of sites that act together to direct dimerization of human foamy virus RNA in vitro. *Virology 229*, 1 (1997), 251–8.

[86] Fan, Q., Lin, E., and Spear, P. G. Insertional mutations in herpes simplex virus type 1 gL identify functional domains for association with gH and for membrane fusion. *Journal of Virology 83*, 22 (2009), 11607–15.

[87] Farnsworth, A., and Johnson, D. C. Herpes simplex virus gE/gI must accumulate in the trans-Golgi network at early times and then redistribute to cell junctions to promote cell-cell spread. *Journal of Virology 80*, 7 (2006), 3167–79.

[88] Farnsworth, A., Wisner, T. W., Webb, M., Roller, R., Cohen, G., Eisenberg, R., and Johnson, D. C. Herpes simplex virus glycoproteins gB and gH function in fusion between the virion envelope and the outer nuclear membrane. *Proceedings of the National Academy of Sciences of the United States of America 104*, 24 (2007), 10187–92.

[89] F.A.S. Frankfurter Allgemeine Sonntagszeitung, Jenseits von Eden, 2012/05/13, 2-3.

[90] Fischer, N., Heinkelein, M., Lindemann, D., Enssle, J., Baum, C., Werder, E., Zentgraf, H., Muller, J. G., and Rethwilm, A. Foamy

virus particle formation. *Journal of Virology 72*, 2 (1998), 1610–5.

[91] FLINT, S. *Principles of virology: molecular biology, pathogenesis, and control of animal viruses.* ASM Press, 2004.

[92] FLOYD, D. L., RAGAINS, J. R., SKEHEL, J. J., HARRISON, S. C., AND VAN OIJEN, A. M. Single-particle kinetics of influenza virus membrane fusion. *Proceedings of the National Academy of Sciences of the United States of America 105*, 40 (2008), 15382–7.

[93] FOSTER, T. P., CHOULJENKO, V. N., AND KOUSOULAS, K. G. Functional characterization of the HveA homolog specified by African green monkey kidney cells with a herpes simplex virus expressing the green fluorescence protein. *Virology 258*, 2 (1999), 365–74.

[94] FOUCHIER, R. A., GARCIA-SASTRE, A., KAWAOKA, Y., BARCLAY, W. S., BOUVIER, N. M., BROWN, I. H., CAPUA, I., CHEN, H., COMPANS, R. W., COUCH, R. B., COX, N. J., DOHERTY, P. C., DONIS, R. O., FELDMANN, H., GUAN, Y., KATZ, J., KLENK, H. D., KOBINGER, G., LIU, J., LIU, X., LOWEN, A., METTENLEITER, T. C., OSTERHAUS, A. D., PALESE, P., PEIRIS, J. S., PEREZ, D. R., RICHT, J. A., SCHULTZ-CHERRY, S., STEEL, J., SUBBARAO, K., SWAYNE, D. E., TAKIMOTO, T., TASHIRO, M., TAUBENBERGER, J. K., THOMAS, P. G., TRIPP, R. A., TUMPEY, T. M., WEBBY, R. J., AND WEBSTER, R. G. Pause on avian flu transmission research. *Science 335*, 6067 (2012), 400–1.

[95] FRANCK, J., AND DYMOND, E. G. Elementary processes of photochemical reactions. *Transactions of the Faraday Society 21*, February (1926).

[96] FREDERICKSEN, B. L., WEI, B. L., YAO, J., LUO, T., AND GARCIA, J. V. Inhibition of endosomal/lysosomal degradation increases the infectivity of human immunodeficiency virus. *Journal of Virology 76*, 22 (2002), 11440–6.

[97] FULLER, A. O., AND SPEAR, P. G. Anti-glycoprotein D antibodies that permit adsorption but block infection by herpes simplex virus 1 prevent virion-cell fusion at the cell surface. *Proceedings of the National Academy of Sciences of the United States of America 84*, 15 (1987), 5454–8.

[98] GALLO, S. A., FINNEGAN, C. M., VIARD, M., RAVIV, Y., DIMITROV, A., RAWAT, S. S., PURI, A., DURELL, S., AND BLUMENTHAL, R. The HIV Env-mediated fusion reaction. *Biochimica et Biophysica Acta 1614*, 1 (2003), 36–50.

[99] GANDHI, M. K., AND KHANNA, R. Human cytomegalovirus: clinical aspects, immune regulation, and emerging treatments. *Lancet Infectious Diseases 4*, 12 (2004), 725–38.

[100] GARNER, J. A. Herpes simplex virion entry into and intracellular transport within mammalian cells. *Advanced Drug Delivery Reviews 55*, 11 (2003), 1497–513.

[101] GENNERICH, A., CARTER, A. P., RECK-PETERSON, S. L., AND VALE, R. D. Force-induced bidirectional stepping of cytoplasmic dynein. *Cell 131*, 5 (2007), 952–65.

[102] GERAGHTY, R. J., KRUMMENACHER, C., COHEN, G. H., EISENBERG, R. J., AND SPEAR, P. G. Entry of alphaherpesviruses mediated by poliovirus receptor-related protein 1 and poliovirus receptor. *Science 280*, 5369 (1998), 1618–20.

[103] GIANNI, T., CAMPADELLI-FIUME, G., AND MENOTTI, L. Entry of herpes simplex virus mediated by chimeric forms of nectin1 retargeted to endosomes or to lipid rafts occurs through acidic endosomes. *Journal of Virology 78*, 22 (2004), 12268–76.

[104] GIANNI, T., CERRETANI, A., DUBOIS, R., SALVIOLI, S., BLYSTONE, S. S., REY, F., AND CAMPADELLI-FIUME, G. Herpes simplex virus glycoproteins H/L bind to cells independently of $\alpha v\beta 3$ integrin and inhibit virus entry, and their constitutive expression restricts infection. *Journal of Virology 84*, 8 (2010), 4013–25.

[105] GIANNI, T., GATTA, V., AND CAMPADELLI-FIUME, G. $\alpha v\beta 3$-integrin routes herpes simplex virus to an entry pathway dependent on cholesterol-rich lipid rafts and dynamin2. *Proceedings of the National Academy of Sciences of the United States of America 107*, 51 (2010), 22260–5.

[106] GODINEZ, W. J., LAMPE, M., WORZ, S., MULLER, B., EILS, R., AND ROHR, K. Deterministic and probabilistic approaches for tracking virus particles in time-lapse fluorescence microscopy image sequences. *Medical Image Analysis 13*, 2 (2009), 325–42.

[107] GOEPFERT, P. A., SHAW, K., WANG, G., BANSAL, A., EDWARDS, B. H., AND MULLIGAN, M. J. An endoplasmic reticulum retrieval signal partitions human foamy virus maturation to intracytoplasmic membranes. *Journal of Virology 73*, 9 (1999), 7210–7.

[108] GOEPFERT, P. A., SHAW, K. L., RITTER, G. D., J., AND MULLIGAN, M. J. A sorting motif localizes the foamy virus glycoprotein to the endoplasmic reticulum. *Journal of Virology 71*, 1 (1997), 778–84.

[109] GOFF, S. P. Retroviridae: The retroviruses and their replication. In *Fields Virology*, D. M. Knipe, P. M. Howley, and D. E. Griffin, Eds., 5 ed. Lippincott Williams & Wilkins, 2007.

[110] GOODE, B. L., DRUBIN, D. G., AND BARNES, G. Functional cooperation between the microtubule and actin cytoskeletons. *Current Opinion in Cell Biology 12*, 1 (2000), 63–71.

[111] GÖPEL, W., AND ZIEGLER, C. *Struktur der Materie: Grundlagen, Mikroskopie und Spektroskopie.* B. G. Teubner Verlagsgesellschaft, 1994.

[112] GRANZOW, H., KLUPP, B. G., FUCHS, W., VEITS, J., OSTERRIEDER, N., AND METTENLEITER, T. C. Egress of alphaherpesviruses: comparative ultrastructural study. *Journal of Virology 75*, 8 (2001), 3675–84.

[113] GRANZOW, H., KLUPP, B. G., AND METTENLEITER, T. C. Entry of pseudorabies virus: an immunogold-labeling study. *Journal of Virology 79*, 5 (2005), 3200–5.

[114] GRUNEWALD, K., DESAI, P., WINKLER, D. C., HEYMANN, J. B., BELNAP, D. M., BAUMEISTER, W., AND STEVEN, A. C. Three-dimensional structure of herpes simplex virus from cryo-electron tomography. *Science 302*, 5649 (2003), 1396–8.

[115] HAARR, L., SHUKLA, D., RODAHL, E., DAL CANTO, M. C., AND SPEAR, P. G. Transcription from the gene encoding the herpesvirus entry receptor nectin-1 (HveC) in nervous tissue of adult mouse. *Virology 287*, 2 (2001), 301–9.

[116] HAHN, B. H., SHAW, G. M., DE COCK, K. M., AND SHARP, P. M. AIDS as a zoonosis: scientific and public health implications. *Science 287*, 5453 (2000), 607–14.

[117] HANSON, G. T., AGGELER, R., OGLESBEE, D., CANNON, M., CAPALDI, R. A., TSIEN, R. Y., AND REMINGTON, S. J. Investigating mitochondrial redox potential with redox-sensitive green fluorescent protein indicators. *Journal of Biological Chemistry 279*, 13 (2004), 13044–53.

[118] Harrison, S. C. Viral membrane fusion. *Nature Structural & Molecular Biology 15*, 7 (2008), 690–8.

[119] Hartschuh, A. Tip-enhanced near-field optical microscopy. *Angewandte Chemie. International Ed. In English 47*, 43 (2008), 8178–91.

[120] Haupts, U., Maiti, S., Schwille, P., and Webb, W. W. Dynamics of fluorescence fluctuations in green fluorescent protein observed by fluorescence correlation spectroscopy. *Proceedings of the National Academy of Sciences of the United States of America 95*, 23 (1998), 13573–8.

[121] He, B., Gross, M., and Roizman, B. The gamma(1)34.5 protein of herpes simplex virus 1 complexes with protein phosphatase 1alpha to dephosphorylate the alpha subunit of the eukaryotic translation initiation factor 2 and preclude the shutoff of protein synthesis by double-stranded RNA-activated protein kinase. *Proceedings of the National Academy of Sciences of the United States of America 94*, 3 (1997), 843–8.

[122] Heim, R., Cubitt, A. B., and Tsien, R. Y. Improved green fluorescence. *Nature 373*, 6516 (1995), 663–4.

[123] Heim, R., Prasher, D. C., and Tsien, R. Y. Wavelength mutations and post-translational autoxidation of green fluorescent protein. *Proceedings of the National Academy of Sciences of the United States of America 91*, 26 (1994), 12501–4.

[124] Heim, R., and Tsien, R. Y. Engineering green fluorescent protein for improved brightness, longer wavelengths and fluorescence resonance energy transfer. *Current Biology 6*, 2 (1996), 178–82.

[125] Heinkelein, M., Pietschmann, T., Jarmy, G., Dressler, M., Imrich, H., Thurow, J., Lindemann, D., Bock, M., Moebes, A., Roy, J., Herchenroder, O., and Rethwilm, A. Efficient intracellular retrotransposition of an exogenous primate retrovirus genome. *EMBO Journal 19*, 13 (2000), 3436–45.

[126] Heiss, G., Lapiene, V., Kukolka, F., Niemeyer, C. M., Brauchle, C., and Lamb, D. C. Single-molecule investigations of a photoswitchable nanodevice. *Small 5*, 10 (2009), 1169–75.

[127] Heldwein, E. E., and Krummenacher, C. Entry of herpesviruses into mammalian cells. *Cellular and Molecular Life Sciences 65*, 11 (2008), 1653–68.

[128] Heldwein, E. E., Lou, H., Bender, F. C., Cohen, G. H., Eisenberg, R. J., and Harrison, S. C. Crystal structure of glycoprotein B from herpes simplex virus 1. *Science 313*, 5784 (2006), 217–20.

[129] Helenius, A., Kartenbeck, J., Simons, K., and Fries, E. On the entry of Semliki forest virus into BHK-21 cells. *Journal of Cell Biology 84*, 2 (1980), 404–20.

[130] Hell, S. W. Far-field optical nanoscopy. *Science 316*, 5828 (2007), 1153–8.

[131] Heneine, W., Switzer, W. M., Sandstrom, P., Brown, J., Vedapuri, S., Schable, C. A., Khan, A. S., Lerche, N. W., Schweizer, M., Neumann-Haefelin, D., Chapman, L. E., and Folks, T. M. Identification of a human population infected with simian foamy viruses. *Nature Medicine 4*, 4 (1998), 403–7.

[132] Herfst, S., Schrauwen, E. J., Linster, M., Chutinimitkul, S., de Wit, E., Munster, V. J., Sorrell, E. M., Bestebroer, T. M., Burke, D. F., Smith, D. J., Rimmelzwaan, G. F., Osterhaus, A. D., and Fouchier, R. A. Airborne transmission of influenza A/H5N1 virus between ferrets. *Science 336*, 6088 (2012), 1534–41.

[133] Herold, B. C., Visalli, R. J., Susmarski, N., Brandt, C. R., and Spear, P. G. Glycoprotein C-independent binding of herpes simplex virus to cells requires cell surface heparan sulphate and glycoprotein B. *Journal of General Virology 75 (Pt 6)* (1994), 1211–22.

[134] Herold, B. C., WuDunn, D., Soltys, N., and Spear, P. G. Glycoprotein C of herpes simplex virus type 1 plays a principal role in the adsorption of virus to cells and in infectivity. *Journal of Virology 65*, 3 (1991), 1090–8.

[135] Hess, S. T., Girirajan, T. P., and Mason, M. D. Ultra-high resolution imaging by fluorescence photoactivation localization microscopy. *Biophysical Journal 91*, 11 (2006), 4258–72.

[136] Hubbard, A. L. Endocytosis. *Current Opinion in Cell Biology 1*, 4 (1989), 675–83.

[137] Hummeler, K., Tomassini, N., and Zajac, B. Early events in herpes simplex virus infection: a radioautographic study. *Journal of Virology 4*, 1 (1969), 67–74.

[138] ICTV. International Committee on Taxonomy of Viruses. Virus taxonomy: 2009 release, `http:// ictvonline. org/ virusTaxonomy. asp? version=2009& bhcp=1` 2012/18/01.

[139] IVANCHENKO, S., GODINEZ, W. J., LAMPE, M., KRAUSSLICH, H. G., EILS, R., ROHR, K., BRAUCHLE, C., MULLER, B., AND LAMB, D. C. Dynamics of HIV-1 assembly and release. *PLoS Pathogens 5*, 11 (2009), e1000652.

[140] JABŁOŃSKI, A. Über den Mechanismus der Photolumineszenz von Farbstoffphosphoren. *Zeitschrift für Physik A Hadrons and Nuclei 94*, 1 (1935), 38–46.

[141] JACKSON, J. O., LIN, E., SPEAR, P. G., AND LONGNECKER, R. Insertion mutations in herpes simplex virus 1 glycoprotein H reduce cell surface expression, slow the rate of cell fusion, or abrogate functions in cell fusion and viral entry. *Journal of Virology 84*, 4 (2010), 2038–46.

[142] JACKSON, J. O., AND LONGNECKER, R. Reevaluating herpes simplex virus hemifusion. *Journal of Virology 84*, 22 (2010), 11814–21.

[143] JANUS, J. *Kinesin-1 is required for nuclear targeting of incoming herpes simplex virus capsids and viral gene expression.* PhD thesis, 2009.

[144] JENTSCH, T. J. Chloride and the endosomal-lysosomal pathway: emerging roles of CLC chloride transporters. *Journal of Physiology 578*, Pt 3 (2007), 633–40.

[145] JENTSCH, T. J. CLC chloride channels and transporters: from genes to protein structure, pathology and physiology. *Critical Reviews in Biochemistry and Molecular Biology 43*, 1 (2008), 3–36.

[146] JHA, N. K., LATINOVIC, O., MARTIN, E., NOVITSKIY, G., MARIN, M., MIYAUCHI, K., NAUGHTON, J., YOUNG, J. A., AND MELIKYAN, G. B. Imaging single retrovirus entry through alternative receptor isoforms and intermediates of virus-endosome fusion. *PLoS Pathogens 7*, 1 (2011), e1001260.

[147] JOHANNSDOTTIR, H. K., MANCINI, R., KARTENBECK, J., AMATO, L., AND HELENIUS, A. Host cell factors and functions involved in vesicular stomatitis virus entry. *Journal of Virology 83*, 1 (2009), 440–53.

[148] JOHNSON, D. C., AND HUBER, M. T. Directed egress of animal viruses promotes cell-to-cell spread. *Journal of Virology 76*, 1 (2002), 1–8.

[149] JONES, S. A., SHIM, S. H., HE, J., AND ZHUANG, X. Fast, three-dimensional super-resolution imaging of live cells. *Nature Methods 8*, 6 (2011), 499–508.

[150] JOO, K. I., TAI, A., LEE, C. L., WONG, C., AND WANG, P. Imaging multiple intermediates of single-virus membrane fusion mediated by distinct fusion proteins. *Microscopy Research and Technique 73*, 9 (2010), 886–900.

[151] KAMIYAMA, H., ZHOU, G., AND ROIZMAN, B. Herpes simplex virus 1 recombinant virions exhibiting the amino terminal fragment of urokinase-type plasminogen activator can enter cells via the cognate receptor. *Gene Therapy 13*, 7 (2006), 621–9.

[152] KAPANIDIS, A. N., LAURENCE, T. A., LEE, N. K., MARGEAT, E., KONG, X., AND WEISS, S. Alternating-laser excitation of single molecules. *Accounts of Chemical Research 38*, 7 (2005), 523–33.

[153] KARASNEH, G. A., AND SHUKLA, D. Herpes simplex virus infects most cell types in vitro: clues to its success. *Virology Journal 8* (2011), 481.

[154] KASHA, M. Characterization of electronic transitions in complex molecules. *Discussions of the Faraday Society 9* (1950), 14–19.

[155] KASSON, P. M., KELLEY, N. W., SINGHAL, N., VRLJIC, M., BRUNGER, A. T., AND PANDE, V. S. Ensemble molecular dynamics yields submillisecond kinetics and intermediates of membrane fusion. *Proceedings of the National Academy of Sciences of the United States of America 103*, 32 (2006), 11916–21.

[156] KERR, M. C., AND TEASDALE, R. D. Defining macropinocytosis. *Traffic 10*, 4 (2009), 364–71.

[157] KHAN, A. S. Simian foamy virus infection in humans: prevalence and management. *Expert Review of Anti-Infective Therapy 7*, 5 (2009), 569–80.

[158] KIRCHHAUSEN, T. Clathrin. *Annual Review of Biochemistry 69* (2000), 699–727.

[159] KLONIS, N., TAN, O., JACKSON, K., GOLDBERG, D., KLEMBA, M., AND TILLEY, L. Evaluation of pH during cytostomal endocytosis and vacuolar catabolism of haemoglobin in plasmodium falciparum. *Biochemical Journal 407*, 3 (2007), 343–54.

[160] KNAUP, B., SCHUNEMANN, S., AND WOLFF, M. H. Subclinical reactivation of herpes simplex virus type 1 in the oral cavity. *Oral Microbiology and Immunology 15*, 5 (2000), 281–3.

[161] KOCH, P., LAMPE, M., GODINEZ, W. J., MULLER, B., ROHR, K., KRAUS-SLICH, H. G., AND LEHMANN, M. J. Visualizing fusion of pseudotyped HIV-1 particles in real time by live cell microscopy. *Retrovirology 6* (2009), 84.

[162] KOYAMA, A. H., AND UCHIDA, T. The mode of entry of herpes simplex virus type 1 into Vero cells. *Microbiology and Immunology 31*, 2 (1987), 123–30.

[163] KRISTENSSON, K., LYCKE, E., ROYTTA, M., SVENNERHOLM, B., AND VAHLNE, A. Neuritic transport of herpes simplex virus in rat sensory neurons in vitro. effects of substances interacting with microtubular function and axonal flow [nocodazole, taxol and erythro-9-3-(2-hydroxynonyl)adenine]. *Journal of General Virology 67 (Pt 9)* (1986), 2023–8.

[164] KRONE, M. R., WALD, A., TABET, S. R., PARADISE, M., COREY, L., AND CELUM, C. L. Herpes simplex virus type 2 shedding in human immunodeficiency virus-negative men who have sex with men: frequency, patterns, and risk factors. *Clinical Infectious Diseases 30*, 2 (2000), 261–7.

[165] KRUMMENACHER, C., BARIBAUD, I., EISENBERG, R. J., AND COHEN, G. H. Cellular localization of nectin-1 and glycoprotein D during herpes simplex virus infection. *Journal of Virology 77*, 16 (2003), 8985–99.

[166] KRUMMENACHER, C., BARIBAUD, I., PONCE DE LEON, M., WHITBECK, J. C., LOU, H., COHEN, G. H., AND EISENBERG, R. J. Localization of a binding site for herpes simplex virus glycoprotein D on herpesvirus entry mediator C by using antireceptor monoclonal antibodies. *Journal of Virology 74*, 23 (2000), 10863–72.

[167] KRUMMENACHER, C., BARIBAUD, I., SANZO, J. F., COHEN, G. H., AND EISENBERG, R. J. Effects of herpes simplex virus on structure and function of nectin-1/HveC. *Journal of Virology 76*, 5 (2002), 2424–33.

[168] KRUMMENACHER, C., CARFI, A., EISEBERG, R. J., AND COHEN, G. H. Entry of herpesviruses into cells: The enigma variations. In *Viral Entry into Host Cells*, S. Pöhlmann and G. Simmons, Eds. Landes Bioscience, 2007, pp. 1–17.

[169] KRUMMENACHER, C., NICOLA, A. V., WHITBECK, J. C., LOU, H., HOU, W., LAMBRIS, J. D., GERAGHTY, R. J., SPEAR, P. G., COHEN, G. H., AND

EISENBERG, R. J. Herpes simplex virus glycoprotein D can bind to poliovirus receptor-related protein 1 or herpesvirus entry mediator, two structurally unrelated mediators of virus entry. *Journal of Virology 72*, 9 (1998), 7064–74.

[170] KRUMMENACHER, C., SUPEKAR, V. M., WHITBECK, J. C., LAZEAR, E., CONNOLLY, S. A., EISENBERG, R. J., COHEN, G. H., WILEY, D. C., AND CARFI, A. Structure of unliganded HSV gD reveals a mechanism for receptor-mediated activation of virus entry. *EMBO Journal 24*, 23 (2005), 4144–53.

[171] KUZMIN, P. I., ZIMMERBERG, J., CHIZMADZHEV, Y. A., AND COHEN, F. S. A quantitative model for membrane fusion based on low-energy intermediates. *Proceedings of the National Academy of Sciences of the United States of America 98*, 13 (2001), 7235–40.

[172] KWON, H., BAI, Q., BAEK, H. J., FELMET, K., BURTON, E. A., GOINS, W. F., COHEN, J. B., AND GLORIOSO, J. C. Soluble V domain of Nectin-1/HveC enables entry of herpes simplex virus type 1 (HSV-1) into HSV-resistant cells by binding to viral glycoprotein D. *Journal of Virology 80*, 1 (2006), 138–48.

[173] KYOUNG, M., SRIVASTAVA, A., ZHANG, Y., DIAO, J., VRLJIC, M., GROB, P., NOGALES, E., CHU, S., AND BRUNGER, A. T. In vitro system capable of differentiating fast Ca^{2+}-triggered content mixing from lipid exchange for mechanistic studies of neurotransmitter release. *Proceedings of the National Academy of Sciences of the United States of America 108*, 29 (2011), E304–13.

[174] LAFFERTY, W. E., DOWNEY, L., CELUM, C., AND WALD, A. Herpes simplex virus type 1 as a cause of genital herpes: impact on surveillance and prevention. *Journal of Infectious Diseases 181*, 4 (2000), 1454–7.

[175] LAFOURCADE, C., SOBO, K., KIEFFER-JAQUINOD, S., GARIN, J., AND VAN DER GOOT, F. G. Regulation of the V-ATPase along the endocytic pathway occurs through reversible subunit association and membrane localization. *PLoS One 3*, 7 (2008), e2758.

[176] LAIRMORE, M. D., AND FRANCHINI, G. Human T-cell leukemia virus types 1 and 2. In *Fields Virology*, D. M. Knipe, P. M. Howley, and D. E. Griffin, Eds., 5 ed. Lippincott Williams & Wilkins, 2007.

[177] LAKADAMYALI, M., RUST, M. J., BABCOCK, H. P., AND ZHUANG, X. Visualizing infection of individual influenza viruses. *Proceedings of the National Academy of Sciences of the United States of America 100*, 16 (2003), 9280–5.

[178] Lakadamyali, M., Rust, M. J., and Zhuang, X. Ligands for clathrin-mediated endocytosis are differentially sorted into distinct populations of early endosomes. *Cell 124*, 5 (2006), 997–1009.

[179] Lakowicz, J., Ed. *Principles of fluorescence spectroscopy*, third edition ed. Springer Science+Business Media, LLC, 2006.

[180] Laquerre, S., Argnani, R., Anderson, D. B., Zucchini, S., Manservigi, R., and Glorioso, J. C. Heparan sulfate proteoglycan binding by herpes simplex virus type 1 glycoproteins B and C, which differ in their contributions to virus attachment, penetration, and cell-to-cell spread. *Journal of Virology 72*, 7 (1998), 6119–30.

[181] Lawrence, R., Yabe, T., Hajmohammadi, S., Rhodes, J., McNeely, M., Liu, J., Lamperti, E. D., Toselli, P. A., Lech, M., Spear, P. G., Rosenberg, R. D., and Shworak, N. W. The principal neuronal gD-type 3-O-sulfotransferases and their products in central and peripheral nervous system tissues. *Matrix Biology 26*, 6 (2007), 442–55.

[182] Lazear, E., Carfi, A., Whitbeck, J. C., Cairns, T. M., Krummenacher, C., Cohen, G. H., and Eisenberg, R. J. Engineered disulfide bonds in herpes simplex virus type 1 gD separate receptor binding from fusion initiation and viral entry. *Journal of Virology 82*, 2 (2008), 700–9.

[183] Le Blanc, I., Luyet, P. P., Pons, V., Ferguson, C., Emans, N., Petiot, A., Mayran, N., Demaurex, N., Faure, J., Sadoul, R., Parton, R. G., and Gruenberg, J. Endosome-to-cytosol transport of viral nucleocapsids. *Nature Cell Biology 7*, 7 (2005), 653–64.

[184] Lehmann, M. J., Sherer, N. M., Marks, C. B., Pypaert, M., and Mothes, W. Actin- and myosin-driven movement of viruses along filopodia precedes their entry into cells. *Journal of Cell Biology 170*, 2 (2005), 317–25.

[185] Lehmann-Che, J., Giron, M. L., Delelis, O., Lochelt, M., Bittoun, P., Tobaly-Tapiero, J., de The, H., and Saib, A. Protease-dependent uncoating of a complex retrovirus. *Journal of Virology 79*, 14 (2005), 9244–53.

[186] Lehmann-Che, J., Renault, N., Giron, M. L., Roingeard, P., Clave, E., Tobaly-Tapiero, J., Bittoun, P., Toubert, A., de The, H., and Saib, A. Centrosomal latency of incoming foamy viruses in resting cells. *PLoS Pathogens 3*, 5 (2007), e74.

[187] LICHTMAN, J. W., AND CONCHELLO, J. A. Fluorescence microscopy. *Nature Methods 2*, 12 (2005), 910–9.

[188] LIN, M. Z., MCKEOWN, M. R., NG, H. L., AGUILERA, T. A., SHANER, N. C., CAMPBELL, R. E., ADAMS, S. R., GROSS, L. A., MA, W., ALBER, T., AND TSIEN, R. Y. Autofluorescent proteins with excitation in the optical window for intravital imaging in mammals. *Chemistry and Biology 16*, 11 (2009), 1169–79.

[189] LINDEMANN, D., AND RETHWILM, A. Foamy virus biology and its application for vector development. *Viruses 3*, 5 (2011), 561–85.

[190] LINIAL, M. Why aren't foamy viruses pathogenic? *Trends in Microbiology 8*, 6 (2000), 284–9.

[191] LINIAL, M. Foamy viruses. In *Fields Virology*, D. M. Knipe, P. M. Howley, and D. E. Griffin, Eds., 5 ed. Lippincott Williams & Wilkins, 2007.

[192] LINIAL, M. L. Foamy viruses are unconventional retroviruses. *Journal of Virology 73*, 3 (1999), 1747–55.

[193] LIU, J., SHRIVER, Z., POPE, R. M., THORP, S. C., DUNCAN, M. B., COPELAND, R. J., RASKA, C. S., YOSHIDA, K., EISENBERG, R. J., COHEN, G., LINHARDT, R. J., AND SASISEKHARAN, R. Characterization of a heparan sulfate octasaccharide that binds to herpes simplex virus type 1 glycoprotein D. *Journal of Biological Chemistry 277*, 36 (2002), 33456–67.

[194] LYCKE, E., HAMARK, B., JOHANSSON, M., KROTOCHWIL, A., LYCKE, J., AND SVENNERHOLM, B. Herpes simplex virus infection of the human sensory neuron. an electron microscopy study. *Archives of Virology 101*, 1-2 (1988), 87–104.

[195] LYMAN, M. G., AND ENQUIST, L. W. Herpesvirus interactions with the host cytoskeleton. *Journal of Virology 83*, 5 (2009), 2058–66.

[196] MARKOSYAN, R. M., COHEN, F. S., AND MELIKYAN, G. B. Time-resolved imaging of HIV-1 Env-mediated lipid and content mixing between a single virion and cell membrane. *Molecular Biology of the Cell 16*, 12 (2005), 5502–13.

[197] MARSH, M., AND HELENIUS, A. Virus entry: open sesame. *Cell 124*, 4 (2006), 729–40.

[198] MARTINEZ-MORENO, M., NAVARRO-LERIDA, I., RONCAL, F., ALBAR, J. P., ALONSO, C., GAVILANES, F., AND RODRIGUEZ-CRESPO, I. Recognition of novel

viral sequences that associate with the dynein light chain LC8 identified through a pepscan technique. *FEBS Letters 544*, 1-3 (2003), 262–7.

[199] MASTERS, B. R. *Confocal Microscopy and Multiphoton Excitation Microscopy.* The Genesis of Live Cell Imaging. SPIE Publications, Bellingham, 2006.

[200] MATZ, M. V., FRADKOV, A. F., LABAS, Y. A., SAVITSKY, A. P., ZARAISKY, A. G., MARKELOV, M. L., AND LUKYANOV, S. A. Fluorescent proteins from nonbioluminescent Anthozoa species. *Nature Biotechnology 17*, 10 (1999), 969–73.

[201] MAURER, U. E., SODEIK, B., AND GRUNEWALD, K. Native 3D intermediates of membrane fusion in herpes simplex virus 1 entry. *Proceedings of the National Academy of Sciences of the United States of America 105*, 30 (2008), 10559–64.

[202] MCCLURE, M. O., AND ERLWEIN, O. Foamy viruses – pathogenic or therapeutic potential? *Reviews in Medical Virology 5*, 4 (1995), 229–37.

[203] MCGEOCH, D. J., DALRYMPLE, M. A., DAVISON, A. J., DOLAN, A., FRAME, M. C., MCNAB, D., PERRY, L. J., SCOTT, J. E., AND TAYLOR, P. The complete DNA sequence of the long unique region in the genome of herpes simplex virus type 1. *Journal of General Virology 69 (Pt 7)* (1988), 1531–74.

[204] MCLAUCHLAN, J., ADDISON, C., CRAIGIE, M. C., AND RIXON, F. J. Noninfectious L-particles supply functions which can facilitate infection by HSV-1. *Virology 190*, 2 (1992), 682–8.

[205] MEIERING, C. D., AND LINIAL, M. L. Historical perspective of foamy virus epidemiology and infection. *Clinical Microbiology Reviews 14*, 1 (2001), 165–76.

[206] MELIKYAN, G. B. Common principles and intermediates of viral protein-mediated fusion: the HIV-1 paradigm. *Retrovirology 5* (2008), 111.

[207] MELIKYAN, G. B., BARNARD, R. J., ABRAHAMYAN, L. G., MOTHES, W., AND YOUNG, J. A. Imaging individual retroviral fusion events: from hemifusion to pore formation and growth. *Proceedings of the National Academy of Sciences of the United States of America 102*, 24 (2005), 8728–33.

[208] MELLMAN, I., FUCHS, R., AND HELENIUS, A. Acidification of the endocytic and exocytic pathways. *Annual Review of Biochemistry 55* (1986), 663–700.

[209] MENOTTI, L., CERRETANI, A., AND CAMPADELLI-FIUME, G. A herpes simplex virus recombinant that exhibits a single-chain antibody to HER2/neu enters cells

through the mammary tumor receptor, independently of the gD receptors. *Journal of Virology 80*, 11 (2006), 5531–9.

[210] MERCER, J., AND HELENIUS, A. Virus entry by macropinocytosis. *Nature Cell Biology 11*, 5 (2009), 510–20.

[211] MERCER, J., SCHELHAAS, M., AND HELENIUS, A. Virus entry by endocytosis. *Annual Review of Biochemistry 79* (2010), 803–33.

[212] METTENLEITER, T. C. Herpesvirus assembly and egress. *Journal of Virology 76*, 4 (2002), 1537–47.

[213] METTENLEITER, T. C. Budding events in herpesvirus morphogenesis. *Virus Research 106*, 2 (2004), 167–80.

[214] METTENLEITER, T. C., KLUPP, B. G., AND GRANZOW, H. Herpesvirus assembly: a tale of two membranes. *Current Opinion in Microbiology 9*, 4 (2006), 423–9.

[215] MILNE, R. S., NICOLA, A. V., WHITBECK, J. C., EISENBERG, R. J., AND COHEN, G. H. Glycoprotein D receptor-dependent, low-pH-independent endocytic entry of herpes simplex virus type 1. *Journal of Virology 79*, 11 (2005), 6655–63.

[216] MIRANDA-SAKSENA, M., BOADLE, R. A., ARMATI, P., AND CUNNINGHAM, A. L. In rat dorsal root ganglion neurons, herpes simplex virus type 1 tegument forms in the cytoplasm of the cell body. *Journal of Virology 76*, 19 (2002), 9934–51.

[217] MIYAUCHI, K., KIM, Y., LATINOVIC, O., MOROZOV, V., AND MELIKYAN, G. B. HIV enters cells via endocytosis and dynamin-dependent fusion with endosomes. *Cell 137*, 3 (2009), 433–44.

[218] MOEBES, A., ENSSLE, J., BIENIASZ, P. D., HEINKELEIN, M., LINDEMANN, D., BOCK, M., MCCLURE, M. O., AND RETHWILM, A. Human foamy virus reverse transcription that occurs late in the viral replication cycle. *Journal of Virology 71*, 10 (1997), 7305–11.

[219] MOLECULARPROBES. Lysotracker probes, `http:// products. invitrogen. com/ ivgn/ product/ L7528 2012/11/04`.

[220] MONTGOMERY, R. I., WARNER, M. S., LUM, B. J., AND SPEAR, P. G. Herpes simplex virus-1 entry into cells mediated by a novel member of the TNF/NGF receptor family. *Cell 87*, 3 (1996), 427–36.

[221] MORENS, D. M., FOLKERS, G. K., AND FAUCI, A. S. Emerging infections: a perpetual challenge. *Lancet Infectious Diseases 8*, 11 (2008), 710–9.

[222] MOROZOV, V. A., COPELAND, T. D., NAGASHIMA, K., GONDA, M. A., AND OROSZLAN, S. Protein composition and morphology of human foamy virus intracellular cores and extracellular particles. *Virology 228*, 2 (1997), 307–17.

[223] MUGGERIDGE, M. I. Characterization of cell-cell fusion mediated by herpes simplex virus 2 glycoproteins gB, gD, gH and gL in transfected cells. *Journal of General Virology 81*, Pt 8 (2000), 2017–27.

[224] MURPHY, D. B., Ed. *Fundamentals of light microscopy and electronic imaging.* John Wiley & Sons, Inc., New York, 2001.

[225] MURRAY, J., WILSON, L., AND KELLIE, S. Phosphatidylinositol-3' kinase-dependent vesicle formation in macrophages in response to macrophage colony stimulating factor. *Journal of Cell Science 113 Pt 2* (2000), 337–48.

[226] MURRAY, S. M., PICKER, L. J., AXTHELM, M. K., AND LINIAL, M. L. Expanded tissue targets for foamy virus replication with simian immunodeficiency virus-induced immunosuppression. *Journal of Virology 80*, 2 (2006), 663–70.

[227] NAGEL, C. H., DOHNER, K., FATHOLLAHY, M., STRIVE, T., BORST, E. M., MESSERLE, M., AND SODEIK, B. Nuclear egress and envelopment of herpes simplex virus capsids analyzed with dual-color fluorescence HSV1(17+). *Journal of Virology 82*, 6 (2008), 3109–24.

[228] NAKANO, A. Spinning-disk confocal microscopy – a cutting-edge tool for imaging of membrane traffic. *Cell Structure and Function 27*, 5 (2002), 349–55.

[229] NASIMUZZAMAN, M., AND PERSONS, D. A. Cell membrane-associated heparan sulfate is a receptor for prototype foamy virus in human, monkey, and rodent cells. *Molecular Therapy* (2012).

[230] NEWCOMB, W. W., TRUS, B. L., CHENG, N., STEVEN, A. C., SHEAFFER, A. K., TENNEY, D. J., WELLER, S. K., AND BROWN, J. C. Isolation of herpes simplex virus procapsids from cells infected with a protease-deficient mutant virus. *Journal of Virology 74*, 4 (2000), 1663–73.

[231] NICOLA, A. V., HOU, J., MAJOR, E. O., AND STRAUS, S. E. Herpes simplex virus type 1 enters human epidermal keratinocytes, but not neurons, via a pH-dependent endocytic pathway. *Journal of Virology 79*, 12 (2005), 7609–16.

[232] NICOLA, A. V., MCEVOY, A. M., AND STRAUS, S. E. Roles for endocytosis and low pH in herpes simplex virus entry into HeLa and Chinese hamster ovary cells. *Journal of Virology 77*, 9 (2003), 5324–32.

[233] NICOLA, A. V., AND STRAUS, S. E. Cellular and viral requirements for rapid endocytic entry of herpes simplex virus. *Journal of Virology 78*, 14 (2004), 7508–17.

[234] NIWA, H., INOUYE, S., HIRANO, T., MATSUNO, T., KOJIMA, S., KUBOTA, M., OHASHI, M., AND TSUJI, F. I. Chemical nature of the light emitter of the Aequorea green fluorescent protein. *Proceedings of the National Academy of Sciences of the United States of America 93*, 24 (1996), 13617–22.

[235] NOBELPRIZE. Nobel prizes in chemistry, `http:// www. nobelprize. org/ nobel_ prizes/ chemistry/ laureates/ 2012/02/22`.

[236] OJALA, P. M., SODEIK, B., EBERSOLD, M. W., KUTAY, U., AND HELENIUS, A. Herpes simplex virus type 1 entry into host cells: reconstitution of capsid binding and uncoating at the nuclear pore complex in vitro. *Molecular and Cellular Biology 20*, 13 (2000), 4922–31.

[237] ORMO, M., CUBITT, A. B., KALLIO, K., GROSS, L. A., TSIEN, R. Y., AND REMINGTON, S. J. Crystal structure of the Aequorea victoria green fluorescent protein. *Science 273*, 5280 (1996), 1392–5.

[238] PADILLA-PARRA, S., MARIN, M., KONDO, N., AND MELIKYAN, G. B. Synchronized retrovirus fusion in cells expressing alternative receptor isoforms releases the viral core into distinct sub-cellular compartments. *PLoS Pathogens 8*, 5 (2012), e1002694.

[239] PATTERSON, G. H., KNOBEL, S. M., SHARIF, W. D., KAIN, S. R., AND PISTON, D. W. Use of the green fluorescent protein and its mutants in quantitative fluorescence microscopy. *Biophysical Journal 73*, 5 (1997), 2782–90.

[240] PELKMANS, L. Secrets of caveolae- and lipid raft-mediated endocytosis revealed by mammalian viruses. *Biochimica et Biophysica Acta 1746*, 3 (2005), 295–304.

[241] PELKMANS, L., BURLI, T., ZERIAL, M., AND HELENIUS, A. Caveolin-stabilized membrane domains as multifunctional transport and sorting devices in endocytic membrane traffic. *Cell 118*, 6 (2004), 767–80.

[242] PELKMANS, L., AND HELENIUS, A. Insider information: what viruses tell us about endocytosis. *Current Opinion in Cell Biology 15*, 4 (2003), 414–22.

[243] PELKMANS, L., KARTENBECK, J., AND HELENIUS, A. Caveolar endocytosis of simian virus 40 reveals a new two-step vesicular-transport pathway to the ER. *Nature Cell Biology 3*, 5 (2001), 473–83.

[244] PELLETT, P. E., AND ROIZMAN, B. The family herpesviridae: A brief introduction. In *Fields Virology*, D. M. Knipe, P. M. Howley, and D. E. Griffin, Eds., vol. 5. Lippincott Williams & Wilkins, 2007.

[245] PEREZ, A., LI, Q. X., PEREZ-ROMERO, P., DELASSUS, G., LOPEZ, S. R., SUTTER, S., MCLAREN, N., AND FULLER, A. O. A new class of receptor for herpes simplex virus has heptad repeat motifs that are common to membrane fusion proteins. *Journal of Virology 79*, 12 (2005), 7419–30.

[246] PERTEL, P. E., FRIDBERG, A., PARISH, M. L., AND SPEAR, P. G. Cell fusion induced by herpes simplex virus glycoproteins gB, gD, and gH-gL requires a gD receptor but not necessarily heparan sulfate. *Virology 279*, 1 (2001), 313–24.

[247] PETIT, C., GIRON, M. L., TOBALY-TAPIERO, J., BITTOUN, P., REAL, E., JACOB, Y., TORDO, N., DE THE, H., AND SAIB, A. Targeting of incoming retroviral Gag to the centrosome involves a direct interaction with the dynein light chain 8. *Journal of Cell Science 116*, Pt 16 (2003), 3433–42.

[248] PICARD-MAUREAU, M., JARMY, G., BERG, A., RETHWILM, A., AND LINDEMANN, D. Foamy virus envelope glycoprotein-mediated entry involves a pH-dependent fusion process. *Journal of Virology 77*, 8 (2003), 4722–30.

[249] PRASHER, D. C., ECKENRODE, V. K., WARD, W. W., PRENDERGAST, F. G., AND CORMIER, M. J. Primary structure of the Aequorea victoria green-fluorescent protein. *Gene 111*, 2 (1992), 229–33.

[250] PRENDERGAST, F. G., AND MANN, K. G. Chemical and physical properties of aequorin and the green fluorescent protein isolated from Aequorea forskalea. *Biochemistry 17*, 17 (1978), 3448–53.

[251] RAHN, E., PETERMANN, P., HSU, M.-J., RIXON, F. J., AND KNEBEL-MÖRSDORF, D. Entry pathways of herpes simplex virus type 1 into human keratinocytes are dynamin- and cholesterol-dependent. *PLoS One 6*, 10 (2011), e25464.

[252] RAYLEIGH. Xxxi. Investigations in optics, with special reference to the spectroscope. *Philosophical Magazine Series 5 8*, 49 (1879), 261–74.

[253] RESKE, A., POLLARA, G., KRUMMENACHER, C., CHAIN, B. M., AND KATZ, D. R. Understanding HSV-1 entry glycoproteins. *Reviews in Medical Virology 17*, 3 (2007), 205–15.

[254] RICHART, S. M., SIMPSON, S. A., KRUMMENACHER, C., WHITBECK, J. C., PIZER, L. I., COHEN, G. H., EISENBERG, R. J., AND WILCOX, C. L. Entry of herpes simplex virus type 1 into primary sensory neurons in vitro is mediated by nectin-1/HveC. *Journal of Virology 77*, 5 (2003), 3307–11.

[255] RINK, J., GHIGO, E., KALAIDZIDIS, Y., AND ZERIAL, M. Rab conversion as a mechanism of progression from early to late endosomes. *Cell 122*, 5 (2005), 735–49.

[256] RIXON, F. J., ADDISON, C., AND MCLAUCHLAN, J. Assembly of enveloped tegument structures (L particles) can occur independently of virion maturation in herpes simplex virus type 1-infected cells. *Journal of General Virology 73 (Pt 2)* (1992), 277–84.

[257] ROCHE, S., BRESSANELLI, S., REY, F. A., AND GAUDIN, Y. Crystal structure of the low-pH form of the vesicular stomatitis virus glycoprotein G. *Science 313*, 5784 (2006), 187–91.

[258] ROIZMAN, B., AND BAINES, J. The diversity and unity of herpesviridae. *Comparative Immunology, Microbiology and Infectious Diseases 14*, 2 (1991), 63–79.

[259] ROIZMAN, B., CARMICHAEL, L. E., DEINHARDT, F., DE THE, G., NAHMIAS, A. J., PLOWRIGHT, W., RAPP, F., SHELDRICK, P., TAKAHASHI, M., AND WOLF, K. Herpesviridae. Definition, provisional nomenclature, and taxonomy. The Herpesvirus Study Group, the International Committee on Taxonomy of Viruses. *Intervirology 16*, 4 (1981), 201–17.

[260] ROIZMAN, B., AND FURLONG, D. The replication of herpesviruses. In *Comprehensive Virology*, H. Fraenkel-Conrat and R. R. Wagner, Eds. Plenum Press, New York, [1974]-c1984, pp. 229–403.

[261] ROIZMAN, B., KNIPE, D. M., AND WHITLEY, R. J. Herpes simplex viruses. In *Fields Virology*, D. M. Knipe, P. M. Howley, and D. E. Griffin, Eds., 5 ed. Lippincott Williams & Wilkins, 2007.

[262] ROIZMANN, B., DESROSIERS, R. C., FLECKENSTEIN, B., LOPEZ, C., MINSON, A. C., AND STUDDERT, M. J. The family Herpesviridae: an update. the Her-

pesvirus Study Group of the International Committee on Taxonomy of Viruses. *Archives of Virology 123*, 3-4 (1992), 425–49.

[263] RUIGROK, R. W., HEWAT, E. A., AND WADE, R. H. Low pH deforms the influenza virus envelope. *Journal of General Virology 73 (Pt 4)* (1992), 995–8.

[264] RUST, M. J., BATES, M., AND ZHUANG, X. Sub-diffraction-limit imaging by stochastic optical reconstruction microscopy (STORM). *Nature Methods 3*, 10 (2006), 793–5.

[265] RUST, M. J., LAKADAMYALI, M., ZHANG, F., AND ZHUANG, X. Assembly of endocytic machinery around individual influenza viruses during viral entry. *Nature Structural & Molecular Biology 11*, 6 (2004), 567–73.

[266] RUTHARDT, N., LAMB, D. C., AND BRAUCHLE, C. Single-particle tracking as a quantitative microscopy-based approach to unravel cell entry mechanisms of viruses and pharmaceutical nanoparticles. *Molecular Therapy 19*, 7 (2011), 1199–211.

[267] SAIB, A., PERIES, J., AND DE THE, H. Recent insights into the biology of the human foamy virus. *Trends in Microbiology 3*, 5 (1995), 173–8.

[268] SAIB, A., PUVION-DUTILLEUL, F., SCHMID, M., PERIES, J., AND DE THE, H. Nuclear targeting of incoming human foamy virus Gag proteins involves a centriolar step. *Journal of Virology 71*, 2 (1997), 1155–61.

[269] SAKISAKA, T., TANIGUCHI, T., NAKANISHI, H., TAKAHASHI, K., MIYAHARA, M., IKEDA, W., YOKOYAMA, S., PENG, Y. F., YAMANISHI, K., AND TAKAI, Y. Requirement of interaction of nectin-1alpha/HveC with afadin for efficient cell-cell spread of herpes simplex virus type 1. *Journal of Virology 75*, 10 (2001), 4734–43.

[270] SATOH, T., ARII, J., SUENAGA, T., WANG, J., KOGURE, A., UEHORI, J., ARASE, N., SHIRATORI, I., TANAKA, S., KAWAGUCHI, Y., SPEAR, P. G., LANIER, L. L., AND ARASE, H. PILRalpha is a herpes simplex virus-1 entry coreceptor that associates with glycoprotein B. *Cell 132*, 6 (2008), 935–44.

[271] SCHELHAAS, M., EWERS, H., RAJAMAKI, M. L., DAY, P. M., SCHILLER, J. T., AND HELENIUS, A. Human papillomavirus type 16 entry: retrograde cell surface transport along actin-rich protrusions. *PLoS Pathogens 4*, 9 (2008), e1000148.

[272] Schweizer, M., Turek, R., Hahn, H., Schliephake, A., Netzer, K. O., Eder, G., Reinhardt, M., Rethwilm, A., and Neumann-Haefelin, D. Markers of foamy virus infections in monkeys, apes, and accidentally infected humans: appropriate testing fails to confirm suspected foamy virus prevalence in humans. *AIDS Research and Human Retroviruses 11*, 1 (1995), 161–70.

[273] Sedy, J. R., Spear, P. G., and Ware, C. F. Cross-regulation between herpesviruses and the TNF superfamily members. *Nature Reviews: Immunology 8*, 11 (2008), 861–73.

[274] Seeger, C., Zoulim, F., and Mason, W. S. Hepadnaviruses. In *Fields Virology*, D. M. Knipe, P. M. Howley, and D. E. Griffin, Eds., 5 ed. Lippincott Williams & Wilkins, 2007.

[275] Shaner, N. C., Campbell, R. E., Steinbach, P. A., Giepmans, B. N., Palmer, A. E., and Tsien, R. Y. Improved monomeric red, orange and yellow fluorescent proteins derived from Discosoma sp. red fluorescent protein. *Nature Biotechnology 22*, 12 (2004), 1567–72.

[276] Shaner, N. C., Steinbach, P. A., and Tsien, R. Y. A guide to choosing fluorescent proteins. *Nature Methods 2*, 12 (2005), 905–9.

[277] Sharp, P. M., and Hahn, B. H. Origins of HIV and the AIDS pandemic. *Cold Spring Harbor Perspectives in Medicine 1*, 1 (2011), a006841.

[278] Shaw, K. L., Lindemann, D., Mulligan, M. J., and Goepfert, P. A. Foamy virus envelope glycoprotein is sufficient for particle budding and release. *Journal of Virology 77*, 4 (2003), 2338–48.

[279] Sherer, N. M., Lehmann, M. J., Jimenez-Soto, L. F., Ingmundson, A., Horner, S. M., Cicchetti, G., Allen, P. G., Pypaert, M., Cunningham, J. M., and Mothes, W. Visualization of retroviral replication in living cells reveals budding into multivesicular bodies. *Traffic 4*, 11 (2003), 785–801.

[280] Shieh, M. T., WuDunn, D., Montgomery, R. I., Esko, J. D., and Spear, P. G. Cell surface receptors for herpes simplex virus are heparan sulfate proteoglycans. *Journal of Cell Biology 116*, 5 (1992), 1273–81.

[281] Shimomura, O., Johnson, F. H., and Saiga, Y. Extraction, purification and properties of aequorin, a bioluminescent protein from the luminous hydromedusan, Aequorea. *Journal of Cellular Physiology 59* (1962), 223–39.

[282] SHUKLA, D., LIU, J., BLAIKLOCK, P., SHWORAK, N. W., BAI, X., ESKO, J. D., COHEN, G. H., EISENBERG, R. J., ROSENBERG, R. D., AND SPEAR, P. G. A novel role for 3-O-sulfated heparan sulfate in herpes simplex virus 1 entry. *Cell 99*, 1 (1999), 13–22.

[283] SHUKLA, D., AND SPEAR, P. G. Herpesviruses and heparan sulfate: an intimate relationship in aid of viral entry. *Journal of Clinical Investigation 108*, 4 (2001), 503–10.

[284] SKEPPER, J. N., WHITELEY, A., BROWNE, H., AND MINSON, A. Herpes simplex virus nucleocapsids mature to progeny virions by an envelopment – deenvelopment – reenvelopment pathway. *Journal of Virology 75*, 12 (2001), 5697–702.

[285] SMITH, J. S., AND ROBINSON, N. J. Age-specific prevalence of infection with herpes simplex virus types 2 and 1: a global review. *Journal of Infectious Diseases 186 Suppl 1* (2002), S3–28.

[286] SODEIK, B. Mechanisms of viral transport in the cytoplasm. *Trends in Microbiology 8*, 10 (2000), 465–72.

[287] SODEIK, B., EBERSOLD, M. W., AND HELENIUS, A. Microtubule-mediated transport of incoming herpes simplex virus 1 capsids to the nucleus. *Journal of Cell Biology 136*, 5 (1997), 1007–21.

[288] SPEAR, P. G., AND LONGNECKER, R. Herpesvirus entry: an update. *Journal of Virology 77*, 19 (2003), 10179–85.

[289] STACKPOLE, C. W. Herpes-type virus of the frog renal adenocarcinoma. I. Virus development in tumor transplants maintained at low temperature. *Journal of Virology 4*, 1 (1969), 75–93.

[290] STANG, E., KARTENBECK, J., AND PARTON, R. G. Major histocompatibility complex class I molecules mediate association of SV40 with caveolae. *Molecular Biology of the Cell 8*, 1 (1997), 47–57.

[291] STANKE, N., STANGE, A., LUFTENEGGER, D., ZENTGRAF, H., AND LINDEMANN, D. Ubiquitination of the prototype foamy virus envelope glycoprotein leader peptide regulates subviral particle release. *Journal of Virology 79*, 24 (2005), 15074–83.

[292] STEINER, I., AND KENNEDY, P. G. Herpes simplex virus latent infection in the nervous system. *Journal of Neurovirology 1*, 1 (1995), 19–29.

[293] Steiner, I., Kennedy, P. G., and Pachner, A. R. The neurotropic herpes viruses: herpes simplex and varicella-zoster. *Lancet neurology 6*, 11 (2007), 1015–28.

[294] Stepanenko, O. V., Shcherbakova, D. M., Kuznetsova, I. M., Turoverov, K. K., and Verkhusha, V. V. Modern fluorescent proteins: from chromophore formation to novel intracellular applications. *Biotechniques 51*, 5 (2011), 313–4, 16, 18 passim.

[295] Stiles, K. M., Milne, R. S., Cohen, G. H., Eisenberg, R. J., and Krummenacher, C. The herpes simplex virus receptor nectin-1 is down-regulated after trans-interaction with glycoprotein D. *Virology 373*, 1 (2008), 98–111.

[296] Stirnnagel, K., Luftenegger, D., Stange, A., Swiersy, A., Mullers, E., Reh, J., Stanke, N., Grosse, A., Chiantia, S., Keller, H., Schwille, P., Hanenberg, H., Zentgraf, H., and Lindemann, D. Analysis of prototype foamy virus particle-host cell interaction with autofluorescent retroviral particles. *Retrovirology 7* (2010), 45.

[297] Stokes, G. G. On the change of refrangibility of light. *Philosophical Transactions of the Royal Society of London 142*, ArticleType: research-article / Full publication date: 1852 / Copyright ©1852 The Royal Society (1852), 463–562.

[298] Subach, F. V., Patterson, G. H., Renz, M., Lippincott-Schwartz, J., and Verkhusha, V. V. Bright monomeric photoactivatable red fluorescent protein for two-color super-resolution sptPALM of live cells. *Journal of the American Chemical Society 132*, 18 (2010), 6481–91.

[299] Subach, F. V., Zhang, L., Gadella, T. W., Gurskaya, N. G., Lukyanov, K. A., and Verkhusha, V. V. Red fluorescent protein with reversibly photoswitchable absorbance for photochromic FRET. *Chemistry and Biology 17*, 7 (2010), 745–55.

[300] Subak-Sharpe, J. H., and Dargan, D. J. HSV molecular biology: general aspects of herpes simplex virus molecular biology. *Virus Genes 16*, 3 (1998), 239–51.

[301] Subramanian, R. P., and Geraghty, R. J. Herpes simplex virus type 1 mediates fusion through a hemifusion intermediate by sequential activity of glycoproteins D, H, L, and B. *Proceedings of the National Academy of Sciences of the United States of America 104*, 8 (2007), 2903–8.

[302] SUENAGA, T., SATOH, T., SOMBOONTHUM, P., KAWAGUCHI, Y., MORI, Y., AND ARASE, H. Myelin-associated glycoprotein mediates membrane fusion and entry of neurotropic herpesviruses. *Proceedings of the National Academy of Sciences of the United States of America 107*, 2 (2010), 866–71.

[303] SUOMALAINEN, M., NAKANO, M. Y., KELLER, S., BOUCKE, K., STIDWILL, R. P., AND GREBER, U. F. Microtubule-dependent plus- and minus end-directed motilities are competing processes for nuclear targeting of adenovirus. *Journal of Cell Biology 144*, 4 (1999), 657–72.

[304] SWITZER, W. M., BHULLAR, V., SHANMUGAM, V., CONG, M. E., PAREKH, B., LERCHE, N. W., YEE, J. L., ELY, J. J., BONEVA, R., CHAPMAN, L. E., FOLKS, T. M., AND HENEINE, W. Frequent simian foamy virus infection in persons occupationally exposed to nonhuman primates. *Journal of Virology 78*, 6 (2004), 2780–9.

[305] SZILAGYI, J. F., AND CUNNINGHAM, C. Identification and characterization of a novel non-infectious herpes simplex virus-related particle. *Journal of General Virology 72 (Pt 3)* (1991), 661–8.

[306] TAKAHASHI, K., NAKANISHI, H., MIYAHARA, M., MANDAI, K., SATOH, K., SATOH, A., NISHIOKA, H., AOKI, J., NOMOTO, A., MIZOGUCHI, A., AND TAKAI, Y. Nectin/PRR: an immunoglobulin-like cell adhesion molecule recruited to cadherin-based adherens junctions through interaction with afadin, a PDZ domain-containing protein. *Journal of Cell Biology 145*, 3 (1999), 539–49.

[307] TAKAI, Y., IRIE, K., SHIMIZU, K., SAKISAKA, T., AND IKEDA, W. Nectins and nectin-like molecules: roles in cell adhesion, migration, and polarization. *Cancer Science 94*, 8 (2003), 655–67.

[308] THOMPSON, N. L., AND LAGERHOLM, B. C. Total internal reflection fluorescence: applications in cellular biophysics. *Current Opinion in Biotechnology 8*, 1 (1997), 58–64.

[309] TIWARI, V., CLEMENT, C., SCANLAN, P. M., KOWLESSUR, D., YUE, B. Y., AND SHUKLA, D. A role for herpesvirus entry mediator as the receptor for herpes simplex virus 1 entry into primary human trabecular meshwork cells. *Journal of Virology 79*, 20 (2005), 13173–9.

[310] TIWARI, V., CLEMENT, C., XU, D., VALYI-NAGY, T., YUE, B. Y., LIU, J., AND SHUKLA, D. Role for 3-O-sulfated heparan sulfate as the receptor for herpes

simplex virus type 1 entry into primary human corneal fibroblasts. *Journal of Virology 80*, 18 (2006), 8970–80.

[311] TIWARI, V., O'DONNELL, C., COPELAND, R. J., SCARLETT, T., LIU, J., AND SHUKLA, D. Soluble 3-O-sulfated heparan sulfate can trigger herpes simplex virus type 1 entry into resistant Chinese hamster ovary (CHO-K1) cells. *Journal of General Virology 88*, Pt 4 (2007), 1075–9.

[312] TIWARI, V., OH, M. J., KOVACS, M., SHUKLA, S. Y., VALYI-NAGY, T., AND SHUKLA, D. Role for nectin-1 in herpes simplex virus 1 entry and spread in human retinal pigment epithelial cells. *FEBS Journal 275*, 21 (2008), 5272–85.

[313] TRILLA, A., TRILLA, G., AND DAER, C. The 1918 "Spanish flu" in Spain. *Clinical Infectious Diseases 47*, 5 (2008), 668–73.

[314] TROY, T. Preparing for bioterrorism, `http:// www. hudson. org/ index. cfm? fuseaction=publication_ details& id=6785& pubType=HI_ opeds` 2012/05/12.

[315] TSIEN, R. Y. The green fluorescent protein. *Annual Review of Biochemistry 67* (1998), 509–44.

[316] TSIEN, R. Y. Spectra of various fluorescent proteins, `http:// www. tsienlab. ucsd. edu/ Documents. htm` 2011/12/14.

[317] TURNER, A., BRUUN, B., MINSON, T., AND BROWNE, H. Glycoproteins gB, gD, and gHgL of herpes simplex virus type 1 are necessary and sufficient to mediate membrane fusion in a Cos cell transfection system. *Journal of Virology 72*, 1 (1998), 873–5.

[318] UMENE, K., AND SAKAOKA, H. Evolution of herpes simplex virus type 1 under herpesviral evolutionary processes. *Archives of Virology 144*, 4 (1999), 637–56.

[319] UNAIDS. Joint United Nations Programme on HIV/AIDS. World AIDS day report, `http:// www. unaids. org/ en/ resources/ presscentre/ pressreleaseandstatementarchive/ 2011/ november/ 20111121wad2011report/` 2012/19/01.

[320] UNGEWICKELL, E., AND BRANTON, D. Assembly units of clathrin coats. *Nature 289*, 5796 (1981), 420–2.

[321] VAN DER SCHAAR, H. M., RUST, M. J., CHEN, C., VAN DER ENDE-METSELAAR, H., WILSCHUT, J., ZHUANG, X., AND SMIT, J. M. Dissecting

the cell entry pathway of dengue virus by single-particle tracking in living cells. *PLoS Pathogens 4*, 12 (2008), e1000244.

[322] VAN GENDEREN, I. L., BRANDIMARTI, R., TORRISI, M. R., CAMPADELLI, G., AND VAN MEER, G. The phospholipid composition of extracellular herpes simplex virions differs from that of host cell nuclei. *Virology 200*, 2 (1994), 831–6.

[323] VANHAESEBROECK, B., LEEVERS, S. J., AHMADI, K., TIMMS, J., KATSO, R., DRISCOLL, P. C., WOSCHOLSKI, R., PARKER, P. J., AND WATERFIELD, M. D. Synthesis and function of 3-phosphorylated inositol lipids. *Annual Review of Biochemistry 70* (2001), 535–602.

[324] VARMUS, H. Retroviruses. *Science 240*, 4858 (1988), 1427–35.

[325] VICENTE-MANZANARES, M., MA, X., ADELSTEIN, R. S., AND HORWITZ, A. R. Non-muscle myosin II takes centre stage in cell adhesion and migration. *Nature Reviews: Molecular Cell Biology 10*, 11 (2009), 778–90.

[326] VOGT, P. K. Historical introduction to the general properties of retroviruses. In *Retroviruses*, J. M. Coffin, S. H. Hughes, and H. E. Varmus, Eds. Cold Spring Harbor Laboratory Press, Cold Spring Harbor (NY), 1997.

[327] WARNER, M. S., GERAGHTY, R. J., MARTINEZ, W. M., MONTGOMERY, R. I., WHITBECK, J. C., XU, R., EISENBERG, R. J., COHEN, G. H., AND SPEAR, P. G. A cell surface protein with herpesvirus entry activity (HveB) confers susceptibility to infection by mutants of herpes simplex virus type 1, herpes simplex virus type 2, and pseudorabies virus. *Virology 246*, 1 (1998), 179–89.

[328] WEISS, R. A. Retrovirus classification and cell interactions. *Journal of Antimicrobial Chemotherapy 37 Suppl B* (1996), 1–11.

[329] WEISSENHORN, W., HINZ, A., AND GAUDIN, Y. Virus membrane fusion. *FEBS Letters 581*, 11 (2007), 2150–5.

[330] WHITBECK, J. C., PENG, C., LOU, H., XU, R., WILLIS, S. H., PONCE DE LEON, M., PENG, T., NICOLA, A. V., MONTGOMERY, R. I., WARNER, M. S., SOULIKA, A. M., SPRUCE, L. A., MOORE, W. T., LAMBRIS, J. D., SPEAR, P. G., COHEN, G. H., AND EISENBERG, R. J. Glycoprotein D of herpes simplex virus (HSV) binds directly to HVEM, a member of the tumor necrosis factor receptor superfamily and a mediator of HSV entry. *Journal of Virology 71*, 8 (1997), 6083–93.

[331] WHITE, J. M., DELOS, S. E., BRECHER, M., AND SCHORNBERG, K. Structures and mechanisms of viral membrane fusion proteins: multiple variations on a common theme. *Critical Reviews in Biochemistry and Molecular Biology 43*, 3 (2008), 189–219.

[332] WHITELEY, A., BRUUN, B., MINSON, T., AND BROWNE, H. Effects of targeting herpes simplex virus type 1 gD to the endoplasmic reticulum and trans-Golgi network. *Journal of Virology 73*, 11 (1999), 9515–20.

[333] WHO. World Health Organization. Global HIV/AIDS response, `http:// www. who. int/ hiv/ pub/ progress_ report2011/ global_ facts/ en/ index. htm` 2012/19/01.

[334] WIEDENMANN, J., IVANCHENKO, S., OSWALD, F., SCHMITT, F., ROCKER, C., SALIH, A., SPINDLER, K. D., AND NIENHAUS, G. U. EosFP, a fluorescent marker protein with UV-inducible green-to-red fluorescence conversion. *Proceedings of the National Academy of Sciences of the United States of America 101*, 45 (2004), 15905–10.

[335] WILK, T., DE HAAS, F., WAGNER, A., RUTTEN, T., FULLER, S., FLUGEL, R. M., AND LOCHELT, M. The intact retroviral Env glycoprotein of human foamy virus is a trimer. *Journal of Virology 74*, 6 (2000), 2885–7.

[336] WILLARD, M. Rapid directional translocations in virus replication. *Journal of Virology 76*, 10 (2002), 5220–32.

[337] WITTELS, M., AND SPEAR, P. G. Penetration of cells by herpes simplex virus does not require a low pH-dependent endocytic pathway. *Virus Research 18*, 2-3 (1991), 271–90.

[338] WOLFSTEIN, A., NAGEL, C. H., RADTKE, K., DOHNER, K., ALLAN, V. J., AND SODEIK, B. The inner tegument promotes herpes simplex virus capsid motility along microtubules in vitro. *Traffic 7*, 2 (2006), 227–37.

[339] WRIGHT, E. R., SCHOOLER, J. B., DING, H. J., KIEFFER, C., FILLMORE, C., SUNDQUIST, W. I., AND JENSEN, G. J. Electron cryotomography of immature HIV-1 virions reveals the structure of the CA and SP1 Gag shells. *EMBO Journal 26*, 8 (2007), 2218–26.

[340] WUDUNN, D., AND SPEAR, P. G. Initial interaction of herpes simplex virus with cells is binding to heparan sulfate. *Journal of Virology 63*, 1 (1989), 52–8.

[341] WUTZLER, P., DOERR, H. W., FARBER, I., EICHHORN, U., HELBIG, B., SAUERBREI, A., BRANDSTADT, A., AND RABENAU, H. F. Seroprevalence of herpes simplex virus type 1 and type 2 in selected German populations-relevance for the incidence of genital herpes. *Journal of Medical Virology 61*, 2 (2000), 201–7.

[342] YE, G. J., VAUGHAN, K. T., VALLEE, R. B., AND ROIZMAN, B. The herpes simplex virus 1 U(L)34 protein interacts with a cytoplasmic dynein intermediate chain and targets nuclear membrane. *Journal of Virology 74*, 3 (2000), 1355–63.

[343] YOKOGAWA. Comparison of CSU series, `http:// www. yokogawa. com/ scanner/ products/ products2. htm` 2012/03/03.

[344] YOON, M., AND SPEAR, P. G. Disruption of adherens junctions liberates nectin-1 to serve as receptor for herpes simplex virus and pseudorabies virus entry. *Journal of Virology 76*, 14 (2002), 7203–8.

[345] YU, S. F., EASTMAN, S. W., AND LINIAL, M. L. Foamy virus capsid assembly occurs at a pericentriolar region through a cytoplasmic targeting/retention signal in Gag. *Traffic 7*, 8 (2006), 966–77.

[346] YU, S. F., SULLIVAN, M. D., AND LINIAL, M. L. Evidence that the human foamy virus genome is DNA. *Journal of Virology 73*, 2 (1999), 1565–72.

[347] ZAGO, A., JOGGER, C. R., AND SPEAR, P. G. Use of herpes simplex virus and pseudorabies virus chimeric glycoprotein D molecules to identify regions critical for membrane fusion. *Proceedings of the National Academy of Sciences of the United States of America 101*, 50 (2004), 17498–503.

[348] ZAMBORLINI, A., RENAULT, N., SAIB, A., AND DELELIS, O. Early reverse transcription is essential for productive foamy virus infection. *PLoS One 5*, 6 (2010), e11023.

[349] ZHANG, J., CAMPBELL, R. E., TING, A. Y., AND TSIEN, R. Y. Creating new fluorescent probes for cell biology. *Nature Reviews: Molecular Cell Biology 3*, 12 (2002), 906–18.

[350] ZHANG, Y., AND MCKNIGHT, J. L. Herpes simplex virus type 1 UL46 and UL47 deletion mutants lack VP11 and VP12 or VP13 and VP14, respectively, and exhibit altered viral thymidine kinase expression. *Journal of Virology 67*, 3 (1993), 1482–92.

[351] Zhang, Y., Sirko, D. A., and McKnight, J. L. Role of herpes simplex virus type 1 UL46 and UL47 in alpha TIF-mediated transcriptional induction: characterization of three viral deletion mutants. *Journal of Virology 65*, 2 (1991), 829–41.

[352] Zhou, G., and Roizman, B. Cation-independent mannose 6-phosphate receptor blocks apoptosis induced by herpes simplex virus 1 mutants lacking glycoprotein D and is likely the target of antiapoptotic activity of the glycoprotein. *Journal of Virology 76*, 12 (2002), 6197–204.

[353] Zhou, G., and Roizman, B. Construction and properties of a herpes simplex virus 1 designed to enter cells solely via the IL-13alpha2 receptor. *Proceedings of the National Academy of Sciences of the United States of America 103*, 14 (2006), 5508–13.

[354] Zhou, Z. H., Dougherty, M., Jakana, J., He, J., Rixon, F. J., and Chiu, W. Seeing the herpesvirus capsid at 8.5 Å. *Science 288*, 5467 (2000), 877–80.

[355] Zhou, Z. H., He, J., Jakana, J., Tatman, J. D., Rixon, F. J., and Chiu, W. Assembly of VP26 in herpes simplex virus-1 inferred from structures of wild-type and recombinant capsids. *Nature Structural Biology 2*, 11 (1995), 1026–30.

List of Abbreviations

3-O-S HS	3-O-Sulfated heparan sulfate
3-OST	3-O-Sulfotransferase
AIDS	acquired immune deficiency syndrome
ALEX	alternating-laser excitation
AOTF	acousto-optic tunable filter
ASLV	avian sarcoma and leukosis virus
AVG	average
B78H1	murine melanoma cell line
BFLA	bafilomycin A1
BHK	baby hamster kidney cell line
BSA	bovine serum albumin
CaSki	human cervical carcinoma cell line
CHO-K1	Chinese hamster ovary cell line
COS	African green monkey kidney fibroblast cell line
CME	clathrin-mediated endocytosis
CTRS	cytoplasmic targeting and retention signal
LC8	cytoplasmic light chain 8
DABCO	1,4-Diazabicyclo[2.2.2]octane
DC	dendritic cells
DC-SIGN	dendritic cell-specific intercellular adhesion molecule grabbing non-integrin
dc virus	dual-color virus
DIC	differential interference contrast
DMEM	Dulbecco's modified eagle medium
DNA	deoxyribonucleic acid
dp	distal pole
D-PBS	Dulbecco's phosphate buffered saline
EBV	Epstein-Barr virus

EE	early endosome
eGFP	enhanced green fluorescent protein
EM	electron microscopy
ER	endoplasmatic reticulum
FBS	fetal bovine serum
FPALM	fluorescence photoactivated localization microscopy
fpm	fluid phase marker
FV	foamy virus
GFP	green fluorescent protein
fpm Alexa647	fluid phase marker dextran Alexa Flour 647
HaCaT	human keratinocyte cell line
HCjE	human conjunctival epithelial cell line
HeLa	human cervical adenocarcinoma cell line *(Henrietta Lacks)*
HIV	human immunodeficiency virus
HHV	human herpesvirus
HCMV	human cytomegalovirus
HEp2	human epidermoid carcinoma cell line
HFF	human foreskin fibroblast cell line
HSPG	heparan sulfate proteoglycan
HSV	herpes simplex virus
HTLV	human T-lymphotropic virus
HveA	herpesvirus entry modulator A, or HVEM
HveC	herpesvirus entry modulator C, or nectin-1
HVEM	herpes virus entry modulator
J	derivative of BHKtk- cell line
LATs	latency-associated transcripts
LE	late endosome
L-particle	light-particle
MA	protein matrix subunit of a viral capsid
MAG	myelin-associated glycoprotein
ME	maturing endosome
MLV	murine leukemia virus
MSD	mean-square-displacement
MTOC	microtubule-organizing center
MW	molecular weight
NA	numerical aperture
NH_4Cl	ammonium chloride

NM-IIA	non-muscle myosin IIA
NMHC-IIA	non-muscle myosin heavy chain IIA
PALM	photoactivated localization microscopy
PBS	phosphate buffered saline
PFA	paraformaldehyde
pfu	plaque forming units
PFV	prototype foamy virus
PFS	point spread function
PILRα	paired immunoglobulin-like type 2 receptor alpha
pp	proximal pole
PREP-particle	pre DNA replication-particle
Prr1	poliovirus receptor-related protein 1, or nectin-1
PtK$_2$	rat kangaroo kidney cell line
RE	recycling endosome
RPE	retinal pigment epithelial cell line
RNA	ribonucleic acid
SDCM	spinning-disk confocal microscope
SFV	simian foamy virus
sptPALM	single particle tracking PALM
STED	stimulated emission depletion
STORM	stochastic optical reconstruction microscopy
SV40	simian virus 40
TGN	trans-Golgi network
TNF	tumor necrosis factor
TIRF	total internal reflection fluorescence
TrIC	tracking image correlation
Vero	African green monkey kidney epithelial cell line
VSV	Vesicular Stomatitis virus
VSV-G	Vesicular Stomatitis virus glycoprotein G
WF	wide-field
wt	wild-type
YFP	yellow fluorescent protein

List of Figures

List of Tables

Acknowledgements